Holography and Strongly Coupled Quantum Field Theories

by

Nikhil Anand

A dissertation submitted to The Johns Hopkins University
in conformity with the requirements for the degree of
Doctor of Philosophy

Baltimore, Maryland
June, 2018

Abstract

The holographic principle, which states that observables in quantum gravity are associated with the boundary of spacetime, has played a crucial role in guiding particle physics research over the past couple of decades. The anti-deSitter space/conformal field theory (AdS/CFT) correspondence is an avatar of the holographic principle and provides an operational *definition* of quantum gravity in AdS space in terms of a dual CFT.

This thesis is comprised of two parts, both of which fall under the broad theme of AdS/CFT. The first part is directly related; it is about the construction of observables in the bulk of three-dimensional AdS space in terms of two-dimensional CFT operators. This is a particularly attractive arena to study quantum gravity because two-dimensional CFTs have an enhanced Virasoro symmetry algebra that rigidly fixes correlators that would be otherwise unconstrained in higher dimensions. This part of the thesis focuses on non-perturbatively defining a bulk AdS "proto-field" ϕ in terms of Virasoro generators acting on a local primary operator $\mathcal{O}$. An exciting application of this work would be to study correlators in black hole backgrounds non-pertubatively.

The second part is indirectly connected to AdS/CFT, but can stand on its own as a numerical prescription to solve quantum field theories (QFTs). QFTs owe their existence to renormalization group flows that begin at ultraviolet CFTs. This suggests that nontrivial information about the flow is encoded into the data that defines the CFT. Typically, this "CFT data" is comprised of the spectrum of local operators present in the theory and the structure constants of the operator algebra. The second part of the thesis explicates a method inspired by holography called "conformal truncation," in which CFT data is used to truncate and diagonalize the Hamiltonian in a strongly interacting QFT. I will demonstrate its applicability in two and three dimensions.

Thesis Committee

Internal Committee Members

Dr. Jared Kaplan (Primary Advisor)
Assistant Professor
Department of Physics & Astronomy
Johns Hopkins Krieger School of Arts & Sciences

Dr. Barry Blumenfeld
Professor
Department of Physics & Astronomy
Johns Hopkins Krieger School of Arts & Sciences

Dr. Nadia Zakamska
Professor
Department of Physics & Astronomy
Johns Hopkins Krieger School of Arts & Sciences

External Committee Members

Greg Eyink
Professor
Department of Applied Mathematics & Statistics
Johns Hopkins Whiting School of Engineering

Benjamin Dodson
Assistant Professor
Department of Mathematics
Johns Hopkins Krieger School of Arts & Sciences

Dedication

To Mom, Dad, Nandan, and Phani Aunty

Acknowledgments

Sic itur ad astra — Virgil

My research over the last five years and this resultant dissertation would not have been possible without the love and support of many people.

First and foremost, I feel truly fortunate to have had Professor Jared Kaplan as my advisor. I have benefited enormously from my conversations with him (physics-related or otherwise) and his total support of my various research ventures. More than anything, the principle lesson that I absorbed from Jared is how to *do* theoretical physics research by example; his take-no-prisoners attitude towards research is one I hope to carry with me for the rest of my life.

I have also learned an enormous amount from conversations with Ibou Bah, Federico Bonetti, David Kaplan, Sandipan Kundu, and Junpu Wang. My collaborators Hongbin Chen, Liam Fitzpatrick, Vincent Genest, Wick Haxton, Charles Hussong, Ami Katz, Zuhair Khandker, Daliang Li, and Matt Walters have also contributed a great deal to my growth as a physicist.

I have had many amazing mentors who first fostered my interest in physics. In particular, I thank my high school teachers Kavita Gupta and Bruce Kawanami for their early encouragement and support. Liam Fitzpatrick, George Fuller, Wick Haxton, Chris Hirata, Hitoshi Murayama, and Jason Rhodes showed me how fun research could be back when I was still an undergrad.

I have been extremely fortunate to have had an incredible group of friends throughout my graduate school career, a list that includes (but is not limited to) Kim Berghaus, Madi Boris, Derek Brehm, Sean Cantrell, Joel Clemmer, Anthony Cordisco, Caroline Huang, Marco Galvani, Tanvi Karwal, Brooks Kinch, Sara Kissinger, Dan Pfeffer, Manav Singh, and Jake Tutmaher. I would like to especially single out Julián Muñoz,

with whom I have shared — and will no doubt continue to share — countless conversations about both life and physics.

I would like to also thank Pam Carmen, Wanda Carter, Kelley Key, and everyone at the front office for helping me meet deadlines, organizing my graduate exams, and so much more. On a related note, I am very grateful to Mark Hall for all the help with travel expenses and reimbursements.

Most importantly, I would like to thank my family: Mom, Dad, Nandan, and Phani Aunty. They have endured the last five years thousands of miles away from me, and I could not have made it this far without their unconditional love and support. This thesis is dedicated to them.

Contents

List of Figures

Chapter 1

Introduction

What one fool can understand, another can.

— Richard P. Feynman

The purpose of particle physics is to understand the fundamental laws of nature. One way we do this is by colliding particles at increasingly higher energies to probe physics at increasingly smaller distances. This fact is encoded in the Heisenberg uncertainty principle:

$$\Delta x \Delta p \geq \frac{\hbar}{2}, \tag{1.0.1}$$

where Δx is the uncertainty in distance, Δp is the uncertainty in momentum, and $\hbar$ is Planck's constant. So the smaller we wish to make Δx — that is, the smaller distances we want to probe — the larger we need to make Δp, the momentum or equivalently the energy, in order for the above principle to hold.

Over the past century, from experiments starting from the simple particle collider of Rutherford's gold foil experiment which determined the existence of the atomic nucleus, to the present-day Large Hadron Collider (LHC) which detected the Higgs particle, we have come to discover that the world of fundamental particles and their interactions is governed by an enormous mathematical framework known as quantum field theory, or 'QFT'. This framework is suited to deal with an infinite set of interacting degrees of freedom, and gives us a recipe for predicting observable quantities from more fundamental principles.

We have also found that QFT is orders of magnitude more far-reaching than physicists of the early 20th century had ever dreamed. It explains and has connections with

such disparate phenomena as superconductivity, water at its critical point, gravity, the physics of early-Universe cosmology, aspects of condensed matter physics, and of course the entire realm of particle physics.

However, there are two major caveats:

- Although the framework of QFT is certainly compatible with gravity at low energies, it is difficult to unify QFT and gravity at very high energies close to and above the Planck scale. The standard program in physics of scattering at higher energies to study smaller length scales seems to inexorably break down due to the formation of black holes. One promising approach to this problem is the holographic principle: the idea that observables in quantum gravity are associated with the *boundary* of spacetime [1]. The most famous and fruitful implementation of the holographic principle is the AdS/CFT correspondence, which *defines* quantum gravity on asymptotically $d+1$-dimensional anti-deSitter ('AdS') spacetime in terms of a d-dimensional conformal field theory ('CFT') that lives on the spatial boundary of AdS [2] [3]. AdS/CFT provides an operational dictionary for calculating quantities in a QFT that, by this duality, reflect features of quantum gravity in AdS space.

- Even without gravity, much of our ability to calculate theoretical predictions and observable signatures in particle physics relies upon the assumption that the systems we study admit some sort of perturbative expansion. That is to say, to reliably calculate anything — such as the scattering amplitude or the spectrum of particles — we often rely on the fact that the interactions only enter in as a small, perturbative effect on top of the larger ensemble. Now, while a subset of phenomena certainly satisfy this assumption, experiments have shown us that some of the most interesting aspects of Nature happen far away from these points. These types of QFTs are called "non-perturbative" or "strongly coupled" QFTs, because they cannot, by definition, be described in a perturbative setting where changes to a system are minuscule.

This PhD thesis is a very small step towards addressing the above open problems: 1) can we glean universal features of quantum gravity from AdS/CFT and 2) can we develop new tools to study strongly coupled QFTs and can we apply them to systems

in the real world? Following this broad outline, this thesis is divided into two parts. Each part can stand alone, although the ideas presented in the second part have been inspired by or can be closely connected to AdS/CFT.

The first part is more directly related, and will focus on aspects of bulk reconstruction in AdS/CFT. By "bulk reconstruction," I mean the exact prescription by which observables in the bulk of AdS space are represented in terms of the dual CFT building blocks, or operators. We will focus on the particular case of theories that live on three-dimensional AdS space, or AdS_3, that are dual to two-dimensional CFTs, or CFT_2s. AdS_3 offers a particularly interesting arena to study holography because of the rich symmetry structure of CFT_2s. Beyond the usual symmetries that are present in any CFT, CFT_2s possess an additional, infinite-dimensional symmetry algebra known as the Virasoro algebra, which we will review momentarily. These additional symmetries constrain physics in the bulk of AdS and describe the emergence of certain universal features of AdS_3 quantum gravity.

This second part is about developing numerical methods to understand QFTs that are strongly coupled at infinite volume.

The main idea is to revisit an old approach to studying QFTs known as Hamiltonian truncation[1]. In Hamiltonian truncation, the Hilbert space of the theory is discretized and truncated in some way. The Hamiltonian of the theory is then numerically diagonalized on this discrete, reduced basis to study the infrared ('IR') dynamics. The point is that as the dimensionality of this basis is made larger, the continuum physics is recovered.

However, in practice, there are many possible implementations of this general framework. One promising method is 'conformal truncation', where the discretized basis is furnished by the eigenstates of the conformal Casimir associated with the UV CFT[2]. The basis is then truncated by setting a maximum Casimir eigenvalue, and the interacting Hamiltonian is then numerically diagonalized on this reduced basis to study the IR physics.

With this overall structure in mind, this thesis is divided into the following chapters:

- In Chapter 2, I show how the Virasoro algebra can be used to construct AdS_3 fields in terms of CFT operators, incorporating the effects of gravitational dressing. I

[1] See [4] for a recent review.
[2] Alternatively, they are the states created by the primary operators of the progenitor CFT.

also show how this definition of a bulk primary gives rise to correlators that agree with bulk perturbation theory. This work was done in collaboration with Hongbin Chen, A. Liam Fitzpatrick, Jared Kaplan, and Daliang Li, and first appeared in [5].

- In Chapter 3, I describe how conformal truncation can be applied to a 1+1-dimensional theory of a quartic scalar at strong coupling. I show how one can construct a (truncated) basis of conformal primaries and compute the Hamiltonian matrix elements between those states. I also show that this method correctly reproduces the physics of the 1+1-dimensional Ising model in the IR at a critical value of the quartic coupling. This work was done in collaboration with Vincent Genest, Emanuel Katz, Zuhair Khandker, and Matthew Walters and first appeared in [6].

- In Chapter 4, I describe ongoing work in applying conformal truncation in 2+1 dimensions again to a quartic scalar theory. This theory flows to the 2+1-dimensional Ising model at a tuned value of the quartic coupling. Since the 2+1-dimensional Ising model is much more complicated than its two-dimensional integrable cousin, this application is an extremely interesting test of conformal truncation. This work is being done in collaboration with Charles Hussong, Emanuel Katz, Zuhair Khandker, and Matthew Walters, and will appear soon.

Chapter 2

Bulk Reconstruction

Hic sunt dracones. — Inscribed on the Hunt-Lenox Globe

2.1 Introduction

To resolve the black hole information paradox in AdS/CFT, we must understand how to describe local AdS dynamics in terms of CFT data and observables. Unfortunately, bulk gauge redundancies could render AdS reconstruction ambiguous, and the existence of black holes at high-energies suggests that local physics may not be well-defined. We will argue that the Virasoro symmetry of CFT_2 provides a sort of beachhead into AdS_3, making it possible to exactly define a bulk 'proto-field' ϕ as a specific linear combination of Virasoro descendants of a given local primary operator $\mathcal{O}$.

The simplest AdS/CFT observable is the vacuum bulk-boundary correlator

$$\langle \phi(X)\mathcal{O}(P)\rangle = \frac{1}{(P\cdot X)^{\Delta}}, \tag{2.1.1}$$

which is determined by conformal symmetry up to an overall constant. From this correlator alone one can derive a formula for a proto-field $\phi(X)$ as a linear combination of global conformal descendants of the primary operator $\mathcal{O}$ [7, 8, 9, 10]. At this level, bulk reconstruction is purely kinematical, following entirely from the assumption that conformal transformations act on ϕ as AdS isometries.

In the case of $\text{AdS}_3/\text{CFT}_2$, Virasoro conformal transformations act as asymptotic symmetries. So it is natural to expect that the bulk-boundary correlator should be

uniquely determined in any geometry that can be related to the vacuum by a Virasoro symmetry. In rather different words, we expect that all correlators of the form

$$\langle \phi(X)\mathcal{O}(z,\bar{z})T(z_1)\cdots T(z_n)\bar{T}(\bar{w}_1)\cdots\bar{T}(\bar{w}_m)\rangle \tag{2.1.2}$$

can be determined by symmetry once we fix a gauge for the bulk gravitational field. This leads to a unique expression for a Virasoro proto-field operator $\phi(X)$ as a linear combination of Virasoro descendants of the CFT_2 primary $\mathcal{O}$. These proto-field operators will automatically 'know' about the bulk geometry associated with heavy distant sources, meaning that they perform bulk reconstruction at an operator level. In this paper we will explain how to identify and explicitly compute $\phi(X)$ as a CFT_2 operator. We will be led to the potentially surprising conclusion that an exact (non-perturbative in c) condition uniquely determines ϕ in our Fefferman-Graham type gauge.

We will determine $\phi(X)$ in two distinct but ultimately equivalent ways. The first is based on an extension of gravitational Wilson lines [11, 12, 13, 14, 15, 16, 17] as OPE blocks [18]. We will introduce a 'bulk-boundary OPE block' that encapsulates the projection of the (non-local) operator $\phi(X)\mathcal{O}(x)$ onto the vacuum sector. This provides an explicit prescription for computing all correlators of the form of equation (2.1.2). Our second method is based purely on imposing Virasoro symmetry, resulting in a very simple, non-perturbative definition for $\phi(X)$. This also makes it possible to determine the correlators of equation (2.1.2) via a simple recursion relation. The proto-field operator that we will obtain has a number of desirable properties:

- Virasoro transformations act on the scalar field $\phi(X)$ as infinitesimal bulk diffeomorphisms preserving the gauge. At the semiclassical level, $\phi(X)$ obeys the Klein-Gordon equation in any vacuum geometry.

- Correlators of ϕ with stress tensors are causal and have only those singularities dictated by the gravitational constraints [19, 20, 21], matching bulk perturbation theory. Correlators of $\phi(X)$ reduce to those of $\mathcal{O}(x)$ when we extrapolate $\phi(X)$ to the boundary. Equation (2.1.2) reduces to $\langle\mathcal{O}\mathcal{O}T\cdots\bar{T}\cdots\rangle$; in fact there is a simple recursion relation that computes vacuum correlators, generalizing well-known relations [22] for correlators of CFT_2 primaries with stress tensors.

With our exact definition for $\phi(X)$, it is possible to study the impact of non-perturbative

gravitational effects on bulk observables. This means that one could study $\phi(X)\phi(Y)$ at short distances, and directly probe near black hole horizons without relying on bulk perturbation theory.

There is a large literature on bulk reconstruction in AdS/CFT employing a variety of philosophies and methods, for example [7, 23, 8, 24, 19, 20, 21, 25, 26, 27, 10, 28, 29, 18, 30, 31, 32, 33, 34].[1] The most common approach expresses bulk fields in terms of local CFT operators integrated against a kernel [7, 8, 24]. We will take a somewhat different approach [35, 36, 37]; our scalar operator $\phi(y,0,0)$ will be expressed in a boundary operator expansion[2] (BOE) [38]

$$\phi(y,0,0) = \sum_{N=0}^{\infty} \lambda_N y^{2h+2N} \mathcal{L}_{-N}\bar{\mathcal{L}}_{-N}\mathcal{O}(0) \tag{2.1.3}$$

where $\mathcal{L}_{-N}$ and $\bar{\mathcal{L}}_{-N}$ are linear combinations of products of Virasoro generators at level N, and $\lambda_N = \frac{(-1)^N}{N!(2h)_N}$. In the global limit ($c \to \infty$), we have $\lim_{c\to\infty} \mathcal{L}_{-N} = L_{-1}^N$. At finite c, we will show that $\mathcal{L}_{-N}\mathcal{O}$ satisfies the bulk primary conditions

$$L_m \mathcal{L}_{-N}\mathcal{O} = 0, \qquad \text{for } m \geq 2. \tag{2.1.4}$$

and similarly for $\bar{\mathcal{L}}_{-N}\mathcal{O}$. Roughly speaking, these conditions say that ϕ is as primary as it can be and still move around under AdS bulk isometries. In the smearing function language, we are computing ϕ as an infinite sum of operators[3] of the schematic form $\mathcal{O}, [T\bar{\partial}^2\mathcal{O}], \cdots, [T\partial^2 T\bar{T}\bar{\partial}^4\mathcal{O}], \cdots$, though we will not express our results in this way.

The outline of this paper is as follows. In section 2.2 we explain the bulk-boundary OPE block idea, and then show how the vacuum $\phi(X)\mathcal{O}(z)$ OPE block can be derived using gravitational or Chern-Simons Wilson lines. We begin section 2.3 by providing an exact algebraic definition for ϕ compatible with the results of section 2.2. Then we show that this simple definition follows from considerations of symmetry. We solve for

[1] We believe the proposal in [33, 34] is different from ours.

[2] The idea of performing bulk reconstruction using a boundary operator expansion was briefly discussed in [35]. The global AdS results have been worked out by M. Paulos in unpublished work. Note that the boundary operator expansion appears local on the boundary, but due to the infinite sum it should really be viewed as a non-local CFT operator, for the same reason that $e^{x\partial}\chi(0) = \chi(x)$ should not be viewed as a local operator at the origin.

[3] As was shown by Kabat and Lifschytz [20, 21], because of the gravitational gauge constraints ϕ must include contributions from the scalar descendants of quasi-primaries with non-zero spin, such as $\partial^\mu\partial^\nu[T_{\mu\nu}\mathcal{O}]$, even though ϕ itself is a bulk scalar field. Thus it's not entirely clear how smearing functions can be used to describe our results.

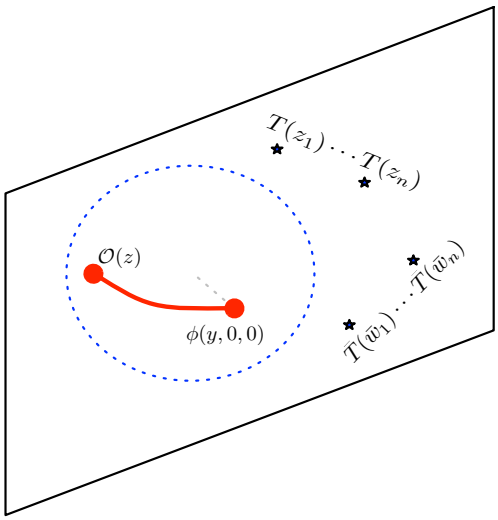

Figure 2.1: This figure portrays a bulk-boundary OPE block used to compute the correlator (2.1.2). The red line denotes the gravitational or Chern-Simons Wilson line, while the blue circle suggests radial quantization around the block, so that it creates a definite linear combination of Virasoro descendants of the identity. The explicit computation involves line integrals over stress tensor correlators.

ϕ explicitly in various cases, and then show how our definition leads to new recursion relations for correlators of ϕ with boundary stress tensors. We collect various technical results and background material in the appendices. Appendix 2.5.3 may be useful for readers who are most familiar with the HKLL [8] smearing procedure, and want to understand how our approach, in the simple global conformal case, can be reduced to theirs. All formulas in this paper are written in Euclidean signature.

2.2 Bulk Reconstruction from Gravitational Wilson Lines

The operator product expansion (OPE) expresses a product of separated local operators $\mathcal{O}_1(x_1)\mathcal{O}_2(x_2)$ as an infinite sum of local operators at a single point. It is very natural to gather the contributions to the OPE that come from a single conformal primary and its descendants. This has been dubbed [18] an 'OPE block'. In the case of CFT_2, the Virasoro OPE blocks can be computed using Chern-Simons Wilson lines [16].

In this work we will be studying an AdS_3 proto-field $\phi(X)$ as a CFT_2 operator, and we focus on Euclidean signature. Although $\phi(X)$ may be somewhat non-local, on the border of a sufficiently large region in the CFT containing $\phi(X)$, we expect that it should still be possible to perform a radial quantization, as shown in figure 2.1. This suggests that we can study OPE blocks involving $\phi(X)$ and other operators. We will be

focusing on the simplest such object, the scalar Virasoro vacuum OPE block

$$\phi(y,0,0)\mathcal{O}(z,\bar{z}) = \frac{y^{2h}}{(y^2+z\bar{z})^{2h}} + \cdots \tag{2.2.1}$$

where the ellipsis denotes non-identity Virasoro generators (e.g. $L_{-6}\bar{L}_{-4}^2$) with coordinate-dependent coefficients, and we have labeled ϕ using the coordinates of the AdS_3 vacuum metric

$$ds^2 = \frac{dy^2 + dzd\bar{z}}{y^2} \tag{2.2.2}$$

Note that we have already identified the contribution of the identity operator in equation (2.2.1) as the vacuum correlator $\langle\phi\mathcal{O}\rangle$, which is fixed by conformal symmetry. All of the remaining terms in equation (2.2.1) would be fixed if we knew all correlators of the form (2.1.2), because the Virasoro generators are just the modes in an expansion of the stress tensors $T(z)$ and $\bar{T}(\bar{z})$.

Building on prior work [16], we will make the following proposal for the $\phi\mathcal{O}$ OPE block. The general asymptotically AdS_3 vacuum metric can be written[4] as [39, 40]

$$ds^2 = \frac{dy^2 + dzd\bar{z}}{y^2} - \frac{6T(z)}{c}dz^2 - \frac{6\bar{T}(\bar{z})}{c}d\bar{z}^2 + y^2\frac{36T(z)\bar{T}(\bar{z})}{c^2}dzd\bar{z} \tag{2.2.3}$$

This amounts to a choice of gauge for the bulk gravitational field. Normally the objects $T(z)$ and $\bar{T}(\bar{z})$ appearing in this equation are viewed as classical functions, but let us instead view them as CFT_2 stress tensor operators. We define the bulk-boundary OPE block as the operator defined by the propagation of a (quantum, first-quantized) particle from the location of $\mathcal{O}$ on the boundary to that of ϕ in the bulk. Formally, this means that the bulk-boundary OPE block can be thought of as a world-line path integral

$$\phi(X)\mathcal{O}(0)|_{\text{vac}} = \int \mathcal{D}Y(\tau)\, e^{-m\int_0^X d\tau\sqrt{g_{\mu\nu}\dot{Y}^\mu\dot{Y}^\nu}}, \tag{2.2.4}$$

where on the LHS we are restricting to the vacuum sector of the operator product. On the RHS we interpret $g_{\mu\nu}$ as a quantum operator dependent on $T, \bar{T}$ as defined

[4] Our construction requires an ability to specify this gauge. This will be possible sufficiently close to the boundary of AdS, but may fail in the presence of sources, or in the context of non-trivial boundary topologies. We expect that the construction may break down in regimes where the dynamics are inconsistent with our gauge choice. We leave a detailed discussion of the regime of validity to future work.

in equation (2.2.3), and $Y^\mu(\tau)$ is world-line connecting ϕ and $\mathcal{O}$. The mass m of the particle will be related to the dimension of $\mathcal{O}$ by $m^2 = 2h(2h-2)$. Equation (2.2.4) defines the OPE block as an infinite sum of products of line integrals of the CFT_2 stress tensor. We have sketched the OPE block in figure 2.1.

In a certain sense, we will use equation (2.2.4) more for conceptual purposes than for computation ones. To use (2.2.4) directly would require defining the path integral measure precisely; in practice, we will circumvent this kind of issue by starting with the exact CFT result for (2.2.4) in the AdS vacuum and uplifting to nonzero $T, \bar{T}$ by performing diffeomorphisms, as we describe below. Nevertheless, it is useful to bear equation (2.2.4) in mind as it intuitively captures what we are trying to achieve in defining $\phi\mathcal{O}$, and furthermore it should agree with our practical definition in a semiclassical limit where ambiguities in the path integral measure do not arise. So when we compute the bulk-boundary OPE block in the presence of operators with dimensions $h_H \propto c$ at large c, then we can approximate $\phi\mathcal{O}$ by including only the semiclassical expectation value $\langle T(z)\rangle \propto \frac{h_H}{c}$. This immediately leads to the correct $\phi\mathcal{O}$ correlators in a semiclassical background, such as that of a BTZ black hole. Relatedly, our prescription will also lead to a $\phi(X)$ that satisfies the Klein-Gordon equation in the semiclassical metric of equation (2.2.3). We review this elementary fact in appendix 2.5.1. We also provide a more detailed discussion of (2.2.4) and its regulation in appendix 2.6.

In the remainder of this section we will use equation (2.2.4) to explicitly compute various correlation functions, and demonstrate that the results reduce to those of [16] when we take ϕ to the boundary. In fact we will find that we can reformulate equation (2.2.4) in terms of sl(2) Wilson lines as

$$\phi(y, z_2, \bar{z}_2)\mathcal{O}(z_1, \bar{z}_1)|_{vac} = P\left\{e^{\int_{z_1}^{z_2} dz A_z + \int_{\bar{z}_1}^{\bar{z}_2} d\bar{z}\bar{A}_{\bar{z}}}\right\}\left(\frac{y}{y^2 + x\bar{x}}\right)^{\Delta}\Bigg|_{x=\bar{x}=0}. \tag{2.2.5}$$

As we will explain in section 2.2.2 (where we also define the notation), this is the most natural generalization of prior Chern-Simons Wilson line results [16] to the case of the bulk-boundary OPE block. It also makes manifest the fact that as we take ϕ to the boundary, we recover the structure of the more conventional $\mathcal{O}(z_2)\mathcal{O}(z_1)$ Virasoro OPE block.

2.2.1 Computing $\phi(X)\mathcal{O}(0)$ from a Diffeomorphism

We will use two facts to formulate an operational definition of equation (2.2.4) that can be used for practical computations. The first is that in pure AdS_3, the first-quantized path integral reduces to $e^{-2h\sigma}$ where σ is the (renormalized) length of a geodesic connecting $\mathcal{O}$ and ϕ. The second fact is an explicit diffeomorphism [40] that relates metrics of the form (2.2.3) to the pure AdS_3 metric. We will elevate this diffeomorphism to an operator equation, defining a change of coordinates parameterized by a function $f_T(z)$ that maps the pure AdS_3 metric to the operator-valued vacuum metric of equation (2.2.3). Then we can use the first fact to evaluate the bulk-boundary OPE block as a functional of $f_T(z)$, which itself depends on the operator $T(z)$. These ideas were inspired by very similar methods that have been used to evaluate Chern-Simons Wilson lines [16] in order to compute Virasoro OPE blocks; we will see in section 2.2.2 that this is not an accident.

The first fact means that in a vacuum metric

$$ds^2 = \frac{du^2 + dwd\bar{w}}{u^2}, \tag{2.2.6}$$

we can write the bulk-boundary correlator as

$$\phi(u,0,0)\mathcal{O}(w,\bar{w}) = \left(\frac{u}{u^2+w\bar{w}}\right)^{2h}. \tag{2.2.7}$$

In the CFT vacuum, this is an exact CFT result, just the standard scalar bulk-to-boundary propagator that can be derived purely from symmetries of the CFT. But now we will generalize it by viewing the coordinates $(u,w,\bar{w})$ as the result of an operator valued diffeomorphism from a general vacuum metric of the form of equation (2.2.3). The diffeomorphism takes the form [40]

$$\begin{aligned} w &\rightarrow f(z) - \frac{2y^2(f'(z))^2\bar{f}''(\bar{z})}{4f'(z)\bar{f}'(\bar{z}) + y^2 f''(z)\bar{f}''(\bar{z})} \\ \bar{w} &\rightarrow \bar{f}(\bar{z}) - \frac{2y^2(\bar{f}'(\bar{z}))^2 f''(z)}{4f'(z)\bar{f}'(\bar{z}) + y^2 f''(z)\bar{f}''(\bar{z})} \\ u &\rightarrow y\frac{4(f'(z)\bar{f}'(\bar{z}))^{\frac{3}{2}}}{4f'(z)\bar{f}'(\bar{z}) + y^2 f''(z)\bar{f}''(\bar{z})} \end{aligned} \tag{2.2.8}$$

and is parameterized by the independent holomorphic and anti-holomorphic functions

$f(z)$ and $\bar{f}(\bar{z})$. This diffeomorphism has the property that the transformed metric is precisely

$$ds^2 = \frac{dy^2 + dzd\bar{z}}{y^2} - \frac{1}{2}S(f,z)dz^2 - \frac{1}{2}S(\bar{f},\bar{z})d\bar{z}^2 + y^2\frac{S(f,z)S(\bar{f},\bar{z})}{4}dzd\bar{z} \tag{2.2.9}$$

where

$$S(f,z) \equiv \frac{f'''(z)f'(z) - \frac{3}{2}(f''(z))^2}{(f'(z))^2} = \frac{12}{c}T(z) \tag{2.2.10}$$

is the Schwarzian derivative. Thus the diffeomorphism maps pure AdS_3 to a general vacuum-sector metric with a non-vanishing stress tensor. Applying this operator valued diffeomorphism to (2.2.7), we obtain the vacuum sector bulk-boundary OPE block[5]

$$\phi(y,z_2,\bar{z}_2)\mathcal{O}(z_1,\bar{z}_1)|_{vac} = (w'(z_1)\bar{w}'(\bar{z}_1))^h \left(\frac{u_2}{u_2^2 + (w_2-w_1)(\bar{w}_2-\bar{w}_1))}\right)^{2h}, \tag{2.2.11}$$

where $u_2, w_2, \bar{w}_2$ are $u, w, \bar{w}$ in (2.2.8) evaluated at $(y, z_2, \bar{z}_2)$, and $w_1, \bar{w}_1$ are evaluated at $(0, z_1, \bar{z}_1)$. This is the key formulation of the bulk-boundary OPE block that will be used in this paper.

To evaluate (2.2.11), we need to solve equation (2.2.10) and its anti-holomorphic equivalent for the functions $f(z)$ and $\bar{f}(\bar{z})$, determining them as functionals of the stress tensor operators $T(z), \bar{T}(\bar{z})$. Then we can evaluate equation (2.2.7) by expanding the coordinates $u, w, \bar{w}$ in terms of $f, \bar{f}$. To carry out this procedure explicitly in $1/c$ perturbation theory, we write

$$f(z) = z + \frac{1}{c}f_1(z) + \frac{1}{c^2}f_2(z) + \cdots \tag{2.2.12}$$

and then solve for the f_n in terms of T using equation (2.2.10). The first two f_n are determined by the differential equations

$$\begin{aligned} f_1'''(z) - 12T(z) &= 0 \\ 2f_1{}^{(3)}(z)f_1'(z) + 3f_1''(z)^2 - 2f_2{}^{(3)}(z) &= 0 \end{aligned} \tag{2.2.13}$$

[5]Note that in deriving this equation, we cut off the divergent near boundary integral at a constant y plane as oppose to the constant y_w plane used in (2.2.7). This shift results in the $(w'(z_1)\bar{w}'(\bar{z}_1))^h$ factor that is essential to reproduce the transformation property of a boundary Virasoro primary.

so for example, the first equation simply leads to $f_1(z) = -6\int_0^z dz'(z-z')^2 T(z')$. Once we solve for the f_n, we can expand (2.2.11) to find the bulk-boundary OPE block[6]

$$\log\phi(y,0,0)\mathcal{O}(z,\bar{z}) = 2h\log\left(\frac{y}{z\bar{z}+y^2}\right) + \underbrace{\frac{h\left(z\bar{z}+y^2\right)f_1'(z) - 2\bar{z}f_1(z)}{c\left(z\bar{z}+y^2\right)}}_{K_T} + \cdots \quad (2.2.14)$$

where the ellipsis denotes both the conjugate anti-holomorphic $K_{\bar{T}}$ terms as well as the perturbation series at order $1/c^2$ and above. The order $1/c$ terms K_T and $K_{\bar{T}}$ are line-integrals of the stress tensors T and $\bar{T}$ against specific kernels. For example, by combining terms above we find that

$$K_T = \frac{12h}{c}\int_0^z dz' \frac{(y^2+z'\bar{z})(z-z')}{y^2+z\bar{z}}T(z') \quad (2.2.15)$$

and similarly for the anti-holomorphic $K_{\bar{T}}$. In the limit $y \to 0$ we recover the kernels [16] for the standard 'boundary-boundary' $\mathcal{O}(z)\mathcal{O}(0)$ OPE block.

At the next order we would obtain the new kernels $K_{TT}, K_{\bar{T}\bar{T}}$, and also the mixed kernel $K_{T\bar{T}}$ which are computed explicitly in appendix 2.7.1. The results are

$$\begin{aligned} K_{TT} &= \frac{72h}{c^2}\int_0^z dz'\int_0^{z'} dz'' \frac{(z-z')^2\left(y^2+\bar{z}z''\right)^2}{\left(z\bar{z}+y^2\right)^2}T\left(z'\right)T\left(z''\right) \\ K_{T\bar{T}} &= -\frac{72hy^2}{c^2\left(z\bar{z}+y^2\right)^2}\int_0^z dz'\left(z-z'\right)^2\int_0^{\bar{z}} d\bar{z}'\left(\bar{z}-\bar{z}'\right)^2 T\left(z'\right)\bar{T}\left(\bar{z}'\right) \end{aligned} \quad (2.2.16)$$

for the bulk-boundary OPE blocks. Note that the first reduces to the expected $\mathcal{O}(z)\mathcal{O}(0)$ kernel (compare to equation 4.40 of [16]) at this order, while the $K_{T\bar{T}}$ kernel vanishes as $y \to 0$, again matching with the expectations for the boundary (where OPE blocks factorize into holomorphic $\times$ anti-holomorphic parts). In the next subsection we will present an alternative derivation that makes this matching explicit to all orders in $1/c$.

[6] We took the logarithm because it renders computations simpler and more transparent [16], but one could easily deal with the full OPE block directly instead. Taking the logarithm of an operator is not at all innocuous in general, but due to our choice of regulator it will not present any problems.

2.2.2 Connection with Chern-Simons Wilson Lines

The sl(2) Wilson line formulation in [16] (based on the earlier work [11]) of the standard OPE block takes the form

$$\mathcal{O}(z_2)\mathcal{O}(z_1) \supset W(z_2, z_1) = P\left\{e^{\int_{z_1}^{z_2} dz^\mu A_\mu^a(z) L_x^a}\right\} \frac{1}{x^{2h}}\bigg|_{x=0}. \tag{2.2.17}$$

First, we will review the notation and some of the results from [16], and then we will see how to generalize (2.2.17) to the expression (2.2.5) above.

In the Wilson line expression (2.2.17), P indicates 'path-ordering', the A_μs are the sl(2) gauge fields, and the L_x^a are the corresponding generators. The variable x is an auxiliary coordinate introduced so that L_x^a can be written in an infinite dimensional representation,

$$L^1 \cong L_{-1} = \partial_x, \qquad L^0 \cong L_0 = x\partial_x + h, \qquad L^{-1} \cong L_1 = \frac{1}{2}x^2\partial_x + hx. \tag{2.2.18}$$

Equation (2.2.17) is the holomorphic part of the OPE block, and a similar anti-holomorphic piece is present in the full block. The boundary condition on A_μ that leads to Virasoro symmetry is

$$A_z|_{y=0} = L^1 + \frac{12}{c} T(z) L^{-1}. \tag{2.2.19}$$

For boundary operators $\mathcal{O}$, we can push the Wilson line connecting $\mathcal{O}(z_2)$ and $\mathcal{O}(z_1)$ onto the boundary so that only the above behavior at $y = 0$ is necessary. When we move one of the $\mathcal{O}$s into the bulk to position $(y, z_2, \bar{z}_2)$, we will first take the Wilson line to be along the boundary from $(0, z_1, \bar{z}_1)$ to $(0, z_2, \bar{z}_2)$, and then to go directly to the bulk point $(y, z_2, \bar{z}_2)$ along constant $(z_2, \bar{z}_2)$. Making the gauge choice $A_y = 0$, the second part of the Wilson line is trivial.

In [16], it was shown that the path-ordered term $P\left\{e^{\int_{z_1}^{z_2} dz^\mu A_\mu^a(z) L_x^a}\right\}$ could equivalently be written as

$$e^{\frac{12h}{c}\int_{z_1}^{z_2} dz T(z) x_T(z)} \tag{2.2.20}$$

after promoting x everywhere to an operator $x_T(z_1)$ that is defined as the (operator

valued) solution to the differential equation

$$-x_T'(z) = 1 + \frac{6T(z)}{c} x_T^2(z), \qquad x_T(z_2) = 0. \tag{2.2.21}$$

In other words,

$$W(z_2, z_1) = \left(e^{\int_{z_1}^{z_2} dz \frac{12T(z)}{c}} x_T(z) \frac{1}{x_T(z_1)^2} \right)^h. \tag{2.2.22}$$

A key point was that x_T is closely related to the uniformizing coordinates f_T defined through the Schwarzian in 2.2.10. In particular,

$$\frac{1}{x_T(z)} \equiv \frac{f_T''(z)}{2f_T'(z)} - \frac{f_T'(z)}{f_T(z) - f_T(z_f)}. \tag{2.2.23}$$

automatically satisfies the constraint (2.2.21).

Now we are ready to derive (2.2.5). The starting point will be our general philosophy that ϕ in a general background follows from ϕ in the AdS vacuum combined with the operator-valued transformation (2.2.8). This results in the bulk-boundary OPE block for $\phi\mathcal{O}$ given by (2.2.11). Our goal will be to write (2.2.11) in terms of the Wilson line building blocks. For concision, let us define the exponential

$$E_T \equiv e^{\frac{6}{c}\int_{z_1}^{z_2} dz' T(z') x_T(z')}. \tag{2.2.24}$$

From the constraint equation (2.2.21), we have

$$\log E_T = -\int_{z_1}^{z_2} dz' \frac{1 + x_T'(z)}{x_T(z)} = \log \left(\frac{2(f_T'(z_2))^{\frac{1}{2}} (f_T'(z_1))^{\frac{3}{2}}}{2(f_T'(z_i))^2 + (f_T(z_2) - f_T(z_1)) f_T''(z_1)} \right) \tag{2.2.25}$$

Furthermore, we see that the OPE block to has the correct semiclassical limit [16]

$$W(z_2, z_1) \cong E_T^2 \frac{1}{x_T^2(z_1)} = \frac{f_T'(z_2) f_T'(z_1)}{(f_T(z_2) - f_T(z_1))^2}. \tag{2.2.26}$$

It is now a straightforward matter to compare (2.2.11) to the RHS of

$$P\left\{ e^{\int_{z_1}^{z_2} dz A_z + \int_{\bar{z}_1}^{\bar{z}_2} d\bar{z} \bar{A}_{\bar{z}}} \right\} \left(\frac{y}{y^2 + x\bar{x}} \right)^{\Delta} \Bigg|_{x=\bar{x}=0} \cong E_T^{\Delta} \bar{E}_T^{\Delta} \left(\frac{y}{y^2 + x_T \bar{x}_T} \right)^{\Delta} \tag{2.2.27}$$

expanded out in terms of their dependence on $f_T, \bar{f}_T$ and confirm that they agree.[7] Thus the conclusion is that the methods of 2.2.1 are entirely consistent with those from [16], and all of the techniques from that paper apply equally well to the bulk-boundary OPE. In particular, one can compute the integration kernels $K_{T\ldots\bar{T}\ldots}$ very efficiently to high orders using the x_T variables [16]; this is a significant technical improvement compared to solving equations like (2.2.13) directly.

We can go further and obtain a simple form for the generalization of (2.2.5) to the case of spinning fields and operators as well. We relegate the details of the derivation to appendix 2.7.3 and simply quote the result here:

$$\langle A_{\mu_1\ldots\mu_\ell}(y,z_2,\bar{z}_2)\mathcal{O}_{h,\bar{h}}(z_1,\bar{z}_1)\rangle = P\left\{e^{\int_{z_1}^{z_2}dzA_z+\int_{\bar{z}_1}^{\bar{z}_2}d\bar{z}\bar{A}_{\bar{z}}}\right\}t^{\mu_1'}_{\mu_1}\ldots t^{\mu_\ell'}_{\mu_\ell}K_{\mu_1',\ldots,\mu_\ell'}(y,x,\bar{x}). \tag{2.2.28}$$

Here, $\mathcal{O}_{h,\bar{h}}$ is a boundary field of weight $(h,\bar{h})$ and $A_{\mu_1,\ldots,\mu_\ell}$ is a bulk field with $\ell = h-\bar{h} \geq 0$ (a similar expression holds for $\ell \leq 0$). The factor $K_{\mu_1,\ldots,\mu_\ell}$ is the vacuum AdS bulk-boundary propagator that we describe in detail in appendix 2.7.3, and the tensor t^μ_ν is a diagonal matrix of the form

$$t^y_y = 1, \qquad t^z_z = 1+\frac{6}{c}\frac{T(z_2)y^4}{\bar{x}^2}, \qquad t^{\bar{z}}_{\bar{z}} = 1+\frac{6}{c}\bar{T}(\bar{z}_2)\bar{x}^2. \tag{2.2.29}$$

Although we have not pursued it directly in this paper, these results can be used to study the reconstruction of massive spinning fields in the bulk.

2.2.3 Evaluating Vacuum Sector Correlators

In this section we will use the bulk-boundary OPE block to compute correlators of $\phi\mathcal{O}$ with products of local stress tensors. These correlators repackage all of the information about the overlap of $\phi\mathcal{O}$ with the Virasoro vacuum sector.

Since $\langle\phi\mathcal{O}\rangle$ is simply given by the first term in equation (2.2.14), ie $\langle\phi(y,0,0)\mathcal{O}(z,\bar{z})\rangle = \left(\frac{y}{y^2+z\bar{z}}\right)^{2h}$, the simplest non-trivial correlator is $\langle\phi\mathcal{O}T\rangle$. It can be computed using

[7] To be systematic, one can just solve for x_T and E_T in terms of $f'(z_2), f''(z_2)$ and substitute.

(2.2.15), giving

$$\frac{\langle\phi(y,0,0)\mathcal{O}(z,\bar{z})T(z_1)\rangle}{\langle\phi(y,0,0)\mathcal{O}(z,\bar{z})\rangle} = \langle K_T T(z_1)\rangle = \frac{12h}{c}\int_0^z dz' \frac{2(z-z')(y^2+z'\bar{z})}{y^2+z\bar{z}}\frac{c}{2(z'-z_1)^4} = \frac{hz^2}{z_1^3(z_1-z)^2}\left(z_1+\frac{2y^2(z_1-z)}{y^2+z\bar{z}}\right) \quad (2.2.30)$$

The computation is suggested pictorially in figure 2.1. This result matches bulk gravitational perturbation theory using AdS_3 Feynman diagrams in our chosen gauge, as we show explicitly in appendix 2.7.4. This is no surprise, as the definition in equation (2.2.4) essentially reproduces gravitational perturbation theory in a first quantized language.

Note that the singularity structure of equation (2.2.30) as z_1 approaches 0 encodes the (expectation value of) the commutator[8] of the stress tensor with ϕ. The fact that the most singular term is of order z_1^{-3} provides a first hint of a powerful symmetry structure that we will discuss in section 2.3.

Naively, one might expect that equation (2.2.30) is only the first term in an infinite perturbation series for this correlation function. However, the higher order contributions need to be regulated in a way that is consistent with Virasoro symmetry and with the fixed dimension $2h$ for the scalar CFT operator $\mathcal{O}$. In the context of Chern-Simons Wilson lines, we proposed a prescription for regulating multi-T correlators in Appendix C.2 of [16] that produces the correct Virasoro OPE blocks. In appendix 2.6, we argue that this regulator can be derived from the generating function of multi-T correlators. Applying this same regulator for the bulk-boundary OPE block, we find that all higher order contributions to $\langle\phi\mathcal{O}T\rangle$ vanish. Thus we claim that equation (2.2.30) is the exact result for this correlation function. We will provide another argument that equation (2.2.30) is exact in section 2.3.

We can also compute the correlators $\langle\phi\mathcal{O}TT\rangle$ and $\langle\phi\mathcal{O}T\bar{T}\rangle$. We provide details of the computations in appendix 2.7.2. The results are that

$$\begin{aligned}&\frac{\langle\phi(y,0,0)\mathcal{O}(z,\bar{z})T(z_1)T(z_2)\rangle}{\langle\phi(y,0,0)\mathcal{O}(z,\bar{z})\rangle}\\ =&\frac{c}{2(z_1-z_2)^4}+\frac{h^2z^4\left(z_1z\bar{z}+y^2(3z_1-2z)\right)\left(z_2z\bar{z}+y^2(3z_2-2z)\right)}{z_1^3z_2^3(z-z_1)^2(z-z_2)^2(z\bar{z}+y^2)^2}\\ &+\frac{2hz^2\left(y^2z\bar{z}z_1z_2(z(z_1+z_2)-4z_1z_2)-z^2\bar{z}^2z_1^2z_2^2+y^4\left(zz_1z_2(z_1+z_2)-3z_1^2z_2^2-z^2(z_1-z_2)^2\right)\right)}{(z-z_1)(z_2-z)z_1^3z_2^3(z_2-z_1)^2(z\bar{z}+y^2)^2}\end{aligned}$$

[8] To any order in a small y expansion, the operator-valued commutator $[\phi(y,0,0),T(z_1)]$ will be a sum of Virasoro descendants of $\mathcal{O}(0)$. However, at finite y this commutator cannot be interpreted as a local CFT operator at z, for the same reason that ϕ itself does not have this interpretation – it is an infinite sum of local operators, and so it is not local.

and

$$\begin{aligned}&\frac{\left\langle \phi\left(y,0,0\right)\mathcal{O}\left(z,\overline{z}\right)T\left(z_1\right)\overline{T}\left(\overline{w}_1\right)\right\rangle}{\left\langle \phi\left(y,0,0\right)\mathcal{O}\left(z,\overline{z}\right)\right\rangle}\\ =&\frac{h^2z^2\bar{z}^2\left(y^2\left(3\bar{w}_1-2\bar{z}\right)+\bar{w}_1z\bar{z}\right)\left(y^2\left(3z_1-2z\right)+z_1z\bar{z}\right)}{z_1^3\overline{w}_1^3\left(z_1-z\right)^2\left(\overline{w}_1-\bar{z}\right)^2\left(z\bar{z}+y^2\right)^2}+\frac{2hy^2z^3\bar{z}^3}{z_1^3\bar{w}_1^3\left(z-z_1\right)\left(\bar{w}_1-\bar{z}\right)\left(z\bar{z}+y^2\right)^2}\end{aligned}$$

These reduce to the expected $\mathcal{O}\mathcal{O}$ correlators as $y\to 0$.

We should also emphasize that in the semiclassical limit, where we include sources with dimensions $h_H\propto c$ as $c\to\infty$, the correlators of ϕ will take the correct form. This follows automatically from the definition of the OPE block in equation (2.2.4) and the form of the vacuum metric in equation (2.2.3). We can compute correlators in a BTZ black hole background when we include a heavy operators $\mathcal{O}_H(\infty)\mathcal{O}_H(0)$, which lead to $\frac{1}{c}\langle T(z)\rangle=\frac{h_H}{c}\frac{1}{z^2}$ in the semiclassical limit. We hope to study these correlators at a non-perturbative level in the future.

2.3 An Exact Algebraic Definition for the Proto-Field $\phi(X)$

Our regulated bulk-boundary OPE block computes vacuum sector correlators exactly, and this suggests that we can obtain an exact definition for the proto-field ϕ built from the Virasoro primary $\mathcal{O}$. Now we provide this definition in a simple algebraic form, which originates from symmetry considerations. Our $\phi(y,0,0)$ will satisfy

$$L_m\phi(y,0,0)|0\rangle=0,\quad \bar{L}_m\phi(y,0,0)|0\rangle=0,\qquad m\geq 2. \tag{2.3.1}$$

This follows from the fact that ϕ is a scalar and the bulk points $(y,0,0)$ are invariant under bulk Virasoro transformations generated by L_m with $m\geq 2$. We explain this in detail in section 2.3.1 and appendix 2.7.

In the following discussion, we will write $\phi\left(y,0,0\right)$ as an expansion in small y or the

boundary OPE expansion (BOE)[9]

$$\phi\left(y,0,0\right)|0\rangle=\sum_{N=0}^{\infty}y^{2h+2N}\left|\phi\right\rangle_{N} \tag{2.3.2}$$

where $|\phi\rangle_N$ is a level N Virasoro descendant of $\mathcal{O}$ in both holomorphic and anti-holomorphic sectors, since we are defining the proto-field ϕ to be made of $\mathcal{O}$ and its descendants.[10] Then the conditions (2.3.1) for $\phi\left(y,0,0\right)$ will be equivalent to saying that $|\phi\rangle_N$ satisfies the following 'bulk primary' conditions:

$$L_{m}\left|\phi\right\rangle_{N}=0,\quad\overline{L}_{m}\left|\phi\right\rangle_{N}=0,\qquad\text{for }m\geq2. \tag{2.3.3}$$

That is, $\phi\left(y,0,0\right)$ will be a sum over these operators ϕ_N of different levels. The $|\phi\rangle_N$ is, in a sense, as close as possible to being a primary itself while still living in the bulk (ie it is a primary that is not quasi-primary). It is an eigenstate of L_0 and is annihilated by all higher generators except L_1. We will say more about the non-trivial action of L_1 in appendix 2.7.

In particular, the conditions (2.3.3) imply that at each level, $|\phi\rangle_N$ factorizes, and can be written in the following form

$$\left|\phi\right\rangle_{N}=\lambda_{N}\mathcal{L}_{-N}\overline{\mathcal{L}}_{-N}|\mathcal{O}\rangle,\qquad\lambda_{N}=\frac{\left(-1\right)^{N}}{N!\left(2h\right)_{N}}. \tag{2.3.4}$$

where $\mathcal{L}_{-N}$ (and $\overline{\mathcal{L}}_{-N}$) are linear combinations of products of holomorphic (and anti-holmorphic) Virasoro generators at level N. Note that, the holomorphic and anti-holomorphic conditions above are independent, which means that $\overline{\mathcal{L}}_{-N}$ will just be $\mathcal{L}_{-N}$ with L replaced by $\overline{L}$.

The conditions (2.3.3) will uniquely determine $|\phi\rangle_N$ (or $\mathcal{L}_{-\mathcal{N}}$) up to an overall normalization (will be explained below). The overall normalization of $|\phi\rangle_N$ is fixed by

[9] In the conventional BCFT case, the bulk theory is a CFT (see [41] for a nice discussion). An identical expansion also applies when studying non-gravitational QFTs in AdS [35], because boundary dilatations correspond to a bulk isometry. When the bulk theory is gravitational, one cannot use pure symmetry or OPE type arguments to prove that this expansion converges, but our results suggest that it can be determined exactly to all orders in y after bulk gauge fixing. It seems reasonable to expect that the small y expansion of ϕ would have a finite radius of convergence, since no terms like $\sim e^{-1/y}$ are allowed by scaling symmetry. We also explain in appendix 2.5.3 that symmetry arguments dictate this global conformal BOE result [35, 10]

[10] More generally, a full bulk field would have terms like $y^{h'+\bar{h}'}|\mathcal{O}_{h',\bar{h}'}\rangle$, where $\mathcal{O}_{h',\bar{h}'}$ is not a descendant of $\mathcal{O}$.

$$L_1^N \overline{L}_1^N \left|\phi\right\rangle_N = (-1)^N N! \left(2h\right)_N \left|\mathcal{O}\right\rangle . \tag{2.3.5}$$

This normalization condition is based on the requirement that we correctly reproduce the vacuum correlator $\langle\phi\mathcal{O}\rangle$,that is, $\langle\phi(y,0,0)\mathcal{O}(z,\bar{z})\rangle = \langle\phi^{\text{global}}\mathcal{O}\rangle = \left(\frac{y}{y^2+z\bar{z}}\right)^{2h}$. ϕ^{global} here is the global bulk field in the HKLL reconstruction [8], which we explain in 2.5.3 is equivalent to

$$\phi^{\text{global}}\left(y,0,0\right)\left|0\right\rangle = \sum_{N=0}^{\infty} y^{2h+2N} \lambda_N L_{-1}^N \overline{L}_{-1}^N \left|\mathcal{O}\right\rangle . \tag{2.3.6}$$

So the requirement that $\langle\phi\mathcal{O}\rangle = \langle\phi^{\text{global}}\mathcal{O}\rangle$ implies that

$$\mathcal{L}_{-N}|\mathcal{O}\rangle = L_{-1}^N|\mathcal{O}\rangle + (\text{other quasi-primaries and their descendants}) \tag{2.3.7}$$

where the terms in the parenthesis are all orthogonal to $\mathcal{O}$ and its global descendants, and will not contribute when computing $\langle\phi\mathcal{O}\rangle$. They are then fixed by solving (2.3.3). When acting on $|\phi\rangle_N$ with $L_1^N \bar{L}_1^N$, the terms in the parenthesis will be killed, that's why we have the normalization condition (2.3.5).[11] It's also true that in the large c limit, our ϕ will reduce to ϕ^{global}, as will be shown in 2.3.2.2 that the terms in the parenthesis are suppressed at large c.

Now let us explain why the conditions (2.3.3) uniquely determine $\mathcal{L}_{-N}$. It is easy to see that they are equivalent to the equations

$$L_{m_1}\cdots L_{m_i}\left|\phi\right\rangle_N = 0, \qquad \sum_i m_i = N \tag{2.3.8}$$

(and similarly for the anti-holomorphic part) where $L_{m_1}\cdots L_{m_i}$ represents the set of all level N products of Virasoro generators with at least one L_{m_i} with $m_i \geq 2$. That is, $L_{m_1}\cdots L_{m_i}$ does not include L_1^N . These conditions say that when $L_{m_1}\cdots L_{m_i}$ decreases the level of $\left|\phi\right\rangle_N$ back to level zero, the result vanishes. There are $p\left(N\right)-1$ independent ways (because we exclude L_1^N) to lower $\left|\phi\right\rangle_N$ to level zero, and thus $\left|\phi\right\rangle_N$ must satisfy $p\left(N\right)-1$ constraint equations. Since all the level N descendants of $\left|\mathcal{O}\right\rangle$ form a $p\left(N\right)$ dimensional space, the above condition will fix the bulk field up to an overall constant.

[11] Specifically, $L_1^N \bar{L}_1^N|\phi\rangle_N = L_1^N \bar{L}_1^N|\phi^{\text{global}}\rangle = \lambda_N L_1^N \bar{L}_1^N L_{-1}^N \bar{L}_{-1}^N|\mathcal{O}\rangle = (-1)^N N!(2h)_N|\mathcal{O}\rangle$.

So $\phi(y,0,0)$ will be uniquely fixed[12] by the constraints (2.3.3) and the normalization condition (2.3.5).

In section 2.3.1 we motivate the definition of ϕ using Virasoro symmetry and the fact that ϕ is a bulk scalar field. We then solve these conditions in various cases in section 2.3.2. In section 2.3.3, we show that our definition of $\phi(y,0,0)$ leads to a powerful recursive algorithm to compute correlators of the form of equation (2.1.2), extending standard recursion relations for correlators of stress tensors with local CFT_2 primary operators. The results exactly agree with those obtained from the bulk-boundary OPE block in section 2.2.

2.3.1 Virasoro Transformations of $\phi(X)$

In this section we will derive (2.3.1) using the fact that ϕ must transform as a bulk scalar. This means that under a coordinate transformation, $\phi(z,\bar{z},y) \to \phi(z',\bar{z}',y')$.

We would like to understand the transformation of ϕ under the action of Virasoro, which is defined on the boundary by $(z,\bar{z}) \to (g(z),\bar{g}(\bar{z}))$. We will constructively demonstrate that there is a unique extension of an infinitesimal boundary Virasoro transformation preserving the Fefferman-Graham gauge. Infinitesimally, we have

$$\epsilon L_m(y,z,\bar{z},S,\bar{S}) \equiv \epsilon(\delta_m y, \delta_m z, \delta_m \bar{z}, \delta_m S, \delta_m \bar{S}). \tag{2.3.9}$$

where $S,\bar{S}$ parameterizes the metric and are defined in (2.2.10). Then the transformation of ϕ under an infinitesimal Virasoro generator L_m is determined by its scalar property:

$$L_m\phi(z,\bar{z},y) = (\delta_m y\partial_y + \delta_m z\partial + \delta_m\bar{z}\bar{\partial})\phi(z,\bar{z},y) \tag{2.3.10}$$

This transformation rule is expected to hold within correlation functions.

[12] This means that ϕ has been fixed exactly (ie non-perturbatively in c, and not just to all orders in a $1/c$ expansion) to all-orders in powers of y. It's less clear if we have determined ϕ exactly in *both* c and y simultaneously, though it would appear that we have for cases where ϕ is inserted into a correlator where the sum over y^{2N} powers has a finite radius of convergence.

We work out the gauge preserving extension of L_m in Appendix 2.7, with the result

$$\delta_m y = \frac{1}{2}(m+1)yz^m \tag{2.3.11}$$

$$\delta_m z = \frac{z^{m-1}\left(\left(m^2+m+z^2S(z)\right)\bar{S}\left(\bar{z}\right)y^4-4z^2\right)}{y^4S(z)\bar{S}\left(\bar{z}\right)-4} \tag{2.3.12}$$

$$\delta_m \bar{z} = \frac{2m(m+1)y^2z^{m-1}}{y^4S(z)\bar{S}\left(\bar{z}\right)-4} \tag{2.3.13}$$

We have verified that these results agree with the action of L_m computed using contour integrals [22] of the stress tensor correlators from section 2.2.3. These results have several notable features. First, they reduce to the expected form of a Virasoro transformation on the boundary:

$$\lim_{y\to 0}(\delta_m y, \delta_m z, \delta_m \bar{z}) = (0, z^{m+1}, 0). \tag{2.3.14}$$

Secondly, the transformation on the coordinates depends on the starting metric through $(S, \bar{S})$. This fact is easy to understand because if no such dependency existed, then we would not be able preserve the Fefferman-Graham form of the metric in general.

The central feature of these transformations is that for $m \geq 2$, points on the line $(y, 0, 0)$ are left invariant:

$$\delta_m(y,0,0) = 0 \quad \text{for } m \geq 2. \tag{2.3.15}$$

Using the scalar property (2.3.10), we find that

$$L_m\phi(y,0,0)|0\rangle = 0, \quad \text{for } m \geq 2. \tag{2.3.16}$$

Including the constraints from $\bar{L}_{\bar{m}}$, we arrive at conditions (2.3.1) satisfied by $\phi(y,0,0)$.

One can also motivate the conditions (2.3.1) satisfied by $\phi(y,0,0)$ by consideration of causality [19, 20, 21, 29]. Correlators of $\phi(y,0,0)$ with boundary stress tensors $T(z)$ necessarily have singularities of the form $\frac{1}{z^2}$, as the stress tensor must be sensitive to the energy-momentum 'charge' of the bulk field, as well as $\frac{1}{z^3}$ singularities, since special conformal transformations move ϕ around in the bulk.[13] However, one may wish to

[13] These singularities could move to a different location in a different gauge, but they cannot be eliminated entirely [20].

forbid branch cuts and higher order singularities such as $\frac{1}{z^n}$ with $n \geq 4$. Our $\phi(y,0,0)$ is constructed to satisfy these requirements. The conditions on ϕ are equivalent to stipulating that the singular terms in the OPE of the stress energy tensor $T(z)$ with $\phi(y,0,0)$ are

$$T(z)\,\phi(y,0,0) \sim \frac{L_{-1}\phi(y,0,0)}{z} + \frac{L_0\phi(y,0,0)}{z^2} + \frac{L_1\phi(y,0,0)}{z^3}. \tag{2.3.17}$$

So there will be no higher order singularities in correlators of ϕ with any number of T. This property also holds for the individual components ϕ_N. One can also see this explicitly in the correlators $\langle\phi\mathcal{O}T\rangle$, $\langle\phi\mathcal{O}TT\rangle$, and $\langle\phi\mathcal{O}T\bar{T}\rangle$ that we computed using bulk-boundary OPE blocks in section 2.2.3, where there are no singularities beyond $\frac{1}{z^3}$, including in the expansions of these expressions in y.

2.3.2 Solving for $\phi(X)$ Explicitly

In this section, we will solve the conditions (2.3.3) and the normalization condition (2.3.5) for $\phi(y,0,0)$ explicitly. We will focus on the holomorphic part of $|\phi\rangle_N = \lambda_N \mathcal{L}_{-N}\bar{\mathcal{L}}_{-N}|\mathcal{O}\rangle$ and solve for $\mathcal{L}_{-N}$, since $\bar{\mathcal{L}}_{-N}$ is just the anti-holomorphic conjugate. In terms of $\mathcal{L}_{-N}$, the conditions are

$$\begin{aligned} &L_m\mathcal{L}_{-N}|\mathcal{O}\rangle = 0, \qquad \text{for } 2 \leq m \leq N \\ &L_1^N\mathcal{L}_{-N}|\mathcal{O}\rangle = N!(2h)_N|\mathcal{O}\rangle \end{aligned} \tag{2.3.18}$$

We first provide an example at low orders in section 2.3.2.1 , and then we obtain an exact, all orders solution in terms of orthogonal quasi-primaries in 2.3.2.2. We also solve these conditions in the large c limit up to order $\mathcal{O}(c^{-2})$ in appendix 2.7.5.3.

2.3.2.1 Explicit Solutions at Low Orders

It is obvious that $|\phi\rangle_0 = |\mathcal{O}\rangle$ and $|\phi\rangle_1 = -\frac{1}{2h}L_{-1}\bar{L}_{-1}|\mathcal{O}\rangle$, and so the first non-trivial case arises at the next level. At level 2, an arbitrary $\mathcal{L}_{-2}$ is given by $\mathcal{L}_{-2} = b_1L_{-1}^2 + b_2L_{-2}$ and the conditions are

$$L_2\left(b_1L_{-1}^2 + b_2L_{-2}\right)|\mathcal{O}\rangle = 0, \tag{2.3.19}$$

$$L_1^2\left(b_1L_{-1}^2 + b_2L_{-2}\right)|\mathcal{O}\rangle = 2!(2h)_2|\mathcal{O}\rangle. \tag{2.3.20}$$

Solving these two equations for b_1 and b_2, we find

$$\mathcal{L}_{-2} = \frac{(2h+1)(c+8h)}{(2h+1)\,c+2h(8h-5)}\left(L_{-1}^2 - \frac{12h}{c+8h}L_{-2}\right) \tag{2.3.21}$$

and $|\phi\rangle_2$ is given by $|\phi\rangle_2 = \lambda_2\mathcal{L}_{-2}\bar{\mathcal{L}}_{-2}|\mathcal{O}\rangle$. One can continue this process at higher orders (we also computed $|\phi\rangle_3$ and $|\phi\rangle_4$ in Appendix 2.7.5.1.), although the explicit expressions become rather complicated. Instead we will see how to solve these equations in general in terms of quasi-primaries.

2.3.2.2 Solution in Terms of Quasi-Primaries

We know that $|\phi\rangle_N$ can be written as the sum of the level N descendants of $\mathcal{O}$. These descendants can be decomposed into quasi-primaries (global primaries) and their global conformal descendants. In this subsection, we will show that the coefficients in this decomposition are determined by the norms of the quasi-primaries. We already saw an obvious example in the global case, as the global descendant $L_{-1}^N\bar{L}_{-1}^N|\mathcal{O}\rangle$ appears as

$$|\phi\rangle_N \supset (-1)^N\frac{1}{N!\,(2h)_N}L_{-1}^N\bar{L}_{-1}^N|\mathcal{O}\rangle = (-1)^N\frac{L_{-1}^N\bar{L}_{-1}^N|\mathcal{O}\rangle}{\left|L_{-1}^N\mathcal{O}\right|^2} \tag{2.3.22}$$

where $\left|L_{-1}^N\mathcal{O}\right|^2 \equiv \langle\mathcal{O}|L_1^NL_{-1}^N|\mathcal{O}\rangle = N!(2h)_N$. We will show that phenomenon is a general feature of the quasi-primary decomposition.

Suppose $\mathcal{L}_{-N}^{\text{quasi}}$ is a linear combination of Virasoro generators that acts on $|\mathcal{O}\rangle$ to create a quasi-primary at level N, with the coefficient of L_{-1}^N in $\mathcal{L}_{-N}^{\text{quasi}}$ normalized to 1. For example, at level two there is a unique $\mathcal{L}_{-2}^{\text{quasi}} = L_{-1}^2 - \frac{2(2h+1)}{3}L_{-2}$. Since there are many quasi-primaries[14] at level N, we will take the quasi-primary created by our chosen generator $\mathcal{L}_{-N}^{\text{quasi}}$ to be orthogonal to all of the other level N quasi-primaries, and normalized to contain exactly L_{-1}^N.

In what follows we will treat the holomorphic and anti-holomorphic descendants of $\mathcal{O}$ separately, since at each level ϕ_N factorizes. Then we will combine the holomorphic and anti-holomorphic pieces and correctly normalize them. Let us define the coefficient

[14] The number of quasi-primaries at level N is $p\,(N)-p\,(N-1)$, where $p\,(N)$ is the number of partitions of N.

of $\mathcal{L}_{-N}^{\text{quasi}}|\mathcal{O}\rangle$ in $|\phi\rangle_N = \lambda_N \mathcal{L}_{-N}|\mathcal{O}\rangle$[15] to be b_N, that is

$$|\phi\rangle_N \supset b_N \mathcal{L}_{-N}^{\text{quasi}}|\mathcal{O}\rangle \tag{2.3.23}$$

When we take the inner product of $|\phi\rangle_N$ with $\mathcal{L}_{-N}^{\text{quasi}}|\mathcal{O}\rangle$, we obtain

$$\langle\mathcal{O}|\left(\mathcal{L}_{-N}^{\text{quasi}}\right)^\dagger|\phi\rangle_N \quad = b_N \left\langle \mathcal{O}\left|\left(\mathcal{L}_{-N}^{\text{quasi}}\right)^\dagger \mathcal{L}_{-N}^{\text{quasi}}\right|\mathcal{O}\right\rangle \equiv b_N \left|\mathcal{L}_{-N}^{\text{quasi}}\mathcal{O}\right|^2, \tag{2.3.24}$$

because $\mathcal{L}_{-N}^{\text{quasi}}|\mathcal{O}\rangle$ is orthogonal to all other states in $|\phi\rangle_N$.

Now, using the conditions defining ϕ_N, we have

$$\langle\mathcal{O}|\left(\left(\mathcal{L}_{-N}^{\text{quasi}}\right)^\dagger - L_1^N\right)|\phi\rangle_N = 0 \tag{2.3.25}$$

because all of the terms in $\left(\mathcal{L}_{-N}^{\text{quasi}}\right)^\dagger - L_1^N$ will include at least one L_m, with $m \geq 2$, and according to the conditions (2.3.8), these terms will all annihilate $|\phi\rangle_N$. Using the normalization condition

$$L_1^N|\phi\rangle_N = \frac{(-1)^N}{N!\,(2h)_N} L_1^N L_{-1}^N|\mathcal{O}\rangle = (-1)^N|\mathcal{O}\rangle, \tag{2.3.26}$$

equation (2.3.25) leads to

$$b_N = \frac{(-1)^N}{\left|\mathcal{L}_{-N}^{\text{quasi}}\mathcal{O}\right|^2}. \tag{2.3.27}$$

So we have shown that the coefficient of the level N quasi-primary $\mathcal{L}_{-N}^{\text{quasi}}$ will be given by the inverse of its norm. Actually, one can show that this is also true even for the global descendants of the quasi-primaries. The holomorphic part of $|\phi\rangle_N$ will be given in the following form:[16]

$$|\phi\rangle_N \propto (-1)^N \left(\frac{L_{-1}^N}{\left|L_{-1}^N\mathcal{O}\right|^2} + \frac{\mathcal{L}_{-N}^{\text{quasi}}}{\left|\mathcal{L}_{-N}^{\text{quasi}}\mathcal{O}\right|^2} + \frac{L_{-1}\mathcal{L}_{-(N-1)}^{\text{quasi}}}{\left|L_{-1}\mathcal{L}_{-(N-1)}^{\text{quasi}}\mathcal{O}\right|^2} + \cdots + \frac{L_{-1}^m\mathcal{L}_{-(N-m)}^{\text{quasi}}}{\left|L_{-1}^m\mathcal{L}_{-(N-m)}^{\text{quasi}}\mathcal{O}\right|^2} + \cdots\right)|\mathcal{O}\rangle.$$

Including the anti-holomorphic part and accounting for the overall coefficient (ie re-

[15] Via an abuse of notation, here $|\phi\rangle_N = \lambda_N\mathcal{L}_{-N}|\mathcal{O}\rangle$, but it should be clear from the context whether $\bar{\mathcal{L}}_{-N}$ is included in the definition of $|\phi\rangle_N$ or not.

[16] It is easy to see $\left|L_{-1}^m\mathcal{L}_{-(N-m)}^{\text{quasi}}\mathcal{O}\right|^2 = m!(2(h+N-m))_m\left|\mathcal{L}_{-(N-m)}^{\text{quasi}}\mathcal{O}\right|^2$.

quiring the coefficient of $L_{-1}^N \bar{L}_{-1}^N$ to be $\lambda_N = \frac{(-1)^N}{\left|L_{-1}^N \mathcal{O}\right|^2}$), we find

$$|\phi\rangle_N = (-1)^N \left|L_{-1}^N \mathcal{O}\right|^2 \left(\frac{L_{-1}^N}{\left|L_{-1}^N \mathcal{O}\right|^2} + \frac{\mathcal{L}_{-N}^{\text{quasi}}}{\left|\mathcal{L}_{-N}^{\text{quasi}} \mathcal{O}\right|^2} + \frac{L_{-1}\mathcal{L}_{-(N-1)}^{\text{quasi}}}{\left|L_{-1}\mathcal{L}_{-(N-1)}^{\text{quasi}} \mathcal{O}\right|^2} + \cdots \right)$$
$$\times \left(\frac{\bar{L}_{-1}^N}{\left|\bar{L}_{-1}^N \mathcal{O}\right|^2} + \frac{\bar{\mathcal{L}}_{-N}^{\text{quasi}}}{\left|\bar{\mathcal{L}}_{-N}^{\text{quasi}} \mathcal{O}\right|^2} + \frac{\bar{L}_{-1}\bar{\mathcal{L}}_{-(N-1)}^{\text{quasi}}}{\left|\bar{L}_{-1}\bar{\mathcal{L}}_{-(N-1)}^{\text{quasi}} \mathcal{O}\right|^2} + \cdots \right) |\mathcal{O}\rangle$$

as the exact solution for $|\phi\rangle_N$ in terms of orthogonal quasi-primaries with our chosen normalization. Note that in a large c expansion, the norms of the non-trivial quasi-primaries (and their descendants) will be proportional to positive powers of c, so that their contributions will be suppressed. But at finite c, or for $h \gtrsim c$, their contributions will be on equal footing with the global conformal descendants ϕ.

As an illustration of the above result, $\lambda_2 \mathcal{L}_{-2}$ in $|\phi\rangle_2$ derived in equation (2.3.21) of last section can be written in the following form:

$$\lambda_2 \mathcal{L}_{-2} = \frac{L_{-1}^2}{2!\,(2h)_2} + \frac{L_{-1}^2 - \frac{2(2h+1)}{3} L_{-2}}{\frac{2}{9}(2h+1)\left(c\,(2h+1) + 2h(8h-5)\right)} = \frac{L_{-1}^2}{\left|L_{-1}^2 \mathcal{O}\right|^2} + \frac{\mathcal{L}_{-2}^{\text{quasi}}}{\left|\mathcal{L}_{-2}^{\text{quasi}}\right|^2} \tag{2.3.28}$$

with $|\mathcal{L}_{-2}^{\text{quasi}} \mathcal{O}|^2 = \frac{2}{9}(2h+1)\left((2h+1)c + 2h(8h-5)\right)$. We also explicitly compute $|\phi\rangle_3$ and $|\phi\rangle_4$ in Appendix 2.7.5.1.

2.3.3 Recursion Relation for Stress-Tensor Correlators

In section (2.2.3) we computed correlators of the form $\langle \phi \mathcal{O} T \cdots \overline{T} \cdots \rangle$ using the bulk-boundary OPE block. In this section, we will derive a recursion relation that can be used to calculate these correlators. Specifically, we will express correlators with $n+1$ stress tensors in terms of a differential operator acting on correlators with fewer stress tensors. This relation generalizes the well-known case of $\langle \mathcal{O}\mathcal{O} T \cdots \overline{T} \cdots \rangle$ correlators [42], which can be derived recursively from the two point function $\langle \mathcal{O}\mathcal{O} \rangle$ using the Virasoro Ward identity.

Suppose we know the correlator with n insertions of T and m insertions of $\overline{T}$,

$$G_{n,m} \equiv \left\langle T(z_1) \cdots T(z_n)\, \overline{T}(\overline{w}_1) \cdots \overline{T}(\overline{w}_m)\, \mathcal{O}(z,\overline{z})\, \phi(y,0,0) \right\rangle, \tag{2.3.29}$$

and now we consider the case of one more T insertion,

$$G_{n+1,m} \equiv \left\langle T(z_1)\cdots T(z_n)\, T(z_{n+1})\, \overline{T}(\overline{w}_1)\cdots \overline{T}(\overline{w}_m)\, \mathcal{O}(z,\overline{z})\, \phi(y,0,0)\right\rangle . \quad (2.3.30)$$

A key feature of stress tensor correlators such as $G_{n+1,m}$ is that as $z_{n+1}\to\infty$, the correlator vanishes. This means that $G_{n+1,m}$ is completely determined by its poles in the z_{n+1} variable. Thus $G_{n+1,m}$ can be computed by taking the OPE of $T(z_{n+1})$ with all the other operators in $G_{n+1,m}$ and only keeping the singular terms. We know the singular terms in the OPE of $T(z_{n+1})$ with $\mathcal{O}(z,\overline{z})$ and $T(z_i)$, which are

$$\begin{aligned} T(z_{n+1})\,\mathcal{O}(z,\overline{z}) &\sim \frac{h\mathcal{O}(z,\overline{z})}{(z_{n+1}-z)^2}+\frac{\partial_z\mathcal{O}(z,\overline{z})}{z_{n+1}-z},\\ T(z_{n+1})\,T(z_i) &\sim \frac{c}{2(z_{n+1}-z_i)^4}+\frac{2T(z_i)}{(z_{n+1}-z_i)^2}+\frac{\partial T(z_i)}{z_{n+1}-z_i}. \end{aligned} \quad (2.3.31)$$

The conditions of equation (2.3.3) tell us that the singular terms in the OPE of $T(z_{n+1})$ with $\phi(y,0,0)$ are given by

$$T(z_{n+1})\,\phi(y,0,0) \sim \frac{L_1\phi(y,0,0)}{z_{n+1}^3}+\frac{L_0\phi(y,0,0)}{z_{n+1}^2}+\frac{L_{-1}\phi(y,0,0)}{z_{n+1}}. \quad (2.3.32)$$

Writing $|\phi\rangle$ as a sum over $|\phi\rangle_N$, that is $|\phi\rangle = \sum_{N=0}^{\infty} y^{2h+2N}|\phi\rangle_N$, we know that the effect of L_0 on $|\phi\rangle$ is to pull down a factor of $h+N$ for each $|\phi\rangle_N$. This is equivalent to taking the derivative with respect to y, so we have

$$L_0\phi(y,0,0) = \frac{1}{2}y\partial_y\phi(y,0,0). \quad (2.3.33)$$

And it's easy to see that

$$L_{-1}\phi(y,0,0) = \partial_x\phi(y,x,\overline{x})\,|_{x,\overline{x}=0}. \quad (2.3.34)$$

Because of translation invariance, the action of L_{-1} on $\phi(y,0,0)$ is equal to a holomorphic partial derivative of all of the other operators, namely $\mathcal{O}(z,\overline{z})$ and other Ts in the correlator $G_{n,m}$.

The term $L_1\phi(y,0,0)$ is more subtle. In general, at finite c we cannot write it as a simple differential operator acting on $\phi(y,0,0)$ itself (see appendix 2.7 for more details).

But since L_{-1} annihilates the vacuum, ie $\langle 0| L_1 = (L_{-1}|0\rangle)^\dagger = 0$, we can commute L_1 with all the other operators on the left. Since we know the action of L_1 on $\mathcal{O}$ and the stress tensor,[17] we can evaluate its action on ϕ within the vacuum sector correlator $G_{n,m}$.

Combining all the above facts, we obtain a recursion relation for computing $G_{n+1,m}$ from $G_{n,m}$ and $G_{n-1,m}$:

$$\begin{aligned} G_{n+1,m} = &\left(-\frac{\partial_z + \sum_{i=1}^n \partial_{z_i}}{z_{n+1}} + \frac{\frac{y}{2}\partial_y}{z_{n+1}^2} - \frac{z\left(2h + z\partial_z\right)}{z_{n+1}^3} + \sum_{i=1}^n \frac{-z_i\left(4 + z_i\partial_{z_i}\right)}{z_{n+1}^3}\right) G_{n,m} \\ &+ \left(\frac{h}{\left(z_{n+1} - z\right)^2} + \frac{\partial_z}{\left(z_{n+1} - z\right)} + \sum_{i=1}^n \left(\frac{2}{\left(z_{n+1} - z_i\right)^2} + \frac{\partial_{z_i}}{z_{n+1} - z_i}\right)\right) G_{n,m} \\ &+ \sum_{i=1}^n \frac{\left\langle T\left(z_1\right) T\left(z_2\right) \cdots T\left(z_{i-1}\right) T\left(z_{i+1}\right) \cdots T\left(z_n\right) \overline{T}\left(\overline{w}_1\right) \cdots \overline{T}\left(\overline{w}_m\right) \mathcal{O}\left(z, \overline{z}\right) \phi\left(y, 0, 0\right)\right\rangle}{2\left(z_{n+1} - z_i\right)^4} \end{aligned}$$

We display the origin of all of these terms in appendix 2.7.6. In appendix 2.7.6, we also use this recursion relation to easily reproduce the correlators $\langle \phi\mathcal{O}T\rangle$, $\langle \phi\mathcal{O}TT\rangle$ and $\langle \phi\mathcal{O}T\bar{T}\rangle$ computed in section 2.2.3 using the bulk-boundary OPE block.

One can derive an identical recursion relation with $T \leftrightarrow \bar{T}$ for adding insertions of the anti-holomorphic stress tensor. Together, these relations precisely determine all vacuum sector correlators of $\phi\mathcal{O}$. In other words, one can view these recursion relations as an alternative definition for the proto-field ϕ, which is entirely equivalent to the definition (3.7.5) and the bulk-boundary OPE block prescription and accompanying regulator from section 2.2.

2.4 Discussion

It is natural to conjecture [19] that complete, interacting scalar fields $\Phi(X)$ in AdS_3 should be written as

$$\Phi(X) = \sum_{\mathcal{O}} \lambda_{\mathcal{O}} \phi_{\mathcal{O}}(X) \tag{2.4.1}$$

where the sum runs over all scalar CFT_2 primaries, and the coefficients $\lambda_{\mathcal{O}}$ are constrained by consistency and causality [19, 20, 21, 29]. Our work does not shed much

[17] The commutators of L_1 with $\mathcal{O}$ and T are simply

$$\begin{aligned} \left[L_1, \mathcal{O}\left(z, \overline{z}\right)\right] &= z\left(2h + z\partial_z\right) \mathcal{O}\left(z, \overline{z}\right), \\ \left[L_1, T\left(z_i\right)\right] &= z_i\left(4 + z_i\partial_{z_i}\right) T\left(z_i\right). \end{aligned} \tag{2.3.35}$$

light on the questions of existence, (non-)uniqueness, and efficient determination of the $\lambda_{\mathcal{O}}$.

However, we have proposed a formula for the local AdS_3 proto-field operator $\phi_{\mathcal{O}}$ built from a specific CFT_2 primary $\mathcal{O}$ and its Virasoro descendants.[18] We argued that our choice of $\phi_{\mathcal{O}}$ has a number of desirable properties, including healthy vacuum-sector correlators that match bulk Witten diagrams, a natural interpretation in any semiclassical vacuum geometry, and Virasoro symmetry transformations implemented as bulk diffeomorphisms. But perhaps the most surprising and intriguing aspect of our analysis is that we have determined $\phi_{\mathcal{O}}$ exactly, based on the extremely simple condition of equation (2.3.1).

Profound lore based on diffeomorphism gauge redundancy and black hole physics suggests that local observables in gravitational theories may be ambiguous[19] or ill-defined. Hopefully our formalism will provide a context where these ideas can be made more precise. It may be that AdS_3 differs significantly from the case of higher dimensions (or $AdS_3 \times X$ spacetimes), where most aspects of bulk gravitational physics cannot be fixed by symmetry, and the gravitational dynamics can depend on many parameters. In $CFT_{\geq 3}$ this difference arises because the OPE of the stress tensor is largely unconstrained, in marked contrast with the CFT_2 case.

How Non-Local is ϕ?

Our construction of ϕ was based on a series expansion in the radial coordinate y, which may be viewed as a gravitational version of the boundary operator expansion of boundary CFT. The non-locality of ϕ (as a CFT operator) arises from the fact that it has been expressed as an infinite sum of local operators. In the global conformal case, one can precisely relate the standard HKLL smearing function to the boundary operator expansion (see appendix 2.5.3), making the non-locality of ϕ manifest. The extent of the non-locality displayed by the exact Virasoro ϕ remains less clear. It should be possible to evaluate this region by computing correlators of ϕ with local CFT operators and investigating the convergence properties of the infinite sum.[20] There may be a more

[18] This may be enough to reconstruct the (toy?) case of a CFT with a low-energy spectrum that is dual to AdS_3 gravity coupled to a free bulk scalar field.

[19] For an example of an interesting recent discussion see [43].

[20] This suggests an amusing exercise – one might Borel resum the boundary operator expansion for ϕ. It seems plausible that the summation defining the Borel series (operator) would appear local, in the

direct method involving a non-perturbative generalization of the smearing procedure.

These questions will be of particular interest when we move from Euclidean to Lorentzian signature. Lorentzian CFT correlators can be obtained from their Euclidean counterparts by analytic continuation, but we do not know to what extent this holds for bulk dynamics. At the very least we will need to have a better understanding of bulk diffeomorphisms, including large transformations to new gauges. From the bulk or Wheeler-DeWitt perspective, the formation and evaporation of a black hole can be pure gauge!

Many recent works have focused on the relationship between bulk and boundary domains of dependence [44, 45, 46, 47, 31] in Lorentzian signature. Some of this work [48] was motivated by putative ambiguities in bulk reconstruction associated with the fact that a bulk operator $\phi(X)$ can be expressed using smearing functions supported on different boundary domains [8]. These ambiguities do not exist for non-gravitational AdS field theory and its non-local boundary dual, as in this case $\phi(X)$ is precisely well-defined. Thus it appears that these ambiguities can only arise from non-perturbative gravitational effects. It would be interesting to exhibit such effects explicitly and to characterize their physical significance in the bulk; perhaps this is possible in AdS_3/CFT_2.

Bulk Locality and Horizons

The primary motivation for studying ϕ is to investigate bulk locality and physics near and beyond black hole horizons [49, 50, 51, 52].

The breakdown of bulk locality can be analyzed using scattering in AdS/CFT [53, 54]. However, one can attack the problem much more directly by studying the operator product $\phi(X)\phi(Y)$ and its expectation value. The correlator $\langle\phi(X)\phi(Y)\rangle$ can differ greatly from that of a free bulk scalar field because it includes the exchange of arbitrary Virasoro descendants of $\mathcal{O}$, or in the language of multi-trace operators, states such as '$[T\partial^2 T\bar{T}\bar{\partial}^4\mathcal{O}]$' built from the OPE of $\mathcal{O}$ with any number of stress tensors. Since the contribution of these states has been fixed exactly, one can compute $\langle\phi(X)\phi(Y)\rangle$ at finite operator dimension h and central charge c and as a function of the geodesic separation between the bulk operators. When $h \ll c$ one might hope to see the breakdown of bulk locality at the Planck scale, and for heavy operators with $h \gg c$ one might see

sense that its series expansion would converge in correlators with all other local operators.

indications of the horizon radius (or some other pathology associated with bulk fields dual to very heavy CFT states). More generally, we would expect that the bulk OPE expansion of $\phi(X)\phi(Y)$ does not exist.

We can also use correlators like $\langle\phi\mathcal{O}_H\mathcal{O}_H\rangle$ and $\langle\phi\phi\mathcal{O}_H\mathcal{O}_H\rangle$ to probe the vicinity of black hole horizons. In these and other high-energy states, we may find that ϕ breaks down deep[21] in the bulk, and it will be interesting to understand when and how. Previously it was unclear how to study such observables in a non-trivial way, since it seemed that one would need to rely on bulk perturbation theory to define them. It appears that our construction surmounts this particular obstacle.

Many aspects of black hole thermodynamics are encoded in the Virasoro algebra at large central charge [55, 56, 57, 58, 59], including various non-perturbative effects that resolve or ameliorate information loss problems [60, 61, 62]. This means that it should be possible to learn about bulk physics in the presence of black holes using Virasoro technology.

Furthermore, general considerations [63] borne out by non-perturbative investigations of Virasoro blocks [62] show that in Euclidean space, pure high-energy quantum states look very different from the BTZ black hole solution in the vicinity of the horizon. This follows from the fact that thermal and BTZ correlators are periodic in Euclidean time, while pure state correlators display completely unsuppressed violations of this periodicity [62]. Thus we have reason to believe that correlators like $\langle\phi\phi\mathcal{O}_H\mathcal{O}_H\rangle$ will tell us about interesting structures near the Euclidean horizon. By decomposing correlators into Virasoro blocks, we can learn which of these effects are universal, and which depend on the details of the CFT data.

Of course the real question is whether black hole horizons appear innocuous to infalling *Lorentzian* observers. We hope to address some of these questions soon.

[21] Due to quantum gravitational effects, or from a failure of our Fefferman-Graham gauge choice.

Appendix: Additional Technical Details and Results

2.5 Background and Review

Here we collect fairly elementary results that may be of interest to some readers, and that provides some useful background material for the main body of the paper.

2.5.1 Klein-Gordon Equation from the Worldline Path Integral

Here we review that first-quantized particles have propagators that satisfy the Klein-Gordon equation. This follows implicitly from the equivalence between the two-point correlator of a free quantum field and the first-quantized propagator. But we can also understand it more directly.

The first quantized propagator is

$$K(x_f, x_i) = \int_{x_i}^{x_f} \mathcal{D}x(t) e^{-m\int_i^f \sqrt{g_{\mu\nu}\dot{x}^\mu \dot{x}^\nu}} \tag{2.5.1}$$

Since K propagates wavefunctions in time, it satisfies the Schrodinger equation, and the idea is that this equation is equivalent to the Klein-Gordon equation. For this purpose we need to define a temporal direction for quantization, though we will find that this choice is irrelevant as the Klein-Gordon equation is covariant. It's convenient to choose $t = \log y$ in our AdS case, so that we have a Lagrangian proportional to $\sqrt{g_{\mu\nu}\dot{x}^\mu \dot{x}^\nu} = \sqrt{1 + \dot{x}^i \dot{x}_i}$. Then the canonical momenta are

$$p^i = -\frac{m\dot{x}^i}{\sqrt{1 + \dot{x}^i \dot{x}_i}} \tag{2.5.2}$$

and we find that the Hamiltonian is $H = \sqrt{m^2 - p^i p^j g_{ij}}$. Interpreting the canonical momenta as covariant derivatives $p_i = \nabla_i$, the square of the Schrodinger equation $\partial_t^2 K = (\nabla_i \nabla^i + m^2)K$ is the Klein-Gordon equation in our chosen coordinate system. Note that one might try to identify $p_i = -i\partial_i$ as ordinary derivatives, but this leads to operator ordering ambiguities after quantization since g_{ij} depends on x^i. The choice $p_i = -i\nabla_i$ resolves these issues; equivalently, there is a particular choice of ordering of factors of g_{ij} and $p_i \to -i\partial_i$ in the Hamiltonian that is equivalent to just setting $p_i = -i\nabla_i$. Presumably, this choice should be correctly determined by a proper treatment of the path integral.

2.5.2 Geodesics in Euclidean AdS$_3$

We would like to identify the geodesics in pure Euclidean AdS$_3$. The analysis is most elegant using the embedding space coordinates

$$\begin{aligned} X_0 &= R\frac{\cosh\tau}{\cos\rho} = \frac{1}{2}\left(\frac{y^2 + z\bar{z} + R^2}{y}\right) \\ X_3 &= R\frac{\sinh\tau}{\cos\rho} = \frac{1}{2}\left(\frac{y^2 + z\bar{z} - R^2}{y}\right) \\ X_z &= R\tan\rho e^{i\theta} = \frac{R}{y}z \\ X_{\bar{z}} &= R\tan\rho e^{-i\theta} = \frac{R}{y}\bar{z} \end{aligned} \tag{2.5.3}$$

where we will set the AdS scale $R = 1$. Then the geodesics satisfy $\ddot{X}_A = X_A$(this equation of motion arises from the action for a point particle in embedding space subject to the constraint $X_A X^A = 1$) which means that

$$X_A(s) = v_A \cosh(s) + u_A \sinh(s) \tag{2.5.4}$$

for vectors v_A and v_A with $v_A u^A = 0$ and $v_A v^A - u_A u^A = 1$. Note that

$$\begin{aligned} y &= \frac{1}{X_0 - X_3} \\ z &= \frac{X_z}{X_0 - X_3} \\ \bar{z} &= \frac{X_{\bar{z}}}{X_0 - X_3} \end{aligned} \tag{2.5.5}$$

so we end up with a simple formula for these coordinates on any geodesic. Note that we have translation symmetry in $z, \bar{z}$ so we may as well set these to zero at a convenient point. One choice is $z = \bar{z} = 0$ at $s = 0$. This means that v_A will have vanishing $z, \bar{z}$ components. A convenient Euclidean parameterization is

$$\begin{aligned} X_0 &= A_0 \cosh(s) + B_0 \sinh(s) \\ X_3 &= A_3 \sinh(s) + B_3 \sinh(s) \\ X_z &= A_z \sinh(s) \\ X_{\bar{z}} &= A_{\bar{z}} \sinh(s) \end{aligned} \tag{2.5.6}$$

We must have $B_3 = \frac{A_0 B_0}{A_3}$ and several other conditions for B_0 and A_3. Then if we set $A_0 = \frac{y_0}{2} + \frac{1}{2y_0}$ then the point $s = z = \bar{z} = 0$ occurs at y_0. Thus we find

$$\begin{aligned} y(s) &= y_0 \frac{e^s \left(y_0^2 + z_0 \bar{z}_0\right)}{e^{2s} z_0 \bar{z}_0 + y_0^2} \\ z(s) &= z_0 \frac{\left(1 - e^{2s}\right) y_0^2}{y_0^2 + e^{2s} z_0 \bar{z}_0} \\ \bar{z}(s) &= \bar{z}_0 \frac{\left(1 - e^{2s}\right) y_0^2}{y_0^2 + e^{2s} z_0 \bar{z}_0} \end{aligned} \tag{2.5.7}$$

Note that at $s = 0$ we have $(y_0, 0, 0)$ while for $s = -\infty$ we have $(0, z_0, \bar{z}_0)$. We can also solve for s in terms of y or z, and then re-parameterize. It's simplest to solve for $s(z)$, which leads to

$$\begin{aligned} y(z) &= \sqrt{1 - \frac{z}{z_0}} \sqrt{y_0^2 + z \bar{z}_0} \\ \bar{z}(z) &= \frac{\bar{z}_0}{z_0} z \end{aligned} \tag{2.5.8}$$

for geodesics beginning on the boundary at z_0 and ending in the bulk at y_0 and $z, \bar{z} = 0$.

2.5.3 Global Reconstruction as a Boundary Operator Expansion

The ideas reviewed in this appendix were briefly explained in [35]. As far as we are aware, the explicit equations in this section were either first obtained by Miguel Paulos, or were derived by us via discussion and collaboration with him. Thus these results should largely be credited to Paulos and the other authors of [35]. A somewhat similar

approach was taken in [10]. Ultimately, the point is that the global conformal generators must act on ϕ as AdS isometries, and this idea dates back to the beginning of AdS/CFT. Throughout this appendix we will always be discussing the global ϕ, which we will usually denote as ϕ^g.

2.5.3.1 Global BOE from HKLL Smearing

Here we will show how to recover the global boundary operator expansion (BOE) for a scalar operator [64]

$$\phi^{\rm g}(y,z,\bar{z}) = y^{2h}\sum_{n=0}^{\infty}\frac{(-1)^n y^{2n}}{n!(2h)_n}\left(L_{-1}\bar{L}_{-1}\right)^n\mathcal{O}(z,\bar{z}) \tag{2.5.9}$$

from the well-known HKLL [24] smearing procedure.

To obtain a free bulk scalar field from a boundary primary, we 'smear' the boundary operator via

$$\phi^{\rm g}(y,0,0) = \frac{2h-1}{\pi}\int dzd\bar{z}\left(\frac{y^2-z\bar{z}}{y}\right)^{2h-2}\mathcal{O}(iz,i\bar{z}) \tag{2.5.10}$$

over the Euclidean region $\bar{z}=z^*$ with $|z|<y$. We can formally re-write this as

$$\phi^{\rm g}(y,0,0) = \frac{2h-1}{\pi}\int_{z\bar{z}<y^2} dzd\bar{z}\left(\frac{y^2-z\bar{z}}{y}\right)^{2h-2}e^{iz\partial+i\bar{z}\bar{\partial}}\mathcal{O}(0) \tag{2.5.11}$$

As the smearing function depends only on $z\bar{z}$, and terms with unequal powers of z and $\bar{z}$ vanish after angular integration, we can change variables to

$$\phi^{\rm g}(y,0,0) = (2h-1)\int_0^{y^2} dx\left(\frac{y^2-x}{y}\right)^{2h-2}P\left(-x\partial\bar{\partial}\right)\mathcal{O}(0) \tag{2.5.12}$$

where $P(a)=\sum_{n=0}^{\infty}\frac{1}{(n!)^2}a^n$. One can do this integral explicitly and find a result with the desired series expansion in $y^2\partial\bar{\partial}$. One way to see this directly is to perform a rescaling $x\to xy^2$ so that

$$\begin{aligned}\phi^{\rm g}(y,0,0) &= (2h-1)y^{2h}\int_0^1 dx\,(1-x)^{2h-2}\,P\left(-x\left(y^2\partial\bar{\partial}\right)\right)\mathcal{O}(0)\\ &= y^{2h}\sum_{n=0}^{\infty}\frac{(-1)^n}{(2h)_n n!}\left(y^2\partial\bar{\partial}\right)^n\mathcal{O}(0)\end{aligned} \tag{2.5.13}$$

which is the desired boundary operator expansion in powers of y.

2.5.3.2 Bulk-Boundary Correlator from BOE

Now we can verify explicitly that we obtain the correct $\langle\phi\mathcal{O}\rangle$ correlator from the boundary operator expansion for ϕ. In fact we will demonstrate a more general result, which makes it possible to compute $\langle\phi^{\mathrm{g}}\mathcal{O}T(z_1)\cdots T(z_n)\rangle$:

$$\begin{aligned}\langle\phi^{\mathrm{g}}(y,0,0)\mathcal{O}(z,\bar{z})T(z_1)\cdots T(z_n)\rangle &= y^{2h}\sum_{n=0}^{\infty}\frac{(-1)^n(y^2\partial_x\partial_{\bar{x}})^n}{n!(2h)_n}\frac{f(z_i,x,z)}{(\bar{z}-\bar{x})^{2h}}\\ &= \frac{y^{2h}}{\bar{z}^{2h}}\sum_{n=0}^{\infty}\frac{1}{n!}\left(-\frac{y^2}{\bar{z}}\partial_x\right)^n f(z_i,x,z)\\ &= \frac{y^{2h}}{\bar{z}^{2h}}f\left(z_i,-\frac{y^2}{\bar{z}},z\right)\end{aligned} \tag{2.5.14}$$

where we define f via $\langle\mathcal{O}(x)\mathcal{O}(z)T(z_1)\cdots T(z_n)\rangle = f(z_i,x,z)(\bar{z}-\bar{x})^{-2h}$, so we have

$$\langle\phi^{\mathrm{g}}(y)\mathcal{O}(z)T(z_1)\cdots T(z_n)\rangle = y^{2h}\left\langle\mathcal{O}\left(-\frac{y^2}{\bar{z}}\right)\mathcal{O}(z)T(z_1)\cdots T(z_n)\right\rangle \tag{2.5.15}$$

The simple special case of interest to us is

$$\langle\phi^{\mathrm{g}}(y,0,0)\mathcal{O}(z,\bar{z})\rangle = \left(\frac{y}{y^2+z\bar{z}}\right)^{2h} \tag{2.5.16}$$

as expected.

2.5.3.3 Symmetries of the Global Boundary Operator Expansion

In this section we will show that global conformal symmetry transformations L_{-1}, L_0, L_1 act as expected on the global conformally reconstructed ϕ.

When we regard ϕ as a bulk field, the global conformal generators should act on it as the differential operators

$$\begin{aligned}L_{-1} &= \partial_z\\ L_0 &= z\partial_z + \frac{1}{2}y\partial_y\\ L_1 &= z^2\partial_z + zy\partial_y - y^2\partial_{\bar{z}}\end{aligned}$$

So the goal is to show that when the quantum operators L_n act on equation (2.5.9) in

accord with this expectation. In what follows, we will show that an L_n transformation applied to $\mathcal{O}$ results in the appropriate differential operator acting on ϕ.

The fact that the translation generators act correctly follows easily because ∂_z commutes with $(y^2\partial\bar{\partial})^n$. For the dilatation L_0 note that

$$\begin{aligned}\delta\phi^{\mathrm{g}} &= y^{2h}\sum_{n=0}^{\infty}\lambda_n y^{2n}(\partial\bar{\partial})^n\,(z\partial+h)\,\mathcal{O}(z,\bar{z})\\ &= (z\partial+h)\,\phi^{\mathrm{g}}+y^{2h}\sum_{n=0}^{\infty}n\,\lambda_n y^{2n}(\partial\bar{\partial})^n\mathcal{O}(z,\bar{z})\\ &= \left(z\partial+\frac{1}{2}y\partial_y\right)\phi^{\mathrm{g}}\end{aligned} \tag{2.5.17}$$

as desired. Note that this is automatic given the structure of expansion, and it does not depend on the form $\lambda_n=\frac{(-1)^n}{n!(2h)_n}$.

Finally, let us check the special conformal transformation L_1; we will see that it can only act appropriately if λ_n take the expected form. We need to compute

$$\begin{aligned}\delta\phi^{\mathrm{g}} =& y^{2h}\sum_{n=0}^{\infty}\lambda_n y^{2n}(\partial\bar{\partial})^n\left(z^2\partial+2hz\right)\mathcal{O}(z,\bar{z})\\ =&\left(z^2\partial+2hz\right)\phi^{\mathrm{g}}+y^{2h}\sum_{n=0}^{\infty}\lambda_n y^{2n}\left[(\partial\bar{\partial})^n,z^2\partial+2hz\right]\mathcal{O}(z,\bar{z})\\ =&z^2\partial\phi^{\mathrm{g}}+zy\partial_y\phi^{\mathrm{g}}+y^{2h}y^2\sum_{n=1}^{\infty}\lambda_n y^{2(n-1)}n\,(2h+n-1)\,\bar{\partial}^n\partial^{n-1}\mathcal{O}\,(z,\bar{z})\\ =&z^2\partial\phi^{\mathrm{g}}+zy\partial_y\phi^{\mathrm{g}}+y^2\bar{\partial}y^{2h}\sum_{n=0}^{\infty}\lambda_{n+1}\,(n+1)\,(2h+n)\,y^{2n}\bar{\partial}^n\partial^n\mathcal{O}\,(z,\bar{z})\\ =&\left(z^2\partial+zy\partial_y-y^2\bar{\partial}\right)\phi^{\mathrm{g}}\end{aligned}$$

where in the last line, we used

$$\lambda_n=-\lambda_{n+1}(n+1)(2h+n). \tag{2.5.18}$$

The same result could also be obtained by demanding that the conformal Casimir acts appropriately on ϕ^{g}, as shown by M. Paulos.

2.6 Regulation: from Classical Backgrounds to Correlators

In section 2.2, we developed an algorithm to compute the correlators $\langle T\dots T\bar{T}\dots\bar{T}\phi\mathcal{O}\rangle$ from the simpler correlator $\langle\phi\mathcal{O}\rangle_{\mu,\bar{\mu}}$ evaluated in states with non-trivial stress tensor vevs:

$$\langle T(z)\rangle_{\mu,\bar{\mu}} = T_{cl}\left(\bar{z}\right), \quad \langle\bar{T}(z)\rangle_{\mu,\bar{\mu}} = \bar{T}_{cl}\left(\bar{z}\right) \tag{2.6.1}$$

The algorithm was to first view $\langle\phi\mathcal{O}\rangle_{\mu,\bar{\mu}}$ as a functional on the vevs $T_{cl}(z)$ and $\bar{T}_{cl}(\bar{z})$. In a series expansion, this functional takes the general form:

$$\begin{aligned}\langle\phi\mathcal{O}\rangle_{\mu,\bar{\mu}} =& \langle\phi\mathcal{O}\rangle_0\left(1+\int dx\tilde{K}_{10}(x)T_{cl}(x)+\int d\bar{x}\tilde{K}_{01}(\bar{x})\bar{T}_{cl}(\bar{x})+\int dx\tilde{K}_{11}(x,\bar{x})T_{cl}(x)\bar{T}_{cl}(\bar{x})+\dots\right)\\ =& \langle\phi\mathcal{O}\rangle_0\left(\sum_{n,\bar{n}=0}^{\infty}\int\prod_{i=1}^{n}dx_i\prod_{\bar{i}=1}^{\bar{n}}d\bar{x}_{\bar{i}}\tilde{K}_{i,\bar{i}}(x_1,\dots x_n,\bar{x}_1,\dots,\bar{x}_{\bar{n}})T_{cl}(x_1)\dots T_{cl}(x_n)\bar{T}_{cl}(\bar{x}_1)\dots\bar{T}_{cl}(\bar{x}_{\bar{n}})\right)\end{aligned}$$

Then we compute the vacuum sector of the operator product $\phi\mathcal{O}$ that includes all contributions from Virasoro descendants of the vacuum[22], which is done by replacing T_{cl} and $\bar{T}_{cl}$ in $\langle O\phi\rangle_{\mu,\bar{\mu}}$ by quantum operators T and $\bar{T}$.

However, generically operators products of T have short distance singularities when two T's approach each other, which will occur due to the integration over positions in (2.6.2). In [16] we empirically discovered a simple regulator (equation C.10 there) that, when applied to the "quantum" version of (2.6.2), produces the correct OPE block. The correlator between the regulated product of T's, denoted as $[T(x_1)\dots T(x_n)]$, and external, unregulated $T(z_i)$s were found to be:

$$\langle T(z_1)\dots T(z_k)[T(x_1)\dots T(x_n)]\rangle = 0, \quad n>k \tag{2.6.2}$$

$$\langle T(z_1)\dots T(z_k)[T(x_1)\dots T(x_n)]\rangle \equiv \sum_{groupings}\prod_{i=1}^{n}\langle T(z_1)\dots T(z_k)T(x_i)\rangle, \quad n\leq k \tag{2.6.3}$$

The sum is over different groupings of $T(z_i)$'s. Note that since in each correlator there is only one $T(x_i)$, the results never diverge as $x_i\to x_j$. Thus the regulator fully specifies correlators of the OPE block with stress tensors.

[22] All other contributions to ϕO involve quantum operators that are not descendants of the vacuum. Thus they do not contribute to the multi-T correlators that we are computing in this appendix.

To summarize, we proposed that the vacuum sector of the $\phi\mathcal{O}$ operator product is:

$$\phi\mathcal{O} = \left[\langle\phi\mathcal{O}\rangle_B|_{T_{cl}\to T,\bar{T}_{cl}\to\bar{T}}\right] + \dots \tag{2.6.4}$$

where the square bracket represents the regularization applied to all products of T and $\bar{T}$'s. In the current context this regulator is defined by (2.6.2-2.6.3). In [16] and this paper, this proposal survived extensive and non-trivial checks by direct computation.

In this appendix, we would like to provide a general argument for this proposal. In particular, we would like to show that, under fairly general assumptions, it correctly extracts multi-T vacuum correlators such as $\langle T(z_1)\dots T(z_n)\bar{T}(\bar{z}_1)\dots\bar{T}(\bar{z}_{\bar{n}})\phi\mathcal{O}\rangle_0$ from simpler core correlators such as $\langle\phi O\rangle_{\mu,\bar{\mu}}$ on a background with non-trivial source. We also show that this algorithm does not seem to rely on conformal symmetry and may work in a wider range of settings.

Suppose we have a generic field theory containing a bosonic quantum operator T. It is possible to construct a classical source for it, such that T has a classical vev:

$$\langle T(x)\rangle_\mu = T_{cl}(x). \tag{2.6.5}$$

We view this equation as a mapping between functions $\mu \leftrightarrow T_{cl}$. We will make the assumption this mapping is one-to-one, and $\mu = 0$ maps to $T_{cl} = 0$. In particular, this assumes that given any $T_{cl}(x)$, there must exist a unique source configuration $\mu(x)$ that sets up this vev. Thus we can write the functional $\mu[T_{cl}]$ as the solution of (2.6.5). Note that the source is defined in the usual way by shifting the action in the Euclidean path integral:

$$S \to S + \int dz\mu(z)T(z) \tag{2.6.6}$$

The input of our algorithm is $\langle X\rangle_{\mu[T_{cl}]}$ as a functional on T_{cl}.

$$\langle X\rangle_{\mu[T_{cl}]} = \langle X e^{\int dz\mu[T_{cl}](z)T(z)}\rangle_0 \tag{2.6.7}$$

Once this is known, we should have enough information to determine vacuum multi-T

correlators $\langle XT(z_1)\dots T(z_n)\rangle_0$. We first compute the simplest of this family:

$$\begin{aligned}\langle XT(z_1)\rangle_{c,0} &= \frac{\delta}{\mu(z_1)}\langle X\rangle_\mu\Big|_{\mu\to 0}\\ &= \int dx_1\,\frac{\delta T_{cl}(x_1)}{\mu(z_1)}\frac{\delta}{\delta T_{cl}(x_1)}\langle X\rangle_{\mu[T_{cl}]}\Big|_{\mu\to 0}\\ &= \langle X\rangle_0\int dx_1\langle T(z_1)T(x_1)\rangle_0\tilde{K}^X_{10}(x_1)\\ &= \langle T(z_1)\left[\langle X\rangle_{\mu[T]}\right]\rangle_0 \end{aligned}\tag{2.6.8}$$

In the second step, we used:

$$\frac{\delta T_{cl}(x_1)}{\mu(z_1)}\Big|_{\mu\to 0} = \frac{\delta}{\mu(z_1)}\langle T(x_1)\rangle_\mu\Big|_{\mu\to 0} = \langle T(z_1)T(x_1)\rangle_0 \tag{2.6.9}$$

$$\frac{\delta\langle X\rangle_{\mu_{[T_{cl}]}}}{\delta T_{cl}(x_1)}\Big|_{\mu\to 0} = \frac{\delta}{\delta T_{cl}(x_1)}\langle X\rangle_0\int dx\tilde{K}^X_1(x)T_{cl}(x)\Big|_{\mu\to 0} = \langle X\rangle_0\tilde{K}^X_1(x_1) \tag{2.6.10}$$

where we have inserted a series expansion of $\langle X\rangle_{\mu_{[T_{cl}]}}$ in the style of (2.6.2), which should exist given the non-singular limit $\langle X\rangle_{\mu[T_{cl}\to 0]} = \langle X\rangle_0$. When we replace $X\to\phi O$, (2.6.8) is precisely the result predicted by inserting (2.6.4) into $\langle T(z_1)\phi\mathcal{O}\rangle$ and evaluate using (2.6.2-2.6.3). We made this clear in the last step.

A slightly more non-trivial example is $\langle XTT\rangle$:

$$\begin{aligned}\langle XT(z_1)T(z_2)\rangle_{c,0} &= \frac{\delta}{\delta\mu(z_1)}\frac{\delta}{\delta\mu(z_2)}\langle X\rangle_\mu\Big|_{\mu\to 0}\\ &= \int dx_2\,\frac{\delta}{\delta\mu(z_1)}\left(\frac{\delta T_{cl}(x_2)}{\delta\mu(z_2)}\frac{\delta}{\delta T_{cl}(x_2)}\langle X\rangle_{\mu[T_{cl}]}\right)\Big|_{T_{cl}\to 0}\\ &= \int dx_2\frac{\delta^2 T_{cl}(x_2)}{\delta\mu(z_1)\delta\mu(z_2)}\frac{\delta}{\delta T_{cl}(x_2)}\langle X\rangle_{\mu[T_{cl}]}\Big|_{T_{cl}\to 0}\\ &\quad+\int dx_1dx_2\frac{\delta T_{cl}(x_2)}{\delta\mu(z_2)}\frac{\delta T_{cl}(x_1)}{\delta\mu(z_1)}\frac{\delta}{\delta T_{cl}(x_1)}\frac{\delta}{\delta T_{cl}(x_2)}\langle X\rangle_{T_{cl}}\Big|_{T_{cl}\to 0}\\ &= \langle X\rangle_0\int dx_1\langle T(z_1)T(z_2)T(x_1)\rangle\tilde{K}^X_1(x_1)\\ &\quad+\langle X\rangle_0\int dx_1dx_2\langle T(z_1)T(x_1)\rangle_0\langle T(z_2)T(x_2)\rangle_0\tilde{K}^X_2(x_1,x_2)\\ &= \langle T(z_1)T(z_2)\left[\langle X\rangle_{\mu[T]}\right]\rangle_0 \end{aligned}\tag{2.6.11}$$

Again this exactly agrees with the result of our OPE block defined with regulator (2.6.3).

It is easy to see why this works to level n, $\langle XT(z_1)\dots T_n(z_n)\rangle$:

$$\langle XT(z_1)\dots T(z_n)\rangle_0 = \frac{\delta}{\mu(z_1)}\dots\frac{\delta}{\mu(z_n)}\langle X\rangle_\mu\Big|_{\mu\to 0} \tag{2.6.12}$$

Each time we add a $T(z_{n+1})$, the corresponding $\frac{\delta}{\delta\mu(z_{n+1})}$ either act on $\langle\mathcal{O}\mathcal{O}\rangle_{T_{cl}}$ as $\int dx_{n+1}\frac{\delta T(x_{n+1})}{\delta\mu(z_{n+1})}\frac{\delta}{\delta T(x_{n+1})}$, where it picks up a single T from the OPE block of $\mathcal{O}\mathcal{O}$, or acts on an existing derivative $\frac{\delta^k T_{cl}(x_{i_k})}{\delta\mu(z_{i_1})\dots\delta\mu(z_{i_k})}\frac{\delta}{\delta T_{cl}(x_{i_k})}$, where it adds a point to a existing multi-T correlator. By construction, there are never two T's from the X OPE block appearing in the same vev. Thus, there are no UV divergences. The result is our OPE block defined with regulator (2.6.3).

To summarize, given the correlator of operator product X on non-trivial backgrounds, $\langle X\rangle_{\mu[T_{cl}]}$, we can extract the vacuum correlator between X and any number of T insertions using:

$$\begin{aligned}\langle T(z_1)\dots T(z_n)X\rangle_0 &= \sum_{groupings}\prod_{i<n}\int dx_n\langle T(z_{i_1})\dots T(z_{i_{k_n}})T(x_i)\rangle\frac{\delta}{\delta T_{cl}(x_i)}\langle X\rangle_{\mu[T_{cl}]}\Big|_{T_{cl}\to 0}\\ &= \langle T(z_1)\dots T(z_n)\left[\langle X\rangle_{\mu[T]}\right]\rangle_0\end{aligned}$$

where in the second line we interpreted the result as computing the correlator between $T(z_1)\dots T(z_n)$ and the OPE block of the operator product X, which is constructed and regulated as given in the first line. This algorithm should work in any field theory as long as the mapping $\langle T\rangle_\mu = T_{cl}$ is one-to-one between μ and T_{cl}.

2.7 Bulk Virasoro Transformations

We would like to find an extension of a boundary Virasoro transformation into the bulk, such that this bulk transformation will preserve the Fefferman-Graham form of the metric. To achieve this, this bulk Virasoro transformation must depend on the initial bulk metric. In other words, the Virasoro transformations acts in the following way:

$$\left(z,\bar{z},y,f,\bar{f}\right)\to\left(\tilde{z},\tilde{\bar{z}},\tilde{y},\tilde{f},\tilde{\bar{f}}\right) \tag{2.7.1}$$

The bulk metric is specified by $\left(f\left(z\right),\bar{f}\left(\bar{z}\right)\right)$, which determines the vev of stress tensors and the boundary Virasoro transformations back to the uniformizing coordinate (2.2.8),

reproduced here:

$$z_u = f(z) - \frac{2y^2 f'^2 \bar{f}''}{4f'\bar{f}' + y^2 f''\bar{f}''}, \quad \bar{z}_u = \bar{f}(\bar{z}) - \frac{2y^2 \bar{f}'^2 f''}{4f'\bar{f}' + y^2 f''\bar{f}''} \tag{2.7.2}$$

$$y_u = 4y \frac{\left(f'\bar{f}'\right)^{\frac{3}{2}}}{4f'\bar{f}' + y^2 f''\bar{f}''} \tag{2.7.3}$$

Collectively, we may denote $P = \left(z, \bar{z}, y, f, \bar{f}\right)$ and the above coordinate map to the uniformizing coordinate is denoted as $P_u(P)$. Given any Virasoro transformation $(g(z), \bar{g}(\bar{z}))$, the way we obtain its bulk completion on any background metric that preserves the Fefferman-Grahm gauge is to first map the original coordinate back to the uniformizing coordinate, and then transform from it to the new coordiante such that the composition is equivalent to $(g(z), \bar{g}(\bar{z}))$ on the boundary. In equations, this means the new point in the $\tilde{P}$ satisfies

$$P_u\left(\tilde{P}\right) = P_u(P) \tag{2.7.4}$$

$$\tilde{f}^{-1} \circ f(z) = g(z), \quad \tilde{\bar{f}}^{-1} \circ \bar{f}(\bar{z}) = \bar{g}(\bar{z}) \tag{2.7.5}$$

We consider a generic background that is specified by $\left(f(z), \bar{f}(\bar{z})\right)$. Then we do a small Virasoro transformation generated by L_m on this background. On the boundary, this transformation is defined as

$$(1 + \epsilon L_m) z = z + \epsilon z^{m+1} \tag{2.7.6}$$

This transformation takes

$$\left(f, \bar{f}\right) \to \left(\tilde{f}, \bar{f}\right) \tag{2.7.7}$$

$\tilde{f}$ is determined by:

$$f^{-1} \circ \tilde{f}(z) = z - \epsilon z^{m+1} \tag{2.7.8}$$

which means

$$\tilde{f} = f - \epsilon z^{m+1} f' \equiv f + \epsilon \delta_m f \tag{2.7.9}$$

We then solve

$$P_u\left(P+\epsilon\delta_m P\right)=P_u\left(P\right) \tag{2.7.10}$$

The solution is (2.3.13), reproduced here:

$$\begin{aligned}\delta_m z &= \frac{z^{m-1}\left(\left(m^2+m+z^2S(z)\right)\bar{S}\left(\bar{z}\right)y^4-4z^2\right)}{y^4S(z)\bar{S}\left(\bar{z}\right)-4} &(2.7.11)\\ \delta_m\bar{z} &= \frac{2m(m+1)y^2z^{m-1}}{y^4S(z)\bar{S}\left(\bar{z}\right)-4} &(2.7.12)\\ \delta_m y &= \frac{1}{2}(m+1)yz^m &(2.7.13)\end{aligned}$$

Note that the f and $\bar{f}$ organize themselves exactly to reproduce S and $\bar{S}$, where

$$\bar{S}=\frac{\bar{f}^{(3)}\bar{f}'-\frac{3}{2}\bar{f}''^2}{\bar{f}'^2}=\frac{12}{c}\bar{T} \tag{2.7.14}$$

Clearly, we see that L_m with $m\geq 2$ will leave points $(y,0,0)$ invariant.

For L_1 this is explicitly not the case. In fact, the action of L_1 is somewhat non-trivial. On a background with $L=0$ (correlators $\langle\phi\mathcal{O}\bar{T}\cdots\bar{T}\rangle$ without any T), we have:

$$L_1\phi\left(y,0,0\right)=\left(-y^2\bar{\partial}-\frac{6}{c}y^4\bar{T}\left(0\right)\partial\right)\phi\left(y,0,0\right). \tag{2.7.15}$$

One way to test whether this is correct is to compute

$$\langle\mathcal{O}(z,\bar{z})\bar{T}(\bar{z}_1)L_1\phi\left(y,0,0\right)\rangle\stackrel{?}{=}\langle\mathcal{O}(z,\bar{z})\bar{T}(\bar{z}_1)\left(-y^2\bar{\partial}-\frac{6}{c}y^4\bar{T}\left(0\right)\partial\right)\phi\left(y,0,0\right)\rangle \tag{2.7.16}$$

Note that the first term on the RHS, which is the naive transformation of ϕ (it's the transformation of ϕ^{global} under L_1), gives a wrong result:

$$\begin{aligned}&-y^2\langle\mathcal{O}(z,\bar{z})\bar{T}(\bar{z}_1)\bar{\partial}\phi\left(y,0,0\right)\rangle\\ =&\frac{2hy^2\bar{z}\left(y^2z\bar{z}\left(2(h-3)\bar{z}_1\bar{z}-3(h-1)\bar{z}_1^2+3\bar{z}^2\right)-z^2\bar{z}^2\bar{z}_1\left((h-1)\bar{z}_1+\bar{z}\right)+3y^4\left(\bar{z}-\bar{z}_1\right)^2\right)}{\left(\bar{z}-\bar{z}_1\right)^2\bar{z}_1^4\left(z\bar{z}+y^2\right)^2}\end{aligned}$$

This is wrong because it has a $\frac{1}{\bar{z}_1^4}$ pole, which is inconsistent with the condition of equation (2.3.3). But the second term

$$-\frac{6}{c}y^4\langle\mathcal{O}(z,\bar{z})[\bar{T}(\bar{z}_1)\bar{T}\left(0\right)]\partial\phi\left(y,0,0\right)\rangle=-3y^4\frac{1}{\bar{z}_1^4}\langle\mathcal{O}(z,\bar{z})\partial\phi\left(y,0,0\right)\rangle=-\frac{6hy^4\bar{z}}{\bar{z}_1^4\left(z\bar{z}+y^2\right)} \tag{2.7.17}$$

has precisely the right form to cancel this pole. Then combining these two terms, we have

$$\begin{aligned}
&\langle \mathcal{O}(z,\bar{z})\bar{T}(\bar{z}_1)\left(-\frac{6}{c}y^4\bar{T}(0)\,\partial - y^2\bar{\partial}\right)\phi(y,0,0)\rangle \\
=&\langle \mathcal{O}(z,\bar{z})\phi(y,0,0)\rangle \frac{2hy^2z\bar{z}^2\left(h\left(y^2\left(2\bar{z}-3\bar{z}_1\right)-z\bar{z}\bar{z}_1\right)+z\bar{z}\left(\bar{z}_1-\bar{z}\right)\right)}{\left(\bar{z}-\bar{z}_1\right)^2\bar{z}_1^3\left(z\bar{z}+y^2\right)^2} \\
=&-\left(2hz+z^2\partial_z\right)\langle O(z,\bar{z})\bar{T}(\bar{z}_1)\phi(y,0,0)\rangle \\
=&-\langle [L_1,\mathcal{O}(z,\bar{z})]\,\bar{T}(\bar{z}_1)\phi(y,0,0)\rangle \\
=&\langle \mathcal{O}(z,\bar{z})\bar{T}(\bar{z}_1)L_1\phi(y,0,0)\rangle
\end{aligned}$$

Similarly, we checked (2.7.15) also work in the case of $\langle \bar{T}\bar{T}\mathcal{O}L_1\phi\rangle$. In particular, we checked that

$$\begin{aligned}
&\langle \bar{T}(\bar{z}_1)\bar{T}(\bar{z}_2)\mathcal{O}(z,\bar{z})L_1\phi(y,0,0)\rangle \\
=&\langle \bar{T}(\bar{z}_1)\bar{T}(\bar{z}_2)\mathcal{O}(z,\bar{z})\left(-y^2\bar{\partial}-\frac{6}{c}\bar{T}(0)y^4\partial\right)\phi(y,0,0)\rangle \\
=&-y^2\langle \bar{T}(\bar{z}_1)\bar{T}(\bar{z}_2)\mathcal{O}(z,\bar{z})\bar{\partial}\phi(y,0,0)\rangle \\
&-\frac{6}{c}y^4\langle \bar{T}(\bar{z}_1)\bar{T}(\bar{z}_2)\bar{T}(0)\rangle\langle \mathcal{O}(z,\bar{z})\partial\phi(y,0,0)\rangle \\
&-\frac{6}{c}y^4\left(\langle \bar{T}(\bar{z}_1)\bar{T}(0)\rangle\langle \bar{T}(\bar{z}_2)\mathcal{O}(z,\bar{z})\partial\phi(y,0,0)\rangle+(z_1\leftrightarrow z_2)\right) \\
=&-\left(2hz+z^2\partial_z\right)\langle \bar{T}(\bar{z}_1)\bar{T}(\bar{z}_2)\mathcal{O}(z,\bar{z})\phi(y,0,0)\rangle \\
=&-\langle \bar{T}(\bar{z}_1)\bar{T}(\bar{z}_2)\,[L_1,\mathcal{O}(z,\bar{z})]\,\phi(y,0,0)\rangle.
\end{aligned} \tag{2.7.18}$$

The fact that these work nicely are non-trivial checks for our method.

2.7.1 Gravitational Wilson Line Computations at Higher Orders

In this section, we provide the details to derive the bulk-boundary OPE block kernels up to order $\frac{1}{c^2}$. First, we need to solve the following equation at large c

$$S(f,z)\equiv\frac{f'''(z)\,f'(z)-\frac{3}{2}\left(f''(z)\right)^2}{\left(f'(z)\right)^2}=\frac{12}{c}T(z) \tag{2.7.19}$$

and determine $f(z)$ and $\overline{f}(\overline{z})$ as functions of the stress tensor operators $T(z), \overline{T}(\overline{z})$. We'll do this by expanding $f(z)$ in terms of large c as follows

$$f(z) = f_0(z) + \sum_{n=1}^{\infty} \frac{f_n(z)}{c^n} \tag{2.7.20}$$

with $f_0(z) = z$ satisfies $S(f_0(z), z) = 0$ at leading order. At order $\frac{1}{c}$ and $\frac{1}{c^2}$, $f_1(z)$ and $f_2(z)$ are determined by the following differential equations

$$\begin{aligned} f_1^{(3)}(z) - 12T(z) &= 0, \\ 2f_1{}^{(3)}(z) f_1'(z) + 3f_1''(z)^2 - 2f_2{}^{(3)}(z) &= 0. \end{aligned}$$

The first equation is easy to solve and the solution with desired boundary condition is

$$f_1(z) = 6\int_0^z dz' (z - z')^2 T(z'). \tag{2.7.21}$$

Using this solution, the second equation in (2.7.21) becomes

$$\begin{aligned} f_2^{(3)} &= f_1^{(3)} f_1' + \frac{3}{2} f_1''^2 \\ &= 144T(z)\int_0^z dz' (z - z') T(z') + 432\int_0^z dz' \int_0^{z'} dz''' T(z') T(z'''). \end{aligned} \tag{2.7.22}$$

And the solution is

$$\begin{aligned} f_2(z) &= 36\int_0^z dz'' (z - z'')^2 \left[2T(z'')\int_0^{z''} dz' (z'' - z') T(z') + 6\int_0^{z''} dz' \int_0^{z'} dz''' T(z') T(z''')\right] \\ &= 72\int_0^z dz' \int_0^{z'} dz'' T(z') T(z'') (z - z')^2 (z - z''). \end{aligned} \tag{2.7.23}$$

Now we can turn to the derivation of the bulk-boundary OPE block kernels. Expanding the coordinates transformation (2.2.8) in terms of large c, i.e. using 2.7.20 with $f_0(z) = z$, we have

$$\begin{aligned} u &= y + \frac{y\left(\bar{f}_1'(\bar{z}) + f_1'(z)\right)}{2c} - \frac{y\left(2y^2 f_1''(z)\bar{f}_1''(\bar{z}) + \left(f_1'(z) - \bar{f}_1'(\bar{z})\right)^2 - 4\left(\bar{f}_2'(\bar{z}) + f_2'(z)\right)\right)}{8c^2} + \mathcal{O}\left(c^{-3}\right) \\ w &= z + \frac{f_1(z) - \frac{1}{2}y^2\bar{f}_1''(\bar{z})}{c} + \frac{2f_2(z) - y^2\left(\left(f_1'(z) - \bar{f}_1'(\bar{z})\right)\bar{f}_1''(\bar{z}) + \bar{f}_2''(\bar{z})\right)}{2c^2} + \mathcal{O}\left(c^{-3}\right) \end{aligned} \tag{2.7.24}$$

and similar expression for $\overline{w}$. Expanding the bulk-boundary two-point function and

using the above result, we find

$$\begin{aligned}
&\log\phi\left(y,z_f,z_f\right)\mathcal{O}\left(z_i,\overline{z}_i\right)\\
=&2h\log\left(\frac{u_f\sqrt{w'\left(z_i\right)\overline{w}'\left(\overline{z}_i\right)}}{u_f^2+\left(w_f-w_i\right)\left(\overline{w}_f-\overline{w}_i\right)}\right)\\
=&2h\log\left(\frac{y}{y^2+z\overline{z}}\right)+\underbrace{\frac{h}{c}\frac{\left(z\overline{z}+y^2\right)f_1'(z)-2\overline{z}f_1(z)}{\left(z\overline{z}+y^2\right)}}_{K_T}\underbrace{-\frac{2hy^2f_1(z)\bar{f}_1\left(\overline{z}\right)}{c^2\left(z\overline{z}+y^2\right)^2}}_{K_{T\overline{T}}}\\
&\underbrace{-\frac{h\left(\left(z\overline{z}+y^2\right)\left(\left(z\overline{z}+y^2\right)\left(f_1'(z)^2-2f_2'(z)\right)+4\overline{z}f_2(z)\right)-2\overline{z}^2f_1(z)^2\right)}{2c^2\left(z\overline{z}+y^2\right)^2}}_{K_{TT}}\\
&+K_{\overline{T}}+K_{\overline{TT}}+\mathcal{O}\left(c^{-3}\right)
\end{aligned}\tag{2.7.25}$$

with $K_{\overline{T}}$ and $K_{\overline{TT}}$ the complex conjugate of K_T and K_{TT} respectively. In the third line of the above equations, we've put the two operators at $\phi\left(y,0,0\right)$ and $\mathcal{O}\left(z,\overline{z}\right)$.

Plugging in the solutions for $f_n,\overline{f}_n$, we have

$$\begin{aligned}
K_T&=\frac{12h}{c}\int_0^z dz'\frac{\left(y^2+z'\overline{z}\right)\left(z-z'\right)}{z\overline{z}+y^2}T\left(z'\right)\\
K_{TT}&=\int_0^z dz'\int_0^{z'}dz''\frac{72h\left(z-z'\right)^2\left(y^2+\overline{z}z''\right)^2}{c^2\left(z\overline{z}+y^2\right)^2}T\left(z'\right)T\left(z''\right)\\
K_{T\overline{T}}&=-\frac{72hy^2}{c^2\left(z\overline{z}+y^2\right)^2}\int_0^z dz'\left(z-z'\right)^2\int_0^{\overline{z}}d\overline{z}'\left(\overline{z}-\overline{z}'\right)^2T\left(z'\right)\overline{T}\left(\overline{z}'\right)
\end{aligned}\tag{2.7.26}$$

Sending $y=0$, we find

$$\begin{aligned}
K_T&\overset{y=0}{\Longrightarrow}\frac{12h}{c}\int_0^z dz'\frac{z'\left(z-z'\right)}{z}T\left(z'\right)\\
K_{TT}&\overset{y=0}{\Longrightarrow}\int_0^z dz'\int_0^{z'}dz''\frac{72h\left(z-z'\right)^2z''^2}{c^2z^2}T\left(z'\right)T\left(z''\right)\\
K_{T\overline{T}}&\overset{y=0}{\Longrightarrow}0
\end{aligned}\tag{2.7.27}$$

which are exactly the boundary-boundary OPE kernels found in [16].

2.7.2 Computations Using the Bulk-Boundary OPE Block

In this section, we'll provide the details for computing $\langle\phi\mathcal{O}TT\rangle$ and $\langle\phi\mathcal{O}T\overline{T}\rangle$ using bulk-boundary OPE block with the regulator proposed in Appendix C.2 of [16] and discussed in details in appendix 2.6. The regulator (2.6.2-2.6.3) is basically saying that when computing $\langle\phi\mathcal{O}T_1\cdots T_n\bar{T}_1\cdots\bar{T}_m\rangle$, the kernels in the OPE block of $\phi\mathcal{O}$ that

will contribute are those whose numbers of T and $\bar{T}$ are equal or less than n and m respectively.

2.7.2.1 $\langle\phi\mathcal{O}T\overline{T}\rangle$

Using the regulator (2.6.2-2.6.3), the kernels in the bulk-boundary OPE of $\phi\mathcal{O}$ that contribute to $\langle\phi\mathcal{O}T\overline{T}\rangle$ are $K_T K_{\bar{T}}$ and $K_{T\bar{T}}$. So $\langle\phi\mathcal{O}T\overline{T}\rangle$ is given by

$$\begin{aligned}\frac{\langle\phi(y,0,0)\,\mathcal{O}(z,\bar{z})\,T(z_1)\,\overline{T}(\overline{w}_1)\rangle}{\langle\phi(y,0,0)\,\mathcal{O}(z,\bar{z})\rangle} &= \langle e^{K_T+K_{\overline{T}}+K_{T\overline{T}}+\cdots}T(z_1)\,\overline{T}(\overline{w}_1)\rangle \\ &= \langle\left(K_T K_{\overline{T}}+K_{T\overline{T}}\right)T(z_1)\,\overline{T}(\overline{w}_1)\rangle\end{aligned}$$

The first term is

$$\begin{aligned}&\langle K_T K_{\overline{T}} T(z_1)\,\overline{T}(\overline{w}_1)\rangle \\ =&\left(\frac{144h^2}{c^2}\int_0^z dz'\int_0^{\bar{z}} d\bar{z}'\frac{\left(y^2+z'\bar{z}\right)(z-z')}{z\bar{z}+y^2}\frac{\left(y^2+\bar{z}'z\right)(\bar{z}-\bar{z}')}{z\bar{z}+y^2}\right)\langle\left[T\left(z'\right)\overline{T}\left(\bar{z}'\right)\right]T(z_1)\,\overline{T}(\overline{w}_1)\rangle \\ =&\frac{h^2z^2\bar{z}^2\left(y^2(3\bar{w}_1-2\bar{z})+\bar{w}_1z\bar{z}\right)\left(y^2(3z_1-2z)+z_1z\bar{z}\right)}{z_1^3\overline{w}_1^3(z-z_1)^2(\bar{w}_1-\bar{z})^2(z\bar{z}+y^2)^2}\end{aligned} \tag{2.7.28}$$

where in the second line we use the regulated four-point function

$$\langle\left[T\left(z'\right)\overline{T}\left(\bar{z}'\right)\right]T(z_1)\,\overline{T}(\overline{w}_1)\rangle=\frac{c^2}{4}\frac{1}{(z'-z_1)^4(\bar{z}'-\overline{w}_1)^4}. \tag{2.7.29}$$

The above result is just the contribution from $\langle\phi\mathcal{O}T\rangle\langle\phi\mathcal{O}\overline{T}\rangle$.

The second term in equation (2.7.28) is

$$\begin{aligned}&\langle K_{T\overline{T}}T(z_1)\,\overline{T}(\overline{w}_1)\rangle \\ =&-\frac{72hy^2}{c^2(z\bar{z}+y^2)^2}\int_0^z dz'\int_0^{\bar{z}}d\bar{z}'\left(z-z'\right)^2\left(\bar{z}-\bar{z}'\right)^2\langle[T\left(z'\right)\overline{T}\left(\bar{z}'\right)]T(z_1)\,\overline{T}(\overline{w}_1)\rangle \\ =&\frac{2hy^2z^3\bar{z}^3}{z_1^3\bar{w}_1^3(z-z_1)(\bar{w}_1-\bar{z})(z\bar{z}+y^2)^2}\end{aligned}$$

So putting these two terms together, we get

$$\begin{aligned}&\frac{\langle\phi(y,0,0)\,\mathcal{O}(z,\bar{z})\,T(z_1)\,\overline{T}(\overline{w}_1)\rangle}{\langle\phi(y,0,0)\,\mathcal{O}(z,\bar{z})\rangle} \\ =&\frac{h^2z^2\bar{z}^2\left(y^2(3\bar{w}_1-2\bar{z})+\bar{w}_1z\bar{z}\right)\left(y^2(3z_1-2z)+z_1z\bar{z}\right)}{z_1^3\overline{w}_1^3(z_1-z)^2(\overline{w}_1-\bar{z})^2(z\bar{z}+y^2)^2}+\frac{2hy^2z^3\bar{z}^3}{z_1^3\bar{w}_1^3(z-z_1)(\bar{w}_1-\bar{z})(z\bar{z}+y^2)^2}\end{aligned}$$

Sending $y \to 0$, the second term vanishes, and the first term will reduce to the boundary four-point function $\left\langle \mathcal{O}(0,0)\,\mathcal{O}(z,\overline{z})\,T(z_1)\,\overline{T}(\overline{w}_1)\right\rangle = \langle \mathcal{O}\mathcal{O}T\rangle\left\langle \mathcal{O}\mathcal{O}\overline{T}\right\rangle = \frac{h^2 z^2 \overline{z}^2}{z^{2h}\overline{z}^{2h} z_1^2 \overline{w}_1^2 (z_1-z)^2 (\overline{w}_1-\overline{z})^2}$ as expected.

2.7.2.2 $\langle \phi \mathcal{O} T T\rangle$

Using the regulator (2.6.2-2.6.3), the kernels in the bulk-boundary OPE of $\phi\mathcal{O}$ that contribute to $\langle\phi\mathcal{O}TT\rangle$ are the identity, K_T, K_{TT} and $K_T K_T$. So $\langle\phi\mathcal{O}TT\rangle$ is given by

$$\begin{aligned}\frac{\langle\phi(y,0,0)\,\mathcal{O}(z,\overline{z})\,T(z_1)\,T(z_2)\rangle}{\langle\phi(y,0,0)\,\mathcal{O}(z,\overline{z})\rangle} &= \left\langle e^{K_T+K_{TT}+\cdots} T(z_1)\,T(z_2)\right\rangle \\ &= \langle T(z_1)\,T(z_2)\rangle + \left\langle \left(K_T + K_{TT} + \frac{K_T K_T}{2}\right) T(z_1)\,T(z_2)\right\rangle .\end{aligned}$$

The first term is trivial and it's just $\langle T(z_1)\,T(z_2)\rangle = \frac{c}{2(z_1-z_2)^4}$.

The first two terms in the second braket give the following contribution

$$\begin{aligned}&\langle K_T T(z_1)\,T(z_2)\rangle + \langle K_{TT} T(z_1)\,T(z_2)\rangle \\ &= \frac{12h}{c}\int_0^z dz' \frac{\left(y^2+z'\overline{z}\right)(z-z')}{z\overline{z}+y^2}\left\langle T(z')\,T(z_1)\,T(z_2)\right\rangle \\ &\quad + \int_0^z dz' \int_0^{z'} dz'' \frac{72h\,(z-z')^2\left(y^2+\overline{z}z''\right)^2}{c^2\left(z\overline{z}+y^2\right)^2}\left\langle\left[T(z')\,T(z'')\right]T(z_1)\,T(z_2)\right\rangle \\ &= \frac{2hz^2\left(y^2 z\overline{z} z_1 z_2\left(z(z_1+z_2)-4z_1z_2\right) - z^2\overline{z}^2 z_1^2 z_2^2 + y^4\left(z z_1 z_2 (z_1+z_2) - 3z_1^2 z_2^2 - z^2(z_1-z_2)^2\right)\right)}{(z-z_1)\,z_1^3 z_2^3\,(z_2-z)\,(z_2-z_1)^2\,(z\overline{z}+y^2)^2}\end{aligned}$$

where in the second line and third line, we used

$$\begin{aligned}\left\langle T(z')\,T(z_1)\,T(z_2)\right\rangle &= \frac{c}{(z_1-z_2)^2\,(z_2-z')\,(z_1-z')^2}, \\ \left\langle\left[T(z')\,T(z'')\right]T(z_1)\,T(z_2)\right\rangle &= \frac{c^2}{4}\left(\frac{1}{(z'-z_1)^4\,(z''-z_2)^4} + \frac{1}{(z'-z_2)^4\,(z''-z_1)^4}\right).\end{aligned}$$

Notice that there is no logarithm in the result of equation (2.7.30). But if one computes $\langle K_T T(z_1)\,T(z_2)\rangle$ and $\langle K_{TT} T(z_1)\,T(z_2)\rangle$ separately, one can see that they both have logarithmic terms, but they cancel out exactly!

The last term in the second bracket of equation (2.7.30) is

$$\begin{aligned}
&\left\langle \frac{K_T K_T}{2} T\left(z_1\right) T\left(z_2\right)\right\rangle \\
=&\int_0^z dz' \int_0^z dz'' \left(\frac{72h^2}{c^2} \frac{\left(y^2+z'\bar{z}\right)\left(z-z'\right)}{z\bar{z}+y^2} \frac{\left(y^2+z''\bar{z}\right)\left(z-z''\right)}{z\bar{z}+y^2}\right)\left\langle\left[T\left(z'\right) T\left(z''\right)\right] T\left(z_1\right) T\left(z_2\right)\right\rangle \\
=&\frac{h^2 z^4\left(z z_1 \bar{z}+y^2\left(3 z_1-2 z\right)\right)\left(z z_2 \bar{z}-2 y^2 z+3 y^2 z_2\right)}{\left(z-z_1\right)^2 z_1^3 z_2^3\left(z_2-z\right)^2}
\end{aligned}$$

which is just the contribution from $\langle\phi\mathcal{O}T\rangle\langle\phi\mathcal{O}T\rangle$.

So putting everything together, we have

$$\begin{aligned}
&\frac{\left\langle\phi\left(y,0,0\right)\mathcal{O}\left(z,\bar{z}\right) T\left(z_1\right) T\left(z_2\right)\right\rangle}{\left\langle\phi\left(y,0,0\right)\mathcal{O}\left(z,\bar{z}\right)\right\rangle} \\
=&\frac{c}{2\left(z_1-z_2\right)^4}+\frac{h^2 z^4\left(z_1 z \bar{z}+y^2\left(3 z_1-2 z\right)\right)\left(z_2 z \bar{z}+y^2\left(3 z_2-2 z\right)\right)}{z_1^3 z_2^3\left(z-z_1\right)^2\left(z-z_2\right)^2\left(z \bar{z}+y^2\right)^2} \\
&+\frac{2 h z^2\left(y^2 z \bar{z} z_1 z_2\left(z\left(z_1+z_2\right)-4 z_1 z_2\right)-z^2 \bar{z}^2 z_1^2 z_2^2+y^4\left(z z_1 z_2\left(z_1+z_2\right)-3 z_1^2 z_2^2-z^2\left(z_1-z_2\right)^2\right)\right)}{\left(z-z_1\right) z_1^3 z_2^3\left(z_2-z\right)\left(z_2-z_1\right)^2\left(z \bar{z}+y^2\right)^2}
\end{aligned}$$

Sending $y \to 0$ the above result does give us $\frac{\langle\mathcal{O}(0,0)\mathcal{O}(z,\bar{z})T(z_1)T(z_2)\rangle}{\langle\mathcal{O}(0,0)\mathcal{O}(z,\bar{z})\rangle}$, which is

$$\begin{aligned}
\frac{\left\langle\mathcal{O}\left(0,0\right)\mathcal{O}\left(z,\bar{z}\right) T\left(z_1\right) T\left(z_2\right)\right\rangle}{\left\langle\mathcal{O}\left(0,0\right)\mathcal{O}\left(z,\bar{z}\right)\right\rangle} &= \frac{1}{\left(z_1-z_2\right)^4}\left[\frac{c}{2}+\frac{h u^2(u(h u-2)+2)}{(u-1)^2}\right] \\
&= \frac{c}{2\left(z_1-z_2\right)^4}+\frac{h z^2\left(h z^2+\frac{2 z_1 z_2\left(z-z_1\right)\left(z-z_2\right)}{\left(z_1-z_2\right)^2}\right)}{z_1^2 z_2^2\left(z-z_1\right)^2\left(z-z_2\right)^2}
\end{aligned}$$

where $u \equiv \frac{z_{12} z_{34}}{z_{13} z_{24}}=\frac{\left(z_1-z_2\right) z}{\left(z_1-z\right) z_2}$ is the cross ratio.

2.7.3 Spinning Bulk Wilson Lines

In this appendix we give the derivation of equation (2.2.28) in the text. To begin, we recall how to write the bulk-to-boundary propagators in the vacuum. The general procedure was described in [65], and takes the form

$$\langle A^{\mu_1,\ldots,\mu_\ell}(y,z_1,\bar{z}_1)\mathcal{O}_{h,\bar{h}}(z_2,\bar{z}_2)\rangle = \left(\frac{y}{y^2+z_{12}\bar{z}_{12}}\right)^{2h} \xi_\pm^{\mu_1}\ldots\xi_\pm^{\mu_\ell}, \quad (\pm=-\mathrm{sgn}(\ell)) \tag{2.7.30}$$

for the case $h-\bar{h}=\ell$ of interest. Here, $(\xi_+^y,\xi_+^z,\xi_+^{\bar{z}})=(yz_1,z_1^2,-y^2)$ is the Killing vector associated with holomorphic special conformal generators, and $(\xi_-^y,\xi_-^z,\xi_-^{\bar{z}})=(y\bar{z}_1,-y^2,\bar{z}_1^2)$ for anti-holomorphic ones.

To promote this to an arbitrary background, we perform the transformation (2.2.8). Because $A_{\mu_1,\ldots,\mu_\ell}$ is a tensor, this transformation includes factors of

$$\frac{\partial x_f^{\mu}}{\partial x^{\mu'}}, \tag{2.7.31}$$

where x_f are the transformed coordinates $(y_f, z_f, \bar{z}_f)$. The transformed coordinates include dependence on the second derivatives of $f, \bar{f}$, and so the above Jacobian factor depends on its third derivatives. These third derivatives $f'''(z_2), \bar{f}'''(\bar{z}_2)$ can be eliminated in terms of the stress tensor $T(z_2), \bar{T}(\bar{z}_2)$ at the point $(z_2, \bar{z}_2)$. Moreover, as before we can eliminate $f'(z_2), f''(z_2)$ in terms of $x_T(z_1)$ and E_T. Making such substitutions, we find that

$$(\xi'_-)_{\mu'} = \frac{\partial x^{\mu}}{\partial x_f^{\mu'}}(\xi_-)_{\mu}(u_2, w_2, \bar{w}_2) = t^{\mu}_{\mu'}\bar{E}_{\bar{T}}^{-2}\bar{f}'(\bar{z}_1)(\xi_-)_{\mu}(y, z, \bar{z}), \tag{2.7.32}$$

where $t^{\mu}_{\mu'}$ is given in (2.2.29). We also have, from massaging (2.2.11) a bit, that

$$\left(\frac{u_2}{u_2^2 + f_{21}\bar{f}_{21}}\right)^{2h} = E_T^{2h}\bar{E}_{\bar{T}}^{2h}(f'(z_1)\bar{f}'(\bar{z}_1))^{-h}\left(\frac{y}{y^2 + x_T(z_1)\bar{x}_{\bar{T}}(\bar{z}_1)}\right)^{2h}. \tag{2.7.33}$$

Multiplying by $(\xi'_-)_{\mu'_1}\ldots(\xi'_-)_{\mu'_\ell}$ and using (2.7.32), we find

$$\begin{aligned}\left(\frac{u_2}{u_2^2 + f_{21}\bar{f}_{21}}\right)^{2h}(\xi'_-)_{\mu'_1}\ldots(\xi'_-)_{\mu'_\ell} &= E_T^{2h}\bar{E}_{\bar{T}}^{2\bar{h}}(f'(z_1))^{-h}(f'(\bar{z}_1))^{-\bar{h}} \\ &\times \left(\frac{y}{y^2 + x_T(z_1)\bar{x}_{\bar{T}}(\bar{z}_1)}\right)^{2h} t^{\mu'_1}_{\mu_1}\ldots t^{\mu'_\ell}_{\mu_\ell}(\xi_-)_{\mu_1}\ldots(\xi_-)_{\mu_\ell}.\end{aligned} \tag{2.7.34}$$

Equation (2.2.28) follows by using the fact that the Wilson line factors simply impose the constraint $x \to x_T(z_1), \bar{x} \to x_{\bar{T}}(\bar{z}_1)$ and produce factors $E_T^{2h}, \bar{E}_{\bar{T}}^{2\bar{h}}$.

2.7.4 Bulk Witten Diagram Computation for $\langle\phi\mathcal{O}T\rangle$

In this section, we will show that the result we obtained for $\langle\phi\mathcal{O}T\rangle$ using bulk-boundary OPE block and the recursion relation agrees with the result of the bulk Witten diagram computation for $\langle\phi(y,0,0)\mathcal{O}(z,\bar{z})T(z_1)\rangle$, shown in Fig. **??**. This should be expected, as the definition of equation (2.2.4) is essentially the first-quantized version of the bulk field theory that leads to the Witten diagram we will discuss. We will first show that the result is exact, using a trick [66] that obviates the need to perform integrals over

AdS_3. Then we will explicitly evaluate the diagram in the large h limit using saddle point approximation (this will give the same exact result), where we can make direct contact with some of the results from section 2.2.

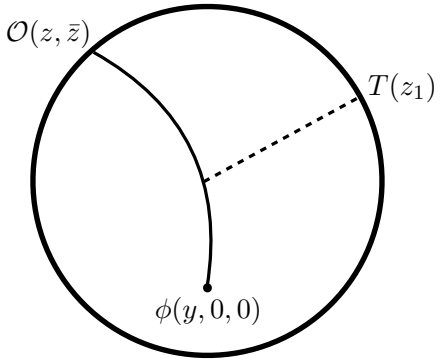

Figure 2.2: Dashed (solid) lines are graviton (scalar) propagators.

In order to compute this diagram, we need four ingredients: the scalar bulk-to-boundary propagator, the scalar bulk-to-bulk propagator, the vertex structure associated with the scalar-graviton interaction, and the graviton bulk-to-boundary propagtor. The standard prescription is to multiply these propagators together, and integrate over the bulk. There are a variety of conventions for normalizing these objects, so we will mostly ignore the overall numerical prefactors, which can be fixed in any case in terms of operator normalizations and the stress tensor Ward identity.

The bulk-to-bulk propagator, specializing to our coordinate set-up, is given by

$$G_{(y,0,0),(y',z',\bar{z}')} = \frac{e^{-2h\sigma}}{1-e^{-2\sigma}}, \tag{2.7.35}$$

where $\sigma \equiv \sigma_{(y',z',\bar{z}'),(y,0,0)}$ is the bulk-bulk geodesic between $(y',z',\bar{z}')$ and $(y,0,0)$

$$\sigma_{(y',z',\bar{z}'),(y,0,0)} = \log\frac{1+\sqrt{1-\xi^2}}{\xi}, \qquad \text{with} \quad \xi = \frac{2yy'}{y^2+y'^2+z'\bar{z}'}. \tag{2.7.36}$$

The scalar bulk-to-boundary propagator is given by

$$K_{(y',z',\bar{z}'),(z,\bar{z})} = \left(\frac{y'}{y'^2+(z-z')(\bar{z}-\bar{z}')}\right)^{2h}, \tag{2.7.37}$$

while can also be written as

$$K_{(y',z',\bar{z}'),(z,\bar{z})} = e^{-2h\sigma_{(y',z',\bar{z}'),(z,\bar{z})}}, \tag{2.7.38}$$

where $\sigma_{(y',z',\bar{z}'),(z,\bar{z})} = \log \frac{y'^2+(z'-z)(\bar{z}'-z)}{y'}$ is the regulated bulk-boundary geodesic length.

The vertex structure is given by $h_{\mu\nu}T_m^{\mu\nu}$, where $T_m^{\mu\nu}$ is the bulk matter stress energy tensor. It can be derived from the bulk equations of motion, and is given by [67]

$$T_m^{\mu\nu} = (g^{\mu\alpha}g^{\nu\beta} + g^{\mu\beta}g^{\nu\alpha})\partial_\alpha K \partial_\beta G - g^{\mu\nu}(g^{\rho\alpha}\partial_\rho K \partial_\alpha G + m^2 KG). \tag{2.7.39}$$

We are interested in the holomorphic part of this tensor object, since the coupling we need is $h_{zz}T_m^{zz}$. In the Fefferman-Graham gauge, it simplifies to

$$T_m^{zz} = 2g^{z\bar{z}}g^{z\bar{z}}\partial_{\bar{z}}K\partial_{\bar{z}}G = -2y^4 G\partial_{\bar{z}}^2 K. \tag{2.7.40}$$

Finally, we need the graviton bulk-to-boundary propagator in this gauge. $h_{zz}(y,z,\bar{z})$ is by definition equal to $-\frac{6T(z)}{c}$, as in equation (2.2.3).[23] So we have

$$\langle h_{zz}(y',z',\bar{z}')T(z_1)\rangle = -\frac{6}{c}\langle T(z')T(z_1)\rangle = \frac{-3}{(z'-z_1)^4} \tag{2.7.41}$$

Putting these ingredients together, the bulk integral corresponding to fig. ?? is then

$$\begin{aligned}\langle \phi(y,z_3,\bar{z}_3)\mathcal{O}(z_2,\bar{z}_2)T(z_1)\rangle = &\int_{\mathrm{AdS}_3}\sqrt{g}dz'd\bar{z}'dy'(-2y'^4)\\ &\times G_{(y,z_3,z_3),(y',z',\bar{z}')}\partial_{\bar{z}}^2 K_{(y',z',\bar{z}'),(z_2,\bar{z}_2)}\frac{-3}{(z'-z_1)^4}.\end{aligned} \tag{2.7.42}$$

The trick [66] to evaluating this kind of Witten diagram integral is first to simplify the problem as much as possible using global conformal invariance, and second to recall

[23] It was also shown [68] using smearing functions that $h_{zz}(y,z,\bar{z})$ is simply given by boundary stress energy tensor $T(z)$:

$$\begin{aligned} h_{zz}(y,z,\bar{z}) &\propto \frac{1}{\pi y^2}\int_{z\bar{z}\le y^2} dz'\bar{z}' T_{zz}\left(z+iz'\right)\\ &= \frac{1}{\pi y^2}\int_0^y rdr\int_0^{2\pi} d\theta T\left(z+ire^{i\theta}\right)\\ &= T(z).\end{aligned}$$

that the bulk scalar Feynman propagator satisfies the Klein-Gordon equation

$$\left(\nabla^2 - m^2\right) G(X,Y) = \delta_{AdS}(X-Y), \tag{2.7.43}$$

where $m^2 = 2h(2h-2)$. This means that if we act with the bulk differential operator $(\nabla^2 - m^2)$ on the Witten diagram that computes $\langle\phi(X)\mathcal{O}(z_2)T(z_1)\rangle$, then we will be left with just the integrand above, with G removed. We can simplify the calculation by shifting z_2 to 0 with a translation, then performing an inversion, and finally shifting $z_3 \to 0$ by another translation.[24] The resulting equation of motion is

$$\begin{aligned}(\nabla^2 - m^2)A(y,z_3,\bar{z}_3) &= -12\Delta(\Delta+1)\bar{z}_1^4 y^\Delta \left(\frac{y}{y^2+z_3\bar{z}_3}\right)^4, \\ A(y,z_3,\bar{z}_3) &\equiv \langle\phi(y',z_3',\bar{z}_3')\mathcal{O}(z_2',\bar{z}_2')T(z_1')\rangle,\end{aligned} \tag{2.7.44}$$

where (y', z_i') are the transformed coordinates. For comparison, the result in (2.2.30) in terms of the transformed coordinates is

$$\langle\phi(y',z_3',\bar{z}_3')\mathcal{O}(z_2',\bar{z}_2')T(z_1')\rangle = \frac{\Delta}{2}\frac{y^\Delta \bar{z}_1^4 z_3^2(3y^2+z_3\bar{z}_3)}{(y^2+z_3\bar{z}_3)^3} = \frac{\Delta}{2}y^{\Delta-4}z_3^2t^2(1+2t), \tag{2.7.45}$$

where $t \equiv \frac{y^2}{y^2+z_3\bar{z}_3}$. Taking $A(y,z_3,\bar{z}_3) = y^{\Delta-4}z^2 f(t)$, the equation of motion is simply

$$f''(t) + \frac{(-\Delta+(\Delta-1)t+4)f'(t)}{(t-1)t} + \frac{2(\Delta-3)f(t)}{(t-1)t^2} - \frac{3\Delta(\Delta+1)t^2}{t-1} = 0 \tag{2.7.46}$$

It is straightforward to check that the result in (2.2.30), i.e. $f(t) = \frac{\Delta}{2}t^2(1+2t)$, satisfies this equation. More constructively, there are two boundary conditions that must be imposed to fix the solution; one of these is that there is no $y^{2-\Delta}$ piece near the boundary, and the other can be chosen so that the correct $\langle\mathcal{O}\mathcal{O}T\rangle$ three-point function is reproduced at $y \sim 0$; since (2.2.30) manifestly satisfies these conditions, it is the correct solution. Thus our result exactly matches the Witten diagram.

Next, at large h, we can also evaluate the integral (2.7.42) directly using saddle point approximation (the result of this saddle point approximation turns out to be exact) and see how the kernel (2.2.15) emerges. After some manipulations, the bulk integral (2.7.42)

[24] Because of the presence of the bulk coordinate y, it is not enough to just take $z_2 \to \infty$, rather, we must actually perform the transformation ($z \to z - z_2$ followed by an inversion) that takes $z_2 \to \infty$.

can be re-cast into a more suggestive form

$$\langle\phi(y,0,0)\mathcal{O}(z,\bar{z})T(z_1)\rangle = 12h(2h+1)\int_{\text{AdS}_3}\frac{dz'd\bar{z}'dy'}{y'^3}e^{-2hL(y',z',\bar{z}')}\frac{e^{-2\sigma_{(y',z',\bar{z}'),(z,\bar{z})}}}{1-e^{-2\sigma_{(y,0,0),(y',z',\bar{z}')}}}y'^2\frac{(z'-z)^2}{(z'-z_1)^4}. \tag{2.7.47}$$

The notation $\sigma_{a,b}$ indicates the (regulated) geodesic length between points a and b. We have also defined $L(y',z',\bar{z}')$ to be the sum of the lengths of geodesics from $(y,0,0)$ to $(y',z',\bar{z}')$ and from $(y',z',\bar{z}')$ to $(z,\bar{z})$, that is

$$L(y',z',\bar{z}') \equiv \sigma_{(y,0,0),(y',z',\bar{z}')} + \sigma_{(y',z',\bar{z}'),(z,\bar{z})}. \tag{2.7.48}$$

In the large h limit, the integral will localize along the geodesics from $(y,0,0)$ to $(z,\bar{z})$ to minimize L. This geodesic parameterized by z' is given by

$$\bar{z}' = \frac{\bar{z}}{z}z', \qquad y'^2 = \left(1-\frac{z'}{z}\right)(y^2+z'\bar{z}), \tag{2.7.49}$$

so that the saddle point approximation to equation (2.7.47) is

$$\langle\phi\mathcal{O}T\rangle \propto \frac{24h^2}{c}e^{-2hL(y,0,0)}\int_0^z dz'\frac{1}{\sqrt{\det\partial^2 L}}\frac{e^{-2\sigma_{(y',z',\bar{z}'),(z,\bar{z})}}}{1-e^{-2\sigma_{(y,0,0),(y',z',\bar{z}')}}}\frac{1}{y'}\frac{(z-z')^2}{(z'-z_1)^4}, \tag{2.7.50}$$

where the determinant is given by

$$\det\partial^2 L = \det\begin{pmatrix}\partial^2_{\bar{z}'}L & \partial_{\bar{z}'}\partial_{y'}L\\ \partial_{y'}\partial_{\bar{z}'}L & \partial^2_{y'}L\end{pmatrix} = \frac{4z^5(z'\bar{z}+y^2)}{z'^2(z'-z)(z\bar{z}+y^2)^4}, \tag{2.7.51}$$

evaluated along the geodesic (2.7.49). Plugging this in (and neglecting an order 1 numerical factor) and performing the z' integral, we obtain

$$\begin{aligned}\langle\phi(y,0,0)\mathcal{O}(z,\bar{z})T(z_1)\rangle \propto& \frac{12h}{c}\langle\phi(y,0,0)\mathcal{O}(z,\bar{z})\rangle\int_0^z dz'\frac{2(z-z')(z'\bar{z}+y^2)}{z\bar{z}+y^2}\frac{c}{2(z'-z_1)^4}\\ =&\langle\phi(y,0,0)\mathcal{O}(z,\bar{z})\rangle\frac{hz^2}{z_1^3(z_1-z)^2}\left(z_1+\frac{2y^2(z_1-z)}{y^2+z\bar{z}}\right)\end{aligned}$$

matching equation 2.2.30 as expected. This demonstrates how the kernel of equation (2.2.15) emerges from a bulk Witten diagram calculation.

2.7.5 Solving for the Quantum Operator ϕ

2.7.5.1 Solutions to the Conditions of equation (2.3.3) at Level 3 and Level 4

In this section, we provide the solutions to the conditions of equation (2.3.3) at level 3 and level 4.

At level 3, $|\phi\rangle_3 = \lambda_3 \mathcal{L}_{-3}\overline{\mathcal{L}}_{-3}|\mathcal{O}\rangle$ and $\lambda_3\mathcal{L}_{-3}$ is given by with

$$\lambda_3\mathcal{L}_{-3} = (-1)^3\left(\frac{L_{-1}^3}{|L_{-1}\mathcal{O}|^2} + \frac{L_{-1}\mathcal{L}_{-2}^{\text{quasi}}}{\left|L_{-1}\mathcal{L}_{-2}^{\text{quasi}}\mathcal{O}\right|^2} + \frac{\mathcal{L}_{-3}^{\text{quasi}}}{\left|\mathcal{L}_{-3}^{\text{quasi}}\right|^2}\right), \tag{2.7.52}$$

where $\mathcal{L}_{-3}^{\text{quasi}} = L_{-1}^3 - 2(h+1)L_{-1}L_{-2} + (h+1)(h+2)L_{-3}$ and the norms are

$$\begin{aligned}\left|L_{-1}\mathcal{L}_{-2}^{\text{quasi}}\mathcal{O}\right|^2 &= 2(h+2)\left|\mathcal{L}_{-2}^{\text{quasi}}\mathcal{O}\right|^2 = \frac{4(2h+1)(h+2)((2h+1)c+2h(8h-5))}{9},\\ \left|\mathcal{L}_{-3}^{\text{quasi}}\right|^2 &= 2h(h+1)(h+2)\left((c-7)h+c+3h^2+2\right).\end{aligned} \tag{2.7.53}$$

At level 4, $|\phi\rangle_4 = \lambda_4\mathcal{L}_{-4}\overline{\mathcal{L}}_{-4}|\mathcal{O}\rangle$ and $\lambda_4\mathcal{L}_{-4}$ is given by

$$\lambda_4\mathcal{L}_{-4} = \frac{L_{-1}^2\mathcal{L}_{-2}^{\text{quasi}}}{\left|L_{-1}^2\mathcal{L}_{-2}^{\text{quasi}}\right|^2} + \frac{L_{-1}\mathcal{L}_{-3}^{\text{quasi}}}{\left|L_{-1}\mathcal{L}_{-3}^{\text{quasi}}\right|^2} + b_{4,1}\mathcal{L}_{-4}^{\text{quasi},(4,1)} + b_{2,2}\mathcal{L}_{-4}^{\text{quasi},(2,2)} \tag{2.7.54}$$

where

$$\begin{aligned}\mathcal{L}_{-4}^{\text{quasi},(4,1)} &= L_{-1}^4 - \frac{4(2h+3)}{375}\left[(16h(2h+11)+267)L_{-4} - 5(6h+9)L_{-2}^2 - 5(16h+49)L_{-1}L_{-3} + 125L_{-1}^2L_{-2}\right],\\ \mathcal{L}_{-4}^{\text{quasi},(2,2)} &= L_{-1}^4 + \frac{16}{9}h(h+3)L_{-2}^2 + \left(\frac{8h}{3}+10\right)L_{-1}L_{-3} - \frac{4}{3}(2h+3)L_{-1}^2L_{-2} + -4(h+3)L_{-4}.\end{aligned} \tag{2.7.55}$$

$\mathcal{L}_{-4}^{\text{quasi},(4,1)}$ and $\mathcal{L}_{-4}^{\text{quasi},(2,2)}$ are not orthogonal to each other. $\mathcal{L}_{-4}^{\text{quasi},(4,1)}$ becomes a null-state when $c = c_{4,1}(h) = -\frac{8h}{5} - \frac{45}{2h+3} + \frac{53}{5}$, and $\mathcal{L}_{-4}^{\text{quasi},(2,2)}$ becomes a null-state when $c = c_{2,2}(h) = 1 - 8h$. The coefficients of them, $b_{4,1}$ and $b_{2,2}$ are given by

$$\begin{aligned}b_{4,1} &= \frac{1125(10c+116h-81)}{8(2h+3)(2h+5)(8h-3)(8h+27)(5c(2h+3)+2(h-1)(8h-33))(2ch+c+2h(8h-5))},\\ b_{2,2} &= \frac{81(2h(16h+19)-5c)}{16h(h+3)(2h+5)(8h-3)(8h+27)(c+8h-1)(2ch+c+2h(8h-5))}.\end{aligned} \tag{2.7.56}$$

They are actually the solution to

$$\begin{pmatrix} \left\langle \mathcal{O} \middle| \left(\mathcal{L}_{-4}^{\text{quasi},(4,1)}\right)^\dagger \mathcal{L}_{-4}^{\text{quasi},(4,1)} \middle| \mathcal{O} \right\rangle & \left\langle \mathcal{O} \middle| \left(\mathcal{L}_{-4}^{\text{quasi},(4,1)}\right)^\dagger \mathcal{L}_{-4}^{\text{quasi},(2,2)} \middle| \mathcal{O} \right\rangle \\ \left\langle \mathcal{O} \middle| \left(\mathcal{L}_{-4}^{\text{quasi},(2,2)}\right)^\dagger \mathcal{L}_{-4}^{\text{quasi},(4,1)} \middle| \mathcal{O} \right\rangle & \left\langle \mathcal{O} \middle| \left(\mathcal{L}_{-4}^{\text{quasi},(2,2)}\right)^\dagger \mathcal{L}_{-4}^{\text{quasi},(2,2)} \middle| \mathcal{O} \right\rangle \end{pmatrix} \begin{pmatrix} b_{4,1} \\ b_{2,2} \end{pmatrix} = \begin{pmatrix} 1 \\ 1 \end{pmatrix}.$$

One can show that for non-orthogonal quasi-primaries at higher order, their coefficients will be given by the solutions to the equation corresponding to the above one at that order. And for global descendants of these non-orthogonal quasi-primaries, their coefficients will be given by a similar equation. These equations can be derived using the method similar to the one in section 2.3.2.2.

2.7.5.2 From Vacuum Sector Correlators to ϕ Via the OPE

We determined the vacuum sector correlators

$$\langle \phi(X)\mathcal{O}(z)T(z_1)\cdots T(z_n)\bar{T}(\bar{z}_1)\cdots\bar{T}(\bar{z}_m)\rangle \tag{2.7.57}$$

using the bulk-boundary OPE block in section 2.2. Thus we can straightforwardly determine the BOE expansion, expressing ϕ_N in terms of Virasoro descendants of $\mathcal{O}$ by studying the multi-OPEs of $\mathcal{O}$ with the various stress tensors.

To perform this analysis explicitly, we start with the $\langle\phi\mathcal{O}\rangle$ correlator and then add more and more T and $\bar{T}$, modifying ϕ_N each time to obtain the correct correaltors. We already found that global BOE of equation (2.3.6) produces the correct $\langle\phi\mathcal{O}\rangle$ correlator (see appendix 2.5.3 for details). Thus the next step is to modify the BOE to achieve the correct $\langle\phi\mathcal{O}T\rangle$ correlators, without disrupting $\langle\phi\mathcal{O}\rangle$. For this purpose it is useful to compute

$$\langle\phi^{\text{global}}(y,0,0)\mathcal{O}(z)T(z_1)\rangle = \frac{h\left(z\bar{z}+y^2\right)^2}{(z_1-z)^2\left(z_1\bar{z}+y^2\right)^2}\langle\phi(y)\mathcal{O}(z)\rangle \tag{2.7.58}$$

as shown via a more general argument in appendix 2.5.3. Now we can subtract this result from the full correlator in equation (2.2.30) to obtain correlators of ϕ_N with the contributions of global conformal descendants of $\mathcal{O}$ removed. Expanding to low order

in y, this is

$$\left(\frac{z\bar{z}}{y}\right)^h \left\langle \mathcal{O}(z)T(z_1)\left(\phi - \phi^{\text{global}}\right)\right\rangle = -\frac{3hy^4}{z_1^4\bar{z}^2} + 2hy^6\left(\frac{1}{z_1^4 z\bar{z}^3} + \frac{2}{z_1^5\bar{z}^3}\right) + \cdots \quad (2.7.59)$$

Notice that the expansion only begins at order y^4, and that as a function of z_1, the location of the stress tensor, each term has a pole at the origin of order 4 or higher. The first observation indicates that the first Virasoro correction occurs in ϕ_2, while the second confirms that these corrections all involve Virasoro descendants of $\mathcal{O}$, ie new quasi-primaries like $[T\mathcal{O}]$. We can match to the Virasoro descendants at levels 2 and 3, namely the operators $L_{-2}\bar{L}_{-1}^2\mathcal{O}$, $L_{-3}\bar{L}_{-1}^3\mathcal{O}$, and $L_{-1}L_{-2}\bar{L}_{-1}^3\mathcal{O}$, by computing correlators such as

$$\langle \mathcal{O}(z,\bar{z})T(z_1)L_{-2}\bar{L}_{-1}^2\mathcal{O}(0)\rangle \approx \frac{2h(2h+1)}{\bar{z}^{2h+2}z^{2h}}\frac{c}{2z_1^4} \quad (2.7.60)$$

where we have neglected terms that are independent of c. Comparing this with equation 2.7.59 at large c, we see that we need to add

$$\delta\phi_2 \approx -\left(\frac{y^4}{2!(2h)_2}\right)\frac{12h}{c}L_{-2}\bar{L}_{-1}^2\mathcal{O}(0) \quad (2.7.61)$$

to ϕ_2 at this order. At order y^6 we would add a linear combination of $L_{-3}\bar{L}_{-1}^3\mathcal{O}$ and $L_{-1}L_{-2}\bar{L}_{-1}^3\mathcal{O}$.

The second step in the analysis is to go back and 'fix' the $\langle\phi\mathcal{O}\rangle$ correlators, as $\delta\phi_2$ above will alter it. To achieve this goal, we simply need to supplement $\delta\phi_2$ to make it proportional to a new level 2 quasi-primary. This leads to

$$\delta\phi_2 \approx \left(\frac{y^4}{2!(2h)_2}\right)\left(L_{-1}^2 - \frac{12h}{c}L_{-2}\right)\bar{L}_{-1}^2\mathcal{O}(0) \quad (2.7.62)$$

to leading order at large c. With this choice, $\delta\phi_2$ will have a vanishing correlator with $\mathcal{O}$, and thus $\langle\phi\mathcal{O}\rangle$ will remain correct.

However, we can determine all of these coefficents more precisely and systematically using the condition of equation (2.3.3), as we'll do in next subsection.

2.7.5.3 Solving for ϕ at Large c

In this section, we'll use the definition of ϕ to derive the leading order terms of the $\frac{1}{c}$ and $\frac{1}{c^2}$ corrections to ϕ.

We know that at the leading order of the large c limit, $\phi(y,0,0)$ will reduce to $\phi^{\text{global}}(y,0,0)$, that is

$$\lim_{c\to\infty}\phi(y,0,0)|0\rangle=\phi^{\text{global}}(y,0,0)|0\rangle=\sum_{N=0}^{\infty}y^{2h+2N}\frac{(-1)^N}{N!\,(2h)_N}\left(L_{-1}\overline{L}_{-1}\right)^N|\mathcal{O}\rangle\,. \tag{2.7.63}$$

We'll expand $\phi(y,0,0)|0\rangle=\sum_{N=0}^{\infty}y^{2h+2N}|\phi\rangle_N$ and write $|\phi\rangle_N$ as follows

$$|\phi\rangle_N=\lambda_N\mathcal{L}_{-N}\overline{\mathcal{L}}_{-N}|\mathcal{O}\rangle\,. \tag{2.7.64}$$

And we'll derive the coefficients of the following terms at order $\frac{1}{c}$ and $\frac{1}{c^2}$ in $\mathcal{L}_{-N}$:

$$\mathcal{L}_{-N}=L_{-1}^N+\frac{1}{c}\sum_{k=2}^{N}\eta_{N,k}L_{-k}L_{-1}^{N-k}+\frac{1}{c^2}\sum_{\substack{k_1,k_2=2\\k_1\geq k_2}}^{N}\kappa_{N,k_1,k_2}L_{-k_1}L_{-k_2}L_{-1}^{N-k_1-k_2}+\mathcal{O}(c^{-3}). \tag{2.7.65}$$

To derive $\eta_{N,k}$, we just need to consider the first two terms in the above equation. Using the condition of equation (2.3.3) we have

$$L_m\left[L_{-1}^N+\frac{1}{c}\sum_{k=2}^{N}\eta_{N,k}L_{-k}L_{-1}^{N-k}\right]|\mathcal{O}\rangle=0+\mathcal{O}\left(c^{-1}\right),\qquad 2\leq m\leq N. \tag{2.7.66}$$

The first term can be calculated exactly as follows[25]

$$\begin{aligned}L_mL_{-1}^N|\mathcal{O}\rangle&=(m+1)!\sum_{i=1}^{N-(m-1)}\begin{pmatrix}N-i\\m-1\end{pmatrix}(h+i-1)\,L_{-1}^{N-m}|\mathcal{O}\rangle\\&=\frac{N!(h\,(m+1)+N-m)}{(N-m)!}L_{-1}^{N-m}|\mathcal{O}\rangle\end{aligned}$$

[25] Equation (2.7.67) comes from the following procedure. We commute L_m with m L_{-1} to get L_0. To do so we need to choose m L_{-1}s from the N L_{-1}s. If the position of the last L_{-1} for these m L_{-1}s is the ith L_{-1} in the N L_{-1}s from the right, then it means that we need to choose $(m-1)$ L_{-1}s from $(n-i)$ L_{-1}s, where there are $\begin{pmatrix}N-i\\m-1\end{pmatrix}$ of ways to do so. Commuting L_m with m L_{-1} will eventually gives us a L_0 times a factor of $(m+1)!$. And there are $(i-1)$ L_{-1}s remained on the right of this L_0, so the eigenvalue of L_0 will be $h+i-1$.

The second term is easy to calculate at leading order of large c, which is given by

$$L_m \sum_{k=2}^{N} \frac{1}{c} \eta_{N,k} L_{-k} L_{-1}^{N-k} |\mathcal{O}\rangle = \eta_{N,m} \frac{m\left(m^2-1\right)}{12} L_{-1}^{N-m} |\mathcal{O}\rangle + \mathcal{O}(c^{-1}) \tag{2.7.67}$$

where we used the Virasoro algebra $[L_m, L_n] = (m-n)L_{m+n} + \frac{m(m^2-1)c}{12}\delta_{m,-n}$.Equating the RHSs of equation (2.7.67) and equation (2.7.67), and solving for $\eta_{N,m}$, we find

$$\eta_{N,m} = -\frac{12(h\,(m+1)+N-m)N!}{(N-m)!m\,(m^2-1)} \tag{2.7.68}$$

To derive κ_{N,k_1,k_2}, we need to use the following conditions,

$$L_{m_2} L_{m_1} \left(L_{-1}^N + \frac{1}{c} \sum_{k=2}^{N} \eta_{N,k} L_{-k} L_{-1}^{N-k} + \frac{1}{c^2} \sum_{\substack{k_1,k_2=2 \\ k_1 \geq k_2}}^{N} \kappa_{N,k_1,k_2} L_{-k_1} L_{-k_2} L_{-1}^{N-k_1-k_2} \right) |\mathcal{O}\rangle = 0 + \mathcal{O}\left(c^{-1}\right), \tag{2.7.69}$$

with $m_1, m_2 \geq 2$ and $m_1 \geq m_2$, because $L_{m_2} L_{m_1}$ acting on the $\frac{1}{c^2}$ terms will contribute to leading order $\mathcal{O}\left(c^0\right)$.

We already know that

$$L_{m_1} \left(L_{-1}^n + \sum_{k=2}^{n} \lambda_{n,k} \frac{1}{c} L_{-k} L_{-1}^{n-k} \right) = 0 + \mathcal{O}\left(c^{-1}\right) \tag{2.7.70}$$

so in the following we only need to consider the remaining contribution of the second term, which comes from $k = m_2$ and $k = m_1 + m_2$,

$$\begin{aligned} L_{m_2} L_{m_1} \sum_{\substack{k=2 \\ k \neq m_1}}^{N} \frac{1}{c} \lambda_{N,k} L_{-k} L_{-1}^{N-k} |\mathcal{O}\rangle = & \frac{m_2\left(m_2^2-1\right)}{12} \Big[\lambda_{N,m_1+m_2} (2m_1+m_2) \\ & + \lambda_{N,m_2} \frac{(N-m_2)!(h\,(m_1+1)+N-m_2-m_1)}{(N-m_2-m_1)!} \Big] L_{-1}^{N-m_1-m_2} |\mathcal{O}\rangle \end{aligned}$$

The third term in equation (2.7.69) give the following leading order contribution

$$\begin{aligned} & L_{m_2} L_{m_1} \sum_{\substack{k_1,k_2=2 \\ k_1 \geq k_2}}^{N} \frac{1}{c^2} \kappa_{n,k_1,k_2} L_{-k_1} L_{-k_2} L_{-1}^{n-k_1-k_2} |\mathcal{O}\rangle \\ = & \left(1+\delta_{m_1,m_2}\right) \kappa_{N,m_1,m_2} \frac{m_1\left(m_1^2-1\right) m_2\left(m_2^2-1\right)}{144} L_{-1}^{N-m_1-m_2} |\mathcal{O}\rangle + \mathcal{O}\left(c^{-1}\right). \end{aligned}$$

So equating the RHSs of the above two equations, and solving for κ_{N,m_1,m_2}, we find

$$\kappa_{N,m_1,m_2} = -\frac{\lambda_{N,m_1+m_2}\left(2m_1+m_2\right)+\lambda_{N,m_2}\frac{(N-m_2)!(h(m_1+1)+N-m_2-m_1)}{(N-m_2-m_1)!}}{\left(1+\delta_{m_1,m_2}\right)\frac{m_1\left(m_1^2-1\right)}{12}}. \tag{2.7.71}$$

So $\mathcal{L}_{-N}$ is by given equation (2.7.65) with $\eta_{N,k}$ and κ_{N,k_1,k_2} given by equation (2.7.68) and equation (2.7.71).

Notice that the $\eta_{N,k}$ and κ_{N,k_1,k_2} we derived above are just the leading order results, ie there are $\frac{1}{c}$ corrections to them. And there are other terms, like L_{-1}^N, at order $\frac{1}{c}$ and $\frac{1}{c^2}$. In general, these $\frac{1}{c}$ corrections should form quasi-primaries and their global descendants, such that $\langle\phi\mathcal{O}\rangle$ will always be given by $\langle\phi\mathcal{O}\rangle = \left\langle\phi^{\text{global}}\mathcal{O}\right\rangle$, which is just the bulk-boundary propagator in vacuum.

2.7.6 Explicit Form of the Stress-Tensor Correlator Recursion and Calculation

We can document the origin of various terms in the recursion relation from section 2.3.3 very explicitly as

$$\begin{aligned}
G_{n+1,m} = &\Bigg(\underbrace{\underbrace{-\frac{\partial_z+\sum_{i=1}^n\partial_{z_i}}{z_{n+1}}}_{L_{-1}\phi}+\underbrace{\frac{\frac{y}{2}\partial_y}{z_{n+1}^2}}_{L_0\phi}\underbrace{-\frac{z\left(2h+z\partial_z\right)}{z_{n+1}^3}}_{-[L_1,\mathcal{O}(z,\bar{z})]}\underbrace{-\sum_{i=1}^n\frac{z_i\left(4+z_i\partial_{z_i}\right)}{z_{n+1}^3}}_{-[L_1,T(Z_i)]}}_{L_1\phi}}_{T(z_{n+1})\phi(y,0,0)}\Bigg)G_{n,m}\\
&+\Bigg(\underbrace{\frac{h}{\left(z_{n+1}-z\right)^2}+\frac{\partial_z}{\left(z_{n+1}-z\right)}}_{T(z_{n+1})\mathcal{O}(z,\bar{z})}+\underbrace{\sum_{i=1}^n\left(\frac{2}{\left(z_{n+1}-z_i\right)^2}+\frac{\partial_{z_i}}{z_{n+1}-z_i}\right)}_{T(z_{n+1})T(z_i)}\Bigg)G_{n,m}\\
&+\underbrace{\sum_{i=1}^n\frac{\left\langle T\left(z_1\right)\cdots T\left(z_{i-1}\right)T\left(z_{i+1}\right)\cdots T\left(z_n\right)\overline{T}\left(\overline{w}_1\right)\cdots\overline{T}\left(\overline{w}_m\right)\mathcal{O}\left(z,\bar{z}\right)\phi\left(y,0,0\right)\right\rangle}{2\left(z_{n+1}-z_i\right)^4}}_{T(z_{n+1})T(z_i)}
\end{aligned} \tag{2.7.72}$$

One can use the above recursion relation to easily derive $\langle\phi\mathcal{O}T\rangle$, $\langle\phi\mathcal{O}TT\rangle$ and $\left\langle\phi\mathcal{O}T\overline{T}\right\rangle$ that we derived in section 2.7.2 using bulk-boundary OPE block. For comparison, we

provide these computations here.

For one T insertion, we have

$$\begin{aligned}\langle\phi(y,0,0)\mathcal{O}(z,\bar{z})T(z_1)\rangle &= \left(-\frac{\partial_z}{z_1}+\frac{\frac{y}{2}\partial_y}{z_1^2}-\frac{z(2h+z\partial_z)}{z_1^3}+\frac{h}{(z_1-z)^2}+\frac{\partial_z}{z_1-z}\right)\langle\phi\mathcal{O}\rangle \\ &= \left(\frac{y}{z\bar{z}+y^2}\right)^{2h}\frac{hz^2\left(z_1\left(z\bar{z}+3y^2\right)-2y^2z\right)}{(z-z_1)^2z_1^3\left(y^2+z\bar{z}\right)}.\end{aligned}$$

For one T and one $\overline{T}$ insertions, we have

$$\begin{aligned}&\left\langle\phi(y,0,0)\mathcal{O}(z,\bar{z})T(z_1)\overline{T}(\overline{w}_1)\right\rangle \\ &= \left(-\frac{\partial_{\bar{z}}}{\overline{w}_1}+\frac{\frac{y}{2}\partial_y}{\overline{w}_1^2}-\frac{\bar{z}(2h+\bar{z}\partial_{\bar{z}})}{\overline{w}_1^3}+\frac{h}{(\overline{w}_1-\bar{z})^2}+\frac{\partial_{\bar{z}}}{\overline{w}_1-\bar{z}}\right)\langle\phi(y,0,0)\mathcal{O}(z,\bar{z})T(z_1)\rangle \\ &= \left(\frac{y}{z\bar{z}+y^2}\right)^{2h}\left(\frac{h^2z^2\bar{z}^2\left(y^2(3\bar{w}_1-2\bar{z})+\bar{w}_1z\bar{z}\right)\left(y^2(3z_1-2z)+z_1z\bar{z}\right)}{z_1^3\overline{w}_1^3(z_1-z)^2(\overline{w}_1-\bar{z})^2(z\bar{z}+y^2)^2}\right. \\ &\qquad\left.+\frac{2hy^2z^3\bar{z}^3}{z_1^3\bar{w}_1^3(z-z_1)(\bar{w}_1-\bar{z})(z\bar{z}+y^2)^2}\right).\end{aligned}$$

For two T insertions, we have

$$\begin{aligned}&\langle\phi(y,0,0)\mathcal{O}(z,\bar{z})T(z_1)T(z_2)\rangle \\ &= \left(-\frac{\partial_z+\partial_{z_1}}{z_2}+\frac{\frac{y}{2}\partial_y}{z_2^2}-\frac{z(2h+z\partial_z)}{z_2^3}-\frac{z_1(4+z_1\partial_{z_1})}{z_2^3}\right)\langle\phi(y,0,0)\mathcal{O}(z,\bar{z})T(z_1)\rangle \\ &\quad+\left(\frac{h}{(z_2-z)^2}+\frac{\partial_z}{z_2-z}+\frac{2}{(z_2-z_1)^2}+\frac{\partial_{z_1}}{z_2-z_1}\right)\langle\phi(y,0,0)\mathcal{O}(z,\bar{z})T(z_1)\rangle \\ &\quad+\frac{c}{2(z_2-z_1)^2}\langle\phi(y,0,0)\mathcal{O}(z,\bar{z})\rangle \\ &= \left(\frac{y}{z\bar{z}+y^2}\right)^{2h}\left[\frac{c}{2(z_1-z_2)^4}+\frac{h^2z^4\left(z_1z\bar{z}+y^2(3z_1-2z)\right)\left(z_2z\bar{z}+y^2(3z_2-2z)\right)}{z_1^3z_2^3(z-z_1)^2(z-z_2)^2(z\bar{z}+y^2)^2}\right. \\ &\quad\left.+\frac{2hz^2\left(y^2z\bar{z}z_1z_2\left(z(z_1+z_2)-4z_1z_2\right)-z^2\bar{z}^2z_1^2z_2^2+y^4\left(zz_1z_2(z_1+z_2)-3z_1^2z_2^2-z^2(z_1-z_2)^2\right)\right)}{(z-z_1)z_1^3z_2^3(z_2-z)(z_2-z_1)^2(z\bar{z}+y^2)^2}\right].\end{aligned}$$

One can see that the above results are exactly what we found in section 2.7.2.

Chapter 3

Conformal Truncation and the 2D Ising Model

This model was suggested to Ising by his thesis adviser, Lenz. Ising solved the one-dimensional model, ..., and on the basis of the fact that the one-dimensional model had no phase transition, he asserted that there was no phase transition in any dimension. As we shall see, this is false. It is ironic that on the basis of an elementary calculation and erroneous conclusion, Ising's name has become among the most commonly mentioned in the theoretical physics literature. But history has had its revenge. Ising's name, which is correctly pronounced "E-zing," is almost universally mispronounced "I-zing." — Barry Simon

3.1 Introduction

The language of quantum field theory underpins our understanding of a vast array of physical phenomena. For strongly-coupled QFTs, however, we face a shortage of robust methods for calculating non-perturbative dynamics. In particular, apart from certain highly specialized examples, it is challenging in most methods to compute time-dependent observables, such as correlation functions of local operators or the wavefunctions of states. A new framework was presetned in [69], called *conformal truncation*, for computing real-time, infinite-volume observables in a non-perturbative QFT in any number of spacetime dimensions, given information about the UV conformal field theory from which it originates. In that work, the method was only tested in examples with a

perturbative or large-N expansion. The goal of the present work is to apply conformal truncation in a truly non-perturbative setting, and in so doing, to lay the groundwork for using this method to study dynamics in general QFTs.

Conformal truncation is a particular implementation of a more general approach known as Hamiltonian truncation (for a recent review, see [70]). The basic strategy is to discretize the QFT Hilbert space in some way and then truncate it to a finite-dimensional subspace. The resulting truncated Hamiltonian can be diagonalized numerically, yielding an approximation to the true QFT spectrum. More importantly, we also obtain an approximation to the actual Hamiltonian eigenstates, which can be used to compute dynamical observables. The heart of any Hamiltonian truncation method is the discretization prescription, since it determines which symmetries are preserved under truncation, how efficiently IR degrees of freedom are captured, and, ultimately, which physical observables are deliverable.

The method proposed in [69] uses conformal symmetry as the organizing principle for truncation. One starts by viewing the QFT in question as arising from a deformed UV CFT. A basis for the QFT Hilbert space is constructed in terms of UV fields and organized into representations of the conformal group, characterized by the quadratic Casimir eigenvalue $\mathcal{C}$. One truncates the basis by specifying some maximum Casimir eigenvalue $\mathcal{C}_{\text{max}}$ and only keeping states below this threshold. In this basis, matrix elements of the Hamiltonian are simply related to OPE coefficients of the UV CFT. Although the basis and Hamiltonian are constructed in the UV, after diagonalization, they describe the entire RG flow of the QFT. In this way, one is using CFT data to study QFT dynamics.

A key feature of conformal truncation is that one can use it to compute real-time, continuum correlation functions. This is largely because the method avoids spacetime compactification or latticization. For two-point functions, one can compute the associated Källén-Lehmann spectral densities, $\rho(\mu)$, which encode the decomposition of these correlators in terms of mass eigenstates,

$$\langle \mathcal{O}(x)\mathcal{O}(0)\rangle = \int d\mu^2\, \rho_{\mathcal{O}}(\mu) \int \frac{d^d p}{(2\pi)^d}\, e^{-ip\cdot x}\, \theta(p_0)\, (2\pi)\delta(p^2-\mu^2). \tag{3.1.1}$$

In [69], we confirmed that conformal truncation indeed correctly reproduces known

spectral densities in a large-N example. Our goal here is to now use conformal truncation to compute fully non-perturbative spectral densities.

To have an independent check of our numerical results, we would like to study a QFT with two properties: (i) it originates from a UV CFT where we know operator dimensions and OPE coefficients so that we can construct the Hamiltonian, and (ii) it has some regime that is strongly-coupled, but with known analytic expressions for correlation functions that we can compare with our conformal truncation results. One QFT that satisfies these requirements is 1+1 dimensional ϕ^4 theory, which can be viewed as the free massless CFT deformed by a mass term and quartic coupling, leading to the full Lagrangian[1]

$$\mathcal{L} = \mathcal{L}_{\text{CFT}} + \delta\mathcal{L} = \frac{1}{2}\partial_\mu\phi\partial^\mu\phi - \frac{1}{2}m^2\phi^2 - \frac{1}{4!}\lambda\phi^4. \tag{3.1.2}$$

The dynamics of this theory are controlled by the dimensionless parameter

$$\bar{\lambda} \equiv \frac{\lambda}{m^2}.$$

Using conformal truncation, we can compute spectral densities for *any* $\bar{\lambda}$. To the best of our knowledge, this is the first calculation of non-perturbative spectral densities in 2D ϕ^4 theory.

For some critical value $\bar{\lambda}_*$, the mass gap closes and the theory flows to a non-trivial IR fixed point in the same universality class as the critical 2D Ising model, a theory for which many exact results are known. We can thus test conformal truncation in a strongly-coupled setting by comparing the IR behavior of our resulting spectral densities in the vicinity of the critical point to the known analytic expressions for the Ising model.

We focus specifically on the local operators ϕ^n and the stress-energy tensor $T_{\mu\nu}$. Our results for the spectral densities of these operators can be summarized as follows:

- We verify explicitly that ϕ^4 theory at $\bar{\lambda}_*$ flows to a non-trivial CFT. Specifically, we compute the spectral density of the trace of the stress tensor, $T^\mu{}_\mu$, and confirm that near criticality it reproduces the 2D Ising prediction in the IR, vanishing as $\bar{\lambda} \to \bar{\lambda}_*$. (Figure 3.7)

[1] The operators in this Lagrangian are normal-ordered, but we have suppressed the typical notation, $:\mathcal{O}:$, with the understanding that *all* local operators in this work are to be normal-ordered.

- We demonstrate universality in the IR behavior of ϕ^n correlators near criticality. In particular, we find that the spectral densities of the even operators ϕ^{2n} all match the Ising model prediction for ϵ, while the odd operators ϕ^{2n-1} match the prediction for σ. (Figures 3.8 and 3.9)
- We compute the Zamolodchikov C-function along the full RG flow. We find that it decreases monotonically from the free central charge $c_{\text{UV}} = 1$, transitioning to the strongly-coupled IR at a scale set roughly by the coupling $\frac{\lambda}{4\pi}$. Near criticality, the IR behavior agrees with the prediction from the Ising model. (Figure 3.12)

It is worth emphasizing that our numerical results for the spectral densities describe the *entire* RG flow, not just the IR regime described by the Ising model. In addition, we can use conformal truncation to compute dynamical observables at any value of the coupling, not just the narrow range near $\bar{\lambda}_*$. We merely choose to focus on the vicinity of the critical point in this work in order to test our framework against analytic results.

There have been many previous applications of Hamiltonian truncation methods to two-dimensional ϕ^4 theory [71, 72, 73, 74, 75, 76, 77, 78, 79, 80, 81, 82, 83, 84, 85, 86, 87, 88, 89, 90]. In particular, Burkardt et al. [73] have proposed using a Fock space basis of symmetric polynomials which in fact match the Casimir eigenstates we use to construct our basis. However, our approach differs somewhat from theirs in practice, as we truncate our basis solely according to Casimir eigenvalue, keeping higher-particle states which they neglect. In addition, we use the conformal structure of the UV theory to simplify the construction of the basis, allowing us to significantly increase the number of states and compute full spectral densities.

Looking forward, conformal truncation can be applied to deformations of more general CFTs, in any number of dimensions, provided we have sufficient knowledge of scaling dimensions and OPE coefficients to construct the Hamiltonian. Conformal truncation can therefore be used to study entire RG flows in a wide range of theories. It would be useful to test the method in examples, such as those studied in [91, 92, 93, 94, 95, 96, 97, 98], where the full flow can be computed using other techniques. Overall, our results for ϕ^4 theory provide a first step toward using this method to study a variety of strongly-coupled dynamics.

The outline of the paper is as follows. In section 4.3, we briefly review the general

framework of conformal truncation and discuss its application to 1+1 dimensional scalar field theory. In section 4.4 we perform some simple consistency checks, numerically reproducing several free field theory spectral densities and then verifying the constraints imposed by the equation of motion and conservation of the stress-energy tensor. In section 3.4, we proceed to strong coupling, studying the behavior of the low-mass spectrum as a function of the coupling $\bar{\lambda}$ in order to determine the point at which the mass gap closes. We then extrapolate the truncated results to determine a prediction for the critical coupling, $\bar{\lambda}_*$, which we compare to previous results in the literature. In section 3.5, we compute spectral densities in the vicinity of the critical point, comparing the results to analytic predictions from the Ising model. We conclude and discuss future directions in section 3.6, while several appendices contain details of our methods.

3.2 Conformal Truncation and Scalar Field Theory

The goal of this work is to use conformal truncation to study the RG flow of 1+1 dimensional ϕ^4 theory, given by the Lagrangian in eq. (3.1.2), to the 2D Ising model. In this section, we introduce all of the necessary ingredients to accomplish this task. We first review the overall approach of conformal truncation and then discuss the details of applying this method to the specific UV CFT of 2D free scalar field theory. Finally, we briefly review spectral densities, which are our main dynamical observable.

3.2.1 Review of Conformal Truncation

Conformal truncation is a method for using CFT data to numerically study the IR dynamics of more general QFTs. This method can be applied to any theory that can be described as an RG flow originating from some UV CFT deformed by one or more relevant operators,

$$S = S_{\text{CFT}} - \lambda \int d^d x \, \mathcal{O}_R(x). \tag{3.2.1}$$

Following the approach presented in [69], a useful basis for the Hilbert space of this theory consists of UV eigenstates of the quadratic Casimir of the conformal group,

$$|\mathcal{C}, \vec{P}, \mu\rangle \equiv \int d^d x \, e^{-iP\cdot x} \mathcal{O}(x)|0\rangle, \tag{3.2.2}$$

where $\mu^2 \equiv P^2$. These basis states are created by primary operators[2] in the original CFT, and are characterized by their Casimir eigenvalue, spatial momentum, and invariant mass (suppressing other possible quantum numbers like the spin ℓ).

The strategy of conformal truncation is to restrict the Hilbert space to the subspace spanned by states with Casimir eigenvalue $\mathcal{C} \leq \mathcal{C}_{\text{max}}$. The full Hamiltonian (CFT + deformation), when restricted to this subspace, can be diagonalized numerically, yielding an approximation to the true spectrum of the IR QFT.

To define the Hamiltonian, we first need to choose a quantization scheme. As discussed in [69], we work in lightcone quantization, with the Hilbert space defined on slices of constant lightcone "time" $x^+ \equiv \frac{1}{\sqrt{2}}(t+x)$. We thus need to compute matrix elements for the associated lightcone Hamiltonian

$$P_+ = P_+^{(\text{CFT})} + \lambda \int d^{d-1}\vec{x}\, \mathcal{O}_R(x^+ = 0, \vec{x}). \tag{3.2.3}$$

By construction, our basis is built from eigenstates of the CFT Hamiltonian, so we only need to compute matrix elements associated with the relevant deformation. These matrix elements are simply Fourier transforms of three-point functions in the original UV CFT,

$$\langle \mathcal{C}, \vec{P}, \mu | \delta P_+ | \mathcal{C}', \vec{P}', \mu' \rangle = \lambda \int d^d x\, d^{d-1}\vec{y}\, d^d z\, e^{i(P\cdot x - P'\cdot z)} \langle \mathcal{O}(x)\mathcal{O}_R(y)\mathcal{O}'(z)\rangle. \tag{3.2.4}$$

We thus only need data from the UV fixed point to study the full RG flow: the spectrum of local operators gives us a complete basis, while the OPE coefficients give us the Hamiltonian matrix elements.

3.2.2 Conformal Basis for 2D Scalar Fields

Our starting point is the 2D free massless scalar in the UV. To apply conformal truncation, we need to first construct the complete set of primary operators built from the scalar field ϕ.[3] This process is more subtle than in higher dimensions, because in 2D ϕ is *not* a primary operator. We can see this by looking at its two-point function, which

[2] In this work, "primary" refers to any operator which is primary with respect to the global conformal group $SO(d,2)$ and thus annihilated by the special conformal generators ($[K_\mu, \mathcal{O}(0)] = 0$). In 2D, this includes operators which are often referred to as "quasi-primary" or "global primary" in the literature.

[3] This basis was originally considered in [99, 100], though with the separate goal of studying bound states in 2D QCD.

is logarithmically divergent,

$$\langle \phi(x)\phi(0)\rangle = \frac{-1}{2\pi}\log|x|. \tag{3.2.5}$$

In order to construct well-defined primary operators, we must instead use the "building blocks"

$$\partial_-\phi, \quad \partial_+\phi, \quad e^{i\alpha\phi}.$$

However, for the purposes of conformal truncation we do not need the latter two, as we now explain.

Consider $\partial_+\phi$. From the equations of motion, we see that $\partial_\pm\phi$ are purely left-moving and right-moving modes, respectively,

$$\partial^2\phi = \partial_-(\partial_+\phi) = \partial_+(\partial_-\phi) = 0. \tag{3.2.6}$$

The left-moving operator $\partial_+\phi$ thus creates particles with zero lightcone momentum P_-. Because we are working in lightcone quantization, these left-moving states are non-dynamical and can be integrated out, setting $\partial_+\phi = 0$ [101].

Now consider the vertex operators $e^{i\alpha\phi}$, parameterized by the variable α. Because of the logarithmic divergence in eq. (3.2.5), these operators require the introduction of an IR scale R,

$$\langle e^{i\alpha\phi(x)}e^{-i\alpha\phi(0)}\rangle = \sum_n \frac{\alpha^{2n}}{(n!)^2}\langle\phi^n(x)\phi^n(0)\rangle = \sum_n \frac{\alpha^{2n}}{n!(2\pi)^n}\log^n\left|\frac{R}{x}\right| = \left(\frac{R}{x}\right)^{\frac{\alpha^2}{2\pi}}. \tag{3.2.7}$$

This IR scale can be absorbed into a redefinition of $e^{i\alpha\phi}$, yielding a well-defined set of primary operators with scaling dimensions $\Delta_\alpha = \frac{\alpha^2}{4\pi}$. However, once we deform the UV CFT by adding the mass term

$$\delta\mathcal{L} = -\frac{1}{2}m^2\phi^2,$$

the resulting Hamiltonian matrix elements for these vertex operators depend on the IR scale, diverging as $R \to \infty$. These divergences "lift" the vertex operators from the theory, such that they have no overlap with the physical low-energy states. This behavior is unsurprising, as vertex operators cease to be independent degrees of freedom in the massive theory.

Consequently, we can ignore both left-moving and vertex operators.[4] Thus our basis consists of primary operators built only from the right-moving mode $\partial_- \phi$, with the general form

$$\boxed{\mathcal{O}(x) = \sum_{\boldsymbol{k}} C_{\boldsymbol{k}}^{\mathcal{O}} \, \partial_-^{k_1} \phi(x) \cdots \partial_-^{k_n} \phi(x),} \tag{3.2.8}$$

for some coefficients $C_{\boldsymbol{k}}^{\mathcal{O}}$ that need to be determined. The method for constructing these primary operators is discussed in appendix 3.7 and will be presented in more detail in [102]. Because these operators only consist of right-moving modes, their associated conformal Casimir eigenvalues are completely fixed by their scaling dimensions,

$$\mathcal{C} = \Delta(\Delta - 2) + \ell^2 = 2\Delta(\Delta - 1). \tag{3.2.9}$$

Setting a maximum Casimir eigenvalue, $\mathcal{C}_{\text{max}}$, is thus equivalent to setting a maximum scaling dimension, Δ_{max}.

The right-moving operators are all annihilated by the original CFT Hamiltonian,

$$[P_+^{(\text{CFT})}, \mathcal{O}(x)] = 0. \tag{3.2.10}$$

This means that *all* states built from these primary operators have zero invariant mass P^2. Thus for the 2D free scalar, the conformal truncation basis states in eq. (3.2.2) take the more restricted form

$$|\mathcal{C}, P_-, \mu = 0\rangle \equiv \int dx^- \, e^{-iP_- x^-} \mathcal{O}(x^-)|0\rangle. \tag{3.2.11}$$

Unlike in higher dimensions, where each primary operator defines a continuum of Casimir eigenstates, parameterized by the invariant mass μ, each 2D operator $\mathcal{O}$ only defines a *single* basis state. For a given $\mathcal{C}_{\text{max}}$, the number of states in our basis is therefore given by the number of primary operators with Casimir eigenvalue below that threshold. It is important to note that this significant reduction of the basis is specific to 2D free field theory (or more generally, 2D theories built from conserved currents). In other CFTs, primary operators are *not* annihilated by P_+, leaving the invariant mass μ

[4] The removal of vertex operators and the restriction to states built from $\partial_- \phi$ is quite similar to the construction of the "Dirichlet basis" discussed in [69].

as a continuous parameter defining a multiplet of Casimir eigenstates for each operator.

After constructing the basis, the next step is to work out Hamiltonian matrix elements. Since $P_+^{(\mathrm{CFT})}$ vanishes in our basis, the full lightcone Hamiltonian only has contributions from the relevant deformations,

$$\boxed{P_+ = \int dx^- \left(\frac{1}{2}m^2\phi^2 + \frac{1}{4!}\lambda\phi^4\right).} \tag{3.2.12}$$

We can compute the Hamiltonian matrix elements by Fourier transforming three-point functions involving ϕ^2 and ϕ^4, following eq. (3.2.4). Because these relevant deformations are *not* primary operators, their three-point functions are not simply a universal kinematic factor multiplied by an overall OPE coefficient. Fortunately, their correlation functions can all easily be computed via Wick contractions. The resulting matrix elements are presented in appendix 3.8.

3.2.3 Review of Spectral Densities

After we have truncated the basis to some $\mathcal{C}_{\max}$ and computed the associated Hamiltonian matrix elements, we can construct the invariant mass operator

$$M^2 = 2P_+P_-. \tag{3.2.13}$$

Because our basis consists of P_- eigenstates, diagonalizing this Lorentz invariant operator is actually equivalent to diagonalizing the lightcone Hamiltonian P_+.

The mass eigenvalues that result from diagonalizing M^2 are an approximation to the spectrum of the IR QFT. However, in addition to the eigenvalues, we also obtain the associated eigenstates $|\mu_i\rangle$, which we can use to compute dynamical IR observables. One natural and important observable for us to study is the spectral density of any local operator $\mathcal{O}(x)$,

$$\rho_{\mathcal{O}}(\mu) \equiv \sum_i |\langle \mathcal{O}(0)|\mu_i\rangle|^2\, \delta(\mu^2 - \mu_i^2). \tag{3.2.14}$$

As shown in eq. (3.1.1), spectral densities encode the same information as real-time, infinite-volume correlation functions. For presenting results, it will be more convenient

to show the integrated spectral density,

$$I_{\mathcal{O}}(\mu) \equiv \int_0^{\mu^2} d\mu'^2\, \rho_{\mathcal{O}}(\mu') = \sum_{\mu_i \leq \mu} |\langle \mathcal{O}(0)|\mu_i\rangle|^2, \tag{3.2.15}$$

which contains the same dynamical information as the spectral density.

3.3 Sanity Checks

In this section, we perform two consistency checks of our conformal truncation method. First, we consider the free field theory limit, $\bar{\lambda} = 0$, and verify that our numerical results for ϕ^n spectral densities match the theoretical predictions. Second, we confirm that the equation of motion and the stress-energy tensor Ward identity are satisfied identically in our framework for any $\bar{\lambda}$, even after truncation.

3.3.1 Spectral Densities in Free Field Theory

Here we consider free massive field theory, obtained by setting $\bar{\lambda} = 0$. In this limit, Hamiltonian matrix elements are diagonal with respect to particle number, which means that we can consider each n-particle sector independently. For each sector, we truncate the basis to some Δ_{max} (or equivalently $\mathcal{C}_{\text{max}}$), diagonalize the lightcone Hamiltonian, and use the resulting approximate mass eigenstates to compute the spectral density of the corresponding scalar operator ϕ^n.

As examples, figure 4.1 shows the integrated spectral densities for ϕ^2, ϕ^3, ϕ^4, and ϕ^5. In each plot, the blue dots are our conformal truncation results and the black line is the theoretical prediction, given by [103]

$$\begin{aligned}\rho_{\phi^n}(\mu) = \frac{n!}{2^n \pi^{n+1}} \int_0^\infty dr\, r K_0(\mu r) \\ \times \Big[2K_0(mr)^n - \big(K_0(mr) + i\pi I_0(mr)\big)^n - \big(K_0(mr) - i\pi I_0(mr)\big)^n\Big],\end{aligned} \tag{3.3.1}$$

where I_0 and K_0 are modified Bessel functions of the first and second kind.

The main plot shows the raw value for the integrated spectral density, while the inset shows the same result normalized by the prediction. For each plot, we also indicate the number of n-particle basis states for the corresponding choice of Δ_{max}. For example, for ϕ^2 we set $\Delta_{\text{max}} = 100$, meaning we have kept all 2-particle states with $\Delta \leq 100$, which

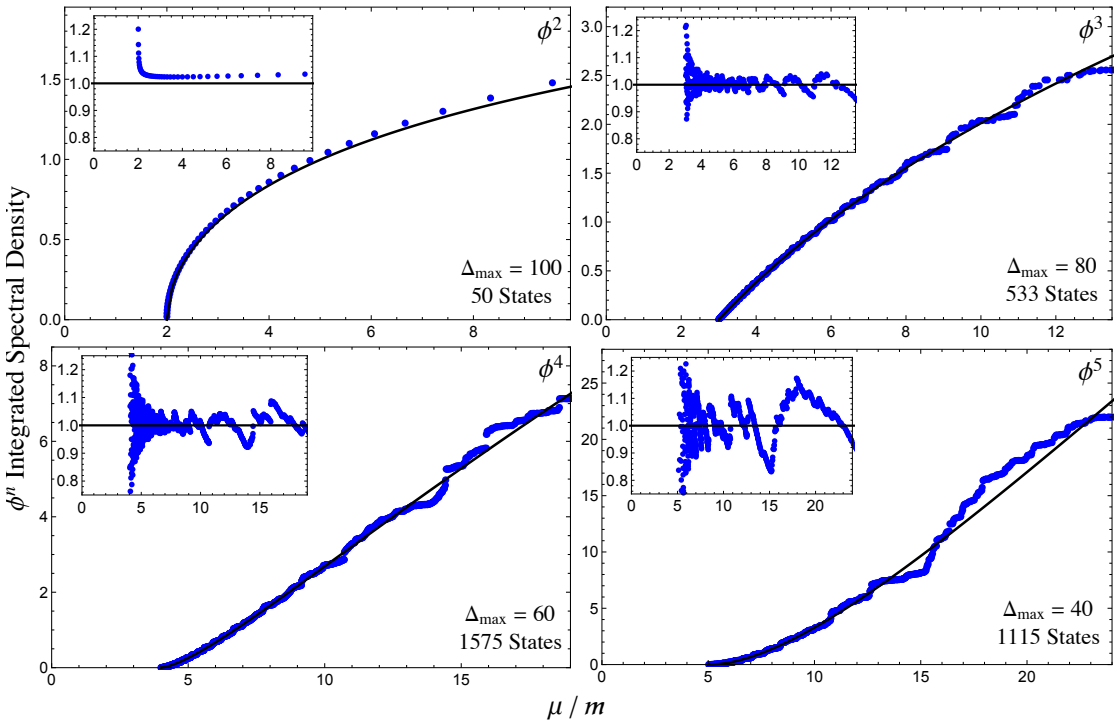

Figure 3.1: Integrated spectral densities for ϕ^2 (upper left), ϕ^3 (upper right), ϕ^4 (lower left), and ϕ^5 (lower right) in massive free field theory ($\bar{\lambda} = 0$), both the raw value (main plot) and normalized by the theoretical prediction (inset). The conformal truncation results (blue dots) for each plot are computed using the Δ_{max} shown, with the corresponding number of n-particle basis states, and compared to the theoretical prediction (black curve).

corresponds to a total of 50 states.

As is evident from the figure, the conformal truncation results correctly reproduce the theoretical expectations for these spectral densities. Similar plots can also be made for ϕ^n with $n > 5$. These plots serve as both a consistency check of our method, ensuring that our basis states and matrix elements have been constructed correctly, as well as a demonstration that our conformal truncation approach can be used to compute full correlation functions.

From the insets in figure 4.1, we see that the numerical results agree with the full functional form of the spectral density to within a few percent over a wide range of μ. The discrepancy slowly begins to increase in the UV, confirming that our basis of primary operators with low conformal Casimir predominantly overlaps with low-mass states [104]. The discrepancy also grows rapidly near the IR threshold $\mu \approx nm$. This is due to the fact that we have truncated to a discrete basis, giving rise to an effective IR

cutoff (see appendix 3.9),

$$\Lambda_{\text{IR}} \sim \frac{m}{\Delta_{\text{max}}}. \tag{3.3.2}$$

Increasing Δ_{max} lowers this effective cutoff, improving our ability to resolve IR mass scales.

3.3.2 Equation of Motion and Ward Identity

In our framework, both the equation of motion (EOM) and the Ward identity for the stress-energy tensor can be phrased as constraints on certain matrix elements of the invariant mass operator M^2. It is convenient to specifically focus on the dynamical part of these matrix elements, $\mathcal{M}_{\mathcal{O}\mathcal{O}'}$, with the overall momentum-conserving delta function removed,

$$\langle \mathcal{C}, P_- | M^2 | \mathcal{C}', P'_- \rangle \equiv 2P_-(2\pi)\delta(P_- - P'_-)\, \mathcal{M}_{\mathcal{O}\mathcal{O}'}. \tag{3.3.3}$$

To derive the matrix element constraints imposed by the EOM, we start with the equation in operator form and act on the vacuum to obtain the relation

$$M^2\phi(0)|0\rangle = m^2\phi(0)|0\rangle + \frac{1}{3!}\lambda\phi^3(0)|0\rangle. \tag{3.3.4}$$

We now act on both sides with an arbitrary basis state $\langle \mathcal{C}, P_-|$, obtaining the constraint

$$\mathcal{M}_{\mathcal{O},\partial\phi} = m^2\langle \mathcal{C}, P_-|\phi(0)\rangle + \frac{1}{3!}\lambda\langle \mathcal{C}, P_-|\phi^3(0)\rangle. \tag{3.3.5}$$

The left side of this equation is an M^2 matrix element mixing the one-particle state with a generic basis state created by any primary operator $\mathcal{O}$. The EOM thus relates this matrix element to the overlap that the $\mathcal{O}$ basis state has with ϕ and ϕ^3. Using the matrix elements presented in appendix 3.8, it is straightforward to check that eq. (3.3.5) indeed holds for any state in our basis. Since the EOM is satisfied at the level of individual matrix elements, it holds exactly for the resulting mass eigenstates, regardless of how we truncate the basis.

The EOM is a useful warmup for the stress-energy tensor Ward identity,

$$P^\mu T_{\mu\nu} = P_+ T_{--} + P_- T_{+-} = 0. \tag{3.3.6}$$

In 2D ϕ^4 theory, the momentum generators are defined as

$$P_- \equiv \int dx^- \left(\partial_- \phi\right)^2, \qquad P_+ \equiv \int dx^- \left(\frac{1}{2} m^2 \phi^2 + \frac{1}{4!}\lambda\phi^4\right). \tag{3.3.7}$$

Given these integral expressions for $P_\pm$, by the Noether construction one would naïvely expect the components T_{--} and T_{+-} to be given by the corresponding integrands. While this expectation is correct for T_{--},[5]

$$T_{--} \equiv \left(\partial_- \phi\right)^2, \tag{3.3.8}$$

it is *not* true for T_{+-}. This subtlety in defining the stress tensor arises from the fact that the scalar field ϕ is not a well-defined primary operator.

To see this concretely, consider the OPE of T_{--} with a general scalar primary operator $\mathcal{O}$ in any 2D CFT,

$$T_{--}(x)\mathcal{O}(y) \sim \frac{-\Delta_\mathcal{O}}{4\pi(x^- - y^-)^2}\mathcal{O}(y) - \frac{1}{2\pi(x^- - y^-)}\partial_-\mathcal{O}(y) + \cdots \tag{3.3.9}$$

where the remaining terms in the expansion are not singular. For the operator ϕ^4, however, we instead have the peculiar expansion

$$T_{--}(x)\phi^4(y) \sim \frac{3}{4\pi^2(x^- - y^-)^2}\phi^2(y) - \frac{1}{2\pi(x^- - y^-)}\partial_-\phi^4(y) + \cdots \tag{3.3.10}$$

Thus ϕ^4 can give rise to ϕ^2, such that the distinction between the two operators is muddied.

We can use the Ward identity to determine the correct form of T_{+-}. Using the OPE, one can check explicitly that eq. (3.3.6) requires

$$\boxed{T_{+-} \equiv \frac{1}{2} m^2 \phi^2 + \frac{1}{4!}\lambda\phi^4 + \frac{1}{16\pi}\lambda\phi^2.} \tag{3.3.11}$$

[5] Note that our definition of T_{--} differs from the standard one (in e.g. [105]) by a factor of 2π.

While there is a discrepancy between this expression for T_{+-} and the integrand of P_+, this appears to be an unavoidable pathology of 2D scalar field theory due to the fact that we have chosen to deform the UV CFT by an ill-defined operator.

Nevertheless, we can confirm that the expression for T_{+-} above is correct by studying the matrix element constraints imposed by the Ward identity. Following the same procedure as the EOM, the Ward identity implies

$$\mathcal{M}_{\mathcal{O},(\partial\phi)^2} = \sqrt{48\pi}\langle \mathcal{C}, P_- | T_{+-}(0)\rangle, \tag{3.3.12}$$

which constrains matrix elements involving the two-particle state created by $(\partial_-\phi)^2$. Using the matrix elements in appendix 3.8, one can check that this constraint is only satisfied if we use the expression for T_{+-} in eq. (3.3.11). This consistency check is important, as we later use this expression to study the stress tensor spectral density in section 3.5.

3.4 Critical Coupling for ϕ^4 Theory

In order to study the RG flow from scalar field theory to the 2D Ising model, we need to determine the critical coupling, $\bar{\lambda}_*$. To do so, we scan over $\bar{\lambda}$, diagonalizing the Hamiltonian for each value of the coupling to obtain the mass spectrum, and look for the following indicators of critical behavior:

- **Vanishing mass gap**. Since in lightcone quantization the vacuum is trivial [106, 107], the mass gap is simply the lowest mass eigenvalue. The critical coupling should therefore correspond to the point at which the lowest eigenvalue goes to zero.

- **Continuous spectrum**. At weak coupling, the lowest eigenvalue corresponds to the one-particle state, which is separated from the two- and three-particle thresholds. At the critical coupling, not only should the lowest eigenvalue hit zero, but this spacing between eigenvalues should also vanish, providing an important consistency check that we have successfully tuned to the critical point.

In this section, we use these criteria to determine the value of the critical coupling. We study the mass spectrum as a function of $\bar{\lambda}$ at various finite values for Δ_{max} and then

extrapolate the results to the limit $\Delta_{\text{max}} \to \infty$ to calculate $\bar{\lambda}_*$. We then compare the value we obtain with previous results and briefly discuss the mapping between critical couplings in lightcone quantization with those in more standard equal-time quantization.

3.4.1 Tuning to the Critical Point

To start, let us look at how the lowest mass eigenvalues depend on the coupling $\bar{\lambda}$. To do so, we truncate our conformal basis to some fixed Δ_{max}, keeping all states below this threshold, then diagonalize the lightcone Hamiltonian for various values of $\bar{\lambda}$. Note that, unlike for the free field theory results in section 4.4, here we include *all* basis states with $\Delta \leq \Delta_{\text{max}}$, regardless of particle number. Because each insertion of $\partial_- \phi$ in a primary operator increases the scaling dimension by 1, this means we include states with up to $n = \Delta_{\text{max}}$ particles.

Because we are only deforming our CFT by the even operators ϕ^2 and ϕ^4, the resulting spectrum can be divided into two independent sectors, depending on whether the eigenstates are odd or even under the $\mathbb{Z}_2$ transformation $\phi \to -\phi$. In the following discussion, we identify the eigenvalues in these two sectors with the notation $\mu^2_{i,\text{odd/even}}$, where the label $i = 1, 2, \ldots$ indicates the magnitude of the eigenvalue, with $i = 1$ corresponding to the lowest eigenvalue in the respective $\mathbb{Z}_2$ sector.

Figure 3.2 shows the lowest mass eigenvalues $\mu^2_{1,\text{odd}}$, $\mu^2_{1,\text{even}}$, and $\mu^2_{2,\text{odd}}$ as functions of $\bar{\lambda}$ for $\Delta_{\text{max}} = 34$, which corresponds to a basis of 12,310 states (the maximum truncation level we consider in this work). As we can see, at $\bar{\lambda} = 0$ these eigenvalues correspond to the 1-, 2-, and 3-particle thresholds, respectively. As the coupling $\bar{\lambda}$ increases, all three of these eigenvalues begin to decrease, eventually reaching zero.[6]

Notice in figure 3.2 that the eigenvalues go to zero at *distinct* values of $\bar{\lambda}$. This is clearly incorrect, as we expect the mass gap and the spacing between eigenvalues to all vanish at the same critical coupling. The discrepancy is due to truncation error, that is, a consequence of restricting our basis to finite Δ_{max}. We expect (and demonstrate below) that the discrepancy disappears in the limit $\Delta_{\text{max}} \to \infty$.

Even at finite Δ_{max}, though, our truncated data places a preliminary bound on the

[6] In particular, the mass eigenvalues cross zero and become negative. This is a signature of spontaneous symmetry-breaking in lightcone quantization [81]. In this work, we focus exclusively on the symmetry-preserving side of the critical point, leaving an analysis of the symmetry-broken phase for future work.

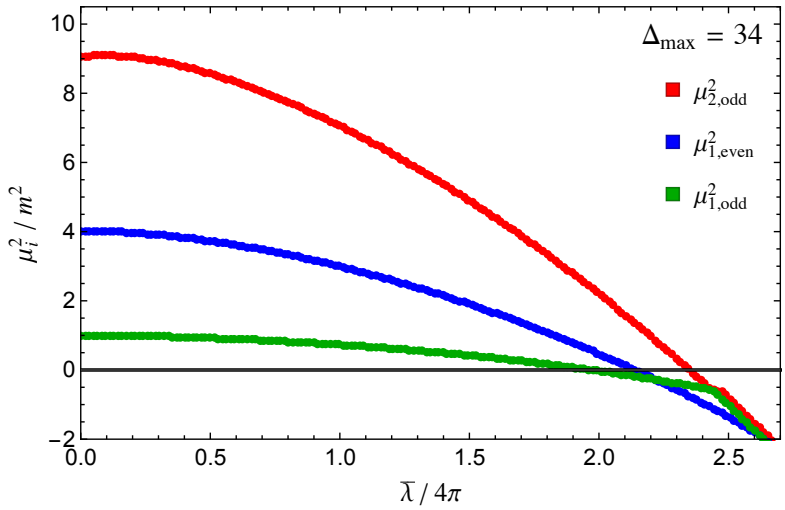

Figure 3.2: The two lowest mass eigenvalues in the odd sector and the lowest eigenvalue in the even sector as a function of $\bar{\lambda}$ for $\Delta_{\max} = 34$ (12,310 basis states).

critical coupling, $\bar{\lambda}_*$. Hamiltonian truncation is a type of variational method, which means that at any $\bar{\lambda}$ the lowest eigenvalue ($\mu^2_{1,\text{odd}}$) always places an *upper bound* on the true mass gap. This in turn means that, for any finite $\Delta_{\max}$, the lowest eigenvalue reaches zero at a coupling strictly above the actual critical coupling. We can thus use the $\Delta_{\max} = 34$ data to obtain the conservative bound

$$\boxed{\frac{\bar{\lambda}_*}{4\pi} \leq 1.98.} \tag{3.4.1}$$

To obtain the correct value for $\bar{\lambda}_*$, we would like to extrapolate in $\Delta_{\max}$. To do this, we need to determine how the spectrum varies with $\Delta_{\max}$. At fixed $\bar{\lambda}$, we find that the dependence of the lowest eigenvalues on $\Delta_{\max}$ is well modeled by

$$\mu_i^2(\Delta_{\max}) = A + \frac{B}{\Delta_{\max}^n}, \tag{3.4.2}$$

where the parameters A, B, and n are $\bar{\lambda}$-dependent. In particular, the exponent n tells us how quickly the truncation result for μ_i^2 converges with $\Delta_{\max}$. We find experimentally that n decreases monotonically with increasing $\bar{\lambda}$, starting with $n \approx 2$ at weak coupling and reaching $n \approx 1$ near the critical point. This behavior for n can be understood as a consequence of the Hamiltonian matrix elements' dependence on $\Delta_{\max}$, as we discuss in appendix 3.9. By fixing $\bar{\lambda}$ and varying $\Delta_{\max}$, we find the best fit for each mass eigenvalue μ_i^2. The resulting parameter A provides the extrapolated value of μ_i^2 for that particular

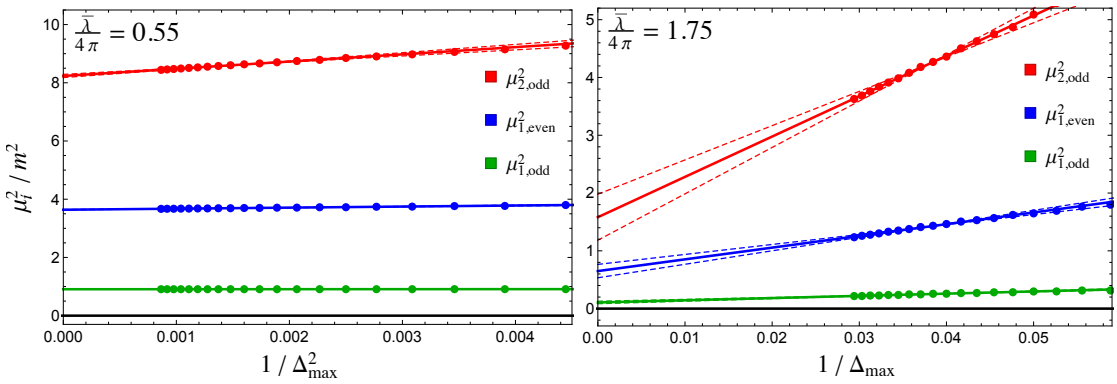

Figure 3.3: Two examples of the dependence of $\mu_{1,\text{odd}}^2$ (green), $\mu_{1,\text{even}}^2$ (blue), and $\mu_{2,\text{odd}}^2$ (red) on Δ_{max}, at fixed $\frac{\bar{\lambda}}{4\pi} = 0.55$ (left) and $\frac{\bar{\lambda}}{4\pi} = 1.75$ (right). The solid lines show the best fit for each $\mu_i^2(\Delta_{\text{max}})$ to the functional form in eq. (3.4.2), with the resulting powers $n = 2.0$ (left) and $n = 1.0$ (right). The y-intercept for each fit provides the extrapolated value of μ_i^2 for $\Delta_{\text{max}} \to \infty$, and the error is estimated by varying the slope by 15% about the mean of the data points.

$\bar{\lambda}$ in the limit $\Delta_{\text{max}} \to \infty$.

Figure 3.3 shows two examples of this procedure, one at $\frac{\bar{\lambda}}{4\pi} = 0.55$ and the other at $\frac{\bar{\lambda}}{4\pi} = 1.75$. The data points show the resulting values for $\mu_{1,\text{odd}}^2$, $\mu_{1,\text{even}}^2$, and $\mu_{2,\text{odd}}^2$ at different Δ_{max}. The solid lines show the best fit for each $\mu_i^2(\Delta_{\text{max}})$, and the resulting y-intercept provides the extrapolated value as $\Delta_{\text{max}} \to \infty$. For the first example, which is clearly far from the critical point, we find that the corrections at finite Δ_{max} fall as $1/\Delta_{\text{max}}^n$ with $n = 2.0$. The second example is much closer to criticality, and the results thus converge more slowly, with $n = 1.0$.

The deviations of the data points from the best-fit curve are highly correlated, since increasing Δ_{max} does not actually change any of the Hamiltonian matrix elements and instead just adds new ones. This correlation between data points makes it more difficult to determine the uncertainty in the extrapolated values for μ_i, and standard estimates which ignore the correlation will typically underestimate the error in the resulting extrapolation. Rather than perform a detailed analysis of the uncertainty, we provide a simple estimate by varying the slope of the best fit line by 15% about the mean of the data points, which corresponds to the dashed lines in figure 3.3.

Carrying out this procedure for each $\bar{\lambda}$, we are able to construct the $\Delta_{\text{max}} \to \infty$ extrapolation for the lowest eigenvalues, shown in figure 3.4. This plot is the analogue of figure 3.2, showing the extrapolated values for $\mu_{1,\text{odd}}^2$, $\mu_{1,\text{even}}^2$, and $\mu_{2,\text{odd}}^2$ as a function of $\bar{\lambda}$. We see that, unlike at finite Δ_{max}, all three eigenvalues reach zero at the same $\bar{\lambda}$,

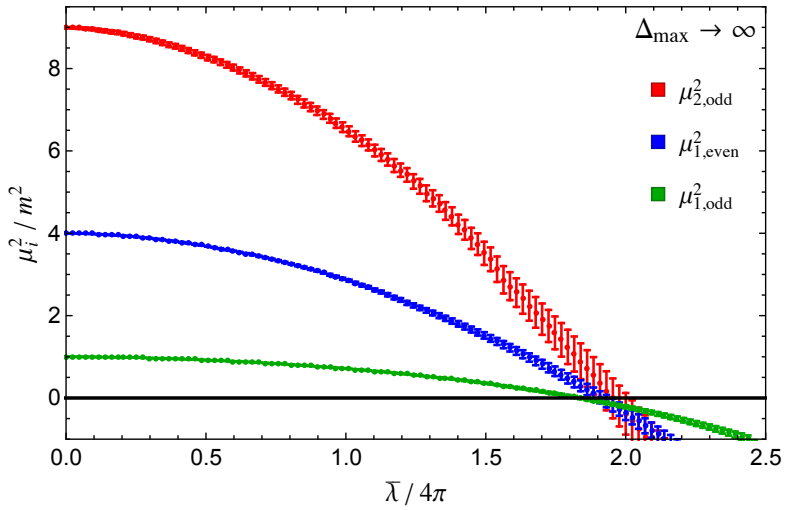

Figure 3.4: The two lowest mass eigenvalues in the odd sector and the lowest eigenvalue in the even sector as a function of $\bar{\lambda}$ in the extrapolated limit $\Delta_{\max} \to \infty$.

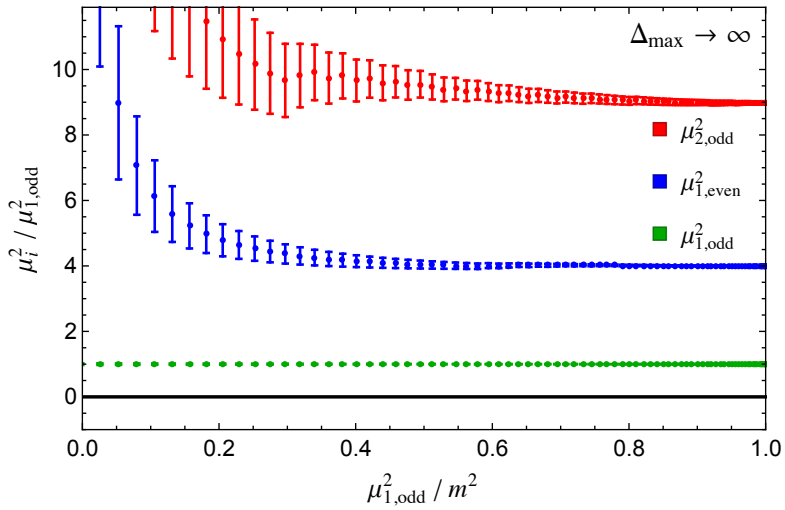

Figure 3.5: The ratio of two lowest mass eigenvalues in the odd sector and the lowest eigenvalue in the even sector to the mass gap as a function of $\mu^2_{1,\text{odd}}$ in the extrapolated limit $\Delta_{\max} \to \infty$.

to within the error bars.

We can now use these extrapolated eigenvalues to determine the critical coupling. Our best estimate clearly comes from the lowest eigenvalue, $\mu^2_{1,\text{odd}}$, which has the least uncertainty in its extrapolation. By measuring the point at which this eigenvalue reaches zero, we obtain the prediction

$$\boxed{\frac{\bar{\lambda}_*}{4\pi} = 1.84 \pm 0.03.} \tag{3.4.3}$$

As another simple check of this extrapolation, figure 3.5 shows the extrapolated ratios of the eigenvalues $\mu^2_{1,\text{even}}$ and $\mu^2_{2,\text{odd}}$ to the mass gap $\mu^2_{1,\text{odd}}$, as a function of the gap. We see that, although the eigenvalues themselves change significantly, their ratios appear to remain fixed at the free field values of 1, 4, and 9, corresponding to the one-, two-, and three-particle thresholds. This matches our expectation that there should be no bound states in ϕ^4 theory.

However, the ratios begin to deviate from the expected values as we near the critical point, indicating that the one-particle state still reaches zero before the two- and three-particle thresholds. This deviation is due to the fact that we have extrapolated these ratios from results with finite Δ_{max}, which limits our IR resolution. These ratios thus provide a useful indicator of the approximate scale of our IR cutoff.

3.4.2 Comparison with Prior Work

The critical coupling of 2D ϕ^4 theory has been studied previously using a variety of computational methods in both lightcone [71, 72, 73] and equal-time quantization [74, 75, 76, 77, 78, 79]. As we briefly summarize below, the value of the critical coupling is dependent on the choice of quantization scheme, such that mapping between the lightcone and equal-time values is rather difficult. We do not attempt a comparison with equal-time results in this work, since it is somewhat tangential to our main goal, and instead focus on comparing our result for $\bar{\lambda}_*$ with values from other lightcone methods. While $\bar{\lambda}_*$ is certainly an important intermediate result of this work, ultimately we are interested in computing physical observables like correlation functions which, unlike the critical coupling, are independent of quantization scheme.

The first study of the critical coupling in lightcone quantization appeared in [71, 72]. This work used the method of discretized lightcone quantization (DLCQ) [108, 109, 110], which is a Hamiltonian truncation method where the underlying QFT Hilbert space is discretized by compactifying the "spatial" lightcone direction x^-. More recently, the critical coupling was studied in [73] using a Hamiltonian truncation method with a basis of symmetric polynomials in momentum space. These results for the critical coupling, along with ours, are summarized below:

Lightcone Method	$\bar{\lambda}_*/(4\pi)$
DLCQ [72]	2.6
Symmetric polynomials [73]	$2.1 \pm .05$
Conformal truncation (this work)	$1.84 \pm .03$

Our extrapolated value for the critical coupling is somewhat lower than the values obtained in both [72] and [73]. There is also some tension between these previous results and our data even before we perform any extrapolation in Δ_{max}. Recall from our discussion above that conformal truncation is a variational method, so that our $\Delta_{\text{max}} = 34$ data places an explicit upper bound on the value of the critical coupling, $\frac{\bar{\lambda}_*}{4\pi} \leq 1.98$. The values reported in [72, 73] are centered above this bound.

Ref. [72] is an older work and does not report error bars, so it is difficult to ascertain the precision of this result for comparison. As for [73], their basis of symmetric polynomials has a one-to-one map to the basis states we use in this work (see appendix 3.7). For this particular theory, our methods are thus completely equivalent in practice, although there are minor technical differences in actual implementation. The maximum basis size considered in [73] consists of 226 total states and corresponds to a subset of our $\Delta_{\text{max}} = 18$ basis. For our results, we have constructed the basis up to $\Delta_{\text{max}} = 34$, which consists of 12,310 states. It is thus possible that the uncertainty in these previous results is somewhat larger than initially estimated, which would allow for compatibility with our higher Δ_{max} results.

Comparison with equal-time results is more subtle, because the value of the critical coupling is quantization scheme dependent. The difference between the two schemes can be seen most easily at the level of Feynman diagrams: there exist mass-renormalization diagrams due to the coupling $\bar{\lambda}$ that appear in equal-time quantization but vanish in lightcone quantization [111]. A given value of the bare coupling $\bar{\lambda}$ thus clearly leads to different physical masses in the two quantization schemes. In principle, it should be possible to resum the missing diagrams in order to convert between lightcone and equal-time results, and ref. [73] proposes such a method. This prescription, however, is inherently non-perturbative due to the need to account for an infinite class of diagrams. While outside the scope of this current work, it would be very interesting and instructive to perform a careful matching between lightcone and equal-time data and to compare

our results to those reported in [74, 75, 76, 77, 78, 79].

3.5 Ising Model Near Critical Temperature

Now that we have confirmed the existence of a critical point and determined the corresponding critical coupling, $\bar{\lambda}_*$, we can turn to the main focus of this work: computing dynamical observables, namely spectral densities, in the vicinity of the fixed point. This IR fixed point is described by the 2D Ising model near the critical temperature T_c,

$$\mathcal{L} = \frac{1}{2}\partial^\mu\phi\partial_\mu\phi - \frac{1}{2}m^2\phi^2 - \frac{1}{4!}\lambda\phi^4 \quad \Rightarrow \quad \mathcal{L}_{\text{Ising}} - m_{\text{gap}}\epsilon, \tag{3.5.1}$$

where the arrow denotes RG flow to the IR. Here $m_{\text{gap}} \to 0$ as $\bar{\lambda} \to \bar{\lambda}_*$, and the deformation by ϵ is equivalent to moving the Ising model away from the critical temperature T_c, with $m_{\text{gap}} \sim |T - T_c|$. This IR theory is famously integrable, such that one can compute its spectral densities analytically. In this section, we use conformal truncation to compute spectral densities in ϕ^4 theory for any $\bar{\lambda}$, then verify that near $\bar{\lambda}_*$ they match the known analytic results for the Ising model, allowing us to test our method in a strongly-coupled example.

Recall that we compute spectral densities by first truncating the basis to some Δ_{max} and then numerically diagonalizing the resulting lightcone Hamiltonian matrix to obtain the approximate mass eigenstates $|\mu_i\rangle$. The integrated spectral density of any operator is then given by eq. (4.3.25).

Specifically, we compute and study the spectral densities of the stress-energy tensor $T_{\mu\nu}$ and the scalar operators ϕ^n. These operators are all initially defined in the UV. For the stress tensor, we can study the spectral densities of individual components. A particularly interesting component is T_{+-}, which in 2D is proportional to the trace,

$$T^\mu{}_\mu = 2T_{+-}.$$

The theoretical prediction for this particular component is that near criticality

$$T_{+-} \Rightarrow m_{\text{gap}}\epsilon. \tag{3.5.2}$$

Note that this vanishes at the critical coupling, since $m_{\text{gap}} \to 0$. By computing the spectral density of T_{+-}, we are thus able to explicitly check whether the stress tensor is traceless at $\bar{\lambda}_*$, which determines whether the critical point corresponds to a CFT. The ability to study the RG flow of the stress tensor is a particularly useful feature of conformal truncation, as other non-perturbative methods typically break translation invariance, making it difficult to reproduce the stress tensor.

For the ϕ^n operators, the expectation is that near criticality their IR description will be in terms of the leading operators in the Ising model, namely, σ (the lowest $\mathbb{Z}_2$-odd operator) and ϵ (the lowest $\mathbb{Z}_2$-even operator). Near the critical point $\bar{\lambda}_*$, we thus expect the *universal* behavior

$$\phi, \phi^3, \phi^5, \ldots \Rightarrow \sigma, \qquad \phi^2, \phi^4, \phi^6, \ldots \Rightarrow \epsilon. \tag{3.5.3}$$

In other words, we expect that near $\bar{\lambda}_*$ the $\mu \to 0$ behavior of the spectral densities ρ_{ϕ^n} will approach the known expressions for ρ_σ or ρ_ϵ, depending on parity.

While not technically an independent degree of freedom (due to the Ward identity), the component T_{--} of the stress tensor is also a useful observable. Its integrated spectral density is equivalent to the Zamolodchikov C-function, which measures the change in central charge between the UV and IR fixed points and is an intrinsic feature of the intermediate RG flow. Using conformal truncation, we can compute the C-function at any coupling $\bar{\lambda}$. Compared to T_{+-} and ϕ^n, however, it is more difficult to extract the Ising model behavior near criticality from T_{--} due to its sensitivity to corrections from UV physics, as we discuss.

3.5.1 Trace of the Stress-Energy Tensor

To begin, let us consider the trace of the stress-energy tensor. In 2D, the trace is proportional to the component T_{+-}, which for ϕ^4 theory takes the form (see section 4.4)

$$T_{+-} = \frac{1}{2}m^2\phi^2 + \frac{1}{4!}\lambda\phi^4 + \frac{1}{16\pi}\lambda\phi^2. \tag{3.5.4}$$

Near the critical coupling, we expect T_{+-} to match onto the 2D Ising prediction in the IR. Exact predictions for the Ising model at $T \neq T_c$ are possible, because the theory is integrable and can be described in terms of a free fermion with mass m_{gap}. The Ising

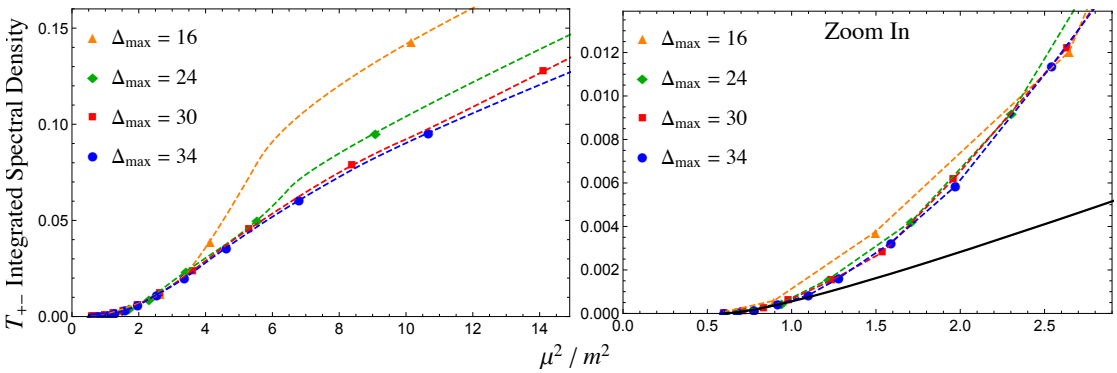

Figure 3.6: Integrated spectral density for T_{+-} at different values of Δ_{max}. The $\Delta_{\text{max}} = 34$ results (blue dots) are at $\frac{\bar{\lambda}}{4\pi} = 1.96$, and the couplings for the remaining results have been chosen such that the mass gap remains fixed. The points are the actual contributions of individual eigenstates to the spectral density, while the dashed lines are interpolations. The right plot is simply a zoomed-in version of the left one, and compares the conformal truncation results to the theoretical IR prediction for the Ising model (black curve).

spectral density for T_{+-} can be computed analytically from its decomposition into Fock space states with two fermions [112],

$$\rho_{T_{+-}}(\mu) = \frac{m_{\text{gap}}^2}{2!}\int \frac{d\theta_1 d\theta_2}{(4\pi)^2}(2\pi)\delta^2(P - p_1 - p_2)\sinh^2\frac{\theta_{12}}{2} = \frac{m_{\text{gap}}^2}{16\pi}\sqrt{1 - \frac{4m_{\text{gap}}^2}{\mu^2}} \quad (T > T_*), \tag{3.5.5}$$

where θ is the rapidity of an individual fermion with $p_\pm = m_{\text{gap}} e^{\pm\theta}$, and $\theta_{ij} \equiv \theta_i - \theta_j$. Near the critical coupling $\bar{\lambda}_*$, we therefore expect the spectral density of T_{+-} to flow to this Ising model prediction in the IR. In particular, recall that $m_{\text{gap}} \to 0$ as $\bar{\lambda} \to \bar{\lambda}_*$, so the spectral density should vanish as we approach criticality, as expected for an IR CFT.

Before comparing the conformal truncation integrated spectral densities with the predictions from the Ising model, we can study their behavior as a function of Δ_{max} to determine how quickly the results converge. When comparing results with different values of Δ_{max}, we have a choice as to which parameter to hold fixed. One obvious choice is to fix the coupling $\bar{\lambda}$ (as we did in the extrapolations in section 3.4), in which case the IR scale m_{gap} will vary as we increase Δ_{max}. Alternatively, we can hold m_{gap} fixed and vary $\bar{\lambda}$. Because we are specifically interested in studying IR dynamics, we choose the latter option, keeping m_{gap} fixed in order to study the convergence of our results relative to this physical IR scale.

Figure 3.6 shows our truncation results for the integrated spectral density of T_{+-} at

four different values of Δ_{max}. The results with the highest truncation level, $\Delta_{\text{max}} = 34$, are at $\frac{\bar{\lambda}}{4\pi} = 1.96$. For the results with lower Δ_{max}, the couplings have thus been chosen to ensure that in each case the mass gap matches that of the $\Delta_{\text{max}} = 34$ spectrum.

As we can see, the $\Delta_{\text{max}} = 34$ results appear to have converged across a wide range of mass scales, suggesting that these results are successfully computing the true spectral densities. Moreover, we see that conformal truncation appears to reconstruct the spectral densities from the IR up, such that even $\Delta_{\text{max}} = 16$ is an accurate approximation to the low-energy dynamics. This behavior appears to confirm our intuition that states with low conformal Casimir in the UV provide the dominant contribution to low-mass states, even at strong coupling.

In the right plot of figure 3.6, we compare our truncation results to the theoretical prediction for the Ising model (black curve). This analytic expression only has one unknown parameter, m_{gap}, which is fixed by setting the lowest eigenvalue $\mu^2_{1,\text{even}} = 4m^2_{\text{gap}}$. In the IR, the conformal truncation results clearly match both the scaling and overall coefficient of the Ising model prediction.

It is worth emphasizing that the correspondence between ϕ^4 theory and Ising model spectral densities should only hold in the deep IR. At higher energy scales μ^2, these theories are not equivalent and thus have distinct spectral densities, which is precisely what we observe in figure 3.6.

Figure 3.7 shows the $\Delta_{\text{max}} = 34$ results for the T_{+-} spectral density at multiple values of $\bar{\lambda}$ near the critical point, again compared to the theoretical prediction from the Ising model. As a rough estimate of the convergence, we have included an envelope surrounding the truncation results whose width corresponds to the difference between these results and those at $\Delta_{\text{max}} = 30$. We see that the spectral density correctly reproduces the Ising model prediction in the IR over a range of couplings. Most importantly, the resulting IR density *vanishes* as $m_{\text{gap}} \to 0$, clearly indicating that the critical theory is described by a CFT.

While this is not surprising, as we already know that the critical point of ϕ^4 theory should be described by the 2D Ising model, this example demonstrates the utility of spectral densities in analyzing the low-energy behavior of strongly-coupled theories. For more general RG flows, where the IR description is unknown, seeing the trace of the stress tensor vanish in conjunction with the mass gap confirms that the UV theory flows

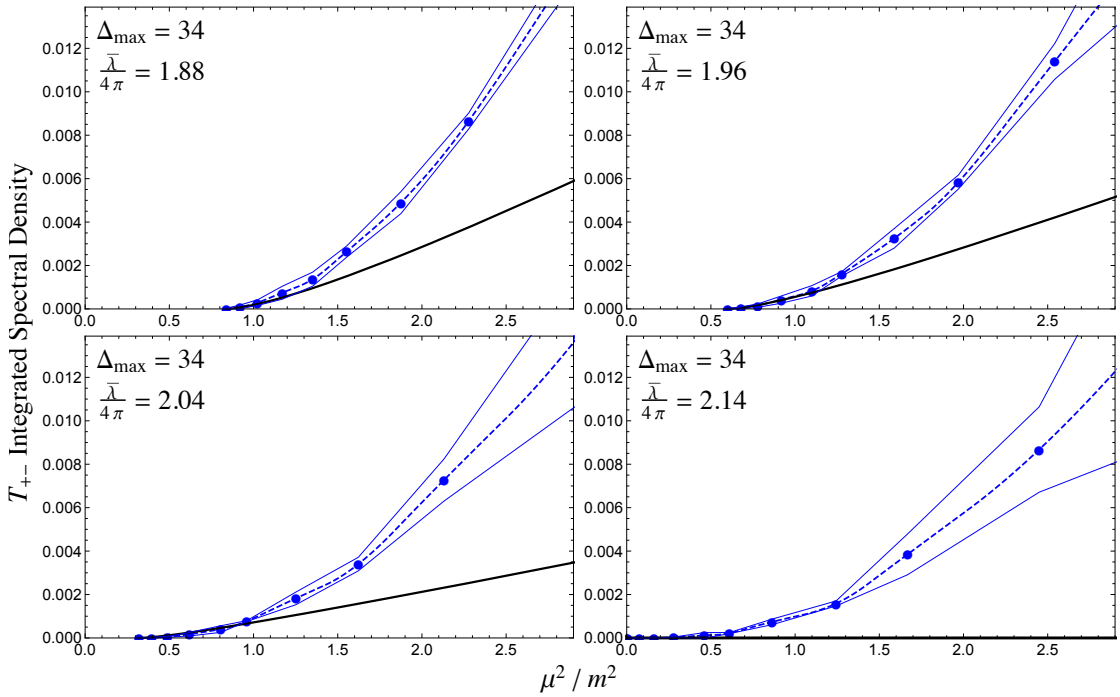

Figure 3.7: Integrated spectral densities for T_{+-}, for $\Delta_{\max} = 34$ and different values of $\bar{\lambda}$, compared to the Ising model prediction (black curve). The thin blue lines indicate the magnitude of the difference between these results and those at $\Delta_{\max} = 30$, providing a rough estimate of the convergence. For reference, the upper right plot corresponds to the same value of the coupling ($\frac{\bar{\lambda}}{4\pi} = 1.96$) as figure 3.6.

to an IR CFT.

The spectral density of the stress tensor trace also clearly delineates which eigenstates correspond to the IR fixed point. As we can see in figure 3.7, the spectral density is zero for roughly the first six points, indicating that these states comprise the IR sector described by the critical Ising model.

3.5.2 Universality in ϕ^n Spectral Densities

Next, we can turn to the scalar operators ϕ^n. Near the critical coupling $\bar{\lambda}_*$, we expect that in the IR these operators will all flow to the lowest dimension operators in the Ising model,

$$\phi^{2n} \Rightarrow \epsilon + \cdots , \quad \phi^{2n-1} \Rightarrow \sigma + \cdots , \tag{3.5.6}$$

where the ellipses denote higher-dimensional operators. We thus expect *universal* behavior in the associated spectral densities as $\mu \to 0$,

$$\rho_{\phi^{2n}}(\mu) \to \rho_\epsilon(\mu), \quad \rho_{\phi^{2n-1}}(\mu) \to \rho_\sigma(\mu) \qquad (\mu \to 0). \tag{3.5.7}$$

The theoretical prediction for the ϵ spectral density is identical to that of T_{+-}, but without the overall factor of m_{gap}^2,

$$\rho_\epsilon(\mu) = \frac{1}{16\pi}\sqrt{1 - \frac{4m_{\text{gap}}^2}{\mu^2}} \qquad (T > T_c). \tag{3.5.8}$$

On the other hand, σ has overlap with all Fock space states with odd numbers of fermions, leading to the more complicated spectral density [113, 114, 115],

$$\rho_\sigma(\mu) = \sum_{n \text{ odd}} \frac{1}{n!} \int \prod_{k=1}^{n} \left(\frac{d\theta_k}{4\pi}\right) (2\pi)\delta^2\Big(P - \sum_k p_k\Big)\, 2^{n-1} \prod_{i \le j} \tanh^2 \frac{\theta_{ij}}{2} \qquad (T > T_c) \tag{3.5.9}$$

However, the contribution of each n-fermion sector begins at $\mu = nm_{\text{gap}}$, which means that in practice we only need to consider the contributions from the states with low fermion number to determine the IR behavior. Moreover, for the mass scales μ^2 that we consider, the overwhelmingly dominant term is the single-fermion contribution, which is a delta function. Thus, the σ integrated spectral density is simply a step function at $\mu^2 = m_{\text{gap}}^2$, with only sub-percent level corrections coming from higher fermion number contributions.

Just like with T_{+-}, we first study the rate of convergence by plotting the ϕ^n spectral densities at various $\Delta_{\max}$ with fixed m_{gap}, as shown in figure 3.8. These plots specifically show ϕ^2 and ϕ^3, with similar results for the other operators. For the highest truncation level, $\Delta_{\max} = 34$, the coupling was fixed to $\frac{\bar{\lambda}}{4\pi} = 1.96$ for ϕ^2 and $\frac{\bar{\lambda}}{4\pi} = 1.69$ for ϕ^3.

We again find that the conformal truncation results converge rather quickly, especially in the IR. The rightmost plots compare the low-mass results to the theoretical predictions for ϵ and σ (black curves). Note that these spectral densities are merely expected to be *proportional* to those of ϵ and σ in the IR, with an unknown $\bar{\lambda}$-dependent overall coefficient for each ϕ^n. These coefficients can be fixed by fitting the overall normalization of the ϕ^n spectral densities to the theoretical predictions. Because we only expect these operators to match the Ising predictions in the IR, we specifically fit the

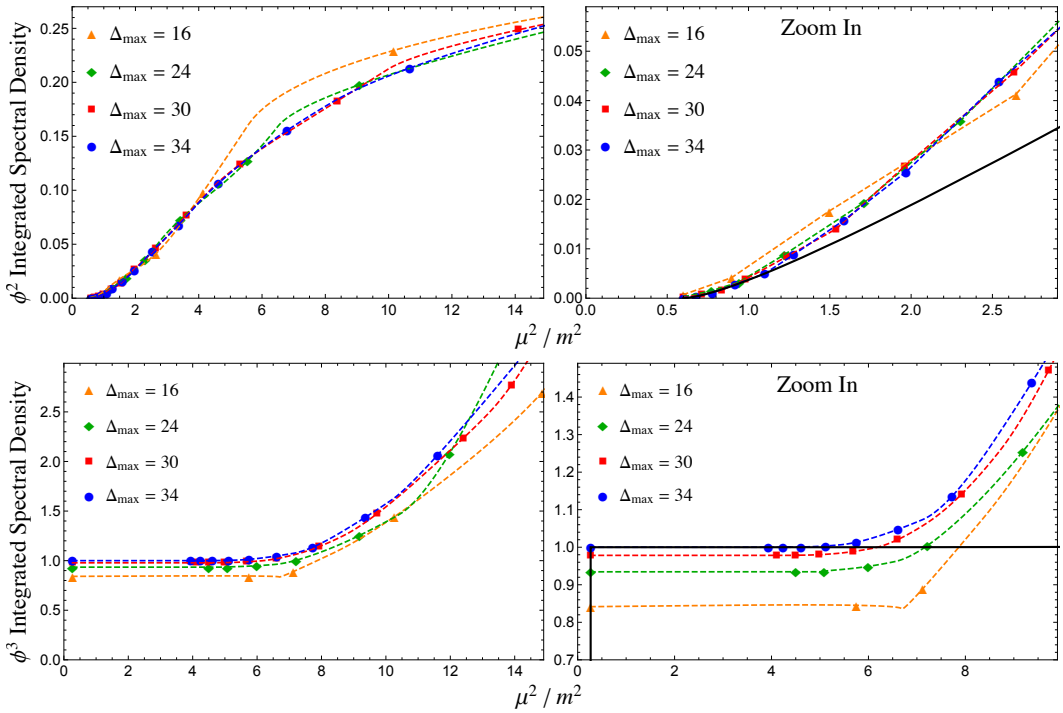

Figure 3.8: Integrated spectral densities for ϕ^2 (top) and ϕ^3 (bottom) at different values of $\Delta_{\max}$. The $\Delta_{\max} = 34$ results (blue dots) are at $\frac{\bar{\lambda}}{4\pi} = 1.96$ (top) and $\frac{\bar{\lambda}}{4\pi} = 1.69$ (bottom), and the couplings for the remaining results have been chosen such that the respective mass gaps remain fixed. The points are the actual contributions of individual eigenstates to the spectral density, while the dashed lines are interpolations. The right plots are simply a zoomed-in version of the left ones, and compare the conformal truncation results to the theoretical IR predictions for ϵ (top) and σ (bottom) in the Ising model.

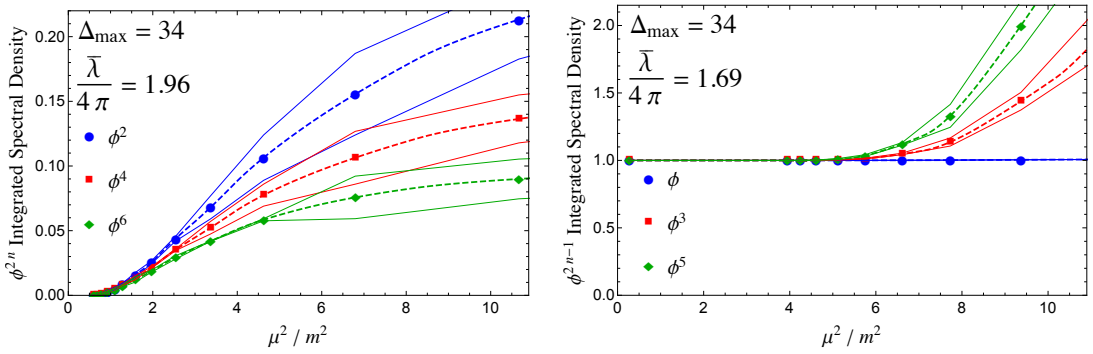

Figure 3.9: Integrated spectral densities for ϕ^2, ϕ^4, and ϕ^6 at $\frac{\bar{\lambda}}{4\pi} = 1.96$ (left) and for ϕ, ϕ^3, and ϕ^5 at $\frac{\bar{\lambda}}{4\pi} = 1.69$ (right), both with $\Delta_{\max} = 34$. The spectral densities in each plot have been rescaled by an overall coefficient such that the first data points match. The thin lines indicate the magnitude of the difference between these results and those at $\Delta_{\max} = 30$, providing a rough estimate of the convergence. In both plots, all three curves converge to the same universal behavior in the IR.

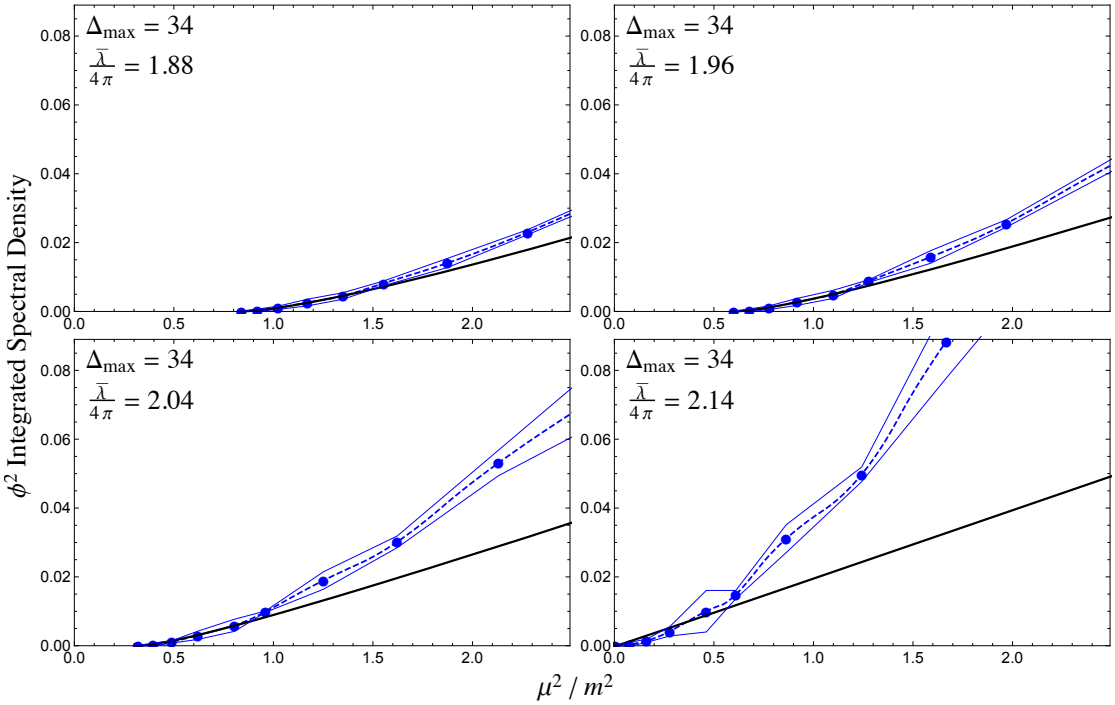

Figure 3.10: Integrated spectral densities for ϕ^2, for $\Delta_{\max} = 34$ and different values of $\bar{\lambda}$, compared to the Ising model prediction for ϵ (black curve). The thin blue lines indicate the magnitude of the difference between these results and those at $\Delta_{\max} = 30$, providing a rough estimate of the convergence. For reference, the upper right plot corresponds to the same value of the coupling ($\frac{\bar{\lambda}}{4\pi} = 1.96$) as figures 3.8 and 3.9.

normalization to the lowest 5 data points. As we can see, both operators match their Ising model predictions at low energies. This is especially noticeable for the ϕ^3 spectral density, which develops a large resonance corresponding to the one-fermion contribution to σ.

Figure 3.9 shows the integrated spectral densities for ϕ^2, ϕ^4, and ϕ^6 (left) and for ϕ, ϕ^3, and ϕ^5 (right). Both plots have $\Delta_{\max} = 34$ and are at the same couplings as figure 3.8. Just like for the stess tensor, we have included an envelope surrounding each spectral density whose width indicates the difference between these results and those at $\Delta_{\max} = 30$. Also, we have again rescaled these results by an overall coefficient, this time such that the very first data points match. In both plots, while the spectral densities are clearly distinct in the UV, they all converge to the same universal behavior in the IR.

This IR universality continues to hold across a range of couplings in the vicinity of $\bar{\lambda}_*$. As an example, figure 3.10 shows the integrated spectral density for ϕ^2 at different values of $\bar{\lambda}$, compared with the ϵ spectral density. While the results match the theoretical

prediction at low energies, the rate of convergence appears to decrease as we push closer to the critical coupling. This is unsurprising, as the resulting spectrum becomes more finely tuned as the mass eigenvalues go to zero, and the truncation results therefore converge more slowly in $\Delta_{\max}$, as we saw in section 3.4.

3.5.3 T_{--} and the Central Charge

Finally, we can consider the stress-energy tensor component $T_{--} \equiv (\partial_- \phi)^2$. The integrated spectral density for this operator is particularly interesting in 2D, because it corresponds to the spectral representation of the Zamolodchikov C-function [116, 117, 118],

$$C(\mu) \equiv \frac{12\pi}{P_-^4} \int_0^{\mu^2} d\mu'^2 \, \rho_{T_{--}}(\mu') = \frac{12\pi}{P_-^4} \sum_{\mu_i \leq \mu} |\langle T_{--}(0)|\mu_i\rangle|^2. \tag{3.5.10}$$

As is well-known, this function monotonically interpolates between the central charges of the UV and IR fixed points. While we can compute $C(\mu)$ for any coupling $\bar{\lambda}$, unfortunately near criticality the Ising model prediction is very sensitive to UV corrections, making the comparison with theory more subtle for this particular observable.

In particular, for RG flows which lead to a non-trivial IR CFT, one could in principle use the spectral density of T_{--} to determine the associated central charge, c_{IR}. In practice, if the IR fixed point is fine-tuned, as in ϕ^4 theory, the resulting truncated spectrum will always have a small but nonzero mass gap. In this case, the C-function will flow to the trivial central charge,

$$C(\mu) \to 0 \text{ as } \mu \to 0 \quad (m_{\text{gap}} \neq 0).$$

If m_{gap} is nevertheless sufficiently small compared to the mass scales of the UV theory, the C-function will still plateau at c_{IR} before eventually falling to zero as $\mu \to 0$. Our ability to extract the IR central charge from the T_{--} spectral density is therefore determined by the size of m_{gap} relative to the other scales characterizing the RG flow.

To be more concrete, the Ising model description of ϕ^4 theory is merely a low-energy effective theory, with an associated cutoff Λ set by the UV parameters m and λ. The stress-energy tensor, and thus the resulting effective Hamiltonian, receive corrections

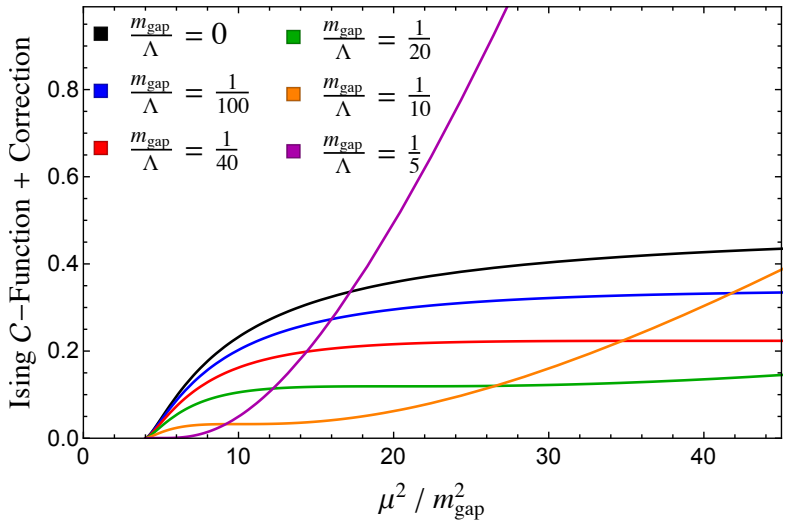

Figure 3.11: Theoretical prediction for the Zamolodchikov C-function in the Ising model effective theory, including the correction from the leading irrelevant operator, for different values of $\frac{m_{\text{gap}}}{\Lambda}$. In the limit $\Lambda \to \infty$ (black curve), the function levels out and approaches the Ising central charge $c_{\text{Ising}} = \frac{1}{2}$. For finite values of Λ, the corrections dramatically alter the function, lowering the plateau and eventually completely eliminating it as $\Lambda \to m_{\text{gap}}$.

from higher-dimensional Ising model operators, suppressed by this cutoff,

$$T_{+-} \approx m_{\text{gap}}\epsilon - \frac{\partial^2 \epsilon}{\Lambda} + \cdots \tag{3.5.11}$$

with the remaining terms suppressed by higher powers of Λ. Using this effective Ising framework, we can determine the effects of these corrections on spectral densities as a function of the ratio $\frac{m_{\text{gap}}}{\Lambda}$. For example, if we include the correction due to the leading irrelevant operator $\partial^2\epsilon$, the prediction for the T_{--} spectral density takes the form

$$\rho_{T_{--}}(\mu) \approx \frac{P_-^4}{4\pi\mu^4}\sqrt{1 - \frac{4m_{\text{gap}}^2}{\mu^2}}\left(m_{\text{gap}}^2 - \frac{m_{\text{gap}}\mu^2}{\Lambda} + \frac{\mu^4}{\Lambda^2}\right). \tag{3.5.12}$$

Figure 3.11 shows the resulting Ising model prediction for the C-function for different values of $\frac{m_{\text{gap}}}{\Lambda}$. In the limit $\Lambda \to \infty$ (black curve), the corrections are negligible and the C-function flattens out, allowing us to extract the central charge $c_{\text{Ising}} = \frac{1}{2}$. However, as we increase m_{gap} relative to the cutoff, the corrections rapidly alter the theoretical prediction, such that the plateau is almost completely removed for $\frac{m_{\text{gap}}}{\Lambda} \gtrsim \frac{1}{10}$.

From this plot, we see that the C-function is very sensitive to corrections from UV physics, such that we must set m_{gap} far below the cutoff to be able to read off c_{IR}

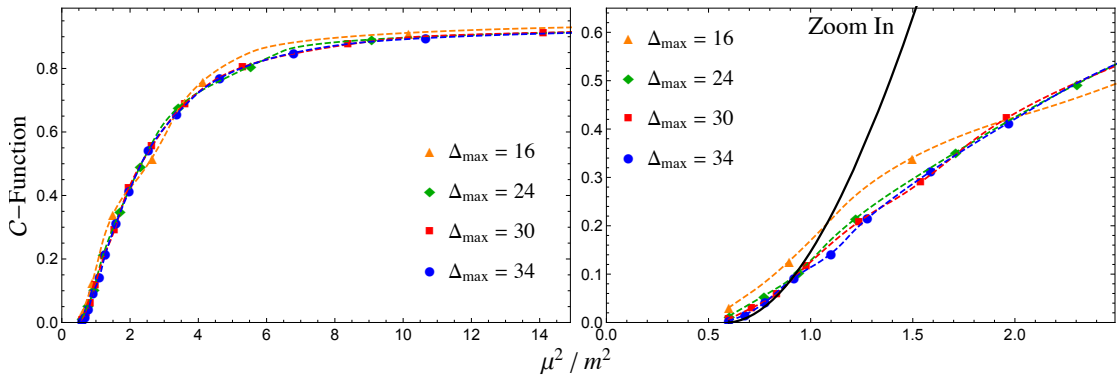

Figure 3.12: Zamolodchikov C-function at different values of $\Delta_{\max}$. The $\Delta_{\max} = 34$ results (blue dots) are at $\frac{\bar{\lambda}}{4\pi} = 1.96$, and the couplings for the remaining results have been chosen such that the mass gap remains fixed. The points are the actual contributions of individual eigenstates to the spectral density, while the dashed lines are interpolations. The right plot is simply a zoomed-in version of the left one, and compares the conformal truncation results to the theoretical IR prediction for the Ising model (black curve), which includes the correction from the leading irrelevant operator (with $\frac{\Lambda}{m} = 1.0$).

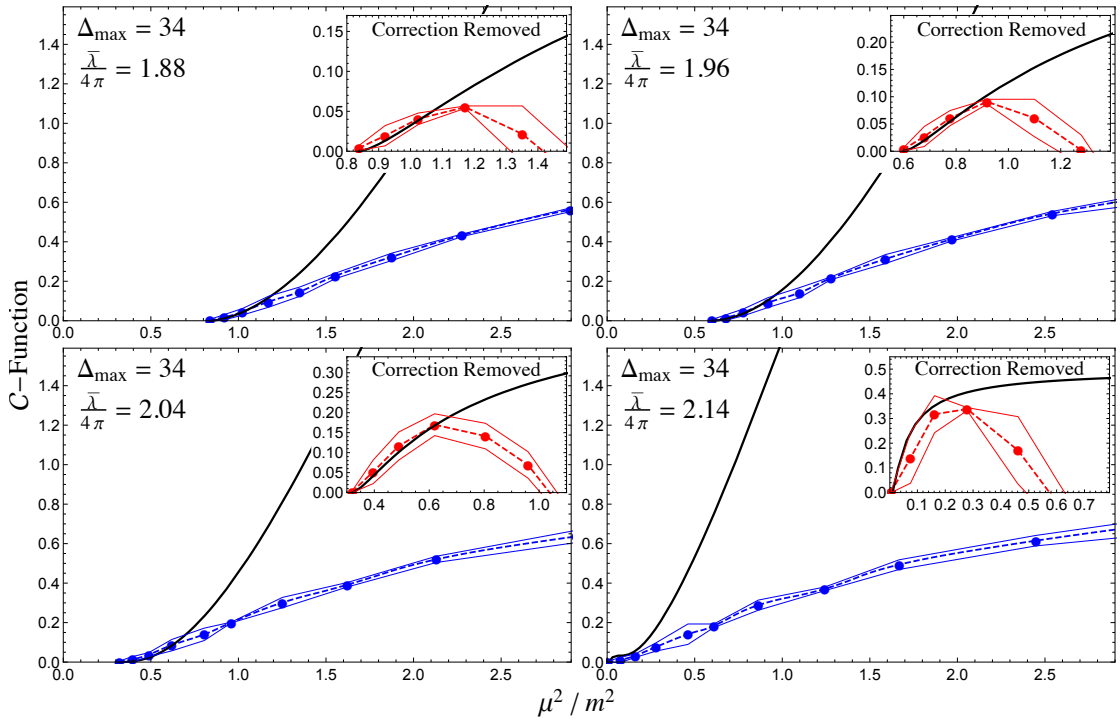

Figure 3.13: Zamolodchikov C-function for $\Delta_{\max} = 34$ and different values of $\bar{\lambda}$. The thin lines surrounding the data points indicate the magnitude of the difference between these results and those at $\Delta_{\max} = 30$, providing a rough estimate of the convergence. Main plots: raw data (blue dots) compared to the Ising model prediction (black curve), which includes the correction from the leading irrelevant operator (with $\frac{\Lambda}{m} = 1.0$). Insets: same data points, but with the expected leading correction removed (red dots), compared with the Ising model prediction (black curve).

directly. More importantly, though, even the IR behavior of $C(\mu)$ changes dramatically due to UV effects. This suggests that we need to account for these irrelevant operators when comparing our numerical results to the predictions from the Ising model.

We can see this clearly in figure 3.12, which shows our conformal truncation results for the C-function at four different values of $\Delta_{\max}$. Just like in previous plots, the couplings have been chosen such that the results all have the same mass gap. In the left plot, we see that the results have converged over a wide range of μ, showing the full RG flow from the free scalar central charge $c_{\text{UV}} = 1$ at high energies to the trivial value of zero in the IR, with the transition scale roughly corresponding to the coupling $\frac{\lambda}{4\pi}$.

However, there appears to be no plateau in the IR corresponding to $c_{\text{Ising}} = \frac{1}{2}$, indicating that the effective cutoff Λ is not sufficiently large compared to m_{gap}. We can confirm this by fitting the IR data points with the Ising model prediction, including the correction from the leading irrelevant operator $\partial^2\epsilon$, as shown in the right plot. The resulting fit yields $\frac{\Lambda}{m} \approx 1.0$, which corresponds to $\frac{m_{\text{gap}}}{\Lambda} \approx 0.4$.

In order to suppress these corrections and isolate the unperturbed Ising model prediction, we therefore must push the mass gap much lower. However, our truncation to $\Delta_{\max} = 34$ limits our IR resolution, setting a lower bound on the value of m_{gap} we can accurately probe with our numerical results. At this truncation level, we are therefore unable to set m_{gap} low enough to ignore these corrections to the C-function.

It is important to note that these corrections to the Ising prediction are *not* a result of truncation error. The effective cutoff Λ is a physical scale at which the Ising model description of ϕ^4 theory breaks down, and these corrections are just a consequence of that fact. Truncation effects merely limit the amount of separation we can obtain between m_{gap} and Λ, or equivalently, how close we can get to the critical point.

Figure 3.13 shows the truncation results for the C-function for $\Delta_{\max} = 34$ and multiple values of $\bar{\lambda}$. In the main plots, we compare these results (blue dots) with the theoretical prediction (Ising + leading correction) with a *fixed* cutoff $\frac{\Lambda}{m} = 1.0$ across the $\bar{\lambda}$ shown. Even though the mass gap changes significantly as we vary $\bar{\lambda}$, the IR data points continue to be well-described by eq. (3.5.12). The insets in these plots confirm this agreement, showing the truncation results for $C(\mu)$ with the expected corrections from $\partial^2\epsilon$ removed (red dots). In the IR, these modified results now match the original Ising model predictions (i.e. without any corrections from irrelevant operators), again

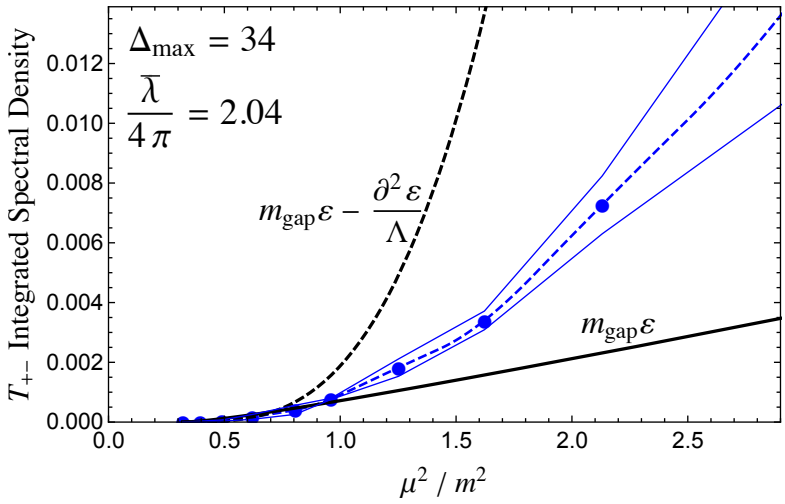

Figure 3.14: Integrated spectral density for T_{+-} at $\Delta_{\text{max}} = 34$ and $\frac{\bar{\lambda}}{4\pi} = 2.04$, compared to the Ising model prediction with (dashed line) and without (solid line) the correction from $\partial^2\epsilon$, with $\frac{\Lambda}{m} = 1.0$. In the IR, the effects from this leading correction are negligible, such that we can safely ignore them. For reference, the numerical results are the same as those in the lower left plot in figure 3.7.

indicating that our truncation results are correctly reproducing the effects due to the cutoff Λ.

One obvious question is whether the corrections due to irrelevant operators also have a significant effect on the integrated spectral densities for T_{+-} and ϕ^n. After all, in the previous subsections we completely ignored these effects when comparing our truncation results with theoretical predictions. Fortunately, unlike for T_{--}, the corrections to those spectral densities are negligible in the IR. As an example, figure 3.14 shows the theoretical prediction for the T_{+-} integrated spectral density, both with and without the leading correction from $\partial^2\epsilon$, compared with the conformal truncation results at $\Delta_{\text{max}} = 34$ and $\frac{\bar{\lambda}}{4\pi} = 2.04$. In the IR, the two theoretical predictions agree, indicating that we can safely ignore the corrections from higher-dimensional operators when comparing with our numerical results.

3.6 Discussion

Conformal truncation, which we introduced in [69], is a new method for performing non-perturbative computations in strongly-coupled QFTs. Unlike other numerical methods, it is formulated in Lorentzian signature and infinite volume and consequently can be used to compute real-time, continuum correlation functions. In this work, we have

used conformal truncation to specifically calculate Källén-Lehmann spectral densities, which are equivalent to two-point functions. To the best of our knowledge, the results presented here constitute the first computation of non-perturbative spectral densities in 2D ϕ^4 theory.

Our main goal has been to check these spectral densities against known analytic results in the IR limit, as a test of our conformal truncation method. As such, we have focused on values of the coupling, $\bar{\lambda}$, near the critical point, where we know the IR theory is described by the 2D Ising model. In section 3.5, we demonstrated that in this regime the spectral densities for several different operators match known Ising spectral densities at low energies, providing a fully non-perturbative check of conformal truncation.

It is worth emphasizing two things. First, our truncation results extend well beyond the deep IR regime described by the Ising model. As we have shown, the spectral densities converge rapidly in Δ_{max} over a wide range of mass scales, μ^2, providing the full RG flow of the corresponding operators. These are novel predictions for non-perturbative two-point functions in ϕ^4 theory. Second, as we vary Δ_{max}, the resulting spectral densities are built from the IR up. That is, the convergence of the spectral densities starts at low mass scales and then extends to larger μ^2 with increasing Δ_{max}. This is evident, for example, in the convergence plots in figure 3.6, where even $\Delta_{\text{max}} = 16$ correctly reproduces the IR. This capacity to preferentially access IR physics is a useful feature of conformal truncation.

Our analysis has taught us some general lessons about conformal truncation. One clear lesson is that conformal truncation becomes less efficient as we increase the separation between the bare parameters in the UV Hamiltonian and emergent IR scales like m_{gap}. From a computational perspective, this is simply because a small value for m_{gap} is the result of fine-tuned cancellations between UV basis states. As m_{gap} decreases, the IR results thus become increasingly sensitive to small corrections from operators with large conformal Casimir. This is most pronounced at a critical point, where m_{gap} vanishes, and explains why in figure 3.4 the error bars increase as we approach criticality. We can also see this behavior in the various spectral density results, where the convergence slows as we tune $m_{\text{gap}} \to 0$. This inability to fully reach criticality at finite Δ_{max} thus makes it difficult to extract observables like critical exponents and central charges using

conformal truncation.

Another important lesson can be drawn by comparing the convergence of our results in sections 3.4 and 3.5. In section 3.5, we found that the spectral densities converged quite rapidly if we held the IR observable m_{gap} fixed. We can contrast this with the mass spectrum results in section 3.4, where we instead held the UV parameter $\bar{\lambda}$ fixed. Even visually, it is clear that the latter results converge much more slowly than the former ones. This is perhaps unsurprising, as mapping precisely between the mass gap and $\bar{\lambda}$ requires reconstructing the *entire* RG flow. Because conformal truncation constructs observables from the IR up, it is thus much more efficient to study low-energy physics directly in terms of IR parameters, rather than UV ones.

Perhaps one way to summarize these observations is that conformal truncation appears to be truly complementary to existing numerical methods. While most methods excel at computing critical observables, conformal truncation is better at studying full RG flows. Conformal truncation can thus deliver something new: real-time, infinite-volume correlation functions computable efficiently in Δ_{max}.

Finally, it is worth commenting that in the space of CFTs, there is a precise sense in which the 2D free scalar CFT is actually the *least* efficient setting for conformal truncation. In 2D free field theory, a primary operator $\mathcal{O}$ only corresponds to a single state in the Hilbert space, as we discussed in section 4.3. For more general theories, each operator $\mathcal{O}$ gives rise to a continuum of states, parameterized by the invariant mass μ. Equivalently, we can think of these additional states as being created by the descendant operators $P^{2n}\mathcal{O}$. Computationally, constructing primary operators is expensive, while including additional descendants is quite cheap. The 2D free scalar CFT thus has the least return in terms of the number of basis states obtained with a given computational power. As a concrete point of comparison, in [69] we considered the 3D free scalar CFT as a starting point for studying the $O(N)$ model in the limit $N \to \infty$. Using conformal truncation, we were able to reproduce the IR spectral density of the singlet operator $\vec{\phi}^2$, in roughly equivalent detail to the results presented here, using just $\Delta_{\text{max}} \sim 5$. The key difference in that work is that we were able to increase the size of our truncated basis with descendants. For this reason, we are optimistic about the capabilities of conformal truncation moving forward to other theories.

Looking ahead, there are several exciting applications of conformal truncation to

pursue:

1) 2D ϕ^4 theory – continued

In this work, we have only studied the symmetry-preserving phase of ϕ^4 theory, focusing particularly on couplings below $\bar{\lambda}_*$. However, as mentioned above, conformal truncation yields results for any $\bar{\lambda}$, so a natural next step is to proceed to the symmetry-broken phase. There is reason to believe that, despite the triviality of the vacuum, spontaneous symmetry-breaking is detectable even in lightcone quantization [81], and some initial work has been done in [83, 82, 84]. It would thus be illuminating to study the behavior of spectral densities in the symmetry-broken phase.

On a different note, it would also be interesting to further study the map between lightcone and equal-time quantization. In particular, it would be instructive to use the prescription presented in [73] to see if one can explicitly map our results to those done in equal-time. This would allow us to compare the value of the critical coupling across the two quantization schemes.

2) 2D Ising model

In this work, we merely used the 2D Ising model to check our method, making use of the fact that an ϵ (temperature) deformation is integrable and can be treated analytically. However, it would be fascinating to use conformal truncation to study the more general case of deforming by both ϵ and σ, which corresponds to the 2D Ising model at $T \neq T_c$ in a magnetic field. While there are already many interesting results [119, 120, 121, 122, 123], full correlation functions in this theory are not known, and conformal truncation could potentially be used to make novel predictions. There are two strategies for doing this.

The first strategy is to again consider ϕ^4 theory, but now with an additional $\mathbb{Z}_2$-odd ϕ^3 deformation. Our results here have confirmed that ϕ^3 flows to σ near criticality, so adding this interaction is equivalent in the IR to deforming the Ising model by a magnetic field. The advantage of this approach is that the UV CFT is still free scalar field theory, so the basis of primary operators is the same one we used in this work. The disadvantage is that flowing all the way from free field theory

is an inefficient use of computational power, using thousands of UV operators to reproduce only a handful of Ising model states.

The second strategy, which we suspect is much more efficient, is to apply conformal truncation directly to the 2D Ising CFT. Indeed, conformal truncation can be initiated from any UV CFT where operator scaling dimensions and OPE coefficients are known up to a desired truncation level. Since the 2D Ising CFT is a minimal model where all of this data is known, it seems more sensible to start directly from this CFT and use conformal truncation to construct and diagonalize the Hamiltonian created by the ϵ and σ deformations.

3) 3D Ising model

Another important feature of conformal truncation is that it can be applied in any number of spacetime dimensions. Thus, a natural goal is to use this method to study the 3D Ising model, about which much less is known than its 2D counterpart. As in 2D, there are two approaches to studying deformations of the 3D Ising model: starting in scalar field theory and flowing to the vicinity of the Ising critical point, which we plan to consider in future work,[7] or starting directly from the Ising CFT and deforming it.

The advantage of starting from free field theory is always that we know operator dimensions and OPE coefficients, which are the necessary ingredients for conformal truncation. By comparison, this data is difficult to obtain in the 3D Ising CFT. A direct application of conformal truncation to the 3D Ising model would require us to know the operator content and OPE coefficients up to a desired Δ_{max}. Over the past several years, there has been remarkable progress in pinning down 3D Ising data using the conformal bootstrap and related techniques [125, 126, 127, 128]. It may turn out that these techniques can provide the CFT data needed to subsequently initiate truncation studies directly around the 3D Ising model. More generally, conformal truncation applications provide an immediate incentive for trying to compute scaling dimensions and OPE coefficients in known CFTs.

[7] See [124] for an alternative proposal for applying Hamiltonian truncation to ϕ^4 theory in higher dimensions.

Appendix: Additional Technical Details and Results

3.7 Basis of Casimir Eigenstates

Our basis consists of total momentum eigenstates built from local operators in the UV CFT,[8]

$$|\mathcal{C}, P\rangle \equiv \int dx\, e^{-iPx}\mathcal{O}(x)|0\rangle, \tag{3.7.1}$$

with the normalization convention

$$\langle \mathcal{C}, P|\mathcal{C}', P'\rangle = 2P(2\pi)\delta(P-P')\,\delta_{\mathcal{O}\mathcal{O}'}. \tag{3.7.2}$$

As our CFT is free scalar field theory, the operators can be written in terms of derivatives acting on the scalar field ϕ,

$$\mathcal{O}(x) = \sum_{\boldsymbol{k}} C^{\mathcal{O}}_{\boldsymbol{k}}\, \partial^{k_1}\phi(x)\cdots\partial^{k_n}\phi(x) \equiv \sum_{\boldsymbol{k}} C^{\mathcal{O}}_{\boldsymbol{k}}\, \partial^{\boldsymbol{k}}\phi(x), \tag{3.7.3}$$

where we have introduced the useful shorthand

$$\partial^{\boldsymbol{k}}\phi \equiv \partial^{k_1}\phi\cdots\partial^{k_n}\phi. \tag{3.7.4}$$

We specifically need to find the linear combinations that correspond to *primary operators*, which are annihilated by the special conformal generator K_μ and create eigenstates

[8] Note that we have suppressed the indices on the coordinates and momentum, with the understanding that all indices are "$-$".

of the conformal quadratic Casimir $\mathcal{C}$,

$$[K_\mu, \mathcal{O}(0)] = 0, \qquad [\mathcal{C}, \mathcal{O}(0)] = \big(\Delta(\Delta-2) + \ell^2\big)\mathcal{O}(0). \tag{3.7.5}$$

There are two ways to obtain the set of primary operators. The first, more direct method is to simply construct linear combinations which satisfy eq. (3.7.5) by brute force. The conformal Casimir and special conformal generator can be written as operators acting on the space of "monomials" $\partial^{\boldsymbol{k}}\phi$, such that constructing primary operators is equivalent to simply organizing the null space of K_μ into eigenstates of $\mathcal{C}$.

The second method, which we use in this work, is to first construct a basis of primary operators built from distinguishable particles, then symmetrize with respect to particle number. In other words, we first find operators of the form

$$\mathcal{O}(x) = \sum_{\boldsymbol{\sigma}} C^{\mathcal{O}}_{\boldsymbol{\sigma}}\, \partial^{\sigma_1}\phi_1(x)\cdots\partial^{\sigma_n}\phi_n(x), \tag{3.7.6}$$

with n distinct fields ϕ_i. We can then remove the labels on ϕ_i to obtain primary operators built from a single scalar field. The advantage of this approach is that the restriction to primary operators and organization into Casimir eigenstates is much simpler for states with distinguishable particles.

The Casimir eigenstates created by these operators can be expressed in terms of n-particle Fock space states. Each operator $\mathcal{O}(x)$ maps to a corresponding "wavefunction" $F_{\mathcal{O}}(p)$, defined as the overlap

$$F_{\mathcal{O}}(p_1,\ldots,p_n) \equiv \langle p_1,\ldots,p_n|\mathcal{O}(0)\rangle, \tag{3.7.7}$$

allowing us to rewrite the corresponding basis states as

$$|\mathcal{C}, P\rangle = \frac{1}{n!}\int \frac{dp_1\cdots dp_n}{(2\pi)^n 2p_1\cdots 2p_n}(2\pi)\delta\Big(P - \sum_i p_i\Big)F_{\mathcal{O}}(p)|p_1,\ldots,p_n\rangle. \tag{3.7.8}$$

The advantage of working with momentum space wavefunctions is that this representation *automatically* restricts our basis to primary operators. This simplification occurs because descendants are created by acting with overall derivatives on primary operators, which in terms of Fock space states simply corresponds to multiplying the wavefunction

by a constant,

$$\partial^k \mathcal{O}(x) \to (p_1 + \cdots + p_n)^k F_{\mathcal{O}}(p) = P^k F_{\mathcal{O}}(p). \tag{3.7.9}$$

Now that we have restricted our basis to primary operators, we can use the methods of [69] to solve for the complete set of eigenfunctions of the conformal quadratic Casimir,

$$\mathcal{C} = -D^2 - \frac{1}{2}(P_\mu K^\mu + K_\mu P^\mu) + \frac{1}{2} L_{\mu\nu} L^{\mu\nu}, \tag{3.7.10}$$

which can be written as the momentum space differential operator,

$$\mathcal{C} = -2 \sum_{i<j} p_i p_j \left(\frac{\partial}{\partial p_i} - \frac{\partial}{\partial p_j} \right)^2. \tag{3.7.11}$$

The resulting Casimir eigenfunctions are multivariate Jacobi polynomials, parameterized by the set of indices $\boldsymbol{\ell} \equiv (\ell_1, \ldots, \ell_{n-1})$,

$$\boxed{F_{\boldsymbol{\ell}}(p) = p_1 \cdots p_n \prod_{i=1}^{n-1} |p|_{i+1}^{\ell_i} P_{\ell_i}^{(2|\ell|_{i-1}+2i-1,1)} \left(\frac{p_{i+1} - |p|_i}{|p|_{i+1}} \right)}, \tag{3.7.12}$$

where we have ignored the overall normalization coefficient and defined

$$|p|_i \equiv \sum_{j=1}^{i} p_j. \tag{3.7.13}$$

These Casimir eigenfunctions can be converted back into local operators simply by making the identification

$$p_i^{k_i} \to \partial^{k_i} \phi_i. \tag{3.7.14}$$

We can see this more concretely by expanding the wavefunctions into sums of monomials, then using the monomial coefficients to construct the corresponding operator,

$$F_{\boldsymbol{\ell}}(p) = \sum_{\boldsymbol{\sigma}} C_{\boldsymbol{\sigma}}^{\boldsymbol{\ell}}\, p_1^{\sigma_1} \cdots p_n^{\sigma_n} \to \mathcal{O}_{\boldsymbol{\ell}}(x) = \sum_{\boldsymbol{\sigma}} C_{\boldsymbol{\sigma}}^{\boldsymbol{\ell}}\, \partial^{\sigma_1} \phi_1(x) \cdots \partial^{\sigma_n} \phi_n(x). \tag{3.7.15}$$

Finally, we can remove the indices on the individual scalar fields to obtain the resulting

primary operator

$$\mathcal{O}_{\boldsymbol{\ell}}(x) = \sum_{\boldsymbol{\sigma}} C_{\boldsymbol{\sigma}}^{\boldsymbol{\ell}}\, \partial^{\sigma_1}\phi(x)\cdots\partial^{\sigma_n}\phi(x) = \sum_{\boldsymbol{k}} \left(\sum_{\boldsymbol{\sigma}\in \mathrm{perm}(\boldsymbol{k})} C_{\boldsymbol{\sigma}}^{\boldsymbol{\ell}} \right) \partial^{\boldsymbol{k}}\phi(x). \tag{3.7.16}$$

As a simple example, let's consider the two-particle Casimir eigenfunction with $\ell = 2$,

$$F_2(p_1,p_2) = p_1 p_2\,(p_1+p_2)^2\, P_2^{(1,1)}\left(\frac{p_2-p_1}{p_1+p_2}\right) = 3p_1^3 p_2 + 3p_1 p_2^3 - 9p_1^2 p_2^2. \tag{3.7.17}$$

This polynomial can be used to construct an operator built from two distinct fields,

$$F_2(p) \to \mathcal{O}_2 = 3\partial^3\phi_1\partial\phi_2 + 3\partial\phi_1\partial^3\phi_2 - 9\partial^2\phi_1\partial^2\phi_2. \tag{3.7.18}$$

We can then replace $\phi_{1,2} \to \phi$ and collect together similar terms to obtain the final operator

$$\mathcal{O}_2 = 6\partial^3\phi\partial\phi - 9(\partial^2\phi)^2. \tag{3.7.19}$$

We thus have a straightforward procedure for constructing the basis of Casimir eigenstates. Starting with the polynomials in (3.7.12), we can convert each wavefunction into a corresponding primary operator built from n distinct fields. We can then obtain operators built from a single scalar field by simply replacing $\phi_i \to \phi$.

An alternative approach would be to first symmetrize the momentum space wavefunctions with respect to particle number, then convert the resulting symmetric polynomials into operators built from a single scalar field. However, this symmetrization procedure is much simpler when implemented at the level of operators. Our approach therefore capitalizes on the relative advantages of both representations of the basis. Working in momentum space trivializes the restriction to primary operators, while converting back to operators in position space trivializes the process of symmetrization.

Because of this need to symmetrize, the set of eigenfunctions in (3.7.12) is overcomplete, which means that multiple polynomials will map to the same final operator (or to linearly dependent combinations of operators). In practice, we therefore only need to use a subset of the Casimir eigenfunctions to span the space of primary operators, using Gram-Schmidt to find the orthogonal linear combinations. A more detailed discussion

of this process, as well as its generalization to higher dimensions, will be presented in future work [102].

In [73] (based on initial work in [129] and [130]), Burkardt et al. considered a basis of Fock space states weighted by symmetric polynomials in momentum space. They then truncated this basis by setting a separate maximum degree for the polynomials in each n-particle sector. The resulting basis states are linear combinations of the Casimir eigenstates we use in this work, such that their truncation scheme is equivalent to setting a different value of Δ_{max} for each particle number in our basis. One can see this explicitly by either computing the wavefunctions $F_{\mathcal{O}}(p)$ of our final basis of Casimir eigenstates or converting the symmetric polynomials used in [73] into local operators built from ϕ. In practice, we find that working in terms of operators, rather than polynomials, greatly simplifies the construction and orthogonalization of the basis.

3.8 Matrix Elements and Operator Overlaps

In this appendix, we use our basis of Casimir eigenstates to compute matrix elements for the invariant mass operator M^2. While we are technically only interested in the matrix elements associated with primary operators, in practice it is simpler to first evaluate the expressions for individual "monomials,"

$$|\partial^{\boldsymbol{k}}\phi, P\rangle \equiv \int dx\, e^{-iPx}\partial^{\boldsymbol{k}}\phi(x)|0\rangle, \tag{3.8.1}$$

which can then be combined to form matrix elements for the primary operators

$$|\mathcal{C}, P\rangle = \sum_{\boldsymbol{k}} C^{\mathcal{O}}_{\boldsymbol{k}}|\partial^{\boldsymbol{k}}\phi, P\rangle. \tag{3.8.2}$$

These monomial matrix elements take the general form

$$\langle\partial^{\boldsymbol{k}}\phi, P|M^2|\partial^{\boldsymbol{k}'}\phi, P'\rangle = 2P(2\pi)\delta(P-P')\,\mathcal{M}_{\boldsymbol{k}\boldsymbol{k}'}. \tag{3.8.3}$$

For the rest of this discussion, we will focus only on the dynamical piece $\mathcal{M}_{\boldsymbol{k}\boldsymbol{k}'}$, suppressing the momentum-conserving kinematic factor. Note that, because our states are

lightcone momentum eigenstates, the matrix elements can be further simplified to

$$\mathcal{M}_{\boldsymbol{k}\boldsymbol{k}'} \equiv \langle \partial^{\boldsymbol{k}}\phi | M^2 | \partial^{\boldsymbol{k}'}\phi \rangle = 2P \langle \partial^{\boldsymbol{k}}\phi | P_+ | \partial^{\boldsymbol{k}'}\phi \rangle. \tag{3.8.4}$$

Constructing $\mathcal{M}_{\boldsymbol{k}\boldsymbol{k}'}$ is thus equivalent to calculating the matrix elements for the lightcone Hamiltonian P_+.

In this work, we specifically consider the scalar field theory arising from the Lagrangian

$$\mathcal{L} = \frac{1}{2}\partial_\mu\phi\partial^\mu\phi - \frac{1}{2}m^2\phi^2 - \frac{1}{4!}\lambda\phi^4, \tag{3.8.5}$$

with the corresponding lightcone Hamiltonian

$$P_+ = \int dx \left(\frac{1}{2}m^2\phi^2 + \frac{1}{4!}\lambda\phi^4 \right). \tag{3.8.6}$$

Note that the Hamiltonian does not receive any contributions from the kinetic term. This is due to the fact that our basis states are only built from the right-moving operator $\partial\phi$, such that every state in the original CFT has invariant mass $\mu^2 = 0$.

The resulting Hamiltonian matrix elements are simply Fourier transforms of CFT three-point functions involving ϕ^2 and ϕ^4. It will therefore be useful to evaluate the general integral[9]

$$\begin{aligned} &\int dx\, dy\, dz\, e^{i(Px-P'z)} \frac{1}{(x-y)^a (y-z)^b (x-z)^c} \\ &\qquad = \frac{2\pi^2 P^{a+b+c-3}\Gamma(a+b-1)}{\Gamma(a)\Gamma(b)\Gamma(a+b+c-1)} \cdot 2P(2\pi)\delta(P-P'). \end{aligned} \tag{3.8.7}$$

3.8.1 Mass Term

Let us first consider the mass term, which in lightcone quantization preserves particle number. We therefore only need to compute the $n \to n$ matrix element

$$\langle \partial^{\boldsymbol{k}}\phi, P | M^2 | \partial^{\boldsymbol{k}'}\phi, P' \rangle = \frac{m^2}{2} \int dx\, dy\, dz\, e^{i(Px-P'z)} \langle \partial^{\boldsymbol{k}}\phi(x)\phi^2(y)\partial^{\boldsymbol{k}'}\phi(z) \rangle. \tag{3.8.8}$$

[9] For simplicity, from now on we will suppress any overall factors of i, as these cancel in the final matrix elements.

The three-point function in the integrand can be written as a sum of Wick contractions,

$$\langle \partial^{\boldsymbol{k}}\phi(x)\phi^2(y)\partial^{\boldsymbol{k}'}\phi(z)\rangle = \sum_{\substack{k_i\in\boldsymbol{k}\\ k'_j\in\boldsymbol{k}'}} \langle \partial^{k_i}\phi(x)\phi^2(y)\partial^{k'_j}\phi(z)\rangle\langle \partial^{\boldsymbol{k}/k_i}\phi(x)\,\partial^{\boldsymbol{k}'/k'_j}\phi(z)\rangle, \quad (3.8.9)$$

where $\boldsymbol{k}/k_i$ simply indicates the vector obtained by removing k_i from $\boldsymbol{k}$.

Each term in this sum cleanly factorizes into a product of interacting and spectating correlation functions. The piece involving the spectating particles can also be computed from Wick contractions

$$\langle \partial^{\boldsymbol{k}/k_i}\phi(x)\partial^{\boldsymbol{k}'/k'_j}\phi(z)\rangle = \frac{A_{\boldsymbol{k}/k_i,\boldsymbol{k}'/k'_j}}{(4\pi)^{n-1}(x-z)^{\Delta+\Delta'-k_i-k'_j}}, \quad (3.8.10)$$

where we have defined the Wick contraction coefficient

$$A_{\boldsymbol{k}\boldsymbol{k}'} \equiv \sum_{\text{pairs}}\prod_{i,j}\Gamma(k_i+k'_j). \quad (3.8.11)$$

The remaining interacting piece can be easily calculated to obtain

$$\langle \partial^{k_i}\phi(x)\phi^2(y)\partial^{k'_j}\phi(z)\rangle = 2\cdot\frac{\Gamma(k_i)\Gamma(k'_j)}{(4\pi)^2(x-y)^{k_i}(y-z)^{k'_j}}. \quad (3.8.12)$$

We can combine these three-point functions with the general integral in eq. (3.8.7) to obtain the final matrix elements

$$\boxed{\mathcal{M}^{(m)}_{\boldsymbol{k}\boldsymbol{k}'} = m^2 N_{\boldsymbol{k}\boldsymbol{k}'}\sum_{\substack{k_i\in\boldsymbol{k}\\ k'_j\in\boldsymbol{k}'}}\Gamma(k_i+k'_j-1)A_{\boldsymbol{k}/k_i,\boldsymbol{k}'/k'_j},} \quad (3.8.13)$$

where we have simplified the expression by introducing the overall coefficient

$$N_{\boldsymbol{k}\boldsymbol{k}'} \equiv \frac{P^{\Delta+\Delta'-2}}{4^n\pi^{n-1}\Gamma(\Delta+\Delta'-1)}. \quad (3.8.14)$$

3.8.2 Interaction Terms

We now turn to the contribution from the quartic interaction, which has two distinct types of matrix elements. The first preserves particle number, and the associated three-point function is similar to that of the mass term, though now there are two particles

from each state participating in the interaction,

$$\langle \partial^{\boldsymbol{k}}\phi(x)\phi^4(y)\partial^{\boldsymbol{k}'}\phi(z)\rangle = \sum_{\substack{k_{i,j}\in\boldsymbol{k}\\ k'_{r,s}\in\boldsymbol{k}'}} \langle \partial^{k_{i,j}}\phi(x)\phi^4(y)\partial^{k'_{r,s}}\phi(z)\rangle\langle \partial^{\boldsymbol{k}/k_{i,j}}\phi(x)\,\partial^{\boldsymbol{k}'/k'_{r,s}}\phi(z)\rangle \tag{3.8.15}$$

We therefore just need to compute the correlation function

$$\langle \partial^{k_{i,j}}\phi(x)\phi^4(y)\partial^{k'_{r,s}}\phi(z)\rangle = 4!\cdot\frac{\Gamma(k_i)\Gamma(k_j)\Gamma(k'_r)\Gamma(k'_s)}{(4\pi)^4(x-y)^{k_i+k_j}(y-z)^{k'_r+k'_s}}. \tag{3.8.16}$$

Using the same approach as the mass term, we then obtain the $n\to n$ matrix elements

$$\boxed{\mathcal{M}^{(n\to n)}_{\boldsymbol{k}\boldsymbol{k}'} = \frac{g}{4\pi}N_{\boldsymbol{k}\boldsymbol{k}'}\sum_{\substack{k_{i,j}\in\boldsymbol{k}\\ k'_{r,s}\in\boldsymbol{k}'}}\frac{\Gamma(k_i)\Gamma(k_j)\Gamma(k'_r)\Gamma(k'_s)\Gamma(k_i+k_j+k'_r+k'_s-1)}{\Gamma(k_i+k_j)\Gamma(k'_r+k'_s)}A_{\boldsymbol{k}/k_{i,j},\boldsymbol{k}'/k'_{r,s}}} \tag{3.8.17}$$

The second type of matrix element changes particle number by two, so we also need to consider the correlation function

$$\langle \partial^{k_i}\phi(x)\phi^4(y)\partial^{k'_{r,s,t}}\phi(z)\rangle = 4!\cdot\frac{\Gamma(k_i)\Gamma(k'_r)\Gamma(k'_s)\Gamma(k'_t)}{(4\pi)^4(x-y)^{k_i}(y-z)^{k'_r+k'_s+k'_t}}. \tag{3.8.18}$$

We then obtain the resulting $n\to n+2$ matrix elements

$$\boxed{\mathcal{M}^{(n\to n+2)}_{\boldsymbol{k}\boldsymbol{k}'} = \frac{g}{4\pi}N_{\boldsymbol{k}\boldsymbol{k}'}\sum_{\substack{k_i\in\boldsymbol{k}\\ k'_{r,s,t}\in\boldsymbol{k}'}}\frac{\Gamma(k'_r)\Gamma(k'_s)\Gamma(k'_t)\Gamma(k_i+k'_r+k'_s+k'_t-1)}{\Gamma(k'_r+k'_s+k'_t)}A_{\boldsymbol{k}/k_i,\boldsymbol{k}'/k'_{r,s,t}}} \tag{3.8.19}$$

3.8.3 Overlap of ϕ^n with Basis States

Using the matrix elements from this appendix, we can construct and diagonalize the truncated matrix M^2. The resulting approximate mass eigenstates can then be used to compute the integrated spectral density for any local operator $\mathcal{O}(x)$, defined in eq. (4.3.25). The approximate eigenstates $|\mu_i\rangle$ are expressed in the UV basis of conformal Casimir eigenstates, so to obtain the integrated spectral density, we need to first compute the overlap of $\mathcal{O}(x)$ with the original basis states. Much like with the matrix elements, in practice it is simpler to evaluate the overlap with the monomial states

$|\partial^{\boldsymbol{k}}\phi, P\rangle$, then arrange them into states created by primary operators,

$$\langle \mathcal{O}(0)|\mathcal{C}', P\rangle = \sum_{\boldsymbol{k}} C_{\boldsymbol{k}}^{\mathcal{O}'} \langle \mathcal{O}(0)|\partial^{\boldsymbol{k}}\phi, P\rangle. \tag{3.8.20}$$

In this work, we are specifically interested in the spectral densities associated with the scalar operators ϕ^n. The corresponding overlap is just the Fourier transform

$$\langle \phi^n(0)|\partial^{\boldsymbol{k}}\phi, P\rangle = \int dx\, e^{iPx} \langle \partial^{\boldsymbol{k}}\phi(x)\phi^n(0)\rangle. \tag{3.8.21}$$

We therefore need to compute the two-point function,

$$\langle \partial^{\boldsymbol{k}}\phi(x)\phi^n(0)\rangle = \frac{n!\Gamma(k_1)\cdots\Gamma(k_n)}{(4\pi)^n x^{\Delta}}, \tag{3.8.22}$$

which we can use to obtain the final overlap

$$\boxed{\langle \phi^n(0)|\partial^{\boldsymbol{k}}\phi, P\rangle = \frac{n!P^{\Delta-1}\Gamma(k_1)\cdots\Gamma(k_n)}{2^{2n-1}\pi^{n-1}\Gamma(\Delta)}.} \tag{3.8.23}$$

3.9 Decoupling of Higher-Dimensional Operators

In this appendix, we use the asymptotic behavior of the M^2 matrix elements to study the convergence of our conformal truncation method. In particular, we would like to understand how both the IR cutoff and corrections to low-energy observables behave as $\Delta_{\text{max}} \to \infty$. Our analysis here is largely based on [79, 80, 124].

In conformal truncation (or any truncation prescription), we divide the Hilbert space of a given QFT into two sectors,

$$\mathcal{H} = \mathcal{H}_L \oplus \mathcal{H}_H, \tag{3.9.1}$$

where $\mathcal{H}_L$ is the truncated subspace spanned by "low" operators with $\Delta \leq \Delta_{\text{max}}$, and $\mathcal{H}_H$ is created by the remaining "high" operators. The full invariant mass operator M^2 thus takes the schematic form

$$M^2 = \begin{pmatrix} \mathcal{M}_{LL} & \mathcal{M}_{LH} \\ \mathcal{M}_{HL} & \mathcal{M}_{HH} \end{pmatrix}. \tag{3.9.2}$$

The matrix $\mathcal{M}_{LL}$, which only acts on the space $\mathcal{H}_L$, corresponds to the truncated version of M^2 we diagonalize to obtain the approximate mass eigenstates at a given $\Delta_{\max}$. However, there are clearly corrections to this approximation due to the remaining matrix elements.

To understand these corrections more concretely, let's write the true mass eigenstates as

$$|\mu_i\rangle = |\mu_i\rangle_L + |\mu_i\rangle_H, \tag{3.9.3}$$

where $|\mu_i\rangle_{L,H} \in \mathcal{H}_{L,H}$. The *exact* eigenvalue equation can then be rewritten solely in terms of operators acting on the truncated space $\mathcal{H}_L$,

$$\Big(\mathcal{M}_{LL} - \mathcal{M}_{LH}(\mathcal{M}_{HH} - \mu_i^2)^{-1}\mathcal{M}_{HL}\Big)|\mu_i\rangle_L = \mu_i^2|\mu_i\rangle_L. \tag{3.9.4}$$

By only diagonalizing the truncated matrix $\mathcal{M}_{LL}$, we've therefore neglected the correction

$$\delta\mathcal{M} \equiv \mathcal{M}_{LH}(\mathcal{M}_{HH} - \mu_i^2)^{-1}\mathcal{M}_{HL}. \tag{3.9.5}$$

The rate of convergence for conformal truncation is thus set by the asymptotic behavior of $\delta\mathcal{M}$ as $\Delta_{\max} \to \infty$. This correction also gives rise to an effective cutoff on our IR resolution, Λ_{IR}, as we cannot accurately reproduce eigenvalues below the scale set by $\delta\mathcal{M}$.

While this correction technically depends on the exact eigenvalues, we're specifically interested in low-mass states. We therefore expect the matrix elements $\mathcal{M}_{HH}$ to be large compared to μ_i^2, which suggests we can approximate the correction as

$$\delta\mathcal{M} \approx \mathcal{M}_{LH}\mathcal{M}_{HH}^{-1}\mathcal{M}_{HL}. \tag{3.9.6}$$

Given this approximation, we can obtain a rough estimate of the IR cutoff by studying the overall magnitude of matrix elements at the edge of our truncation, involving operators with dimension $\Delta_H \sim \Delta_{\max}$.

Recall that for ϕ^4 theory, there are three contributions to the Hamiltonian matrix:

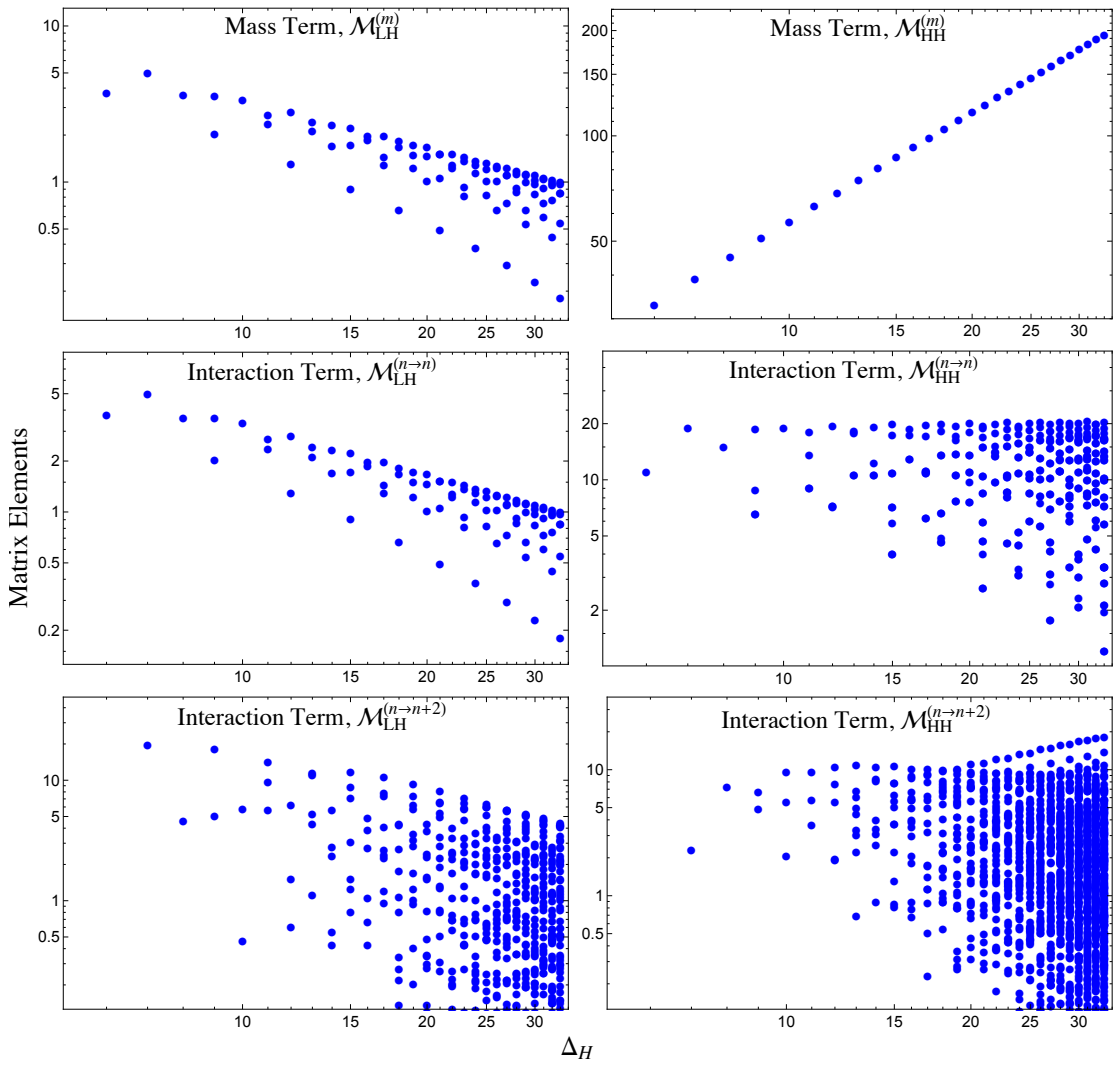

Figure 3.15: Three-particle Casimir eigenstate matrix elements, with overall factors of m^2 and $\frac{\lambda}{4\pi}$ removed, as a function of the larger of the two operator scaling dimensions, Δ_H, for the mass term (top), $n \to n$ interaction (middle) and $n \to n+2$ interaction (bottom). Left: matrix elements involving the lowest-dimension operator ($\Delta_L = 3$). Right: matrix elements where both operators have dimension Δ_H.

the mass term, the $n \to n$ interaction term, and the $n \to n+2$ interaction term. Figure 3.15 shows how the individual matrix elements for these three contributions vary with Δ_H for the case of $n = 3$ particles (the other particle sectors are similar). The plots on the left correspond to the 'LH' matrix elements, where we have chosen the light state to be the lowest three-particle state, with $\Delta_L = 3$, while the plots on the right correspond to 'HH' matrix elements.

From these plots, we can roughly read off the dependence of the largest matrix

elements on Δ_H. For the mass matrices, we find

$$\mathcal{M}_{LH}^{(m)} \sim \frac{1}{\sqrt{\Delta_H}}, \qquad \mathcal{M}_{HH}^{(m)} \sim \Delta_H. \tag{3.9.7}$$

Based on eq. (3.9.6), we can use this asymptotic behavior to estimate the IR cutoff,

$$\Lambda_{\text{IR}}^2 \sim \frac{|\mathcal{M}_{LH}|^2}{\mathcal{M}_{HH}} \sim \frac{m^2}{\Delta_{\text{max}}^2}. \tag{3.9.8}$$

This estimate matches our free field theory results in section 4.4, as the corrections to the three-particle threshold (as well as the other n-particle thresholds) approximately vanish as $1/\Delta_{\text{max}}^2$.

For the interaction matrices, the $\mathcal{M}_{LH}$ terms also decrease as $\Delta_H \to \infty$, though the $n \to n+2$ matrix elements appear to fall off more slowly than the mass term, suggesting that those elements will provide the dominant contribution at large Δ_{max}. The corresponding $\mathcal{M}_{HH}$ elements are either approximately constant ($n \to n$) or slowly increasing ($n \to n+2$), which indicates that they are both subdominant compared to the rapidly growing mass term.

These matrix elements thus explain the observed behavior of the eigenvalue extrapolations in figure 3.3. At weak coupling, the mass term contribution dominates the IR cutoff, such that the corrections scale as $1/\Delta_{\text{max}}^2$. As we increase the coupling, the ϕ^4 $\mathcal{M}_{LH}$ elements begin to contribute more strongly, slowing the rate of convergence and leading to roughly $1/\Delta_{\text{max}}$ corrections near the critical point.

More generally, we learn from these results that the linear growth of the mass term *guarantees convergence* in 2D ϕ^4 theory. Because the matrix elements mixing higher-dimensional operators with our truncated basis all decrease as we increase Δ_{max}, the suppression from the mass term ensures that our IR cutoff must vanish *at least* as quickly as $1/\Delta_{\text{max}}$.

Chapter 4

Conformal Truncation and the 3D Ising Model

They are already putting my ideas into practice! — Tommy Wiseau

4.1 Introduction

We've seen that conformal truncation works at strong coupling, correctly demonstrating the emergence of the Ising fixed point from the RG flow of ϕ^4 theory in two spacetime dimensions. We'd like to push forward now, on to three dimensions at strong coupling! In this brief chapter, I will discuss some ongoing work to extend conformal truncation to the three-dimensional Ising model. Much of the set-up follows from [69], although there the authors only considered the perturbative and large-N regimes. These regimes only test a subset of the conformal basis (in particular, only the two and three-particle states). In the following sections, I will describe ongoing work to attempt this analysis to strong coupling. I will explicate the method to construct the full basis of primary operators in three dimensions as well as sanity checks we have performed to test this basis.

4.2 Conformal Truncation and Scalar Field Theory

Like in two dimensions, our starting point in 3D is the free scalar, which we deform by a mass term and a quartic interaction:

$$S = \int d^3x \, \frac{1}{2}(\partial_\mu \phi)^2 - \frac{1}{2}m^2\phi^2 - \frac{\lambda}{4!}\phi^4. \tag{4.2.1}$$

Obviously, since we are in three dimensions, we have an additional lightcone direction $x^\perp$ in addition to the usual lightcone directions $x^\pm \equiv \frac{1}{\sqrt{2}}(t \pm x)$, where x^+ is treated as time. The metric therefore takes the form

$$ds^2 = 2dx^+dx^- - dx^{\perp 2}. \tag{4.2.2}$$

Associated with the coordinates are the momenta $p_\mu = i\partial_\mu$ where

$$p^2 = 2p_+p_- - p_\perp^2. \tag{4.2.3}$$

The UV CFT is clearly that of a free scalar, which on a fixed time slice can be expanded in creation and annihilation operators

$$\phi(x) = \int \frac{dp_- dp_\perp}{(2\pi)^2\sqrt{2p_-}}(e^{-ip\cdot x}a_p + e^{ip\cdot x}a_p^\dagger). \tag{4.2.4}$$

These operators obey the usual commutation relations

$$[a_p, a_q^\dagger] = (2\pi)^2\delta^2(p-q). \tag{4.2.5}$$

ϕ is normalized such that

$$[\phi(x), \pi(y)] \equiv [\phi(x), \partial_-\phi(y)] = \frac{i}{2}\delta^2(x-y). \tag{4.2.6}$$

Our normalization for the Fock space states are

$$|p\rangle \equiv \sqrt{2p_-}a_p^\dagger|0\rangle, \qquad \langle p|q\rangle = 2p_-(2\pi)^2\delta^2(p-q). \tag{4.2.7}$$

Our basis will be constructed from Casimir eigenstates, which can be thought of as

a Fourier transform of a local operator acting on the vacuum

$$|\mathcal{C}, \ell; \vec{P}, \mu\rangle \equiv \int d^d x \, e^{-iP\cdot x} \mathcal{O}(x)|0\rangle. \tag{4.2.8}$$

These eigenstates are normalized such that

$$\langle \mathcal{C}, \ell; \vec{P}, k|\mathcal{C}', \ell'; \vec{P}', k'\rangle = 2P_-(2\pi)^2\delta^2(P-P')\delta_{\mathcal{C}\mathcal{C}'}\delta_{\ell\ell'}\delta_{kk'}. \tag{4.2.9}$$

4.3 Conformal Truncation and Scalar Field Theory

4.3.1 3D Scalar Field Theory

Our work will largely follow the conventions and notation introduced in [69], but for completeness we provide a quick summary of those details here.

Our starting point is a UV CFT of a free scalar field ϕ with the Lagrangian

$$\mathcal{L}_{\text{CFT}} = \frac{1}{2} : \partial_\mu \phi \partial^\mu \phi :, \tag{4.3.1}$$

where the notation $: \mathcal{O} :$ indicates that the operator should be normal-ordered. We will work in 2+1 dimensions in lightcone coordinates, which are defined by $x^\pm \equiv \frac{1}{\sqrt{2}}(t \pm x)$, as well as the tranverse direction $x^\perp$. The coordinate x^+ is treated as the "time" direction and the metric is given by

$$ds^2 = 2dx^+dx^- - dx^{\perp 2}. \tag{4.3.2}$$

The associated momenta are given by $p_\mu = i\partial_\mu$, from which we can determine the Lorentz invariant quantity

$$p^2 = 2p_+p_- - p_\perp^2. \tag{4.3.3}$$

Our goal will be to determine the IR spectrum and eigenstates by diagonalizing the invariant mass-squared operator in a frame with total momentum $\vec{P}$. In three dimensions, in terms of the momentum generators, this means diagonalizing

$$M^2 = 2P_+P_- - P_\perp^2. \tag{4.3.4}$$

We will diagonalize this operator on a basis of Casimir eigenstates associated with the

UV free scalar. The free scalar field can be expanded in terms of its mode functions

$$\phi(x) = \int \frac{d^2p}{(2\pi)^2\sqrt{2p_-}} \left(e^{-ip\cdot x}a_p + e^{ip\cdot x}a_p^\dagger\right), \tag{4.3.5}$$

where

$$\left[a_p, a_q^\dagger\right] = (2\pi)^2\delta(p-q). \tag{4.3.6}$$

This expansion for $\phi(x)$ leads to an expression for the lightcone hamiltonian P_+ (as well as the other lightcone momenta) in terms of oscillator modes, as we will see momentarily. We will then diagonalize the mass-squared operator by similarly expressing our complete basis states in terms of mode functions, truncating at some maximum Casimir eigenvalue to obtain a finite-dimensional matrix.

After expanding in oscillator modes, the CFT Hamiltonian takes the form

$$P_+^{(\mathrm{CFT})} = \int \frac{d^2p}{(2\pi)^2} a_p^\dagger a_p \frac{p_\perp^2}{2p_-}. \tag{4.3.7}$$

The deformations to the UV CFT that we will study are the mass term and a quartic interaction, given by

$$\delta\mathcal{L} = -\frac{1}{2}m^2\phi^2 - \frac{1}{4!}\lambda\phi^4. \tag{4.3.8}$$

This results in the following corrections to the lightcone Hamiltonian, respectively:

$$\delta P_+^{(m)} = \int \frac{d^2p}{(2\pi)^2} a_p^\dagger a_p \frac{m^2}{2p_-}, \tag{4.3.9}$$

and

$$\delta P_+^{(\lambda)} = \frac{\lambda}{24}\int \frac{d^2pd^2qd^2k}{(2\pi)^6\sqrt{8p_-q_-k_-}} \left(\frac{4a_p^\dagger a_q^\dagger a_k^\dagger a_{p+q+k}}{\sqrt{2(p_-+q_-+k_-)}} + \text{ h.c. } + \frac{6a_p^\dagger a_q^\dagger a_k a_{p+q-k}}{\sqrt{2(p_-+q_--k_-)}}\right). \tag{4.3.10}$$

4.3.2 Conformal Basis for 3D Scalar Fields

The conformal truncation prescription amounts to diagonalizing M^2 on a basis of Casimir eigenstates. In this section, we will explain how to construct these eigenstates and how the basis is modified in the presence of the mass deformation.

Our starting point in the UV is the free massless scalar field, and so our basis is

comprised of primary (and descendant) operators of the free scalar. In order to construct these operators, we have the following building blocks

$$\phi, \qquad \partial_+\phi, \qquad \partial_-\phi, \qquad \partial_\perp\phi. \tag{4.3.11}$$

By the equations of motion $\partial_+\phi = \frac{\partial_\perp^2}{2\partial_-}\phi$, so that we can focus on only the $\partial_-\phi$ and $\partial_\perp\phi$ building blocks.

The procedure to construct a basis of Casimir eigenstates from these building blocks was first presented in [69]. The idea is to first start with the "all-minus" subset of the basis, comprised of operators built only out of ϕ and ∂_- derivatives. Then, the other states are obtained by acting on the all-minus states with the Pauli-Lubanski operator.

However, that method fails to capture *all* of the primary states, so that the resultant basis is incomplete. This can be demonstrated by example. If we start with with states built out of ϕ and $\partial_-\phi$, the Pauli-Lubanski operator will fail to produce states that are schematically like $\partial^\mu\phi\cdots\phi\cdots\partial_\mu\phi$. The reason is that the Pauli-Lubanski operator is

$$W = P_-\sum_i\left(p_{i\perp}\partial_{i-} + \frac{p_{i\perp}^2}{2p_{i-}}\partial_{i\perp}\right) - P_\perp\sum_i p_{i-}\partial_{i-} - \sum_i\frac{p_{i\perp}^2}{2p_{i-}}\sum_j p_{j-}\partial_{j\perp}, \tag{4.3.12}$$

which effectively replaces an instance of $\partial_-\phi$ with $\partial_\perp\phi$ when it acts on an operator (in the total momentum frame where $P_\perp = 0$). In this way, one can start with the all-minus component of a generic operator and then generate the rest of the spin multiplet by acting repeatedly with the Pauli-Lubanski operator. The problem with doing this becomes apparent when we consider primary operators which involve contractions of some of the derviatives. Given an all-minus component, we can act with W to turn a ∂_- to a $\partial_\perp$. However, we will never be able to obtain primaries which involve a contraction of derivatives which gives, e.g. $\partial_+\partial_\perp\phi\cdots\phi\cdots\partial_-\partial_\perp\phi$.

Our approach in this work will be more pedestrian. We will simply start with the building blocks eq. (4.3.11) and construct the linear combinations that are primary with a brute-force algorithm. These operators take the form

$$\mathcal{O}(x) = \sum_{\{m_n\}} C^{\mathcal{O}}_{\{m_n\}}\partial^{m_1}\phi(x)\partial^{m_2}\phi(x)\cdots\partial^{m_n}\phi(x), \tag{4.3.13}$$

for some yet-to-be-determined coefficients $C^{\mathcal{O}}_{\{m_n\}}$. We can express these operators in

momentum space by inserting a complete set of states:

$$\begin{aligned}|\mathcal{O};\vec{P},\mu\rangle &= \frac{1}{n!}\int \frac{d^2p_1\cdots d^2p_n}{(2\pi)^{2n}2p_{1-}\cdots 2p_{n-}}\langle p_1,\ldots,p_n|\mathcal{O};\vec{P},\mu\rangle|p_1,\ldots,p_n\rangle \\ &= \frac{1}{n!}\int \frac{d^2p_1\cdots d^2p_n}{(2\pi)^{2n}2p_{1-}\cdots 2p_{n-}}(2\pi)^3\delta^3\left(\sum_i p_i - P\right)F_{\mathcal{O}}(p)|p_1,\ldots,p_n\rangle,\end{aligned} \tag{4.3.14}$$

where the wavefunction $F_{\mathcal{O}}(p)|p_1,\ldots,p_n\rangle$ is just given by the overlap of the operator with a Fock space state

$$F_{\mathcal{O}}(p) = \langle\mathcal{O}(0)|p_1,\ldots,p_n\rangle = \sum_{\{m_n\}} C^{\mathcal{O}}_{\{m_n\}}p_1^{m_1}\cdots p_n^{m_n}. \tag{4.3.15}$$

We can therefore focus on determining these polynomials, which are simply the Fourier transforms of local operators.

In order to determine these wavefunctions, we must find the operators that are annihilated by the special conformal transformations K_μ. As differential operators acting on a generic monomial $P_+^aP_-^bP_\perp^c\phi$, they take the form

$$\begin{aligned}K_- &= 2P_+\frac{\partial^2}{\partial P_+^2} + 2P_\perp\frac{\partial^2}{\partial P_+\partial P_\perp} + 2\Delta_\phi\frac{\partial}{\partial P_+} + P_-\frac{\partial^2}{\partial P_\perp^2}, \\ K_\perp &= -2P_+\frac{\partial^2}{\partial P_+\partial P_\perp} - 2P_-\frac{\partial^2}{\partial P_-\partial P_\perp} - P_\perp\frac{\partial^2}{\partial P_\perp^2} - 2\Delta_\phi\frac{\partial}{\partial P_\perp} - 2P_\perp\frac{\partial^2}{\partial P_+\partial P_-}, \\ K_+ &= 2P_-\frac{\partial^2}{\partial P_-^2} + 2P_\perp\frac{\partial^2}{\partial P_-\partial P_\perp} + 2\Delta_\phi\frac{\partial}{\partial P_-} + P_+\frac{\partial^2}{\partial P_\perp^2}.\end{aligned} \tag{4.3.16}$$

We could determine the primary operators by then finding the null space of these operators acting on the space of monomials. However, this basis of primary operators is actually not the final basis we are after.

To explain why, we first note that we are interested in deforming the CFT Hamiltonian by a mass term (and interaction terms), as given in eq. (4.3.9). As explained first in [69], and reviewed in Appendix 4.5, the presence of this mass term results in a divergence in the mass matrix elements. Regulating this divergence with an ϵ prescription, we find some eigenstates that are lifted out of the spectrum and those that remain finite as $\epsilon \to 0$. The eigenstates corresponding to the finite matrix elements are a reshuffling of the original primary basis, such that these states satisfy *Dirichlet* boundary conditions. Explicitly, this means operators which have at least one factor of P_- on each particle insertion to cancel against the Lorentz invariant measure of the mass deformation. In

momentum space, this corresponds to wavefunctions of the type

$$p_{1-}p_{2-}\cdots p_{n-}\,(\cdots)\,, \tag{4.3.17}$$

where the second set of ellipses indicates a generic function of p_{i-}, $p_{i\perp}$, and p_{i+}. We will therefore introduce the following notation to specify a Dirichlet basis state:

$$|\mathcal{O};\vec{P},\mu\rangle = \frac{1}{n!}\int \frac{d^2p_1\cdots d^2p_n}{(2\pi)^{2n}2p_{1-}\cdots 2p_{n-}}(2\pi)^3\delta^3\left(\sum_i p_i - P\right) p_{1-}p_{2-}\cdots p_{n-}\bar{F}_{\mathcal{O}}(p)|p_1,\cdots,p_n\rangle, \tag{4.3.18}$$

where $\bar{F}_{\mathcal{O}}(p)$ indicates the Dirichlet wavefunction.

One might be tempted to create a basis for the Dirichlet states by taking a list of all primary operators and throwing out those that do not satisfy Dirichlet boundary conditions. Unfortunately, this resultant basis would be incomplete, because acting with P_- can cause an operator without Dirichlet boundary conditions to become Dirichlet. Therefore, we need to include both the Dirichlet primaries and the non-primary Dirichlet operators for which acting with K produces non-Dirichlet states. But since these, too, are not in general orthonormal, and we lack a good systematic way to identify an orthonormal subset of them, we opted to abandon the primaries altogether. Instead our approach for obtaining the Dirichlet basis is more brute-force; we will tabulate all possible Dirichlet states below a given $\mathcal{C}_{\text{max}}$ and find an orthonormal subset using the Gram-Schmidt process. Details of our implementation can be found in Appendices 4.5 and 4.7.

Finally, to complete the discussion on our basis states, we must note that μ as it appears in eq. (4.3.14) is still a continuous parameter. It denotes the kinetic energy of the state i.e. its eigenvalue under P^2. In order to obtain a complete, *discrete* basis, we must introduce some prescription to discretize over this parameter. A general way to do this is to integrate μ weighted by functions that carry some index $k \in \mathbb{Z}_{\geq 0}$:

$$\begin{aligned}|\mathcal{O};\vec{P},k\rangle = &\int d\mu^2 f(\mu)g_k(\mu)\\ &\times\frac{1}{n!}\int \frac{d^2p_1\cdots d^2p_n}{(2\pi)^{2n}2p_{1-}\cdots 2p_{n-}}(2\pi)^3\delta^3\left(\sum_i p_i - P\right) p_{1-}p_{2-}\cdots p_{n-}\bar{F}_{\mathcal{O}}(p)|p_1,\cdots,p_n\rangle,\end{aligned} \tag{4.3.19}$$

where $f(\mu)$ is a measure that we have freedom to choose. The region of integration

for μ is supposed to be taken from $[0,\infty)$. The reason that it is non-negative is that there is a Wightman prescription for the 2-pt. function of these operators that ensures positivity of the lightcone momenta. However, the integral will diverge and must be regulated. For this reason, we have to introduce a UV cutoff Λ. Cutting off the integral and rescaling the region of integration to $[0,1]$ we find that our final states are given by

$$\boxed{\begin{aligned}|\mathcal{O};\vec{P},k\rangle &= \frac{1}{\sqrt{2\pi}P_-^{n+|\boldsymbol{\lambda}_-|}\Lambda^{\frac{n-5}{2}+|\boldsymbol{\lambda}_\perp|}}\int_0^1 \frac{d\bar{\mu}^2}{\bar{\mu}^{\frac{n-3}{2}+|\boldsymbol{\lambda}_\perp|}}g_k(\bar{\mu}) \\ &\times \frac{1}{n!}\int \frac{d^2p_1\cdots d^2p_n}{(2\pi)^{2n}2p_{1-}\cdots 2p_{n-}}(2\pi)^3\delta^3\left(\sum_i p_i - P\right)p_{1-}p_{2-}\cdots p_{n-}\bar{F}_{\mathcal{O}}(p)|p_1,\cdots,p_n\rangle,\end{aligned}} \tag{4.3.20}$$

where we have defined the dimensionless $\bar{\mu}\equiv\frac{\mu}{\Lambda}$ and $|\boldsymbol{\lambda}_{-,\perp}|$ count the number of $-$ and $\perp$ derivatives in $\bar{F}_{\mathcal{O}}(p)$, respectively. We have introduced a slightly different integration measure than the one used in [69]. In [69], the proposed weight functions $g_k(\mu)$ were Jacobi polynomials of degree k. The motivation for doing this was that the Jacobi polynomials were the natural orthogonal polynomials with respect to the spectral density. In other words, the integration measure was chosen to be the spectral density for that operator. The disadvantage with this method is that the spectral density is different for each Casimir eigenstate. In this paper, we are going to adopt a different approach here and discretize μ into linearly spaced bins democratically for different Casimir eigenstates:

$$g_k(\bar{\mu}) = \frac{1}{\sqrt{\bar{\mu}_k^2-\bar{\mu}_{k-1}^2}}\left[\theta(\bar{\mu}^2-\bar{\mu}_{k-1}^2)-\theta(\bar{\mu}^2-\bar{\mu}_k^2)\right], \tag{4.3.21}$$

where θ is the Heaviside step function. The purpose of the above equation is to the set the region of integration in $\bar{\mu}$ to be in a bin between $\bar{\mu}_{k-1}$ and $\bar{\mu}_k$. Truncating at some $k_{\max}$, we can obtain a discrete, finite-dimensional basis of Dirichlet states. The normalization of these weight functions is chosen such that

$$\int_0^1 d\bar{\mu}^2 g_k(\bar{\mu})g_{k'}(\bar{\mu}) = \delta_{kk'}. \tag{4.3.22}$$

This completes our discussion of computing the Dirichlet basis. To summarize: we

tabulate all possible monomials $P_+^a P_-^b P_\perp^c \phi$ that satisfy Dirichlet boundary conditions and obtain the orthonormal linear combinations through a Gram-Schmidt procedure. We discretize in μ using the weight functions in eq. (4.3.21) and truncate at some $\mathcal{C}_{\text{max}}$, k_{max} obtain our final discrete, truncated basis.

4.3.3 Review of Spectral Densities

After we have truncated the basis to some $\mathcal{C}_{\text{max}}$ and computed the associated Hamiltonian matrix elements, we can construct the invariant mass operator

$$M^2 = 2P_+P_- - P_\perp^2. \tag{4.3.23}$$

Because our basis consists of P_- eigenstates, and we work in a frame where $P_\perp = 0$, diagonalizing this Lorentz invariant operator is actually equivalent to diagonalizing the lightcone Hamiltonian P_+.

The mass eigenvalues that result from diagonalizing M^2 are an approximation to the spectrum of the IR QFT. However, in addition to the eigenvalues, we also obtain the associated eigenstates $|\mu_i\rangle$, which we can use to compute dynamical IR observables. One natural and important observable for us to study is the spectral density of any local operator $\mathcal{O}(x)$,

$$\rho_{\mathcal{O}}(\mu) \equiv \sum_i |\langle \mathcal{O}(0)|\mu_i\rangle|^2 \, \delta(\mu^2 - \mu_i^2). \tag{4.3.24}$$

As shown in eq. (3.1.1), spectral densities encode the same information as real-time, infinite-volume correlation functions. For presenting results, it will be more convenient to show the integrated spectral density,

$$I_{\mathcal{O}}(\mu) \equiv \int_0^{\mu^2} d\mu'^2 \, \rho_{\mathcal{O}}(\mu') = \sum_{\mu_i \le \mu} |\langle \mathcal{O}(0)|\mu_i\rangle|^2, \tag{4.3.25}$$

which contains the same dynamical information as the spectral density.

4.4 Sanity Checks

In this section, we perform consistency checks in the free massive theory where $\lambda = 0$. We then compare with theoretical predictions, which gives us a nontrivial check of the Dirichlet basis.

In section 4.4.1, we first explain how to compute the theoretical predictions for the spectral density associated with a generic local operator $\mathcal{O}_{\mu_1,\ldots,\mu_\ell}(x)$. We then compare these analytic answers to the numerical results obtained from conformal truncation. We will primarily focus on comparisons involving the energy-momentum tensor.

4.4.1 Spectral Densities in Free Field Theory

Let's briefly review some details about spectral densities of operators in free massive theory. The spectral density is the decomposition of the two-point correlation function in terms of mass eigenstates:

$$\langle \mathcal{O}(x)\mathcal{O}(0)\rangle = \int d\mu^2 \rho_{\mathcal{O}}(\mu) \int \frac{d^2P}{(2\pi)^2 2P_0} e^{-iP\cdot x}. \tag{4.4.1}$$

For brevity, we have omitted any tensor structure, but the operators appearing on the LHS could, for example, be various components of spinning operators. In a free theory, we can expand the correlator on the LHS in terms of Fock space modes:

$$\begin{aligned}\langle \mathcal{O}(x)\mathcal{O}(0)\rangle &= \frac{1}{n!}\int \frac{d^3p_1\cdots d^3p_n}{(2\pi)^{3n}} \prod_i (2\pi)\delta(p_i^2 - m^2)|\langle \mathcal{O}(0)|p_1,\ldots,p_n\rangle|^2 e^{-i(\sum_i p_i)\cdot x} \\ &= \int \frac{d\mu^2}{2\pi}\frac{1}{n!}\int \frac{d^3p_1\cdots d^3p_n}{(2\pi)^{3n}} \left(\prod_i (2\pi)\delta(p_i^2 - m^2)\right)(2\pi)^3\delta^3\left(P - \sum_i p_i\right)|\langle \mathcal{O}(0)|p_1,\ldots,p_n\rangle| \\ &\quad \times \int \frac{d^2P}{(2\pi)^2 2P_0} e^{-iP\cdot x},\end{aligned} \tag{4.4.2}$$

where we inserted a complete set of states and used the fact that $d^3P = d\mu^2 \frac{d^2P}{2P_0}$. Equating this to eq. (4.4.1), we can therefore obtain an explicit equation for the spectral density associated with any local operator $\mathcal{O}$:

$$\rho_{\mathcal{O}}(\mu) = \frac{1}{2\pi n!}\int \frac{d^3p_1\cdots d^3p_n}{(2\pi)^{3n}} \left(\prod_i (2\pi)\delta(p_i^2 - m^2)\right)(2\pi)^3\delta^3(P - \sum_i p_i)|\langle \mathcal{O}(0)|p_1,\ldots,p_n\rangle|^2. \tag{4.4.3}$$

This formula also holds for operators with spin, so that we can compare theoretical predictions for spectral densities of various components of spinning operators. The simplest way to apply eq. (4.4.3) is to compute the overlap $|\langle\mathcal{O}(0)|p_1,\ldots,p_n\rangle|$, evaluate the integrals in the total momentum frame $P=(\mu,\vec{0})$, $p_i=(E_i,\vec{p}_i)$, and then perform a boost to the lightcone frame. Let's see how this works for a few examples.

Consider the spectral density associated with the simplest two-particle operator ϕ^2. The overlap of this operator with the two-particle Fock space state is simply

$$\langle\phi^2(0)|p_1,p_2\rangle=2. \tag{4.4.4}$$

Plugging this into eq. (4.4.3), and evaluating in the frame

$$P=(\mu,\vec{0}),\qquad p_1=(E_1,\vec{p}_1),\qquad p_2=(E_2,\vec{p}_2), \tag{4.4.5}$$

we find

$$\rho_{\phi^2}(\mu)=\frac{1}{4\pi\mu}\theta(\mu-2m). \tag{4.4.6}$$

Note that the step function signifies that the two-particle spectral density starts at the two-particle threshold, as expected. There is no need to boost this answer to the lightcone frame as this spectral density is associated with the scalar two-point function $\langle\phi^2\phi^2\rangle$. We can repeat this analysis for any ϕ^n operator which gives the spectral density

$$\rho_{\phi^n}(\mu)=\frac{n!(\mu-nm)^{n-2}}{(n-2)!(4\pi)^{n-1}2\mu}. \tag{4.4.7}$$

Now let's consider a more nontrival example of the stress-energy tensor. It is given by

$$T_{\mu\nu}=\frac{3}{4}\partial_\mu\phi\partial_\nu\phi-\frac{1}{4}\eta_{\mu\nu}\partial_\sigma\phi\partial^\sigma\phi-\frac{1}{4}\phi\partial_\mu\partial_\nu\phi+\frac{1}{2}m^2\eta_{\mu\nu}\phi^2. \tag{4.4.8}$$

Let's start with the all minus component T_{--}. The overlap is given by

$$\langle T_{--}(0)|p_1,p_2\rangle=-\frac{1}{4}\left(6p_{1-}p_{2-}-p_{1-}^2-p_{2-}^2\right). \tag{4.4.9}$$

We can evaluate the integrals in eq. (4.4.3) by noting that

$$p_{1\pm}=\frac{1}{\sqrt{2}}(E_1\pm p_{1x}),\qquad p_{2\pm}=\frac{1}{\sqrt{2}}(E_2\pm p_{2,x}), \tag{4.4.10}$$

which gives

$$\tilde{\rho}_{T_{--}}(\mu) = \frac{\mu^4 - 8\mu^2 m^2 + 48m^4}{2048\pi\mu}, \tag{4.4.11}$$

where the tilde indicates that we still need to boost to the lightcone frame. We have computed the spectral density associated with T_{--} in the frame $(P_+, P_-, P_\perp) = \left(\frac{\mu}{\sqrt{2}}, \frac{\mu}{\sqrt{2}}, 0\right)$ while the lightcone frame is given by $(P_+, P_-, P_\perp) = \left(\frac{\mu^2}{2P_-}, P_-, 0\right)$. In lightcone coordinates, a boost which sends a vector $V_+ \to \tau V_+$ takes $V_- \to \tau^{-1} V_-$ to preserve the lightcone inner product. We therefore need $\tau = \frac{\mu}{\sqrt{2}P_-}$ so that $\rho_{T_{--}} = \tau^{-4}\tilde{\rho}_{T_{--}}$, since there are four minus indices in $\langle T_{--}T_{--}\rangle$. We therefore get

$$\boxed{\rho_{T_{--}}(\mu) = \frac{P_-^4(\mu^4 - 8\mu^2 m^2 + 48m^4)}{512\pi\mu^5}.} \tag{4.4.12}$$

We can apply this procedure to generate the spectral densities for the remaining components. Note that

$$\langle T_{-\perp}(0)|p_1, p_2\rangle = -\frac{1}{4}(3p_{1-}p_{2\perp} + 3p_{1\perp}p_{2-} - p_{1-}p_{1\perp} - p_{2-}p_{2\perp}), \tag{4.4.13}$$

which gives

$$\boxed{\rho_{T_{-\perp}}(\mu) = \frac{P_-^2(\mu^2 - 4m^2)^2}{512\pi\mu^3}.} \tag{4.4.14}$$

Finally, we have

$$\langle T_{\perp\perp}(0)|p_1, p_2\rangle = -\frac{1}{4}(4p_{1\perp}p_{2\perp} + 2p_{1+}p_{2-} + 2p_{1-}p_{2+} - p_{1\perp}^2 - p_{2\perp}^2) - m^2\eta_{\perp\perp}, \tag{4.4.15}$$

which gives

$$\boxed{\rho_{T_{\perp\perp}}(\mu) = \frac{\mu^4 - 8m^2\mu^2 + 88m^4}{512\pi\mu}.} \tag{4.4.16}$$

Now that we have theoretical predictions for these spectral densities, we can compare them to those obtained from conformal truncation. In order to do this, we will need the overlaps of the UV operators with our eigenstates in order to compute the cumulative overlap in eq. (4.3.25). That is to say, in order to compute eq. (4.3.25), we can insert a resolution of the identity corresponding to our basis

$$I_{\mathcal{O}}(\mu) = \sum_{\mu_i \leq \mu} \sum_{\tilde{\mathcal{O}}} |\langle \mathcal{O}(0)|\tilde{\mathcal{O}}\rangle\langle\tilde{\mathcal{O}}|\mu_i\rangle|^2. \tag{4.4.17}$$

The second piece $\langle\tilde{\mathcal{O}}|\mu_i\rangle$ merely picks out that operator of our eigenvector. Meanwhile, the overlaps $\langle\mathcal{O}(0)|\tilde{\mathcal{O}}\rangle$ are given by

$$\langle\mathcal{O}(0)|\tilde{\mathcal{O}}\rangle = \frac{P_-^{d_-}\Lambda^{\frac{n-1}{2}+d_\perp}}{\sqrt{2\pi}}\left(\frac{2}{\frac{n+1}{2}+d_\perp}\right)\left(\frac{\mu_k^{\frac{n+1+2d_\perp}{2}}-\mu_{k-1}^{\frac{n+1+2d_\perp}{2}}}{\sqrt{\mu_k^2-\mu_{k-1}^2}}\right)\times\mathcal{I}^{\text{inner}}_{\mathcal{O}\tilde{\mathcal{O}}}. \quad (4.4.18)$$

$d_{-,\perp}$ count the number of minus and perp derivatives in $\mathcal{O}$. And $\mathcal{I}^{\text{inner}}_{\mathcal{O}\tilde{\mathcal{O}}}$ is the inner product between $\mathcal{O}$ and $\tilde{\mathcal{O}}$ as defined in eq. (4.5.21)[1].

In Fig. 4.1, we show the spectral densities of the operators ϕ^2 through ϕ^5. We see that the numerical results agree with the theoretical prediction for the spectral density for a wide range of μ. Our IR cutoff is set by k_{max}, where

$$\Lambda_{\text{IR}} \sim \frac{\Lambda_{\text{UV}}}{k_{\text{max}}} \quad (4.4.19)$$

and at $k_{\text{max}} = 100$, we see that the IR cutoff is small enough that the spectral density is within a few percent of the theoretical prediction even for $\mu \gg m$. In Figs. 4.2 and 4.3, we show the spectral densities for T_{--}, $T_{-\perp}$, which similarly agree with the analytic predictions. Similar plots exist for the remaining components and also agree closely with the theoretical result.

[1]Note that the wavefunction corresponding to $\mathcal{O}$ isn't necessarily one that satisfies the Dirichlet boundary conditions which we introduce in later sections.

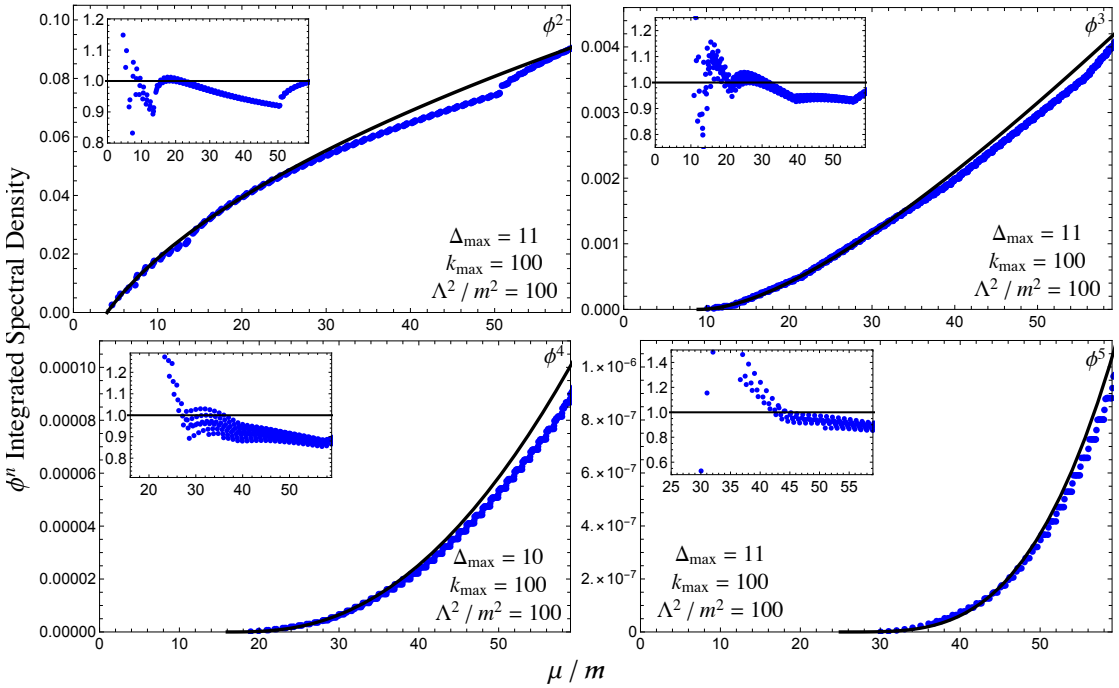

Figure 4.1: Integrated spectral densities for ϕ^2 (upper left), ϕ^3 (upper right), ϕ^4 (lower left), and ϕ^5 (lower right) in massive free field theory ($\lambda = 0$), both the raw value (main plot) and normalized by the theoretical prediction (inset). The conformal truncation results (blue dots) for each plot are computed using the Δ_{max} shown, with the corresponding number of n-particle basis states, and compared to the theoretical prediction (black curve).

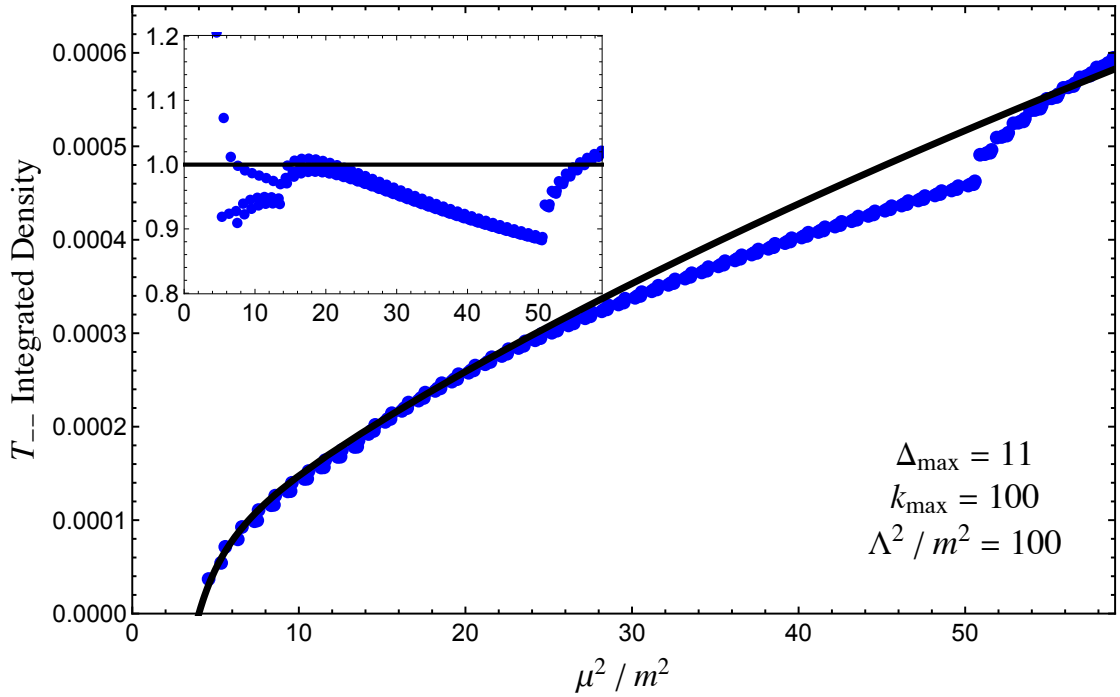

Figure 4.2: Integrated spectral densities for the stress tensor component T_{--} in massive free field theory ($\lambda = 0$), both the raw value (main plot) and normalized by the theoretical prediction (inset). The conformal truncation results (blue dots) for each plot are computed using the $\Delta_{\max}$ shown, with the corresponding number of n-particle basis states, and compared to the theoretical prediction (black curve).

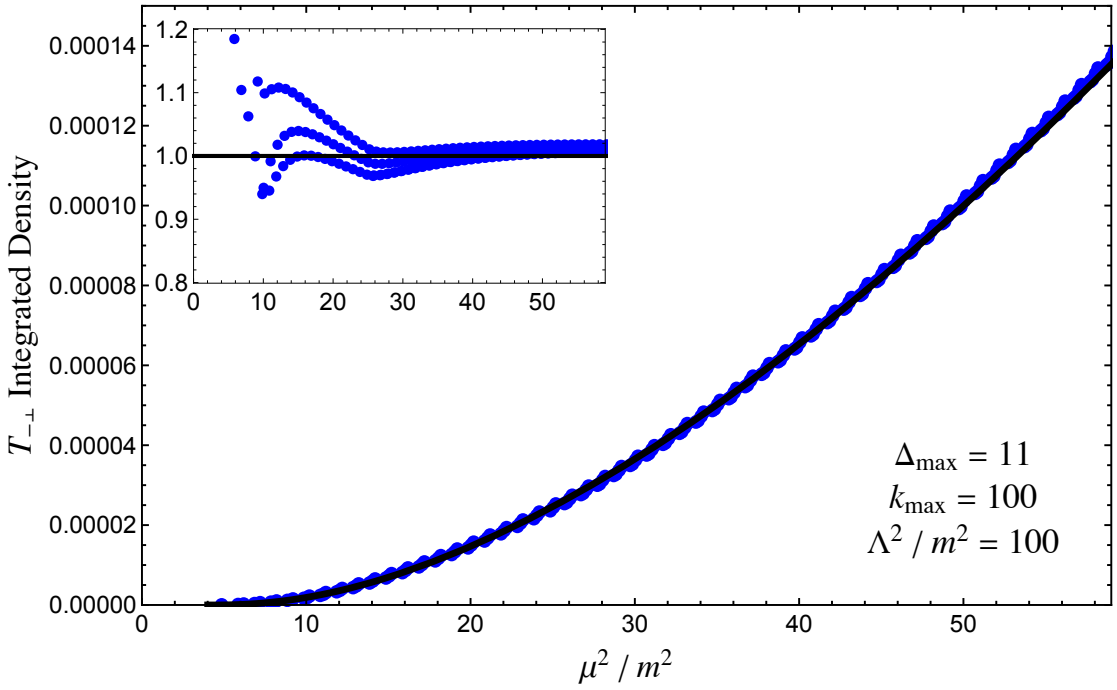

Figure 4.3: Integrated spectral densities for $T_{-\perp}$ in massive free field theory ($\lambda = 0$), both the raw value (main plot) and normalized by the theoretical prediction (inset). The conformal truncation results (blue dots) for each plot are computed using the $\Delta_{\max}$ shown, with the corresponding number of n-particle basis states, and compared to the theoretical prediction (black curve).

Appendix: Additional Technical Details and Results

4.5 Constructing the Basis of Dirichlet States

The construction of the Dirichlet basis from the basis of Casimir eigenstates was first introduced in [69]. We will briefly review that approach below and then explain how it can be generalized to arbitrary particle number.

By definition, the original basis of Casimir eigenstates consists of eigenstates of the CFT Hamiltonian. However, once we introduce a relevant mass deformation to the Hamiltonian

$$\delta P_+^{(m)} = \int \frac{d^2p}{(2\pi)^2} a_p^\dagger a_p \frac{m^2}{2p_-}, \tag{4.5.1}$$

there are IR divergences associated with the mass matrix whenever any individual light-cone momentum of an n-particle eigenstate go to zero. If we regulate these divergences by introducing a small parameter ϵ, the resultant mass spectrum contains two types of eigenstates: those that diverge as $\epsilon \to 0$ and those that remain finite. The states that diverge in this limit are lifted out of the spectrum, such that we can focus on the low-lying sector. The states that remain finite can be seen as a specific linear combination of Casimir eigenstates, a reshuffling of the original UV basis such that their eigenvalues are finite in the limit $\epsilon \to 0$. In practice, this reshuffling gives rise to a "Dirichlet" wavefunction $\tilde{F}_{\mathcal{O}}^{(n)}(p)$ that is schematically the product of the lightcone momenta times a wavefunction which we denote $\bar{F}_{\mathcal{O}}^{(n)}(p)$:

$$F_{\mathcal{O}}^{(n)}(p) \to \tilde{F}_{\mathcal{O}}^{(n)}(p) \sim p_{1-} p_{2-} \cdots p_{n-} \bar{F}_{\mathcal{O}}^{(n)}(p). \tag{4.5.2}$$

We will drop the (n) superscript for brevity.

It is important to note that the size of the Dirichlet basis is smaller than that of the original Casimir basis. While every Dirichlet state has this overall factor of $p_{1-}\cdots p_{n-}$, we cannot obtain it from starting with the UV basis and simply tacking on the product of momenta. These states consist of *specific* linear combinations of UV primaries that are orthogonal with respect to an inner product, and in the following section we outline how to numerically compute them.

4.5.1 Two-Particle Example

Before we move onto the general case, we briefly review how the Dirichlet basis arises in a simple two-particle example. We will show how the addition of a mass deformation to the Hamiltonian reshuffles the basis, resulting in a divergent piece that is lifted out of the IR spectrum and a finite piece that is a physical state.

To see this, consider a truncated 2-particle basis consisting of the operators ϕ^2 and T_{--}, where T_{--} is given by[2]

$$T_{--} = \phi\partial_-^2\phi - 3(\partial_-\phi)^2. \tag{4.5.3}$$

In momentum space, we can express the wavefunction associated with T_{--} as

$$\int d^3x\, e^{ix\cdot P}\langle\phi\partial_-^2\phi(x) - 3(\partial_-\phi)^2(x)|p_1,p_2\rangle = [6p_{1-}p_{2-} - (p_1^2+p_2^2)]\times\delta(P-p_1-p_2), \tag{4.5.4}$$

Let's first start with the simple example of the mass term matrix element between ϕ^2. We find

$$\langle\phi^2;P'|2P_-\delta P_+^{(m)}|\phi^2,P\rangle = 2P_-m^2\int\frac{d^2k_1d^2k_2}{(2\pi)^4 2k_{1-}2k_{2-}}(2\pi)^3\delta^3(k_1+k_2-P')(2\pi)^3\delta^3(k_1+k_2-P) \times\left(\frac{1}{k_{1-}}+\frac{1}{k_{2-}}\right). \tag{4.5.5}$$

Already, we can see how the divergence will arise. We see that when any of the $k_{i-}\to 0$, the integral above will exhibit a divergence which will need to be regulated. In fact, the delta functions cause the two integrals above to collapse to a single integral and introducing an ϵ regulator and performing that integral using the coordinate transformations

[2] Up to a normalization constant that we will ignore as it is not important for this discussion.

in Appendix 4.5.2, we find

$$\langle \phi^2; P' | 2P_- \delta P_+^{(m)} | \phi^2, P \rangle = 2P_- (2\pi)^2 \delta(\vec{P} - \vec{P}') \frac{m^2}{\mu} \left(\frac{1}{\sqrt{P_- \epsilon}} + \mathcal{O}(\epsilon) \right), \tag{4.5.6}$$

where $P^2 = \mu^2$. As expected, this matrix element diverges as $1/\sqrt{\epsilon}$. Now, performing the same exercise for the other operator T_{--}, we find

$$\langle T_{--}; P' | 2P_- \delta P_+^{(m)} | T_{--}; P \rangle = 2P_- (2\pi)^2 \delta^2(\vec{P} - \vec{P}') \frac{m^2}{\mu} \left(\frac{P_-^{7/2}}{\sqrt{\epsilon}} + \mathcal{O}(\epsilon) \right). \tag{4.5.7}$$

We can also similarly compute the matrix element between T_{--} and ϕ^2. Ignoring overall numerical factors and the μ dependence, we find that the divergent part of the matrix elements looks like

$$M^2 \sim \frac{1}{\sqrt{\epsilon}} \begin{pmatrix} P_-^{-1/2} & P_-^{3/2} \\ P_-^{3/2} & P_-^{7/2} \end{pmatrix} \tag{4.5.8}$$

This matrix has two eigenvalues: 0 and one that diverges as $\epsilon \to 0$, which is $\sim \frac{1}{\sqrt{\epsilon}}$. If we look at the eigenvector corresponding to the former, we find that it is just a linear combination

$$\begin{pmatrix} P_-^2 & 1 \end{pmatrix} = -P_-^2 \phi^2 + T_{--} = -(p_1 + p_2)^2 \phi^2 + T_{--} = -\phi \partial_-^2 \phi - (\partial_- \phi)^2 + T_{--}. \tag{4.5.9}$$

We see that the $\phi \partial_-^2 \phi$ cancels against the same term in T_{--}, leaving just a term proportional to $(\partial_- \phi)^2$. The effect of the Dirichlet boundary condition is to therefore to *reshuffle* the basis and remove the problematic piece in T_{--}. The reduced Dirichlet basis, which in this case consists of the single eigenstate corresponding to the operator $(\partial_- \phi)^2$, is the finite eigenstate, while the divergent piece is lifted out of the spectrum. In effect, the Dirichlet basis consists of reshuffling of the original basis such that the operators that remain have a product of momenta $p_{1-} p_{2-} \cdots p_{n-}$ necessary to cancel against the IR divergence.

The purpose of this example was to show how the Dirichlet basis arises from the standard conformal primary basis once we deform by a mass term. We see that the size of the Dirichlet basis is smaller than that of the original basis (and this behavior will persist as we increase the size of the basis). In practice, one could construct the Dirichlet states by finding the finite linear combinations of eigenstates, which amounts to

determining the kernel of the divergent part of the mass matrix. However, our approach will simply be to construct these states by demanding that every Dirichlet state has a product of momenta $p_{1-}p_{2-}\cdots p_{n-}$ and using their associated inner product. We will describe this in the next section.

4.5.2 General Case

While the above method for constructing the Dirichlet basis can be generalized, in this work we will explicitly construct the basis of Dirichlet states from their associated inner product. This basis is identical to what is obtained by starting with Casimir eigenstates and demanding that they satisfy Dirichlet boundary conditions, but it is computationally more efficient to implement. We leave the details of our numerical algorithm to section 4.7; below we will derive the Dirichlet inner product and explain the symmetrization procedure to obtain our final basis states.

Our Dirichlet states take the form as in eq. (4.6.5), which we reproduce here:

$$|\mathcal{O};\vec{P},k\rangle = \frac{1}{\sqrt{2\pi}P_-^{n+|\boldsymbol{\lambda}_-|}\Lambda^{\frac{n-5}{2}+|\boldsymbol{\lambda}_\perp|}}\int_0^1 \frac{d\bar{\mu}^2}{\bar{\mu}^{\frac{n-3}{2}+|\boldsymbol{\lambda}_\perp|}}g_k(\bar{\mu}) \\ \times \frac{1}{n!}\int \frac{d^2p_1\cdots d^2p_n}{(2\pi)^{2n}2p_{1-}\cdots 2p_{n-}}(2\pi)^3\delta^3\left(\sum_i p_i - P\right)p_{1-}p_{2-}\cdots p_{n-}\bar{F}_{\mathcal{O}}(p)|p_1,\cdots,p_n\rangle, \tag{4.5.10}$$

where we have substituted in the Dirichlet wavefunction in eq. (4.5.2). The inner product then takes the form

$$\langle\mathcal{O}';\vec{P}',k'|\mathcal{O};\vec{P},k\rangle = \frac{2P_-(2\pi)^2\delta^2(\vec{P}-\vec{P}')}{2^n n!}\frac{1}{2\pi P_-^{2n+|\boldsymbol{\lambda}_-|+|\boldsymbol{\lambda}'_\perp|}\Lambda^{n-5+|\boldsymbol{\lambda}_\perp|+|\boldsymbol{\lambda}'_-|}} \\ \times\int_0^1 \frac{d\bar{\mu}^2}{\bar{\mu}^{\frac{n-3}{2}+|\boldsymbol{\lambda}_\perp|}}\int_0^1 \frac{d\bar{\mu}'^2}{\bar{\mu}'^{\frac{n-3}{2}+|\boldsymbol{\lambda}_\perp|}}g_k(\bar{\mu}^2)g_{k'}(\bar{\mu}'^2)(2\pi)\delta(\bar{\mu}^2-\bar{\mu}'^2) \\ \times\int \frac{d^2p_1\cdots d^2p_n}{(2\pi)^{2n}}(2\pi)^3\delta^3\left(\sum_i p_i - P\right)p_{1-}\cdots p_{n-}\bar{F}_{\mathcal{O}}(p)\bar{F}_{\mathcal{O}'}(p). \tag{4.5.11}$$

Using the equations of motion and the choice of our reference frame of $P_\perp = 0$, the set of delta functions can be recast as

$$\delta^3\left(\sum_i p_i - P\right) = \delta\left(\sum_i \frac{p_{i\perp}^2}{2p_{i-}} - \frac{\mu^2}{2P_-}\right)\delta\left(\sum_i p_{i-} - P_-\right)\delta\left(\sum_i p_{i\perp}\right). \tag{4.5.12}$$

Here, it is useful to define dimensionless variables

$$x_i \equiv \frac{p_{i-}}{P_-}, \qquad\qquad y_i \equiv \frac{p_{i\perp}}{\mu}, \tag{4.5.13}$$

so that the wavefunctions have a scaling set by

$$\tilde{F}_{\mathcal{O}}(p) = \mu^{|\boldsymbol{\lambda}_\perp|} P_-^{n+|\boldsymbol{\lambda}_-|} x_1 \cdots x_n \bar{F}_{\mathcal{O}}(x, y), \tag{4.5.14}$$

where $|\boldsymbol{\lambda}_\perp|$ counts the number of $P_\perp$ derivatives while $|\boldsymbol{\lambda}_-|$ counts the number of P_- derivatives in $\bar{F}_{\mathcal{O}}(p)$. These scaling factors cancel against the factors coming from the $\bar{\mu}$ integration measure. Since our weight functions are *defined* to be orthonormal when integrated over μ^2 with unit measure, the inner product factorizes into an orthogonal piece with respect to k and k' and a piece that depends on $\mathcal{O}$ and $\mathcal{O}'$:

$$\langle \mathcal{O}'; \vec{P}', k' | \mathcal{O}; \vec{P}, k \rangle = 2P_-(2\pi)^2 \delta^2(\vec{P} - \vec{P}') \delta_{kk'} \mathcal{I}_{\mathcal{O}'\mathcal{O}}. \tag{4.5.15}$$

To determine $\mathcal{I}_{\mathcal{O}'\mathcal{O}}$, we can choose integration variables defined by

$$\begin{aligned}
x_1 &= (1-z_1)(1-z_2)(1-z_3)\cdots(1-z_{n-1}), \\
x_2 &= \quad z_1(1-z_2)(1-z_3)\cdots(1-z_{n-1}), \\
x_3 &= \quad\quad z_2(1-z_3)\cdots(1-z_{n-1}), \\
&\vdots \qquad\qquad \ddots \\
x_n &= \quad\quad\quad\quad\quad\quad z_{n-1},
\end{aligned} \tag{4.5.16}$$

where the z_i range from $[0, 1]$, and

$$\begin{aligned}
y_1 &= -(y_2 + y_3 + \cdots + y_n), \\
y_2 &= \tilde{y}_1 \sqrt{z_1(1-z_1)\cdots(1-z_{n-1})} - z_1(y_3 + \cdots + y_n), \\
y_3 &= \tilde{y}_2 \sqrt{z_2(1-z_2)\cdots(1-z_{n-1})} - z_2(y_4 + \cdots + y_n), \\
&\vdots \\
y_n &= \tilde{y}_{n-1} \sqrt{z_{n-1}(1-z_{n-1})}.
\end{aligned} \tag{4.5.17}$$

In these variables, the original set of delta functions we had simply reduce to

$$\delta^3\left(\sum_i p_i - P\right) \to \frac{2}{\mu^3}\delta\left(\sum_i^{n-1} \tilde{y}_i^2 - 1\right). \tag{4.5.18}$$

Introducing angular variables for the remaining $\tilde{y}$ variables to implement this constraint

$$\begin{aligned}
\tilde{y}_1 &= \sin\theta_1 \sin\theta_2 \cdots \sin\theta_{n-2}, \\
\tilde{y}_2 &= \cos\theta_1 \sin\theta_2 \cdots \sin\theta_{n-2}, \\
\tilde{y}_3 &= \cos\theta_2 \sin\theta_3 \cdots \sin\theta_{n-2}, \\
&\vdots \\
\tilde{y}_{n-1} &= \cos\theta_{n-2},
\end{aligned} \tag{4.5.19}$$

where $\theta_i \in [0,\pi]$ for $i = 1,\ldots,n-3$ and $\theta_{n-2} \in [0,2\pi]$, we find that the inner product becomes

$$\langle \mathcal{O}'; \vec{P}', k' | \mathcal{O}; \vec{P}, k\rangle = 2P_-(2\pi)^2\delta^2(\vec{P}-\vec{P}')\delta_{kk'}\mathcal{I}_{\mathcal{O}'\mathcal{O}}, \tag{4.5.20}$$

with

$$\boxed{\begin{aligned}
\mathcal{I}_{\mathcal{O}'\mathcal{O}} = \frac{1}{n!2^n(2\pi)^{2n-3}} \int dz_1 \cdots dz_{n-1} \left(\prod_i z_i^{\frac{3}{2}}(1-z_i)^{\frac{5}{2}i-1}\right) \\
\times \int d\theta_1 \cdots d\theta_{n-2} \left(\prod_j \sin^{j-1}\theta_j\right) \bar{F}_{\mathcal{O}}(z,\theta)\bar{F}_{\mathcal{O}'}(z,\theta).
\end{aligned}} \tag{4.5.21}$$

To obtain our final Dirichlet states, we tabulate a list of Dirichlet monomials at and below a given maximum Casimir eigenvalue $\mathcal{C}_{\max}$. This set of monomials will be overcomplete, so in order to determine the complete orthonormal basis, we compute the Gram matrix using eq. (4.5.21) between different monomials. We then determine the final basis by performing a QR decomposition on the Gram matrix, the details of which we leave to Appendix 4.7.

4.6 Matrix Elements and Operator Overlaps

In this section, we compute the matrix elements between the invariant mass M^2 and the Dircichlet basis states. The mass operator can be written in terms of momentum

generators as

$$M^2 = 2P_+P_- - P_\perp^2. \tag{4.6.1}$$

However, since the Hamiltonian deformations we will study do not break translational invariance, we can choose a reference frame where P_- is fixed and $P_\perp = 0$. We can therefore compute the simpler matrix elements

$$\langle \mathcal{O}'; \vec{P}', k' | M^2 | \mathcal{O}; \vec{P}, k \rangle = 2P_- \langle \mathcal{O}'; \vec{P}', k' | P_+ | \mathcal{O}; \vec{P}, k \rangle. \tag{4.6.2}$$

These matrix elements take the form

$$\langle \mathcal{O}'; \vec{P}', k' | M^2 | \mathcal{O}; \vec{P}, k \rangle = 2P_-(2\pi)^2 \delta^2(\vec{P} - \vec{P}') \mathcal{M}_{\mathcal{O},\mathcal{O}',k,k'}. \tag{4.6.3}$$

We will suppress the overall kinematic factor and focus on the matrix elements $\mathcal{M}_{\mathcal{O},\mathcal{O}',k,k'}$ for the remainder of this section.

4.6.1 Kinetic Term

We begin by computing the M^2 matrix elements in the original CFT. As shown in [69], the CFT Hamiltonian can be expressed in terms of raising and lowering operators as

$$P_+^{(\mathrm{CFT})} = \int \frac{d^2p}{(2\pi)^2} a_p^\dagger a_p \frac{p_\perp^2}{2p_-}. \tag{4.6.4}$$

Note that this term preserves particle number, so that we consider sectors with differing particle number separately. As discussed in section 4.5, our Dirichlet states take the form

$$\begin{aligned} |\mathcal{O}; \vec{P}, k\rangle = &\frac{1}{\sqrt{2\pi} P_-^{n+|\boldsymbol{\lambda}_-|} \Lambda^{\frac{n-5}{2}+|\boldsymbol{\lambda}_\perp|}} \int_0^1 \frac{d\bar{\mu}^2}{\bar{\mu}^{\frac{n-3}{2}+|\boldsymbol{\lambda}_\perp|}} g_k(\bar{\mu}) \\ &\times \frac{1}{n!} \int \frac{d^2p_1 \cdots d^2p_n}{(2\pi)^{2n} 2p_{1-} \cdots 2p_{n-}} (2\pi)^3 \delta^3 \left(\sum_i p_i - P \right) p_{1-} p_{2-} \cdots p_{n-} \bar{F}_{\mathcal{O}}(p) |p_1, \cdots, p_n\rangle. \end{aligned} \tag{4.6.5}$$

Inserting eq. (4.6.4) in between two states and using the coordinate transformations in eqs. (4.5.16), (4.5.17), and (4.5.19) we find that

$$\boxed{\mathcal{M}^{(\mathrm{CFT})}_{k,k';\mathcal{O},\mathcal{O}'} = \Lambda^2 \left(\frac{\mu_k^2 + \mu_{k-1}^2}{2} \right) \delta_{k,k'} \mathcal{I}_{\mathcal{O},\mathcal{O}'}.} \tag{4.6.6}$$

4.6.2 Mass Term

The first deformation we consider to the UV Hamiltonian is the mass term, which results in a correction

$$\delta P_+^{(m)} = \int \frac{d^2p}{(2\pi)^2} a_p^\dagger a_p \frac{m^2}{2p_-}. \tag{4.6.7}$$

Like the kinetic term, this term preserves particle number. We can use the same coordinate transformations as in the inner product and kinetic terms to arrive at

$$\boxed{\begin{aligned}\mathcal{M}^{(m)}_{k,k';\mathcal{O},\mathcal{O}'} = \delta_{k,k'} \frac{m^2}{(n-1)!2^n(2\pi)^{2n-3}} \int dz_1 \cdots dz_{n-1} \left(\prod_i z_i^{\frac{3}{2}}(1-z_i)^{\frac{5}{2}i-1}\right)\left(\frac{1}{z_{n-1}}\right) \\ \times \int d\theta_1 \cdots d\theta_{n-2} \left(\prod_j \sin^{j-1}\theta_j\right) \bar{F}_{\mathcal{O}}(z,\theta)\bar{F}_{\mathcal{O}'}(z,\theta).\end{aligned}} \tag{4.6.8}$$

4.6.3 Quartic Interaction

We now move onto the more nontrivial deformation of a quartic interaction to the Hamiltonian, which gives rise to a Hamiltonian correction of the form

$$\delta P_+^{(\lambda)} = \frac{\lambda}{24} \int \frac{d^2p d^2q d^2k}{(2\pi)^6\sqrt{8p_-q_-k_-}} \left(\frac{4a_p^\dagger a_q^\dagger a_k^\dagger a_{p+q+k}}{\sqrt{2(p_-+q_-+k_-)}} + \text{ h.c. } + \frac{6a_p^\dagger a_q^\dagger a_k a_{p+q-k}}{\sqrt{2(p_-+q_--k_-)}} \right). \tag{4.6.9}$$

This deformation contains two types of terms, one that changes particle number and one that preserves it. We will refer to the former, which corresponds to the first two terms in eq. (4.6.9), as the n-to-$n+2$ interaction since it changes particle number by two. We will call the latter type of term in eq. (4.6.9) the n-to-n interaction.

Unlike the kinetic and mass terms, the interaction terms give rise to matrix elements that depend separately on both μ and μ'. In other words, the discretization integrals over μ and μ' do not collapse into one simple integral, but instead depend on μ and μ' through the ratio

$$\boxed{\alpha \equiv \frac{\mu}{\mu'}.} \tag{4.6.10}$$

For this reason, we will introduce the useful notation

$$\langle \mathcal{O}'; \vec{P}', k' | \delta M^2 | \mathcal{O}; \vec{P}, k \rangle = 2P_-(2\pi)^2 \delta^2(\vec{P} - \vec{P}') \times \frac{\lambda\Lambda}{2\pi} \frac{1}{P_-^{2n+|\boldsymbol{\lambda}_-|+|\boldsymbol{\lambda}'_\perp|} \Lambda^{n-5+|\boldsymbol{\lambda}_\perp|+|\boldsymbol{\lambda}'_-|}} \int_0^1 \frac{d\bar{\mu}^2}{\bar{\mu}^{\frac{n-3}{2}+|\boldsymbol{\lambda}_\perp|}} \int_0^1 \frac{d\bar{\mu}'^2}{\bar{\mu}'^{\frac{n-3}{2}+|\boldsymbol{\lambda}_\perp|}} g_k(\bar{\mu}^2) g_{k'}(\bar{\mu}'^2) \mathcal{M}_{\mathcal{O}\mathcal{O}'}(\alpha). \tag{4.6.11}$$

The computation of $\mathcal{M}_{\mathcal{O}\mathcal{O}'}(\alpha)$ for the interaction terms will be the main focus of the following two sections. We will explain the details of the discretization procedure in the interaction matrix elements in section **??**.

4.6.3.1 n-to-$n+2$ Interaction

Let's first consider the n-to-$n+2$ interaction, which gives rise to the following matrix element between an n particle state and an $n+2$ particle state:

$$\begin{aligned} \mathcal{M}^{(n\text{-to-}n+2)}_{\mathcal{O}\mathcal{O}'}(\alpha) = \frac{\lambda}{6(n-1)!} \int \frac{d^2p_1 \cdots d^2p_n}{(2\pi)^{2n} 2p_{1-} \cdots 2p_{n-}} (2\pi)^3 \delta^3 \left(\sum_i p_i - P \right) p_{1-} \cdots p_{n-} \bar{F}_{\mathcal{O}}(p) \\ \times \int \frac{d^2p'_1 \cdots d^2p'_{n+2}}{(2\pi)^{2n+4} 2p'_{1-} \cdots 2p'_{n+2-}} (2\pi)^3 \delta^3 \left(\sum_i p'_i - P' \right) p'_{1-} \cdots p'_{n+2-} \bar{F}_{\mathcal{O}'}(p') \\ \times 2p_{2-}(2\pi)^2 \delta^2(p_2 - p'_4) \cdots 2p_{n-}(2\pi)^2 \delta^2(p_n - p'_{n+2}). \end{aligned} \tag{4.6.12}$$

It is useful to switch to the dimensionless variables defined in eq. (4.5.13) separately for the both the primed and unprimed variables. That is, we take eq. (4.5.16)-(4.5.17) for the unprimed variables and

$$\begin{aligned} x'_1 &= (1-z'_1)(1-z'_2)(1-z'_3)\cdots(1-z'_{n+1}), \\ x'_2 &= \quad z'_1(1-z'_2)(1-z'_3)\cdots(1-z'_{n+1}), \\ x'_3 &= \quad z'_2(1-z'_3)\cdots(1-z'_{n+1}), \\ &\vdots \quad \ddots \\ x'_{n+2} &= \quad z'_{n+1} \end{aligned} \tag{4.6.13}$$

for the primed coordinates and analogously for eq. (4.5.17). We then find

$$\mathcal{M}^{(n\text{-to-}n+2)}_{\mathcal{O}\mathcal{O}'}(\alpha) = \frac{\lambda n\sqrt{(n+1)(n+2)}}{24\pi}\frac{1}{\mu'}\alpha^{\frac{n-3}{2}}\int dz_1\cdots dz_{n-1}d\tilde{y}_1\cdots d\tilde{y}_{n-1}\left(\prod_{i=1}^{n-1} z_i^{\frac{3}{2}}(1-z_i)^{\frac{5}{2}i+1}\right)$$
$$\times\,\delta\left(\sum_i^{n-1}\tilde{y}_{n-1}^2-1\right)\bar{F}_{\mathcal{O}}(z,\tilde{y})\int dz_1'dz_2'd\tilde{y}_1'd\tilde{y}_2'\,z_1'^{\frac{1}{2}}(1-z_1')^{\frac{1}{2}}z_2'^{\frac{1}{2}}(1-z_2')^2$$
$$\times\,\delta\left(\tilde{y}_1'^2+\tilde{y}_2'^2+\alpha^2\sum_{i=1}^{n-1}\tilde{y}_i^2-1\right)\bar{F}_{\mathcal{O}'}(z',\tilde{y},\tilde{y}'). \tag{4.6.14}$$

The first delta function constrains the $n-1$ $\tilde{y}$'s, which correspond to the variables of the "spectator" particles, to a sphere of radius 1. The other delta function for the interacting particles constrains $\tilde{y}'$ to a sphere of radius $1-\alpha^2$, which constrains $\alpha \leq 1$. Physically, this is due to the fact that the n-to-$n+2$ interactions can only increase the kinetic energy due to the creation of two additional particles. Parameterizing these two spheres with angular variables for the spectators and interacting particles we obtain

$$\boxed{\begin{aligned}&\mathcal{M}^{(n\text{-to-}n+2)}_{\mathcal{O}\mathcal{O}'}(\alpha) = \frac{1}{(n-1)!3\pi^{2n}2^{3n+4}}\frac{1}{\mu'}\alpha^{\frac{n-3}{2}}\\&\times\int dz_1\cdots dz_{n-1}dz_1'dz_2'\left(\prod_{i=1}^{n-1} z_i^{\frac{3}{2}}(1-z_i)^{\frac{5}{2}i+1}\right)z_1'^{\frac{1}{2}}(1-z_1')^{\frac{1}{2}}z_2'^{\frac{1}{2}}(1-z_2')^2\\&\times\int d\theta_1\cdots d\theta_{n-2}d\theta'\left(\prod_j \sin^{j-1}\theta_j\right)\bar{F}_{\mathcal{O}}(z,\theta)\bar{F}_{\mathcal{O}}(z',\theta',\theta,\alpha).\end{aligned}} \tag{4.6.15}$$

4.6.3.2 n-to-n Interaction

Finally, we turn to the n-to-n part of the quartic interaction. It takes the form

$$\begin{aligned}\mathcal{M}^{(n-\text{to}-n)}_{\mathcal{O}\mathcal{O}'}(\alpha) = \frac{\lambda n(n-1)}{4}\frac{1}{n!}\int\frac{d^2p_1\cdots d^2p_n}{(2\pi)^{2n}2p_{1-}\cdots 2p_{n-}}(2\pi)^3\delta^3\left(\sum_i p_i - P\right)p_{1-}\cdots p_{n-}\bar{F}_{\mathcal{O}}(p)\\ \times\int\frac{d^2p_1'\cdots d^2p_n'}{(2\pi)^{2n}2p_{1-}'\cdots 2p_{n-}'}(2\pi)^3\delta^3\left(\sum_i p_i' - P'\right)p_{1-}'\cdots p_{n-}'\bar{F}_{\mathcal{O}}(p')\\ \times 2p_{3-}(2\pi)^2\delta^2(p_3-p_3')\cdots 2p_{n-}(2\pi)^2\delta^2(p_n-p_n').\end{aligned} \tag{4.6.16}$$

Performing the coordinate transforms in eqs. (4.5.16)-(4.5.17) for both the primed and unprimed coordinates, we find

$$\begin{aligned}\mathcal{M}^{(n-\text{to}-n)}_{\mathcal{O}\mathcal{O}'}(\alpha) =& \frac{\lambda n(n-1)\alpha^{\frac{n-3}{2}}}{16\pi\mu'}\int dz_1 d\tilde{y}_1 dz_1' d\tilde{y}_1' \sqrt{z_1(1-z_1)z_1'(1-z_1')} \\ &\times \delta\left(\sum_i \tilde{y}_i^2 - 1\right)\delta\left(\tilde{y}_1'^2 + \alpha^2\sum_{i=2}\tilde{y}_i^2 - 1\right) \\ &\times \int dz_2\cdots dz_{n-1}d\tilde{y}_2\cdots d\tilde{y}_{n-1}\left(\prod_{i>1} z_i^{\frac{3}{2}}(1-z_i)^{\frac{5i-3}{2}}\right) F_{\mathcal{O}}(z,\tilde{y})F_{\mathcal{O}}(z',\tilde{y}').\end{aligned} \tag{4.6.17}$$

We can use the delta functions to perform the integration over the $\tilde{y}$ coordinates of the interacting particles. Note that they impose the constraints

$$\tilde{y}_1 = \pm\sqrt{1-r^2}, \qquad\qquad \tilde{y}_1' = \pm\sqrt{1-\alpha^2 r^2}, \tag{4.6.18}$$

where

$$r^2 \equiv \tilde{y}_2^2 - \tilde{y}_3^2 \cdots - \tilde{y}_{n-1}^2. \tag{4.6.19}$$

Note that when $\alpha = 1$, the two constraints coincide, and the range of integration r is taken to be between $[0,1]$. Similarly, when $\alpha < 1$, the reality condition on $\tilde{y}_1$ requires $r \in [0,1]$, which automatically satisfies the constraint on $\tilde{y}_1'$. However, when $\alpha > 1$, the reality condition on $\tilde{y}_1'$ provides a stronger constraint and requires $r \in [0, \alpha^{-1}]$.

Defining spherical coordinates for the remaining spectators

$$\begin{aligned}\tilde{y}_2 &= r\sin\theta_1\sin\theta_2\cdots\sin\theta_{n-3}, \\ \tilde{y}_3 &= r\cos\theta_1\sin\theta_2\cdots\sin\theta_{n-3}, \\ \tilde{y}_4 &= r\cos\theta_2\sin\theta_3\cdots\sin\theta_{n-3}, \\ &\vdots \\ \tilde{y}_{n-1} &= r\cos\theta_{n-3},\end{aligned} \tag{4.6.20}$$

and defining

$$\bar{F}_{\mathcal{O}\pm} \equiv \bar{F}_{\mathcal{O}}(\tilde{y}_1 = \pm\sqrt{1-r^2}), \qquad\qquad \bar{F}_{\mathcal{O}'\pm} \equiv \bar{F}_{\mathcal{O}'}(\tilde{y}_1 = \pm\sqrt{1-\alpha^2 r^2}), \tag{4.6.21}$$

the matrix element can be summarized as

$$\begin{aligned}
&\mathcal{M}_{\mathcal{O}\mathcal{O}'}^{(n\text{-to-}n)}(\alpha) = \frac{1}{(n-2)!\pi^{2n-2}2^{3n+2}}\frac{1}{\mu'}\alpha^{\frac{n-3}{2}} \\
&\times \int dz_1 \cdots dz_{n-1} dz_1' \sqrt{z_1(1-z_1)z_1'(1-z_1')} \left(\prod_{i>1} z_i^{\frac{3}{2}}(1-z_i)^{\frac{5i-3}{2}}\right) \\
&\times \int_0^{\min\left(1,\alpha^{-1}\right)} dr \int d\theta_1 \cdots d\theta_{n-3} \left(\prod_j \sin^{j-1}\theta_j\right) \frac{r^{n-3}}{\sqrt{(1-r^2)(1-\alpha^2 r^2)}} \\
&\times \left(\sum_{\pm} \bar{F}_{\mathcal{O}}(z,r,\theta)\right)\left(\sum_{\pm} \bar{F}_{\mathcal{O}'}(z,\alpha r,\theta)\right).
\end{aligned} \tag{4.6.22}$$

4.7 Details of Code and Algorithms

Broadly speaking, the goal of the program is to reduce as many computations as possible to pure linear algebra operations. This allows us both to avoid a great deal of repeated work and to take advantage of established libraries for linear algebra. So in order to do this, we need a basis for all relevant operators and we need to express the quantities of interest as vectors and matrices on this basis.

Our computation begins with a naive list of all Dirichlet monomials having total scaling dimension below some cutoff $\mathcal{C}_{\max}$. We intend to use this as a basis for all states below the cutoff, but since it's vastly overcomplete (see section 4.5) we must first eliminate all of the redundant monomials, the first step of which is to compute the Gram matrix containing the inner products of all of the monomials in the naive list with all of the others. Before computing the Gram matrix, we normalize the input monomials so that it's easier to distinguish floating point epsilons from inner products which just happen to be small.

With the Gram matrix in hand, there are a number of ways to produce an orthogonal basis from the overcomplete one, the simplest of them being a QR decomposition. However, the QR decomposition of a rank-deficient matrix is not unique, and the Gram matrix is rank-deficient due to the basis being overcomplete. This is a mixed blessing: while it means that off-the-shelf QR decomposition functions will often yield a correct but non-useful basis, it also means that we have a lot of freedom to arrange to produce the most convenient basis possible.

Our implementation uses the Modified Gram-Schmidt Algorithm feeding in monomi-

als one at a time starting with the monomials with the most evenly distributed powers of P_- and $P_\perp$. This produces a basis where the fewest possible monomials are used, which is desirable because it's $O(N^2)$ easier to compute matrix elements between single monomials than between arbitrary superpositions of them. The evenly distributed exponents on the monomials means that each individual monomial will have fewer unique permutations, again simplifying the computation of the matrix elements.

Note that the Gram-Schmidt process produces exponentially compounding roundoff errors in the coefficients of the output vectors because each coefficient depends on all of the ones before it. Because of this problem, we found that we had to use 128-bit precision floating point numbers to keep epsilons from growing to sizes comparable to the actual answers; if one were to increase total scaling dimension beyond what we attempted, one would likely need to increase the precision further, which could quickly create performance bottlenecks.

Having finished Gram-Schmidt and obtained a basis of orthonormal states, the next step is to actually compute the matrix elements between these states. All of the matrix elements are bilinear in the two states' reduced wavefunctions $\bar{F}$, which themselves are sums of permutations of ordered monomials. This suggests a second layer of linear algebra structure: we can represent the orthonormal basis states as vectors on the (non-orthonormal) space of ordered monomials which appear in them.

We refer to this latter space as the 'minimal basis' and write the orthonormal polynomial basis as a matrix P whose columns each represent one of the polynomials, with entry (i, j) giving the contribution of minimal basis monomial i to orthonormal polynomial j. Now, to produce matrix elements between the orthonormal basis polynomials, we can simply compute the matrix elements M_{ij} between minimal basis monomials and transform them to $P^T M P$, producing exactly the desired matrix. Note that M and P are precisely the same size in our implementation, thanks to our choice of orthogonalization of the naive basis – if we had not deliberately selected one which used as few individual monomials as possible, M could have been several times larger.

The matrix M is properly a 4th-order tensor relating the kth μ^2 partition of monomial m to the k'th μ^2 partition of monomial m', i.e. we're computing the entries $M_{mkm'k'}$. For computation simplicity, however, we actually treat this as a matrix: if there are N_m minimal basis monomials and N_k μ^2 partitions, then M is an $N_m N_k \times$

$N_m N_k$ matrix where each pair of monomials has its own $N_k \times N_k$ block.

We compute M block by block, first getting an overall factor a by doing all of the integrals not involving μ^2, then computing a discretization matrix D and multiplying it by a. The entry D_{ij} contains the integral of all μ^2 factors across the appropriate window:

$$D_{ij} = \int_{i/N_k}^{(i+1)/N_k} d\mu^2 \int_{j/N_k}^{(j+1)/N_k} d\mu'^2 f(\mu^2, \mu'^2). \tag{4.7.1}$$

For the kinetic and mass matrices, $f(\mu^2, \mu'^2)$ is just proportional to $\delta(\mu^2 - \mu'^2)$, while for the interaction matrices it's close to a polynomial in μ^2/μ'^2. We memoized each discretization matrix in a hash table keyed by $f(\mu^2, \mu'^2)$, so a matrix element calculation can be represented with the following pseudocode:

```
for each unique permutation of m and m':
    do integrals to get {numerical factor a} and {list of which f appear};
    for each f which appears:
        answer += a * D(f);
return answer * degeneracy;
```

from a given unique permutation; which is of course the same for every unique permutation so it becomes an overall factor.

Once all of the minimal basis matrices M have been computed, everything else is just standard matrix algebra. In particular, the Hamiltonian is just

$$\sum_i P^T M_i P, \tag{4.7.2}$$

summed over the kinetic, mass, and interaction terms. Interesting quantities like eigenvalues can just be computed using ordinary matrix libraries, taking care to take advantage of a few important simplifications. First, the matrix is very "block sparse", i.e. it is a matrix sparsely populated with dense blocks: the kinetic and mass terms are block diagonal by particle number, while the interaction is block banded, with nonzero blocks 2 particle numbers above and 2 particle numbers below the diagonal.

Bibliography

[1] L. Susskind, "The World as a hologram," *J.Math.Phys.* **36** (1995) 6377–6396, arXiv:hep-th/9409089 [hep-th].

[2] J. M. Maldacena, "The Large N limit of superconformal field theories and supergravity," *Adv.Theor.Math.Phys.* **2** (1998) 231–252, arXiv:hep-th/9711200 [hep-th].

[3] E. Witten, "Anti-de Sitter space and holography," *Adv.Theor.Math.Phys.* **2** (1998) 253–291, arXiv:hep-th/9802150 [hep-th].

[4] A. J. A. James, R. M. Konik, P. Lecheminant, N. J. Robinson, and A. M. Tsvelik, "Non-perturbative methodologies for low-dimensional strongly-correlated systems: From non-abelian bosonization to truncated spectrum methods," *ArXiv e-prints* (Mar., 2017) , arXiv:1703.08421 [cond-mat.str-el].

[5] N. Anand, H. Chen, A. L. Fitzpatrick, J. Kaplan, and D. Li, "An Exact Operator That Knows Its Place," arXiv:1708.04246 [hep-th].

[6] N. Anand, V. X. Genest, E. Katz, Z. U. Khandker, and M. T. Walters, "RG flow from ϕ^4 theory to the 2D Ising model," *JHEP* **08** (2017) 056, arXiv:1704.04500 [hep-th].

[7] T. Banks, M. R. Douglas, G. T. Horowitz, and E. J. Martinec, "AdS dynamics from conformal field theory," arXiv:hep-th/9808016 [hep-th].

[8] A. Hamilton, D. N. Kabat, G. Lifschytz, and D. A. Lowe, "Local bulk operators in AdS/CFT: A Boundary view of horizons and locality," *Phys.Rev.* **D73** (2006) 086003, arXiv:hep-th/0506118 [hep-th].

[9] M. Miyaji, T. Numasawa, N. Shiba, T. Takayanagi, and K. Watanabe, "Continuous Multiscale Entanglement Renormalization Ansatz as Holographic Surface-State Correspondence," *Phys. Rev. Lett.* **115** no. 17, (2015) 171602, arXiv:1506.01353 [hep-th].

[10] Y. Nakayama and H. Ooguri, "Bulk Locality and Boundary Creating Operators," *JHEP* **10** (2015) 114, arXiv:1507.04130 [hep-th].

[11] H. L. Verlinde, "Conformal Field Theory, 2-D Quantum Gravity and Quantization of Teichmuller Space," *Nucl. Phys.* **B337** (1990) 652.

[12] E. Hijano, P. Kraus, and R. Snively, "Worldline approach to semi-classical conformal blocks," arXiv:1501.02260 [hep-th].

[13] J. de Boer and J. I. Jottar, "Entanglement Entropy and Higher Spin Holography in AdS_3," *JHEP* **04** (2014) 089, arXiv:1306.4347 [hep-th].

[14] M. Ammon, A. Castro, and N. Iqbal, "Wilson Lines and Entanglement Entropy in Higher Spin Gravity," *JHEP* **10** (2013) 110, arXiv:1306.4338 [hep-th].

[15] M. Besken, A. Hegde, E. Hijano, and P. Kraus, "Holographic conformal blocks from interacting Wilson lines," *JHEP* **08** (2016) 099, arXiv:1603.07317 [hep-th].

[16] A. L. Fitzpatrick, J. Kaplan, D. Li, and J. Wang, "Exact Virasoro Blocks from Wilson Lines and Background-Independent Operators," arXiv:1612.06385 [hep-th].

[17] M. Besken, A. Hegde, and P. Kraus, "Anomalous dimensions from quantum Wilson lines," arXiv:1702.06640 [hep-th].

[18] B. Czech, L. Lamprou, S. McCandlish, B. Mosk, and J. Sully, "A Stereoscopic Look into the Bulk," *JHEP* **07** (2016) 129, arXiv:1604.03110 [hep-th].

[19] D. Kabat, G. Lifschytz, and D. A. Lowe, "Constructing local bulk observables in interacting AdS/CFT," *Phys. Rev.* **D83** (2011) 106009, arXiv:1102.2910 [hep-th].

[20] D. Kabat and G. Lifschytz, "CFT representation of interacting bulk gauge fields in AdS," *Phys. Rev.* **D87** no. 8, (2013) 086004, arXiv:1212.3788 [hep-th].

[21] D. Kabat and G. Lifschytz, "Decoding the hologram: Scalar fields interacting with gravity," *Phys. Rev.* **D89** no. 6, (2014) 066010, arXiv:1311.3020 [hep-th].

[22] P. H. Ginsparg, "Applied Conformal Field Theory," arXiv:hep-th/9108028 [hep-th].

[23] I. Bena, "On the construction of local fields in the bulk of AdS(5) and other spaces," *Phys. Rev.* **D62** (2000) 066007, arXiv:hep-th/9905186 [hep-th].

[24] A. Hamilton, D. N. Kabat, G. Lifschytz, and D. A. Lowe, "Holographic representation of local bulk operators," *Phys. Rev.* **D74** (2006) 066009, arXiv:hep-th/0606141.

[25] I. Heemskerk, D. Marolf, J. Polchinski, and J. Sully, "Bulk and Transhorizon Measurements in AdS/CFT," *JHEP* **10** (2012) 165, arXiv:1201.3664 [hep-th].

[26] K. Papadodimas and S. Raju, "An Infalling Observer in AdS/CFT," *JHEP* **10** (2013) 212, arXiv:1211.6767 [hep-th].

[27] D. Kabat and G. Lifschytz, "Bulk equations of motion from CFT correlators," *JHEP* **09** (2015) 059, arXiv:1505.03755 [hep-th].

[28] M. Guica and D. L. Jafferis, "On the construction of charged operators inside an eternal black hole," arXiv:1511.05627 [hep-th].

[29] D. Kabat and G. Lifschytz, "Locality, bulk equations of motion and the conformal bootstrap," *JHEP* **10** (2016) 091, arXiv:1603.06800 [hep-th].

[30] Y. Nakayama and H. Ooguri, "Bulk Local States and Crosscaps in Holographic CFT," *JHEP* **10** (2016) 085, arXiv:1605.00334 [hep-th].

[31] T. Faulkner and A. Lewkowycz, "Bulk locality from modular flow," arXiv:1704.05464 [hep-th].

[32] A. Almheiri, T. Anous, and A. Lewkowycz, "Inside Out: Meet The Operators Inside The Horizon," arXiv:1707.06622 [hep-th].

[33] H. Verlinde, "Poking Holes in AdS/CFT: Bulk Fields from Boundary States," arXiv:1505.05069 [hep-th].

[34] A. Lewkowycz, G. J. Turiaci, and H. Verlinde, "A CFT Perspective on Gravitational Dressing and Bulk Locality," arXiv:1608.08977 [hep-th].

[35] M. F. Paulos, J. Penedones, J. Toledo, B. C. van Rees, and P. Vieira, "The S-matrix Bootstrap I: QFT in AdS," arXiv:1607.06109 [hep-th].

[36] B. Carneiro da Cunha and M. Guica, "Exploring the BTZ bulk with boundary conformal blocks," arXiv:1604.07383 [hep-th].

[37] M. Guica, "Bulk fields from the boundary OPE," arXiv:1610.08952 [hep-th].

[38] J. L. Cardy and D. C. Lewellen, "Bulk and boundary operators in conformal field theory," *Phys. Lett.* **B259** (1991) 274–278.

[39] M. Banados, "Three-dimensional quantum geometry and black holes," arXiv:hep-th/9901148 [hep-th]. [AIP Conf. Proc.484,147(1999)].

[40] M. M. Roberts, "Time evolution of entanglement entropy from a pulse," *JHEP* **12** (2012) 027, arXiv:1204.1982 [hep-th].

[41] P. Liendo, L. Rastelli, and B. C. van Rees, "The Bootstrap Program for Boundary CFT," arXiv:1210.4258 [hep-th].

[42] P. Di Francesco, P. Mathieu, and D. Senechal, *Conformal Field Theory*. Graduate Texts in Contemporary Physics. Springer-Verlag, New York, 1997. http://www-spires.fnal.gov/spires/find/books/www?cl=QC174.52.C66D5::1997.

[43] D. L. Jafferis, "Bulk reconstruction and the Hartle-Hawking wavefunction," arXiv:1703.01519 [hep-th].

[44] B. Czech, J. L. Karczmarek, F. Nogueira, and M. Van Raamsdonk, "The Gravity Dual of a Density Matrix," *Class. Quant. Grav.* **29** (2012) 155009, arXiv:1204.1330 [hep-th].

[45] R. Bousso, B. Freivogel, S. Leichenauer, V. Rosenhaus, and C. Zukowski, "Null Geodesics, Local CFT Operators and AdS/CFT for Subregions," *Phys. Rev.* **D88** (2013) 064057, arXiv:1209.4641 [hep-th].

[46] I. A. Morrison, "Boundary-to-bulk maps for AdS causal wedges and the Reeh-Schlieder property in holography," *JHEP* **05** (2014) 053, arXiv:1403.3426 [hep-th].

[47] X. Dong, D. Harlow, and A. C. Wall, "Reconstruction of Bulk Operators within the Entanglement Wedge in Gauge-Gravity Duality," *Phys. Rev. Lett.* **117** no. 2, (2016) 021601, arXiv:1601.05416 [hep-th].

[48] A. Almheiri, X. Dong, and D. Harlow, "Bulk Locality and Quantum Error Correction in AdS/CFT," *JHEP* **04** (2015) 163, arXiv:1411.7041 [hep-th].

[49] S. D. Mathur, "The Information paradox: A Pedagogical introduction," *Class. Quant. Grav.* **26** (2009) 224001, arXiv:0909.1038 [hep-th].

[50] S. D. Mathur, "The Information paradox and the infall problem," *Class. Quant. Grav.* **28** (2011) 125010, arXiv:1012.2101 [hep-th].

[51] A. Almheiri, D. Marolf, J. Polchinski, and J. Sully, "Black Holes: Complementarity or Firewalls?," arXiv:1207.3123 [hep-th].

[52] A. Almheiri, D. Marolf, J. Polchinski, D. Stanford, and J. Sully, "An Apologia for Firewalls," *JHEP* **09** (2013) 018, arXiv:1304.6483 [hep-th].

[53] M. Gary, S. B. Giddings, and J. Penedones, "Local bulk S-matrix elements and CFT singularities," *Phys. Rev.* **D80** (2009) 085005, arXiv:0903.4437 [hep-th].

[54] J. Maldacena, D. Simmons-Duffin, and A. Zhiboedov, "Looking for a bulk point," arXiv:1509.03612 [hep-th].

[55] A. L. Fitzpatrick, J. Kaplan, and M. T. Walters, "Universality of Long-Distance AdS Physics from the CFT Bootstrap," *JHEP* **1408** (2014) 145, arXiv:1403.6829 [hep-th].

[56] A. L. Fitzpatrick, J. Kaplan, and M. T. Walters, "Virasoro Conformal Blocks and Thermality from Classical Background Fields," arXiv:1501.05315 [hep-th].

[57] T. Anous, T. Hartman, A. Rovai, and J. Sonner, "Black Hole Collapse in the 1/c Expansion," arXiv:1603.04856 [hep-th].

[58] C. T. Asplund, A. Bernamonti, F. Galli, and T. Hartman, "Holographic Entanglement Entropy from 2d CFT: Heavy States and Local Quenches," *JHEP* **02** (2015) 171, arXiv:1410.1392 [hep-th].

[59] P. Caputa, J. Simon, A. Stikonas, and T. Takayanagi, "Quantum Entanglement of Localized Excited States at Finite Temperature," arXiv:1410.2287 [hep-th].

[60] A. L. Fitzpatrick, J. Kaplan, D. Li, and J. Wang, "On Information Loss in AdS_3/CFT_2," arXiv:1603.08925 [hep-th].

[61] A. Liam Fitzpatrick and J. Kaplan, "On the Late-Time Behavior of Virasoro Blocks and a Classification of Semiclassical Saddles," arXiv:1609.07153 [hep-th].

[62] H. Chen, C. Hussong, J. Kaplan, and D. Li, "A Numerical Approach to Virasoro Blocks and the Information Paradox," arXiv:1703.09727 [hep-th].

[63] V. Balasubramanian, B. Czech, V. E. Hubeny, K. Larjo, M. Rangamani, and J. Simon, "Typicality versus thermality: An Analytic distinction," *Gen. Rel. Grav.* **40** (2008) 1863–1890, arXiv:hep-th/0701122 [hep-th].

[64] K. Goto and T. Takayanagi, "CFT descriptions of bulk local states in the AdS black holes," arXiv:1704.00053 [hep-th].

[65] A. L. Fitzpatrick, E. Katz, D. Poland, and D. Simmons-Duffin, "Effective Conformal Theory and the Flat-Space Limit of AdS," *JHEP* **1107** (2011) 023, arXiv:1007.2412 [hep-th].

[66] E. D'Hoker, D. Z. Freedman, and L. Rastelli, "AdS/CFT 4-point functions: How to succeed at z-integrals without really trying," *Nucl. Phys.* **B562** (1999) 395–411, arXiv:hep-th/9905049.

[67] E. D'Hoker, D. Z. Freedman, S. D. Mathur, A. Matusis, and L. Rastelli, "Graviton exchange and complete 4-point functions in the AdS/CFT correspondence," *Nucl. Phys.* **B562** (1999) 353–394, arXiv:hep-th/9903196.

[68] D. Kabat, G. Lifschytz, S. Roy, and D. Sarkar, "Holographic representation of bulk fields with spin in AdS/CFT," *Phys. Rev.* **D86** (2012) 026004, arXiv:1204.0126 [hep-th].

[69] E. Katz, Z. U. Khandker, and M. T. Walters, "A Conformal Truncation Framework for Infinite-Volume Dynamics," *JHEP* **07** (2016) 140, arXiv:1604.01766 [hep-th].

[70] A. J. A. James, R. M. Konik, P. Lecheminant, N. J. Robinson, and A. M. Tsvelik, "Non-perturbative methodologies for low-dimensional strongly-correlated systems: From non-abelian bosonization to truncated spectrum methods," arXiv:1703.08421 [cond-mat.str-el].

[71] A. Harindranath and J. P. Vary, "Solving two-dimensional ϕ^4 theory by discretized light-front quantization," *Phys. Rev.* **D36** (1987) 1141–1147.

[72] A. Harindranath and J. P. Vary, "Stability of the Vacuum in Scalar Field Models in $1+1$ Dimensions," *Phys. Rev.* **D37** (1988) 1076–1078.

[73] M. Burkardt, S. S. Chabysheva, and J. R. Hiller, "Two-dimensional light-front ϕ^4 theory in a symmetric polynomial basis," *Phys. Rev.* **D94** (2016) 065006, arXiv:1607.00026 [hep-th].

[74] D. Lee, N. Salwen, and D. Lee, "The diagonalization of quantum field Hamiltonians," *Phys. Lett.* **B503** (2001) 223–235, arXiv:hep-th/0002251 [hep-th].

[75] T. Sugihara, "Density matrix renormalization group in a two-dimensional $\lambda\phi^4$ Hamiltonian lattice model," *JHEP* **05** (2004) 007, arXiv:hep-lat/0403008 [hep-lat].

[76] D. Schaich and W. Loinaz, "An improved lattice measurement of the critical coupling in ϕ_2^4 theory," *Phys. Rev.* **D79** (2009) 056008, arXiv:0902.0045 [hep-lat].

[77] A. Milsted, J. Haegeman, and T. J. Osborne, "Matrix product states and variational methods applied to critical quantum field theory," *Phys. Rev.* **D88** (2013) 085030, arXiv:1302.5582 [hep-lat].

[78] P. Bosetti, B. De Palma, and M. Guagnelli, "Monte Carlo determination of the critical coupling in ϕ_2^4 theory," *Phys. Rev.* **D92** (2015) 034509, arXiv:1506.08587 [hep-lat].

[79] S. Rychkov and L. G. Vitale, "Hamiltonian truncation study of the ϕ^4 theory in two dimensions," *Phys. Rev.* **D91** (2015) 085011, arXiv:1412.3460 [hep-th].

[80] S. Rychkov and L. G. Vitale, "Hamiltonian truncation study of the ϕ^4 theory in two dimensions. II. The $\mathbb{Z}_2$-broken phase and the Chang duality," *Phys. Rev.* **D93** (2016) 065014, arXiv:1512.00493 [hep-th].

[81] J. S. Rozowsky and C. B. Thorn, "Spontaneous symmetry breaking at infinite momentum without P^+ zero modes," *Phys. Rev. Lett.* **85** (2000) 1614–1617, arXiv:hep-th/0003301 [hep-th].

[82] D. Chakrabarti, A. Harindranath, L. Martinovic, and J. P. Vary, "Kinks in discrete light cone quantization," *Phys. Lett.* **B582** (2004) 196–202, arXiv:hep-th/0309263 [hep-th].

[83] D. Chakrabarti, A. Harindranath, L. Martinovic, G. B. Pivovarov, and J. P. Vary, "Ab initio results for the broken phase of scalar light front field theory," *Phys. Lett.* **B617** (2005) 92–98, arXiv:hep-th/0310290 [hep-th].

[84] D. Chakrabarti, A. Harindranath, and J. P. Vary, "A transition in the spectrum of the topological sector of ϕ_2^4 theory at strong coupling," *Phys. Rev.* **D71** (2005) 125012, arXiv:hep-th/0504094 [hep-th].

[85] A. Coser, M. Beria, G. P. Brandino, R. M. Konik, and G. Mussardo, "Truncated Conformal Space Approach for 2D Landau-Ginzburg Theories," *J. Stat. Mech.* **1412** (2014) P12010, arXiv:1409.1494 [hep-th].

[86] J. Elias-Miro, M. Montull, and M. Riembau, "The renormalized Hamiltonian truncation method in the large E_T expansion," *JHEP* **04** (2016) 144, arXiv:1512.05746 [hep-th].

[87] Z. Bajnok and M. Lajer, "Truncated Hilbert space approach to the 2d ϕ^4 theory," *JHEP* **10** (2016) 050, arXiv:1512.06901 [hep-th].

[88] B. Elliott, S. S. Chabysheva, and J. R. Hiller, "Application of the light-front coupled-cluster method to ϕ^4 theory in two dimensions," *Phys. Rev.* **D90** (2014) 056003, arXiv:1407.7139 [hep-ph].

[89] S. S. Chabysheva and J. R. Hiller, "Light-front ϕ_2^4 theory with sector-dependent mass," arXiv:1612.09331 [hep-th].

[90] N. Christensen, "Diagonalizing the Hamiltonian of $\lambda\phi^4$ Theory in 2 Space-Time Dimensions," arXiv:1603.01273 [hep-ph].

[91] A. B. Zamolodchikov, "From tricritical Ising to critical Ising by thermodynamic Bethe ansatz," *Nucl. Phys.* **B358** (1991) 524–546.

[92] P. Fendley, H. Saleur, and A. B. Zamolodchikov, "Massless flows I: The sine-Gordon and $O(n)$ models," *Int. J. Mod. Phys.* **A8** (1993) 5717–5750, arXiv:hep-th/9304050 [hep-th].

[93] P. Fendley, H. Saleur, and A. B. Zamolodchikov, "Massless flows II: The exact S-matrix approach," *Int. J. Mod. Phys.* **A8** (1993) 5751–5778, arXiv:hep-th/9304051 [hep-th].

[94] C. Ahn, G. Delfino, and G. Mussardo, "Mapping between the Sinh-Gordon and Ising Models," *Phys. Lett.* **B317** (1993) 573–580, arXiv:hep-th/9306103 [hep-th].

[95] G. Delfino, G. Mussardo, and P. Simonetti, "Correlation functions along a massless flow," *Phys. Rev.* **D51** (1995) 6620–6624, arXiv:hep-th/9410117 [hep-th].

[96] G. Delfino and G. Mussardo, "The spin-spin correlation function in the two-dimensional Ising model in a magnetic field at $T = T_c$," *Nucl. Phys.* **B455** (1995) 724–758, arXiv:hep-th/9507010 [hep-th].

[97] G. Delfino and G. Mussardo, "Non-integrable aspects of the multi-frequency Sine-Gordon model," *Nucl. Phys.* **B516** (1998) 675–703, arXiv:hep-th/9709028 [hep-th].

[98] G. Mussardo, V. Riva, G. Sotkov, and G. Delfino, "Kink scaling functions in 2D non-integrable quantum field theories," *Nucl. Phys.* **B736** (2006) 259–287, arXiv:hep-th/0510102 [hep-th].

[99] E. Katz, G. Marques Tavares, and Y. Xu, "Solving 2D QCD with an adjoint fermion analytically," *JHEP* **05** (2014) 143, arXiv:1308.4980 [hep-th].

[100] E. Katz, G. Marques Tavares, and Y. Xu, "A solution of 2D QCD at Finite N using a conformal basis," arXiv:1405.6727 [hep-th].

[101] L. Chao, "Light-cone quantization of scalar field," *Mod. Phys. Lett.* **A8** (1993) 3165–3172.

[102] N. Anand, V. X. Genest, E. Katz, Z. U. Khandker, and M. T. Walters, "Conformal Basis for Scalar Field Theory." In progress.

[103] S. Groote, J. G. Korner, and A. A. Pivovarov, "A new technique for computing the spectral density of sunset type diagrams: Integral transformation in configuration space," *Phys. Lett.* **B443** (1998) 269–275, arXiv:hep-ph/9805224 [hep-ph].

[104] A. L. Fitzpatrick, J. Kaplan, E. Katz, and L. Randall, "Decoupling of High Dimension Operators from the Low Energy Sector in Holographic Models," arXiv:1304.3458 [hep-th].

[105] P. Di Francesco, P. Mathieu, and D. Sénéchal, *Conformal Field Theory*. Springer-Verlag, 1997.

[106] H. Leutwyler, J. R. Klauder, and L. Streit, "Quantum field theory on lightlike slabs," *Nuovo Cim.* **A66** (1970) 536–554.

[107] T. Maskawa and K. Yamawaki, "The Problem of $P^+ = 0$ Mode in the Null Plane Field Theory and Dirac's Method of Quantization," *Prog. Theor. Phys.* **56** (1976) 270.

[108] H. C. Pauli and S. J. Brodsky, "Solving Field Theory in One Space One Time Dimension," *Phys. Rev.* **D32** (1985) 1993.

[109] H. C. Pauli and S. J. Brodsky, "Discretized Light Cone Quantization: Solution to a Field Theory in One Space One Time Dimensions," *Phys. Rev.* **D32** (1985) 2001.

[110] S. J. Brodsky, H.-C. Pauli, and S. S. Pinsky, "Quantum chromodynamics and other field theories on the light cone," *Phys. Rept.* **301** (1998) 299–486, arXiv:hep-ph/9705477 [hep-ph].

[111] M. Burkardt, "Light front quantization of the Sine-Gordon model," *Phys. Rev.* **D47** (1993) 4628–4633.

[112] A. Cappelli and J. I. Latorre, "Perturbation Theory of Higher Spin Conserved Currents Off Criticality," *Nucl. Phys.* **B340** (1990) 659–691.

[113] B. Berg, M. Karowski, and P. Weisz, "Construction of Green Functions from an Exact S Matrix," *Phys. Rev.* **D19** (1979) 2477.

[114] B. M. McCoy, C. A. Tracy, and T. T. Wu, "Two-Dimensional Ising Model as an Exactly Solvable Relativistic Quantum Field Theory: Explicit Formulas for n Point Functions," *Phys. Rev. Lett.* **38** (1977) 793–796.

[115] T. T. Wu, B. M. McCoy, C. A. Tracy, and E. Barouch, "Spin-spin correlation functions for the two-dimensional Ising model: Exact theory in the scaling region," *Phys. Rev.* **B13** (1976) 316–374.

[116] A. Zamolodchikov, "Irreversibility of the Flux of the Renormalization Group in a 2D Field Theory," *JETP Lett.* **43** (1986) 730–732.

[117] A. Cappelli, D. Friedan, and J. I. Latorre, "C Theorem and Spectral Representation," *Nucl. Phys.* **B352** (1991) 616–670.

[118] G. Mussardo, *Statistical Field Theory*. Oxford Univ. Press, 2010.

[119] G. Delfino, G. Mussardo, and P. Simonetti, "Non-integrable quantum field theories as perturbations of certain integrable models," *Nucl. Phys.* **B473** (1996) 469–508, arXiv:hep-th/9603011 [hep-th].

[120] G. Delfino, P. Grinza, and G. Mussardo, "Decay of particles above threshold in the Ising field theory with magnetic field," *Nucl. Phys.* **B737** (2006) 291–303, arXiv:hep-th/0507133 [hep-th].

[121] A. Zamolodchikov and I. Ziyatdinov, "Inelastic scattering and elastic amplitude in Ising field theory in a weak magnetic field at $T > T_c$: Perturbative analysis," *Nucl. Phys.* **B849** (2011) 654–674, arXiv:1102.0767 [hep-th].

[122] P. Fonseca and A. Zamolodchikov, "Ising spectroscopy I: Mesons at $T < T_c$," arXiv:hep-th/0612304 [hep-th].

[123] A. Zamolodchikov, "Ising Spectroscopy II: Particles and poles at $T > T_c$," arXiv:1310.4821 [hep-th].

[124] M. Hogervorst, S. Rychkov, and B. C. van Rees, "Truncated conformal space approach in d dimensions: A cheap alternative to lattice field theory?," *Phys. Rev.* **D91** (2015) 025005, arXiv:1409.1581 [hep-th].

[125] S. El-Showk, M. F. Paulos, D. Poland, S. Rychkov, D. Simmons-Duffin, *et al.*, "Solving the 3d Ising Model with the Conformal Bootstrap II. c-Minimization and Precise Critical Exponents," arXiv:1403.4545 [hep-th].

[126] F. Gliozzi and A. Rago, "Critical exponents of the 3d Ising and related models from Conformal Bootstrap," *JHEP* **10** (2014) 042, arXiv:1403.6003 [hep-th].

[127] F. Kos, D. Poland, D. Simmons-Duffin, and A. Vichi, "Precision islands in the Ising and $O(N)$ models," *JHEP* **08** (2016) 036, arXiv:1603.04436 [hep-th].

[128] D. Simmons-Duffin, "The Lightcone Bootstrap and the Spectrum of the 3d Ising CFT," *JHEP* **03** (2017) 086, arXiv:1612.08471 [hep-th].

[129] S. S. Chabysheva, B. Elliott, and J. R. Hiller, "Symmetric multivariate polynomials as a basis for three-boson light-front wave functions," *Phys. Rev.* **E88** (2013) 063307, arXiv:1307.4964 [physics.comp-ph].

[130] S. S. Chabysheva and J. R. Hiller, "Basis of symmetric polynomials for many-boson light-front wave functions," *Phys. Rev.* **E90** (2014) 063310, arXiv:1409.6333 [hep-ph].

Vita

Nikhil Anand grew up in Bangalore, India and Cupertino, California. He received his B.A. in physics from the University of California, Berkeley in 2013. As an undergrad, his research focused on the direct detection of dark matter particles. He enrolled in the physics PhD program at Johns Hopkins University in 2013 and received an M.A. in 2015.

In the fall of 2018, Nikhil will start as a postdoctoral fellow at McGill University to continue his career in theoretical physics.